Anticancer activity of sulforaphane and allyl isothiocyanate-conjugated silicon quantum dots

A thesis submitted for the Degree of Doctor of Philosophy

By

Peng Liu

Norwich Medical School

September 2017

© This copy of the thesis has been supplied on condition that anyone who consults it is understood to recognise that its copyright rests with the author and that use of any information derived there-from must be in accordance with current UK Copyright Law. In addition, any quotation or extract must include full attribution.

Abstract

Dietary isothiocyanates (ITCs) from cruciferous vegetables (CVs) have been shown to possess chemopreventive and chemotherapeutic effects in many cellular and animal studies but with only limited success in humans. The aim of this thesis is to further evaluate the bioactivities of ITCs and the mechanisms behind, and the potential of multi-functional nano-conjugates to maximize the beneficial effects of ITCs in cancer therapy.

The effects of sulforaphane (SFN), one of the most studied ITCs, were examined on human hepatocytes (HHL5) and hepatocarcinoma (HepG2) cells. Results showed that SFN was more toxic towards HHL5 than HepG2, and that the high basal levels of Nrf2/GSH/ROS enabled HepG2 cells to benefit from the protective effects of SFN against H_2O_2-induced cell death, apoptosis and DNA damage. Three of the metabolites of SFN were also examined in terms of their anticancer activities, and were demonstrated to exhibit similar cytoprotective activity, but weaker cytotoxic effects than SFN. Allyl isothiocyanate (AITC), another common dietary ITC, showed biphasic effects on cell viability, DNA damage and migration in HepG2 cells, and on endothelial cell tube formation in a 3D model. siRNA knockdown of Nrf2 and GSH inhibition abolished the stimulatory effects of low dose AITC on cell migration as well as low dose AITC induced protection against DNA damage. The lack of selectivity and the biphasic effects of ITCs could present undesirable risks in the context for cancer prevention and treatment.

The bioactivities of novel AITC-conjugated silicon quantum dots (AITC-SiQDs) were compared with AITC, and their cellular uptake was monitored by detecting the intrinsic fluorescence of SiQDs. AITC-SiQDs demonstrated similar activity as AITC at high doses whilst lacking the low dose stimulatory effects. In addition, AITC-SiQDs induced a long-lasting activation of Nrf2 *via* translocation into the nucleus, which correlated positively with their cellular uptake. ROS were involved in the anticancer effects of AITC-SiQDs. Taken together, these data provide novel insights into the anticancer properties of ITCs and highlight the possibility of application of nanotechnology to optimize their potential in cancer treatment.

Acknowledgment

Firstly, I would like to express my sincere gratitude to my supervisors, Dr Yongping Bao and Dr Yimin Chao for their guidance and support. Also, big thanks to all members of Dr Bao and Chao's lab, past and present, for the help and friendship throughout my PhD.

I am grateful to Dr Richard Bowater, Professor Andrea Munsterberg, Dr Stuart Rushworth, Dr Paul Thomas and Dr Zhigang Zhou for the help with comet assay, the CAM assay, flow cytometry, confocal microscopy and 3D culture respectively. Special thanks to Dr Qi Wang, Dr Sophia Akbareian, Dr Christopher Dacosta and Ms Wei Wang, for their input and advices during these years of my PhD.

My sincerest thanks also go to Dr Stephen Robinson and all members of his lab (and Didi and Huvi) for their kindness and lending hands (and fluffiness).

I would like to thank my family for all their love and support encouraging me to pursuit my dream of being a scientist. Special thanks to my fiancé Samuel Atkinson and his family, who have been there for me in the good and not so good times. I would like to dedicate this thesis for you Sam, thank you for all the wonder you have done for me over the years, and I am looking forward to the future with you.

Finally, I would like to acknowledge UEA, John and Pamela Salter Trust for the financial support for my project.

To finish with a traditional Chinese poem:

A Traveller's Song

By Meng Jiao (751-814), translated by Yanshen Zhang and Bosi Wei

Through a kind mother's hands passed the thread

That made the clothes I journeying wear.

Tightly tightly she wove them then,

Dreading year after year of no return.

Can the young grass ever repay

The spring sun's kindly rays?

Contents

Abbreviations

γ-GCS	γ-glutamylcysteine synthetase
γ-GT	γ-glutamyl transferase
AITC	allyl isothiocyanate
AITC-SiQDs	AITC-conjugated SiQDs
ARE	antioxidant responsive element
Akt	protein kinase B
ASAP	ascorbic acid phosphate
BSA	bovine serum albumin
BSO	D,L-buthionine sulfoximine
CAM	chorioallantoic membrane
CG	cysteinylglycinase
Chk2	checkpoint kinase 2
CLSM	confocal laser scanning microscopy
CM	conditioned medium
CVs	cruciferous vegetables
CYP	cytochrome P450
DMEM	dulbecco's modified eagle medium
DMSO	dimethyl sulphoxide
DSB	double strand breaks
DTT	dithiothreitol
EC	endothelial cell
ECM	extracellular matrix
EGCG	epigallocatechin-3-gallate
EGF	epidermal growth factor
EGFR	epidermal growth factor receptor
EGM-2	endothelial cell growth medium 2
EMT	epithelial to mesenchymal transition
EPR	enhanced permeability and retention
ERK	extracellular signal-related kinase
ESP	epithiospecifier protein
FBS	foetal bovine serum
FGF	fibroblast growth factor
FOXO	forkhead box-O

GSH	glutathione
GSK3β	glycogen synthase kinase-3β
GST	glutathione S-transferase
H&E	hematoxylin and eosin
HCC	hepatocellular carcinoma
HDAC	histone deacetylase
HIF-1α	hypoxia inducible factor-1alpha
HO-1	heme oxygenase-1
HPLC	high-performance liquid chromatography
HR	homologous recombination
HREs	hypoxia-responsive elements
HRP	horseradish peroxidase
IC50	half-maximal inhibitory concentration
IL	interleukin
ITCs	Isothiocyanates
JNK	c-jun N-terminal kinase
Keap1	Kelch-like ECH-associated protein 1
MAPK	mitogen-activated protein kinase
mBBr	monobromobimane
MMP	matrix metalloproteinase
MQW	MillQ-water
MSA	methanesulfonic acid
MTT	3-(4,5-Dimethyilthiazol-2-yl)-2,5-diphenyltetrayolium bromide
NAC	N-acetyl-L-cysteine
NAT	N-acetyl transferase
NER	nucleotide excision repair
NF-kB	nuclear factor-kappa B
NH_2-SiQDs	amine-capped SiQDs
NHEJ	non-homologous end-joining
NP40	Nonidet P40 lysis buffer
NPs	nanoparticles
NQO1	NAD(P)H: quinone oxidoreductase-1
Nrf2	nuclear factor E2-related factor 2
NSAIDs	non-steroidal anti-inflammatory drugs

PBS	phosphate buffered saline
PDGF	platelet-derived growth factor
PEG	polyethylene glycol
PEITC	phenethyl isothiocyanate
PFA	paraformaldehyde
PGA	polyglycolic acid
PHDs	prolyl hydroxylases
PI	propidium iodide
PI3K	Phosphatidylinositol 3-kinase
PL	photoluminescence
PLA	polylactic acid
PLL	poly-l-lysine
PVA	polyvinyl alcohol
QDs	quantum dots
ROS	reactive oxygen species
RT	room temperature
SDS-PAGE	sodium dodecyl sulphate polyacrylamide gel electrophoresis
SFN	sulforaphane
SFN-Cys	sulforaphane cysteine
SFN-CG	sulforaphane cysteinylglycine
SFN-GSH	sulforaphane glutathione
SFN-NAC	Sulforaphane N-acetylcysteine
SiQDs	silicon quantum dots
siRNA	small interfering RNA or silencing RNA
SSB	single-strand breaks
STAT3	signal transducer and activator of transcription 3
TGF-β	transforming growth factor beta
TNF-alpha	tumour necrosis factor alpha
TRAIL	tumour necrosis factor-related apoptosis-inducing ligand
TrxR1	thioredoxin reductase 1
UGT	UDP-glucuronosyltransferase
VEGF	vascular endothelial growth factor
VHL	von Hippel-Lindau

List of Figures

List of Tables

Chapter 1. Introduction

1.1 Chemoprevention and phytochemicals

Cancer is a leading burden on public health around the world and has been a major research focus for at least two decades[1]. The increasing understanding of cancer pathobiology has led to a molecular approach to treatment and more important, developing chemopreventive strategies. The concept of chemoprevention is defined as the use of non-toxic chemicals to prevent or interfere with the development or progression of the neoplastic process that leads to cancer[2]. Clinically, chemoprevention can be categorized as primary, secondary, or tertiary. Primary chemoprevention is suited for the general population and for those who may be at increased risk of disease. Secondary chemoprevention is intended for patients with premalignant lesions that may progress to an invasive disease. Tertiary chemoprevention is targeted to prevent disease recurrence or additional disease in those individuals who have already received therapy. At the molecular level, cancer chemoprevention is characterized by the disruption of, or at least the delay of, multiple pathways and processes among the three stages of carcinogenesis: initiation, promotion, and progression[2,3]. Generally accepted examples of these agents include dietary phytochemicals and non-steroidal anti-inflammatory drugs (NSAIDs).

Chemoprevention by dietary phytochemicals, is now considered to be an inexpensive, readily applicable, acceptable and accessible approach to cancer control and management[4–6]. Phytochemicals are bioactive non-nutrient chemical compounds found in plant foods, e.g. fruits, vegetables, grains, nuts, and seeds. They often are categorized into groups based on their chemical structure, such as polyphenols, organosulfur compounds, carotenoids, alkaloids, and nitrogen-containing compounds. Several organizations such as the World Health Organization, the American Cancer Society, the American Institute of Cancer Research and the National Cancer Institute, have established dietary guidelines to help people reduce the cancer risk[7]. It has been estimated that at least 20% of all cancers can be prevented by consumption of diets rich in vegetables and fruits (>400 g/day)[8].

Chemopreventive phytochemicals can interfere with different steps of the carcinogenesis process. According to the conventional classification originally proposed by Lee Wattenberg, chemopreventive agents are subdivided into two main categories: blocking agents and suppressing agents[9]. Some inhibit metabolic activation of the procarcinogens to their ultimate electrophilic species, or their subsequent interaction with DNA, or advance the

detoxification and elimination of the carcinogens. These agents therefore block tumour initiation (blocking agents). Others suppress the later steps (promotion and progression) by inducing apoptosis, interfering with cell proliferation, inhibiting angiogenesis and metastasis, etc. They are considered as suppressing agents. The understanding of the carcinogenic process at the cellular and molecular level has progressed and this blocking and suppressing categorization is now considered as an oversimplification. The ability of any single chemopreventive phytochemical should be recognized as the outcome of the combination of several distinct sets of intracellular effects as it may target numerous cellular molecules and events in different situations.

Although various cellular and animal models have confirmed the benefit derived from many phytochemicals against cancer, the clinical utilization of phytochemicals is limited[6,10,11]. The cause can be ascribed to a number of factors: human genetic variation may modify the response to phytochemicals in population-based studies; a precise assessment of the mechanisms by which the phytochemicals act in different physiological and pathological situations is necessary before they can be tested in human intervention trials; and like the disposition of drugs and any other xenobiotics, the bioactivity of phytochemicals is largely dependent on the absorption, metabolism, distribution and excretion in our body. In addition to the low solubility and/or stability of many phytochemicals, achieving sustained therapeutic levels at the target site remains a challenge due to the digestive system. Thus, further studies are needed to confirm the molecular mechanisms behind the bioactivities of phytochemicals and to explore advanced delivery systems for targeted and controlled release.

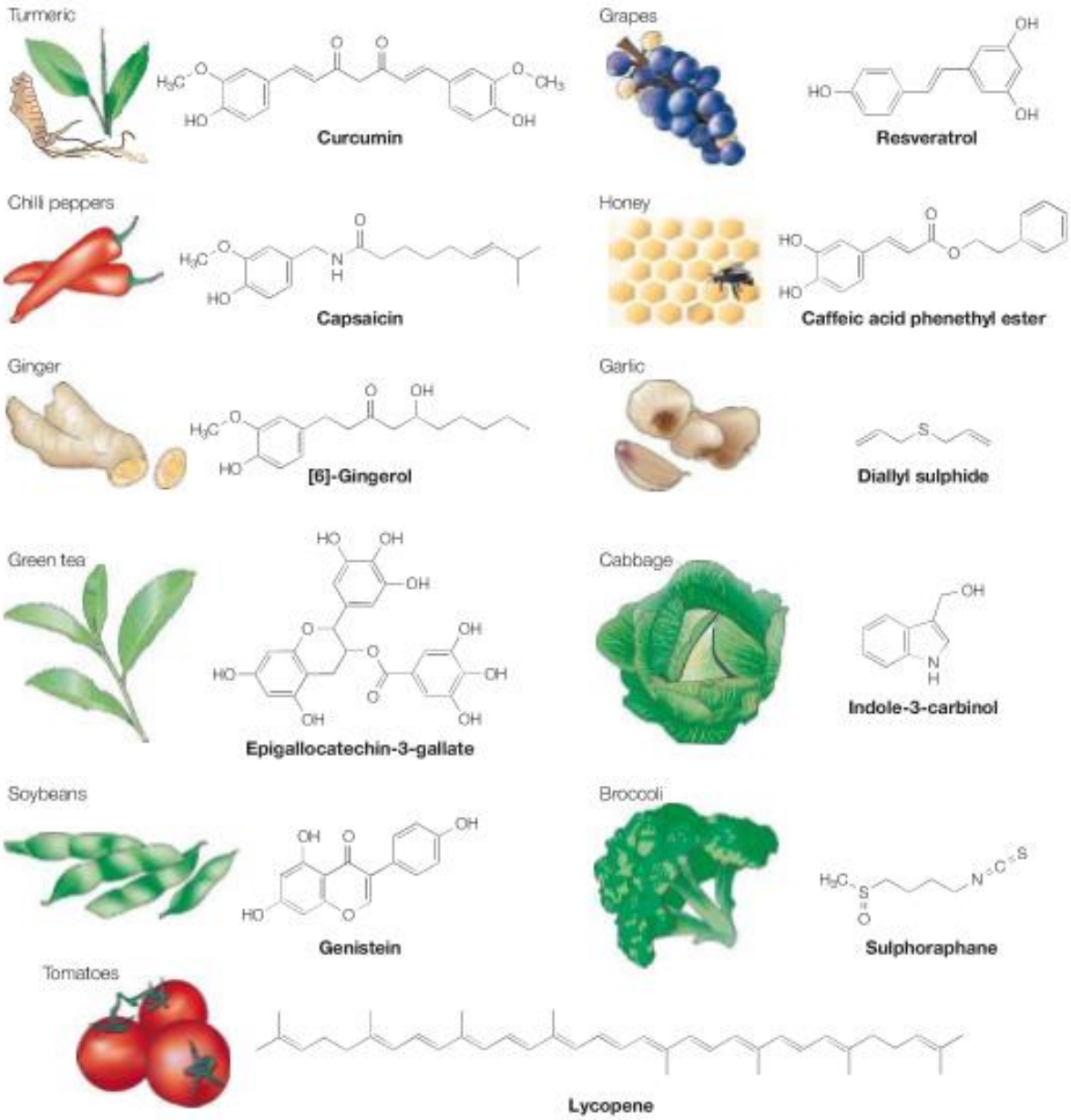

Figure 1.1 Representative chemoprevention phytochemicals and their dietary sources[7].

1.2 Dietary isothiocyanates

Isothiocyanates (ITCs) have been identified as the chemopreventive phytochemicals from cruciferous vegetables (CVs) that belong to the Cruciferae family. Commonly consumed CVs include the *Brassica* genus such as broccoli, brussels sprouts, cabbage, cauliflower, kale, mustard, turnips and Chinese cabbage; and others such as horseradish, wasabi and watercress. There are many nutrients and phytochemicals that CVs provide, including folate, carotenoids, vitamins C, E and K, minerals and fiber. However, a group of sulfur-containing chemicals known as glucosinolates (β-thioglucoside N-hydroxysulfate) can only be found in CVs. Glucosinolates remain stable within the cytoplasm until they come into contact with the endogenous plant enzyme, β-thioglucoside glucohydrolase (EC 3.2.3.1), also named myrosinase, which is expressed on the external surface of the plant cell wall. This could happen when plant is ruptured by chewing, cooking or insect attack. The hydrolysis reaction leads to a variety of products. At neutral pH (6–7), the major glucosinolate hydrolysis products are stable ITCs (Figure 1.2). Alternatively, thioglucosidases in human gut microflora can hydrolyse the consumed glucosinolates to ITCs and indoles with lower efficiency[12].

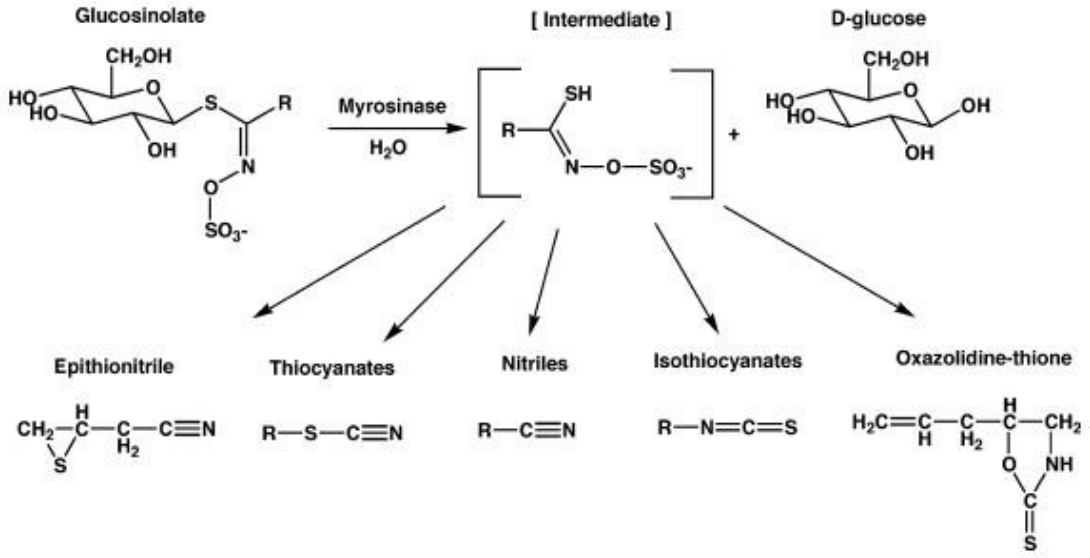

Figure 1.2 The general structures of glucosinolates and their degradation products[13].

One of the most studied of the ITCs is sulforaphane (1-isothiocyanate-(4R)-(methylsulfinyl) butane, SFN). First isolated from broccoli in 1992[388], SFN is derived from glucoraphanin (4-methylsulfinylbutyl glucosinolate) (Figure 1.3). It is abundant in broccoli and broccoli sprouts, with reports demonstrating that the SFN concentration in broccoli

sprout was about 10 times higher than that of mature broccoli[14]. The hydrolysis of glucoraphanin via myrosinase typically generates SFN as the major product but this is dependent on the reaction conditions such as pH, availability of ions (Fe^{2+}), and the presence of epithiospecifier protein (ESP)[15,16].

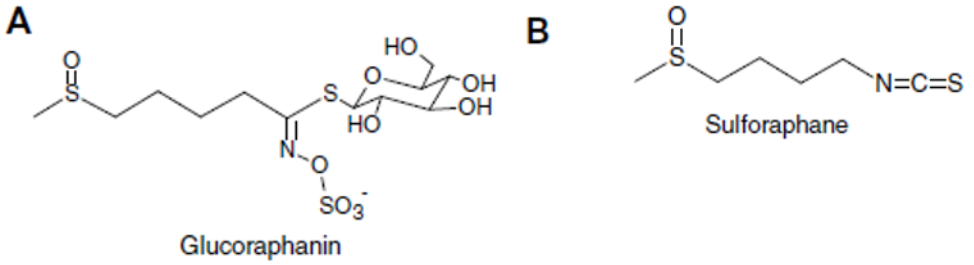

Figure 1.3 Structures of glucosinolate precursor glucoraphanin (A) and its isothiocyanate hydrolysis product sulforaphane (B).

Another ITCs on which this study focused was allyl isothiocyanate (AITC), also known as mustard oil. It is derived from the glucosinolate, sinigrin, which is particularly abundant in mustard, horseradish and wasabi[17,18](Figure 1.4). AITC is a liquid at ambient temperature and is responsible for the pungent taste as it activates the transient receptor potential A1 channel in sensory neurons[19]. Therefore, synthetic AITC is often used as a food additive to enhance flavour.

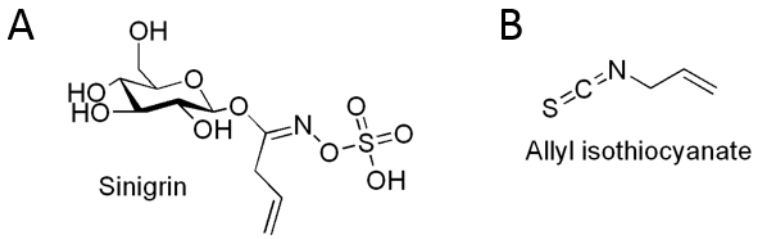

Figure 1.4 Structures of glucosinolate precursor sinigrin (A) and its isothiocyanate hydrolysis product allyl isothiocyanate (B).

The average intake of CVs was 11.3 g/day according to data from 40684 Spanish[20]. Higher intake was reported in Asian countries. For example, habitual Brassica consumption among healthy Shanghai women was 98 g/day[21]. The glucosinolate contents of common Brassica were summarized by McNaughton and Marks. Broccoli usually contains 19.3–127.5

mg glucoraphinin/100 g fresh weight, which is equivalent to 44.2–292.1 µmol SFN/100 g if 100% converted, however that average losses during cooking are approximately 36%[22]. Since ESP activity is negatively correlated with the formation of SFN in broccoli[16], heating of broccoli enhances SFN absorption as the ESP denatures; while over-heating broccoli reduced SFN bioavailability by deactivating myrosinase[23,24]. Also, the absorption of ITCs was delayed in the case of cooked broccoli compared to raw broccoli[25]. Apart from cooking conditions, the bioavailability of ITCs also depends on plant myrosinase[26] and glucosinolates status, food matrix[27], intestinal microbiota[28] as well as genetic differences in humans. For example, ITCs are metabolized by glutathione S-transferases (GSTs). Individuals with a homozygous deletion of the GSTM1 or GSTT1 gene cannot produce the corresponding GST enzyme, which results in slower elimination of ITCs after CV consumption[29]. Several epidemiological studies have suggested that GST gene polymorphisms interact with the bioavailability and anti-carcinogenic effects of CVs, examples see section 1.2.4.

1.2.1 Metabolism of ITCs

ITCs undergo extensive first-pass metabolism in the gut epithelium or liver via the mercapturic acid pathway summarized in Figure 1.5. After absorption by passive diffusion across the gastrointestinal epithelium and the capillary endothelium, ITCs bind rapidly and reversibly to thiols of plasma proteins and cross the membrane into cells when they are first conjugated with glutathione (GSH). Although it can occur nonenzymically, this conjugation is more likely to occur with the activity of GSTs *in vivo*[30]. The peak intracellular accumulation of ITCs is reached within 0.5-3 hours of exposure and could be up to several hundred-fold over their extracellular concentration (millimolar level), which is critical for their anticarcinogenic activity[31,32]. However this high cellular accumulation followed by a rapid membrane transporter-mediated export has also been observed[33]. The GSH conjugates then undergo further enzymatic cleavage sequentially to the cysteinylglycine conjugate and cysteine conjugate via γ-glutamyl transferase (γ-GT) and cysteinylglycinase (CG) respectively, both enzymes being localized on the extracellular surface of the plasma membrane. The resulting cysteine conjugates are transported to the liver where they form N-acetylcysteine conjugates by N-acetyl transferase (NAT), and then finally transported to the kidney and excreted in urine.

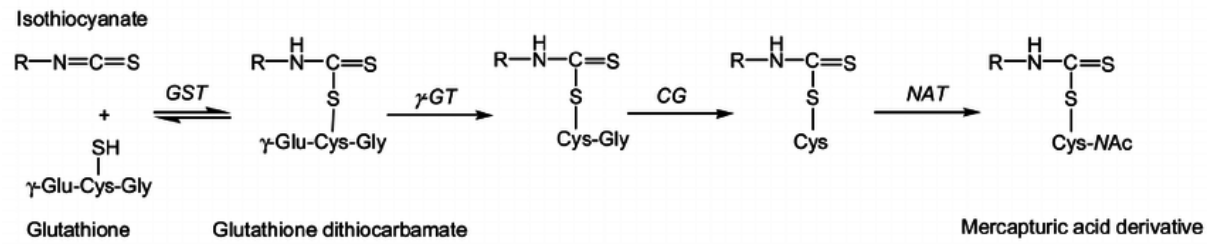

Figure 1.5 Metabolism of ITCs by the mercapturic acid pathway. R: is the aliphatic or aromatic substituent of the ITC[34].

1.2.2 Pharmacokinetics of ITCs

In 2002, Ye *et al* reported that after giving four human subjects a single dose of 200 µmol broccoli sprous ITCs (largely SFN, with lesser amounts of iberin and erucin), the plasma concentrations peaked between 0.943 and 2.27 µM at 1 hour and declined with first-order kinetics (half-life times of 1.77 ± 0.13 hours), about half of the dose was excreted (58.3 ± 2.8%) after 8 hours[35]. Human perfusion experiments showed that 74 ± 29% of SFN from broccoli extracts can be absorbed in the jejunum and a portion of that returns to the lumen of the jejunum as GSH conjugates[36]. Gasper *et al* reported that plasma SFN level reached over 7.3 µM in human subjects eating 'SuperBroccoli' soup[37]. After consuming 180 µmol per day ITCs, the plasma concentration of ITC and SFN reached 2.2 µM and 0.32 µM respectively, and ITCs were detected in the synovial fluids of the patients (0.5 µM)[38]. In another study, an oral dose of broccoli sprout preparation containing 200 µmol SFN was given to eight healthy females. SFN metabolites were readily measurable in breast tissue after 1 hour. The mean accumulation was 1.45 ± 1.12 pmol/mg tissue in the right breast and 2.00 ± 1.95 pmol/mg in the left breast. This not only confirmed the distribution level of SFN in human body but also showed it can accumulate at different levels in different tissues[39].

Using animal models further data on tissue distribution have been reported. ITC metabolites are inclined to accumulate at the bladder, followed by liver and kidney. Lower concentrations were detected in plasma, skin, and lung tissue in female mice[40]. In rat, tissue uptake of SFN was the greatest in the stomach then bladder and declined rapidly in gastro-intestinal tract while tissue levels of SFN in the colon, prostate and several other organs were very low compared to those in the bladder and stomach[41]. The tissues containing the highest concentration of AITC-derived radioactivity were the intestinal mucosa, liver, kidneys, and bladder, followed by the lungs and spleen. The brain and heart exhibited very low concentrations of radioactivity[42,43]. According to Zhang *et al*, orally administered AITC was

selectively delivered to cancer tissue in the bladder through urinary excretion in two rat bladder cancer models *in vivo* (an orthotopic model and a subcutaneous model)[44].

The cumulative renal excretion after 72 hours following a single oral intake of broccoli extract containing 111 μmol of ITCs was 80% in human[45]. In another study, ingestion of CVs (51 or 224 μmol of ITCs) led to a urinary excretion of 69 and 75%, respectively within 48 hours[46]. The clearance of SFN and its metabolites follows first-order kinetics in humans. In urine around 12% is excreted as SFN, less than 1% as SFN-GSH and SFN-CG conjugates, around 23% as SFN-Cys and around 68% as SFN-NAC in the 24 hours after consumption[37]. Munday *et al* reported the recovery of a mean of 76% AITC as NAC conjugate within 24 hours in the urine after dosing with 25 or 250 μmol/kg body weight, with an average concentration nearly 10 times higher than that in blood[47].

While the effects of long-term, low-level dietary exposure are not as well understood, there is evidence from animal models suggesting that SFN may accumulate in tissue after repeated feeding[41], however one human study indicated the urinary elimination pattern was not significantly altered even after repeated dosing (oral broccoli sprout extracts containing 25 μmol ITC at 8 hours intervals for 7 days)[48]. Another study concluded 200 μmol/day of SFN-rich extracts for a maximum period of 20 weeks was safe with no Grade 3 adverse events in men with recurrent prostate cancer[49]. The highest level yet given during a clinical trial was reported as around 450 μmol/day (80 mg/day) of SFN in the form of powdered broccoli sprout extract for one week to healthy adults, and no severe treatment-related adverse events was noted[50].

1.2.3 Anticancer mechanisms of ITCs

The chemical structures of ITCs consist of a functional group - N = C = S with various side chains. The central carbon atom of the functional group makes ITCs powerful electrophiles which react readily with sulfur-, nitrogen- and oxygen-based biological nucleophiles, in particular, amines and thiols[51]. Thus, directly biological effects may be due to the modification of reactive cysteine, selenocysteine or amine residues in various proteins (Figure 1.6). Indeed, the cytoprotective effect of ITCs is largely achieved by the binding of ITCs to sulfhydryl groups of Kelch-like ECH-associated protein 1 (Keap1) resulting in the activation of nuclear factor E2-factor related factor (Nrf2). Lewis *et al* reported that ITCs are time-dependent inactivators of cysteine-dependent protein tyrosine phosphatases[52].

Tubulin was found to be covalently modified by ITCs at Cys303 and Cys347, leading to cell growth arrest and microtubule polymerization disruption[53]. The activity of MEKK1 and DNA topoisomerase IIα were reported to be inhibited by ITCs via modification of their cysteine residues[54,55]. The anti-inflammatory properties of ITCs have also been linked with their ability to covalently bind multiple cysteine residues of recognition membrane receptors, which blocks downstream nuclear factor-kappa B (NF-kB) activation[56]. Other protein sulfhydryl groups readily interact with ITCs including heat shock protein 90β and glyceraldehyde-3-phosphate dehydrogenase[57]. ITCs can also bind to the N-terminal proline residue of macrophage migration inhibitory factor[58,59] and to the N-terminal amino acids of key oncogenic molecules such as transforming growth factor beta (TGF-β) and insulin[60].

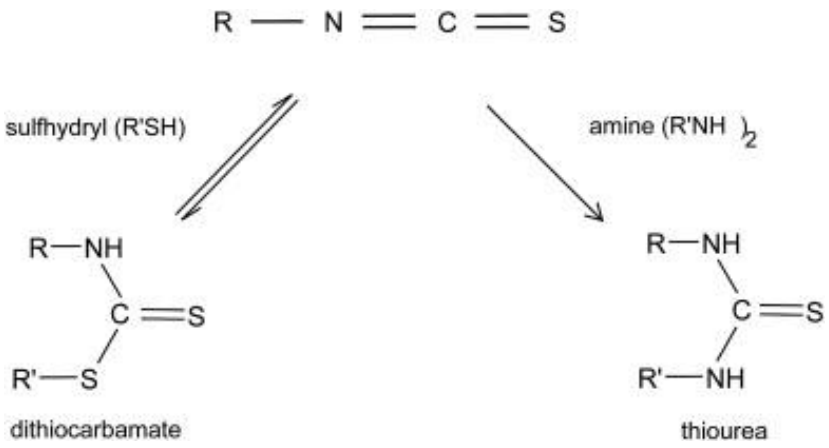

Figure 1.6 The reactivity from the –N=C=S group in ITCs. Reaction with amines to generate stable thiourea derivatives, whereas reaction with thiols generates labile dithiocarbamate adducts[61].

1.2.3.1 Effect on phase I and phase II enzymes

The up-regulation of the xenobiotic-detoxifying phase II enzymes and/or the down-regulation of the xenobiotic-activating phase I enzymes by ITCs is thought to be an important step in blocking chemically-induced carcinogenesis. The inhibitory effect of SFN on Cytochrome P450 (CYP) 1A1, 2E1, 2B1, 2B2, and 3A4 has been reviewed in rat and human hepatocytes, respectively[62]. AITC reduced the expression and function of CYP3A4 and CYP2B6 in HepG2 cells[63]. Structural influence of ITCs on CYP expression has also been reported[64].

ITCs are known as potent naturally occurring inducers of phase II enzymes in both animals and humans, including drug-detoxifying enzymes such as GST, NAD(P)H: quinone

oxidoreductase-1 (NQO1), UDP-glucuronosyltransferase (UGT); antioxidant defence enzymes such as heme oxygenase-1(HO-1), thioredoxin reductase 1 (TrxR1); and enzymes for GSH synthesis, such as α-glutamylcysteine synthetase (γ-GCS)[65–67]. Molecular studies have shown that the induction on these phase II enzymes from ITCs depends on the antioxidant responsive element (ARE) present in the upstream region of their genes, the regulation of which is associated with disruption of Nrf2-Keap1 interactions and mitogen-activated protein kinase (MAPK) activation[68]. There are three families in MAPK: extracellular signal-related kinase (ERK), c-jun N-terminal kinase (JNK), and p38 MAPK. Activated by upstream signalling kinases such as MAPK kinase and MAPKK kinase, MAPK is phosphorylated in both threonine (T) and tyrosine in the activation loop and the central amino acid defines individual MAPKs: glutamic acid (E) for ERK, proline (P) for JNK and glycine (G) for p38 MAPK[69]. Studies have demonstrated that the upregulation of Nrf2/ARE-dependent gene expression by ITCs was mediated by MAPK pathway[70–72].

Phosphatidylinositol 3-kinase (PI3K) is another intracellular signalling kinase that is implicated in the regulation of Nrf2/ARE-dependent gene expression. The downstream Ser/Thr kinase of PI3K is protein kinase B (Akt), which has shown to regulate the activation of glycogen synthase kinase-3β (GSK3β). GSK3β can directly phosphorylate and suppress the activity of Nrf2 protein by nuclear exclusion[73]; or contribute to the degradation of Nrf2 in a Keap1-independent manner[74]; or activate tyrosine kinase Fyn which phosphorylate Nrf2 at tyrosine 568[75]. Shang *et al* reported that SFN ameliorated experimental diabetic nephropathy *in vitro*, at least in part, via the GSK3β/Fyn/Nrf2 signalling pathway[76]. The activation of PI3K/Akt signalling regulated cell survival and Nrf2-driven HO-1 expression in SFN-treated human mesothelioma cells[77]. Others reported that SFN stimulated the phosphorylation of PI3K leading Nrf2-mediated HO-1 expression against Hepatitis C virus replication *in vitro*[78]. It has also been demonstrated *in vivo* that broccoli sprouts significantly retard prostate tumour growth, which is accompanied by the suppression of the Akt-dependent kinase pathway[79]. According to Li *et al*, MAPK (ERK, JNK and p38) and PI3K/Akt signalling pathways played no significant role in SFN-induced Nrf2 nuclear translocation in human hepatocytes, but blocking ERK and JNK decreased SFN-induced TrxR-1 mRNA by about 20%; whereas blocking p38 and PI3K/AKT increased TrxR-1 transcription[80].

ITCs can also disrupt Keap1 and Nrf2 protein interactions. Nrf2 is a member of the basic leucine-zipper NF-E2 family, regulating the expression of more than 200 genes. It can bind to ARE (5'-(G/A)TGA(G/C)nnnGC(G/A)-3') sites as a cis-acting element in the 5'-flanking

region of the genes. Under basal conditions, Nrf2 is sequestered in the cytoplasm by redox-sensitive Keap1, which associates with Cul3 and brings Nrf2 in close proximity to Cul3-based E3 ligase complex so Nrf2 degrades via ubiquitin-26S proteasomal pathway[81]. With a half-life of around 20 minutes[82], Nrf2 is maintained at a low cellular level. However, under redox stress, the Keap1-Nrf2-ubiquitin assembly is disturbed and consequently releases Nrf2 which then translocates to the nucleus and heterodimerizes with small Mafs, binds to ARE, leading to transcription of ARE-dependent genes. Different mechanistic models have been proposed for Nrf2 activation: In the 'hinge and latch' model, cysteine residues of Keap1 (C273 and C288 as the most studied ones for the ubiquitination of Nrf2) are covalently modified, which leads to the conformational changes that makes the orientation of Nrf2 not suitable for ubiquitin ligase activity by Keap1-Cul3 complex[83]; while other models propose the covalent modification of cysteine residue(s) in Cul3 binding Keap1 leads to the dissociation of Keap1-Cul3 interaction[84]; alternative mechanisms for Nrf2 stabilization in response to inducers, such as nucleocytoplasmic shuttling of Keap1, ubiquitination of Keap1, and Nrf2 as a direct sensor, etc., have also been reported[85,86]. All result in Nrf2 escaping from proteasomal degradation, accumulating in the cell along with newly *de novo* synthesized Nrf2, and translocating to the nucleus.

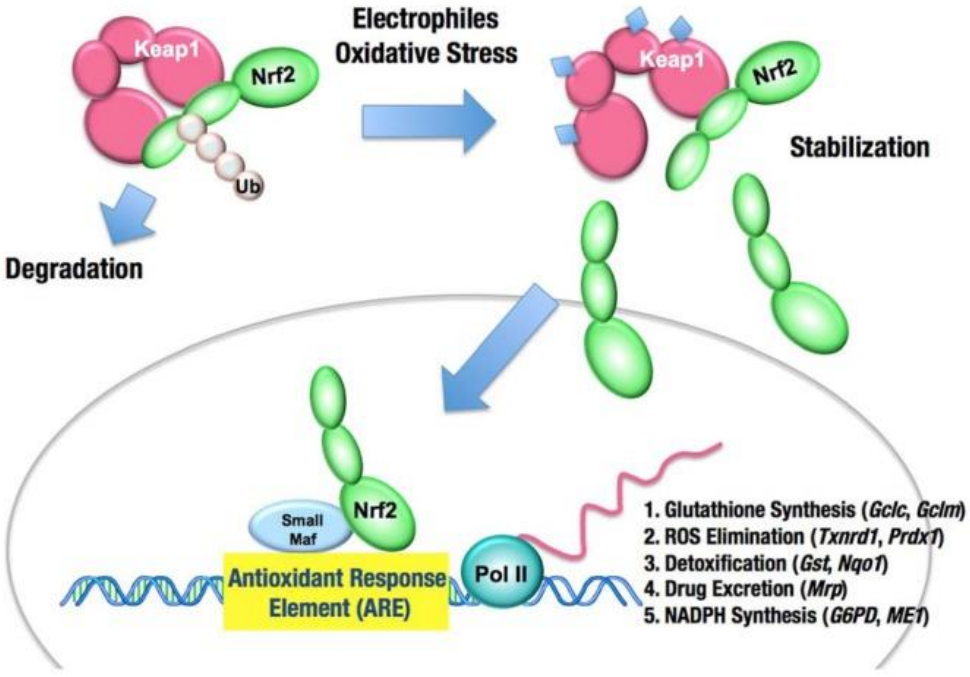

Figure 1.7 Schematic representation of the Keap1-Nrf2-ARE system[87]. Under basal conditions, Nrf2 is sequestered in the cytoplasm by an adaptor subunit of Cullin 3-based E3 ubiquitin ligase, Keap1, which promotes its degradation by the ubiquitin proteasome pathway. While

under redox stress, the inducer-modified and Nrf2-bound Keap1 is inactivated, which leads to the release of Nrf2. Together with the newly synthesized Nrf2 proteins, they translocate into the nucleus, bind with small Maf proteins to the ARE in the regulatory regions of target genes.

The prevailing molecular mechanism of regulation of Nrf2 signalling by ITCs is through their covalent modification of Keap1 on one or more of the 27 cysteine residues on Keap1[88]. The loss of intracellular GSH due to ITC metabolism can increase cellular oxidative stress at least in the short term, thus promoting release of Nrf2 from Keap1 and triggering increased *de novo* Nrf2[86]. Others reported that SFN suppressed Nrf2 proteasomal degradation leading to its prolonged half-life and transcriptional activity[89]. *In vivo* studies have confirmed the activation of Nrf2 signalling is behind the protective effects of ITCs. Pre-treatment with SFN before methylmercury exposure resulted in a decrease in mercury accumulation in the brain and liver of wild-type but not Nrf2-deficient mice[90], topical application of 100 nmol of SFN per day for 14 days decreased the incidence of skin tumour in the Nrf2(+/+) mice compared with the vehicle-treated group, and no chemoprotective effect was observed in the Nrf2(−/−) mice group[91]. Others reported that SFN up-regulated the expression of Nrf2 and its downstream genes *in vivo*. Nrf2 expression as well as the mRNA expression of HO-1 and NQO1 were found to be significantly increased in the heart of SFN-treated mice both at 3 months (0.5 mg/kg daily in five days of each week) and 6 months (3 months after 3-month SFN treatment)[92]. Co-administration of SFN (50 mg/kg, every other day for 60 days) rescued rotenone induced inhibition of Nrf2, HO-1 and NQO1 expression in the cerebral cortex and striatum[93]. A 7 day oral application of AITC (15 mg/kg body weight) in mice resulted in a significant increase in nuclear Nrf2 and HO-1 expression in the liver[94].

1.2.3.2 Other anticarcinogenic properties

Hanahan and Weinberg have defined six basic common hallmarks underlying cancer progression. These are 1) sustaining proliferative signalling; 2) evading growth suppressors; 3) resisting cell death (apoptosis); 4) enabling replicative immortality; 5) inducing angiogenesis; 6) activating invasion and metastasis[95]. Inhibition of one or more of these hallmarks can achieve anticancer therapeutic effects. Accumulating evidence suggests that ITCs have a broad spectrum of molecular targets to suppress cancer growth and progression. ITCs act on certain molecular targets like survivin and NF-kB that are vital for cancer cell

proliferation and survival[94,96]. Specific activation of MAP kinases such as ERK, JNK and p38 in response to ITC treatment was shown to be involved in inducing cell cycle arrest and cell death[97]. Other studies suggested that ITCs have a role in cancer epigenetics[98,99], inflammation[94,100], and metabolism[66,101], etc. A number of studies have indicated that ITCs may target cancer stem cells in different types of cancer[102–104]. Discussion below focuses on the effect of ITCs on apoptosis, DNA damage, cell migration and angiogenesis.

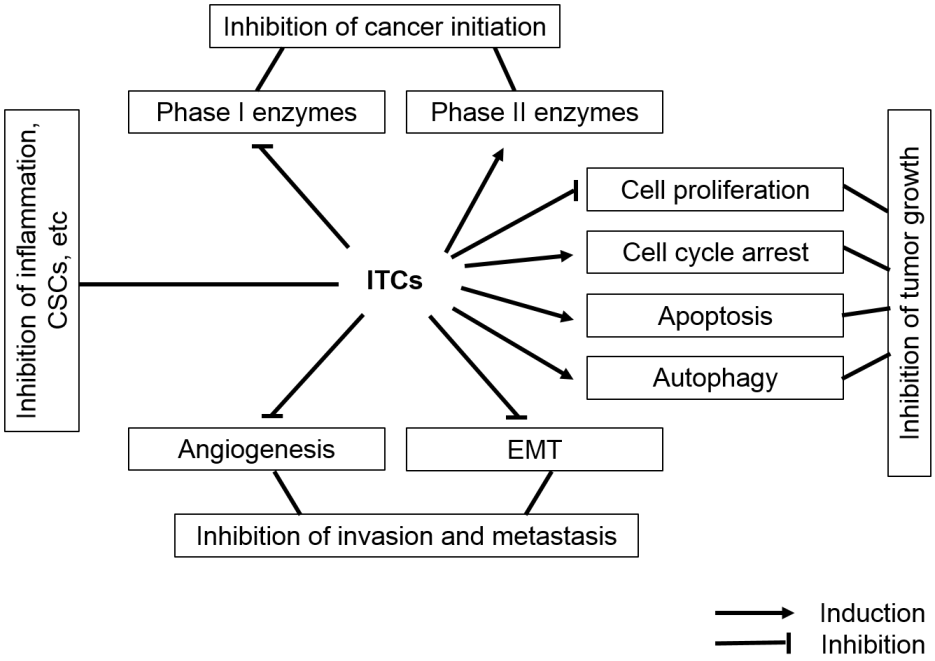

Figure 1.8 Chemotherapeutic targets of ITCs.

Effect on apoptosis

Apoptosis, or programmed cell death, is a physiologic process for removal unwanted cells to maintain tissue homeostasis, which is characterized by several morphologic changes including condensation of the cytoplasm and nucleus, DNA fragmentation and plasma membrane blebbing[105]. Reduced apoptosis or its resistance plays a vital role in carcinogenesis. There are three pathways by which apoptosis can be activated: the intrinsic mitochondrial, intrinsic endoplasmic reticulum, and extrinsic (or death receptor) pathways. Malignant cells can have a disrupted balance of pro-apoptotic and anti-apoptotic proteins, reduced caspase function and impaired death receptor signalling, which facilitates tumour development and metastasis[106]. Treatments that can restore the apoptotic pathways

towards normality therefore have the potential to eliminate cancer cells, or to sensitize resistant cancer cells to conventional treatments[107].

ITCs induce apoptosis in cancer cells by activating both extrinsic and intrinsic pathways[108]. SFN was found to induce endoplasmic reticulum[109] and mitochondrial[110] stress related apoptosis. It also inactivated the inhibitors of apoptosis proteins[111]. SFN also sensitizes human cholangiocarcinoma to cisplatin via the downregulation of anti-apoptotic proteins such as Bcl-2 and XIAP[112]. AITC induced mitochondrion-mediated apoptosis in human bladder cancer cells, which depended entirely on mitotic arrest which caused by AITC direct binding to cysteine residues of tubulins; and was mediated via Bcl-2 phosphorylation at Ser70 which caused by AITC induced activation of JNK[113]. According to Li *et al*, the apoptosis induced by AITC stems primarily from ROCK1/PTEN/PI3K signalling, resulting in dephosphorylation of cofilin, which binds to G-actin and translocates to mitochondria, culminating in the dysfunction of mitochondria[114].

Effect on DNA damage

The genome DNA is constantly exposed to various insults, which can cause DNA damage. DNA damage is then recognized and repaired by the intrinsic DNA damage response machinery. DNA repair, if unsuccessful, may cause cellular senescence, oncogenesis, or apoptosis. Multiple types of DNA damage as well as the corresponding repair mechanisms in humans have been reviewed by Curtin *et al*[115], including base modification (repaired by direct repair and base excision repair), base mismatch (repaired by mismatch repair), intrastrand crosslinks (ICL), and DNA–protein crosslinks [repaired by ICL repair and nucleotide excision repair (NER)], stalled replication forks [repaired by homologous recombination (HR), NER, and the Fanconi Anemia pathway], single-strand breaks (SSB; repaired by BER and HR) and double strand breaks [DSB; repaired by HR and non-homologous end-joining (NHEJ)]. The most deleterious DNA damage is DSBs, while the most common one is SSBs. They both can be caused by endogenous reactive oxygen species (ROS) as well as exogenous insults such as ionizing radiation and chemotherapeutic agents[116]. Interestingly, DSB repair depends on the phase of the cell cycle. HR is an error free pathway but is most predominant during late S and G2 phase, factors involved in HR include the MRN complex, CtIP, BRCA1, BRCA2, RAD51, etc. While NHEJ is active during all phases of the cell cycle but is error-prone, factors involved in NHEJ include the Ku complex (a heterodimer of Ku70/Ku80), DNA-PK catalytic subunits,

DNA ligase IV, etc. NHEJ is thought to be the primary means of repair for therapeutically induced DSBs resulting from irradiation, radiomimetics, topoisomerase poisons, and ROS-inducing treatments[115]. In addition, an alternative form of NHEJ, namely, alt-NHEJ, is also involved in DSB repaire[117].

The DNA damage caused by ITCs has been reported to involve the production of ROS[118,119] and cause cell growth arrest, autophagy and apoptosis[120,121]. On the other hand, ITCs enhance the acetylation and subsequent degradation of critical DNA repair proteins, such as CtIP[122]. Piberger *et al* reported that SFN inhibited the repair against (+)-anti-BPDE-induced DNA damage *in vitro* within the first 12 hours but not the later repair period up to 24 hours, and this may due to SFN impairing the xeroderma pigmentosum A protein, which is essential for NER[123]. SFN also induced a loss of DNA repair proteins Ku70, Ku80 and XRCC4 in human pancreatic cancer cells and enhanced irradiation effects[124]. Charron *et al* reported DNA strand breaks after 3 hours AITC consumption in human but this effect dissipated by 6 hours[125]. *In vitro*, AITC caused Cu(II)-mediated and oxidative DNA damage in HL60 cells[126]. It also induced replication-associated DNA damage response and exhibited synergistic effect with radiation in non-small cell lung cancer cells[127]. Interestingly, lower concentrations of AITC were able to induce genotoxicity in the mutant cells for the TP53 gene compared to wild-type bladder cancer cells[121].

Effect on cell migration

Cell migration is a fundamental step for embryonic development, wound repair, immune responses, and tumor invasion and metastasis. The dissemination of tumor cells from the primary site is the leading cause of death for solid tumors (carcinomas, sarcomas, and central nervous system tumors)[128]. Tumor metastasis consists of several steps, starting with cancer cells detaching from the primary tumor, to invade the basement membranes and local mesenchymal tissues, to undergo transendothelial migration into blood or lymphatic vessels (intravasation), to attach to the vessel wall in the distant organ and migrate out of the vessel (extravasation), and finally colonize and proliferate at the secondary sites. There are two properties common to invasion and metastasis, one is the epithelial to mesenchymal transition (EMT) that loosens the primary tumor cell mass, the other is growth factor-induced cell motility[128,129].

ITCs have also been reported to reduce the invasive potential of cancer cells. The anti-cell migratory effect of SFN was associated with matrix metalloproteinase (MMP) suppression[130,131] and epidermal growth factor receptor (EGFR) down-regulation[132]. It inhibited the migration and invasion of triple-negative SUM159 human breast cancer cells through suppressing the Hedgehog pathway[133], and hypoxia-induced migration of human cancer cells[134]. It also suppressed EMT in various cancer cells[135–137]. Combination of lapatinib, a commonly used drug that interrupts signalling from EGFR and HER2/neu, with SFN overcomes drug resistance and inhibits migration of HER2 positive breast cancer cells[138]. AITC influenced cell adhesion, migration and metalloproteinase gene expression in SK-Hep1 cells[139], and suppressed the epidermal growth factor (EGF) induced invasion and migration in HT29 cells via the suppression of MAPK pathway[140]. A low oral dose of AITC (1 mg/kg) significantly inhibited the development and muscle invasion of the orthotopic bladder cancers but was ineffective against the subcutaneous xenografts of the same cancer cells in the same animals, which may due to the higher level of AITC in urinary compared to that in plasma[44].

Effect on angiogenesis

Angiogenesis is defined as the formation of blood vessels from pre-existing vasculature. Most blood vessels are quiescent in the adult. However, physiological angiogenesis is active in the uterus and ovary during the menstrual cycle, placenta during pregnancy, skeletal muscle after exercise, and regenerating tissues following injury[141]. When dysregulated, angiogenesis can contribute to a range of pathological conditions, including cancer. It is a complicated process with many stages and molecular interaction between different cell types. Generally speaking, angiogenesis initiates when hypoxic, inflammatory or tumour cells release a plethora of pro-angiogenic growth factors, such as vascular endothelial growth factors (VEGFs), angiopoietin 2, platelet-derived growth factor (PDGF) or fibroblast growth factors (FGFs), and lead to the angiogenic phenotype, triggering the removal of pericytes from nearby capillaries and the degradation of the extracellular matrix (ECM) by proteases like MMPs. Endothelial cells (ECs) then loosen their intercellular junctions, proliferate, and migrate onto newly forming and remodelling ECM. Finally, ECs re-establish their junctions and are covered by new mural cells (pericytes in medium-sized and smooth muscle cells in large vessels) and ECM to form tube-like structures[141].

As early as 1971, J. Folkman proposed that inhibiting tumour angiogenesis might be a valuable therapy against cancer as angiogenesis is critical for tumour growth and metastasis[95]. When a tumour exceeds a few millimetres in diameter, hypoxia and nutrient-deprivation trigger and/or sustain the persistent release of pro-angiogenic growth factors in the tumour microenvironment. Due to the dysregulation of the angiogenic signalling, the arising tumour vasculature is continuously remodelled, and is therefore leaky, tortuous and fragile[142]. The tumour microenvironment, including ECs, mural cells, tumour associated fibroblasts, tumour-associated macrophages, lymphatic ECs, etc., is now considered as important as the tumour cells for tumour progression and angiogenesis.

ECs have been reported as a novel target of ITC action both *in vitro* and *in vivo*. SFN showed time- and concentration-dependent inhibitory effects on hypoxia-induced mRNA expression of VEGF and its receptor VEGFR2, as well as two angiogenesis-associated transcription factors, hypoxia inducible factor-1alpha (HIF-1α) and c-Myc, in an immortalized human microvascular endothelial cell line[143]. It also inhibited VEGF expression in pericytes[144]. Another study showed the inhibition of forkhead box-O (FOXO)/AKT pathway as one of the molecular mechanisms by which SFN inhibits angiogenesis[145]. 15 μM SFN clearly induced G2/M arrest and disrupted mitotic progression in bovine aortic endothelial cells. In addition, daily intravenous administration of SFN (100 nmol/day, for 7 days) significantly suppressed angiogenesis progression in female mice bearing VEGF-impregnated Matrigel plugs[146]. The combination of SFN and tumour necrosis factor-related apoptosis-inducing ligand (TRAIL) was more effective in inhibiting markers of angiogenesis in prostate cancer orthotopic model[147]. AITC not only significantly inhibited endothelial cell migration, invasion, and tube formation *in vitro*, but also downregulated the pro-angiogenic factors such as VEGF, interleukin (IL)-1β , IL-6, granulocyte macrophage colony-stimulating factor, tumour necrosis factor alpha (TNF-alpha)[148] and nitric oxide[149] in the serum cytokine profiles of angiogenesis-induced mice. It also showed significant inhibition of *in vivo* angiogenesis in the peritoneum of Ehrlich ascites tumour cells-bearing mice, associated with a reduced VEGF production[150].

1.2.4 Epidemiological studies of ITCs

The epidemiological evidence regarding the consumption of dietary ITCs as chemopreventive agents has been inconsistent. Summarized below are findings for lung, colorectal, breast, prostate, pancreatic and liver cancer.

High CV intake was significantly associated with improved lung cancer-specific survival among Chinese women[151]; and reduced the lung cancer risk among Japanese male nonsmokers[152]. While in a Caucasian population, high intakes of CVs reduced lung cancer risk among GSTM1 positive individuals but not among GSTM1 null individuals[153].

Broccoli, in particular, exhibited protective benefits against colorectal neoplasms according to a meta-analysis of 33 articles[154]. However, no association was found between urinary ITC concentration and colorectal cancer risk among Chinese women who carried either the GSTM1 or GSTT1 gene[155] and among Chinese men with GST gene variants[156].

In the case of breast cancer, intake of CVs showed a statistically significant association with a decreased risk of breast cancer among premenopausal Japanese women[157], and African-American women[158]. However, no association with recurrence or mortality were found using data from the After Breast Cancer Pooling Project, which includes prospective data from US and Chinese breast cancer survivors[159].

A significantly decreased prostate cancer risk was observed overall in the CV intake group in a meta-analysis of 7 cohort and 6 population-based case-control studies[160]. Others also reported that after diagnosis CV consumption may reduce risk of prostate cancer progression[161]. However, treatment with 200 μM/day of SFN-rich extracts lead to more than 50% prostate specific antigen (PAS) declines only in 1 out of 20 patients who had recurrent prostate cancer in a phase II study[49]. No recommendation can be made for the use of ITCs in managing prostate cancer morbidity and mortality[162].

A significantly decreased risk of pancreatic cancer was reported to be associated with the high intake of CV[163], though cohort studies on this relationship are limited. For example, a nonsignificant inverse association was observed with CV consumption among 81,922 women and men in the Swedish Mammography Cohort and the Cohort of Swedish Men[164]; and no association was found in the Hawaii-Los Angeles Multiethnic Cohort[165].

In a randomized, placebo-controlled trial in Qidong, intake of 400 μM glucoraphanin nightly for 2 weeks altered the disposition of aflatoxin and phenanthrene in 200 healthy participants, both of which contribute to the high risk of HCC in that region[166]. On the other hand, no association between urinary ITC exposure and liver cancer risk was found in a nested case-control study including Chinese men and women[167]. Consumption of CVs (around 125 g) at least once a week also showed no significant association with liver cancer risk reduction in data from case-control studies conducted in Italy and Switzerland[168].

For rectal cancer, the consumption of CVs even showed a positive association in a prospective study of Dutch women[169]. 17 human intervention studies with broccoli or glucoraphanin or SFN were found on PubMed with consistent results in blood glucose and lipid profile and for molecular parameters of oxidative stress, while less solid evidence was found with regard to protection against cancer[170].

1.2.5 Hormetic effect of ITCs

Hormesis is generally defined as a biphasic dose response to an exogenous or endogeneous factor (chemical agents exercise, dietary restriction, oxidative stress, temperature, etc.) characterized by low dose stimulation or beneficial effects, and high dose inhibition or adverse effects. From an evolutionary perspective, hormesis may be viewed as an adaptive response to homeostasis disruption within complex biological systems[171]. The highly consistent quantitative features of the hormetic dose responses at the cell, organ, and organismic level has important implications in drug discovery, clinical trials and toxicological risk assessment for pharmaceutical agents[172].

Some phytochemicals, including ITCs, have been reported to exhibit biphasic dose responses *in vitro* with low doses activating adaptive cellular stress response pathways that increase the expression of cytoprotective proteins including antioxidant enzymes, protein chaperones, growth factors and mitochondrial proteins. Examples of such pathways include the MAPK, Nrf2/ARE, sirtuin/FOXO and NF-κB pathways[173,174]. Indeed, the hormetic effect of ITCs have been observed as cytotoxic effects at higher doses (see previous sections), and cytoprotective effects at lower doses. Low concentrations of ITCs promoted cell proliferation and provided protection against oxidative injuries in human mesenchymal stem cells; while high concentrations exacerbated DNA damage, induced cell cycle arrest and cell death[175,176]. 2 μM SFN showed no toxicity in wild-type mouse embryonic fibroblasts yet provided protection against a spectrum of xenobiotics[177]. With an IC_{50} of 25 μM in immortalised human hepatocytes, SFN (≤5 μM) showed protective effect against H_2O_2 and CdSe quantum dot induced cytotoxicity[80,178].

However, the hormetic dose response from endogenous or exogenous agents can contribute to the development of cancer, through low doses having a stimulatory effect on cancer cell proliferation, transformation, and resistance[179]. A few investigations have shown that at low concentration (1-5 μM) ITCs promoted cancer cell proliferation and migration, stimulated angiogenesis, and offered protection against free-radical mediated cell

death[180,181]. These results suggest that ITCs may either prevent or promote tumour development depending on the dose and the nature of the target cells.

The amounts of ITCs normally consumed by humans from diet or concentrated supplements could be within the low dose stimulatory range (see section 1.2.2), and cause adverse health consequences. A schematic concept for the benefits and risks of dietary ITCs is proposed in Figure 1.9. It is therefore crucial to understand the mechanisms of action of the hormetic effects of ITCs and evaluate detailed dose-response studies for their safety and effectiveness regarding cancer management.

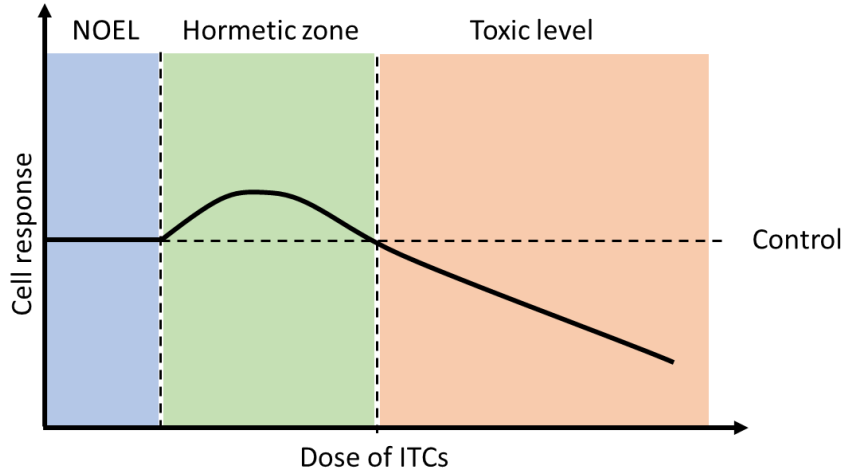

Figure 1.9 A schematic concept on the hormetic effect of ITCs adapted from[180]. NOEL, No Observed Effect Level.

1.3 Nanotechnology against cancer

Nanotechnology has been widely used in the development of new strategies for drug delivery and cancer therapy. Generally, nanotechnology refers to application of an incredibly small scale between 1 and 100 nm. The National Cancer Institute currently recommends that the size of the nanoparticles (NPs) used in biomedicine should be 10-100 nm, the upper limit of NP size is not strictly defined but the lower limit is fixed based on the threshold for first-pass elimination by the kidney[182]. Nanotechnology is playing a role in providing both diagnostics and therapeutics for cancer, with the potential to provide novel nanodevices for *in vitro* molecular measurements of pathophysiology, targeted therapies with optimized therapeutic index and *in vivo* molecular monitors as a diagnostic of drug efficacy[183,184], etc. Albumin-bound paclitaxel nanospheres (Abraxane®) and liposome-encapsulated daunorubicin (DaunoXome®) are two of successful examples of natural product formulations based on nanotechnological approaches.

1.3.1 Delivery of phytochemicals by nanoparticles

Nano formulations of phytochemicals essentially follow the general principles of nanotechnology. Many successful examples of nanoformulations with enhanced cellular bioavailability and anticancer activities have been reported *in vitro*[185]. In animal studies, curcumin loaded NPs exhibited superior tumor regression compared to free curcumin against prostate[186], pancreatic[187], cervical[188] and glioma[189] cancer. Quercetin-loaded NPs had more than 1.5-fold higher tumor growth inhibition in human A549 lung tumor xenograft mice model[190]. Resveratrol-loaded NPs suppressed glucose metabolism and tumor growth in CT26 tumor-bearing mice[191]. Siddiqui *et al* reported that the encapsulation of epigallocatechin-3-gallate (EGCG) achieved over 10-fold dose advantage for its proapoptotic and angiogenesis inhibitory effects[192]. More recently, the same group reported an oral formulation of EGCG NPs for the treatment of prostate cancer in a preclinical setting[193]. Hsieh *et al* coated gold NPs with EGCG, which exhibited improved anticancer efficacy against bladder[194] and melanoma[195] cancer in mouse models.

Targeted delivery of phytochemicals can be enhanced by incorporating target ligands, such as folic acid, antibodies and aptamers, on the surface of NPs[196–198]. Furthermore, new classes of stimuli-responsive multifunctional NPs have been developed. For example, Ji *et al* reported curcumin-loaded nanodroplets achieved controlled release into targeted

tumor under ultrasound-mediated vaporization[199]. Other studies applied pH- and/or thermos-responsive NPs to improve the bioavailability of phytochemicals in the targeted tissue[200,201].

The use of nanotechnology for the delivery of combined chemotherapeutics has also been explored. A docetaxel-curcumin nanoformulation showed a synergistic effect on tumor growth inhibition *in vivo* without any obvious side effects[202]. An intravenous injection of a lactoferrin-tethered magnetic nanocapsule co-delivering doxorubicin and curcumin followed by magnetic targeting in brain tumor-bearing mice not only achieved high accumulation at the targeted site but also more efficiently suppressed cancer growth *in vivo* than the delivery of either drug alone[203]. Another combinatorial nanomedicine based on 5-fluorouracil and curcumin enhanced the anticancer effects in colon cancer cells and prolonged plasma concentration in a pharmacokinetic study[204]. Following systemic administration of quercetin phosphate NPs, a significant downregulation in Wnt16 expression was observed and further yielded a synergistic antitumor effect with cisplatin in a stroma-rich bladder carcinoma model[205]. Other phytochemicals such as polyphenols EGCG and resveratrol have also been reported to sensitize cancer cells to different chemotherapeutics via nanoparticulate delivery system[206,207]. Combined co-delivery of curcumin and resveratrol reduced prostate cancer incidence in PTEN knockout mice[208].

Several studies have reported the advantages of NPs as delivery system for ITCs. Hossein *et al* reported that SFN-loaded monomethoxypoly (ethylene glycol)–poly (e-caprolactone) (mPEG–PCL) micelles with encapsulation efficiency of 86% and sustained release of SFN, caused increased cytotoxicity and apoptosis in the MCF-7 cell line compared to SFN[209]. From the same lab, a SFN-loaded PCL-PEG-PCL was also reported. The encapsulation efficiency was only 19% but the SFN loaded micelles increased the circulation period and the therapeutic efficacy of SFN *in vivo*[210]. A SFN-loaded gold-coated iron oxide NP (Fe3O4@Au) was studied as a potential delivery system to improve the efficiency and stability of SFN. FITC via thiolated polyethylene glycol was coated on the surface of the NPs to enable the evaluation of cellular delivery with fluorescence microscopy, in addition, folic acid was conjugated with the NPs to enhance the targeted delivery. An average of 2.8 mmol/g of SFN was loaded onto the surface of NPs. Compared to free SFN, these NPs increased apoptosis in the MCF-7 cells[211]. AITC-loaded poly-lactic-co-glycolic acid (PLGA) NPs provided protection against degradation and exhibited sustained release of AITC, leading to stronger toxicity in cancerous HeLa and MDA-MB-231 cells[212]. Another AITC nanoemulsion

was prepared by Li *et al*, yielding satisfactory aqueous solubility and chemical stability[213]. Lipid NPs were used as carriers for phenethyl isothiocyanate (PEITC) which enhanced the protection against cigarette smoke condensate induced DNA damage and the ability to activate protective apoptosis in bronchial epithelial cells both *in vitro* and *ex vivo*[214]. The liposomal formulation of cisplatin and PEITC showed enhanced toxicity toward human non-small cell lung cancer cells compared to when administered together free[215]. Overall, these studies indicate that nanotechnology has great potential for delivering phytochemicals such as ITCs as chemopreventive reagents.

1.3.2 Silicon quantum dots

Amongst the various types of nanomaterials, semiconductor NPs, also referred to as quantum dots (QDs), exhibit unique electronic and optical properties and can be developed as novel intravascular or cellular probes for both bio-imaging and therapeutic purposes.

QDs have optical properties such as tunable light emission wavelengths, intense fluorescence, resistance against photobleaching and simultaneous excitation of multiple colours, all of which give the advantages of QDs as luminescent labels in cell biology. Compared with conventional dyes the advantages of QDs include 1) narrow emission spectrum and broad excitation spectrum with the Stokes' shift effect providing more sensitivity and multiplicity of detection; 2) increased brightness, i.e. similar emission saturation and quantum yield with less variation of self-quenching; 3) increased photostability for 3D optical imaging[216,217]. Furthermore, QDs are considered to be energy donors, and the possibility for energy transfer between quantum dot particles and cell molecules has the potential to induce the generation of ROS and/or free radicals and to provoke apoptosis of the cells[218]. It has been speculated that the energy donor capacity of QDs could be utilized as novel photosensitizers or at least as potentiators of conventional photosensitizing drugs in photodynamic therapy of cancer[219,220]. Last but not least, QDs can provide novel functionality as a traceable and targeted drug delivery system by conjugation with drug molecules[221]. The size of such carriers (~10-20 nm in diameter) diminishes their renal clearance and uptake by the reticulo-endothelial system prolonging their blood circulation; The QD core can provide as a structural scaffold for loading of various types of drug molecules; by tuning their size and surface properties. Suitable pharmacokinetics can be achieved from either systemic administration or a targeted delivery; and the entirety can

be checked through the process of biodistribution and intracellular uptake via fluorescence[222].

Within the family of QDs, silicon QDs (SiQDs) have been preferred in biomedicine application because of their low inherent toxicity in comparison to all II-VI types of QDs which are heavy metal based (e.g., cadmium, lead, arsenic, etc.). The photoluminescence (PL) mechanism in SiQDs can be explained by quantum confinement effects[223] while their physiochemical properties largely depend on the surface reconstruction and termination[224]. Adding protecting groups onto the particle surface can not only prevent agglomeration, but also protect the particle from its surrounding environment, and provides multiple functionalization. The highest surface coverage can be achieved with hydrogen-capping (producing H-terminated SiQDs), however H-terminated SiQDs are photochemically unstable and prone to oxidation. Further functionalization usually involves the formation of stable covalent bonds between surface silicon atoms and carbon, nitrogen or oxygen species (Figure 1.10). For example, carbon-bonded species can be attached via hydrosilylation by exposing H-terminated SiQDs to terminal alkenes or alkynes (alkylation), long organic ligands such as 1-octene, 1-undecene and 1, 9-decadiene. This was reported to prevent aggregation of SiQDs and improve their stability leading to an enhanced PL efficiency[225]. Other water dispersible SiQDs have been produced by modifying the surface with amines, the resultant SiQDs exhibited strong blue PL with quantum yield about 22% and pH stability over a wide range (pH 4-14)[226].

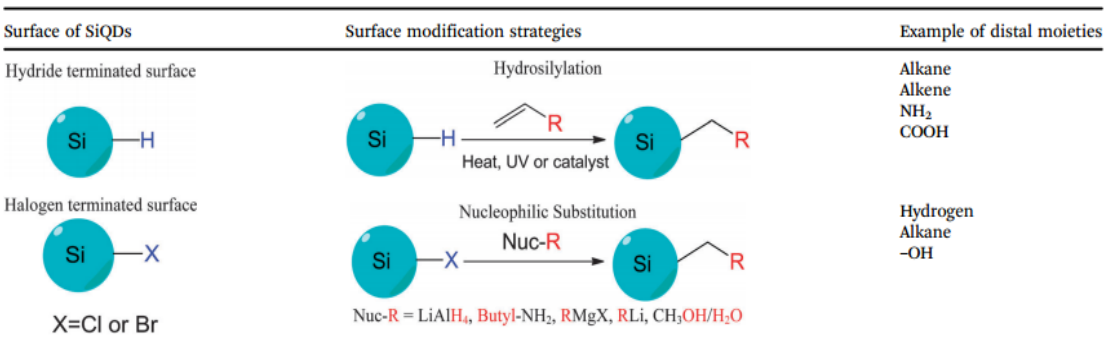

Figure 1.10 Schematic strategies of surface modification of SiQDs by forming covalent linkages[227].

Bio-application of SiQDs is a dynamically evolving field, various kinds of SiQDs have been used as optical labels for imaging and in drug delivery systems. Alkyl-capped SiQDs enhanced intracellular accumulation in malignant cells via cholesterol-dependent endocytosis[228]. Carbohydrate-capped SiQDs were reported with a selective internalization by

cancer cells than noncancerous cells[229]. Thiourea-capped SiQDs exhibited EGFR mediated targeting in cancer cells[230]. Wang *et al* reported a co-encapsulation system of quercetin and SiQDs in polymer NPs that achieved simultaneous *in vitro* imaging and improved the biocompatibility of quercetin[231]. However, SiQDs are much less well understood in terms of their fundamental photophysics than the particles made from direct gap semiconductors such as CdSe. Furthermore, the complete characterization of the surface remains a challenge, particularly when considering the incomplete coverage on silicon surfaces. For these reasons, there are few applications of SiQDs in biology at present, thus development of this technology is actively needed.

1.4 Aims of the study

SFN has been shown to possess chemopreventive activity against different cancers *in vitro* and *in vivo*. 15 clinical studies have been registered to investigate its anticancer effect (www.clinicaltrials.gov, accessed at 19/07/2017). The development of rational chemoprevention strategies requires deep understanding of the mechanisms of the agent. There is still on-going research regarding to the multimodal actions of SFN but based on the reviewed literature, little work has been done focusing on: 1) the selectivity of SFN between normal and cancer cells; 2) bioactivities of its metabolites; and 3) its role in tumour angiogenesis. The bioactivity of ITCs (and any other phytochemicals) can also be influenced by diverse pharmacokinetic parameters which leads to additional logistical problems regarding the application of an optimized delivery system.

To further study these research topics, the objectives of this research are twofold. Firstly, the bioactivity of SFN (and its metabolites) will be investigated in two liver cell lines: HHL5 and HepG2 representing human liver normal and cancer cells respectively. The effects of SFN on cell viability, DNA damage, apoptosis, intracellular ROS and GSH, cell motility and Nrf2 signalling will be determined as well as the protective effect of SFN against oxidative stress. The role of Nrf2 in SFN's bioactivities will be examined by siRNA silencing. *In vitro* cell models using human endothelial cells HUVECs as well as *ex vivo* and *in vivo* models will be used to investigate the anti-tumour and anti-angiogenic effect of SFN. Secondly, SiQDs will be explored as a delivery system for AITC. The biological activity of novel AITC-conjugated SiQDs (AITC-SiQDs) will be investigated in terms of their effects on cancer cell viability, DNA damage, migration and angiogenesis in comparison to AITC; and the cellular uptake will be monitored *via* the intrinsic fluorescence of SiQDs.

Chapter 2. Materials and Methods

2.1 Materials

2.1.1 Cell lines

The liver is responsible for major metabolic process within the human body, and remains a poorly characterised organ in cancer research despite of the fact that the hepatocellular carcinoma is the sixth most common malignancy and the third most common cause of mortality worldwide[232]. Relatively low therapeutic selectivity and high drug resistance are two major issues in liver cancer chemotherapy. It is also reported that liver is one of the target organs for NPs after they gain entry into the body through any of the possible routes[233,234]. Here two liver cell lines have been used: HHL5 and HepG2. HHL5, the immortalized human hepatocyte-derived line 5, was provided by Professor Arvind Patel, Medical Research Council Virology Unit, UK[235]. HepG2 cell line, human Caucasian hepatocyte carcinoma cells taken from a primary hepatoblastoma, was obtained from American Type Culture (ATCC, Manassas, USA).

Other cell lines used include human umbilical vein endothelial cells (HUVECs) and murine MII perivascular cells (M2) which were obtained from TCS Cellworks and provided by Dr Zhigang Zhou[236] respectively. The Caco-2 cell line was established from a moderately well-differentiated colorectal adenocarcinoma obtained from a 72-year-old patient[237]. It could differentiate spontaneously when reaching confluence and express enterocyte-like phenotype and enzyme activities[238]. Here studies were carried out in the undifferentiated cancer colonic phenotype of Caco-2 cells only.

2.1.2 Reagents

SFN was purchased from Toronto Research Chemicals. AITC, 3-(4,5-Dimethyilthiazol-2-yl)-2,5-diphenyltetrayolium bromide (MTT), dimethyl sulfoxide (DMSO), DL-Buthionine sulfoximine (BSO), N-acetyl-L-cysteine (NAC) and Bradford reagent were all purchased from Sigma-Aldrich. Complete protease inhibitors were obtained from Roche Applied Science. All other reagents used see Method section 2.2.

SiQDs were provide by Dr Chao's lab. AITC-SiQDs were synthesized and characterized as reported in Mehrnaz Behray's PhD Thesis (100025408). Thermal Gravimetric Analysis estimated the quantity of ligands on the surface of SiQDs as 60% (w/w). Hence, in average 5.88 mmol/g of AITC was loaded onto the surface of SiQDs. Based on this, working concentration of AITC-SiQDs was calculated as below to compare with AITC.

Table 1. Concentrations of NPs compared to AITC

AITC (μM)	2.5	5	10	20	40	80	160	320
AITC-SiQDs (μg/ml)	0.41	0.83	1.7	3.3	6.6	13.2	26.4	52.8

2.2 Methods

2.2.1 Cell culture

HHL5, HepG2, Caco-2 and M2 cells were cultured in Dulbecco's Modified Eagle's Medium (DMEM, Gibco) containing 4.5 g/L D-glucose and Non-Essential Amino Acids, supplemented with 10% heat-inactivated foetal bovine serum (FBS, Invitrogen), 1% L-glutamine (200 mM, Gibco), penicillin (100 U/ml) and streptomycin (100 mg/ml) at 37°C, 5% (v/v) CO_2. HUVECs were cultured in Endothelial Cell Growth Medium 2 (EGM-2, PromoCell) supplemented with penicillin (100 U/ml) and streptomycin (100 mg/ml) at 37°C, 5% (v/v) CO_2.

HUVECs were used between the fifth and ninth passages and M2 were used between passages 35 and 40 for all experiments. For these two cell lines, cells were grown in flasks coated with 10 µg/ml type-I collagen.

For subculture, cells were usually grown in T75 flasks (10 ml medium) incubated at 37°C, 5% CO_2 and cell culture medium were changed every 2-3 days. Subculture was carried out according to the standard operating procedures (SOPs) in a Class II Biological Safety Cabinet when cells reached 80% confluence. Prior to subculture, cells were checked for ideal confluency, morphology and any signs of contamination. Medium was aspirated from the tissue culture flasks and the cell layer was washed with phosphate buffered saline (PBS) twice. Then 1 ml of trypsin-EDTA (0.05%) was added for 5-10 mins at 37°C, 5% CO_2 until the cells were detached from the base of the flask. Trypsin was neutralized with 9 ml of culture medium and a cell suspension formed through several pipetting cycles. Cells were counted using a hemocytometer. The cell suspension was centrifuged for 5 mins at 200 g to form a cell-pellet, which was then re-suspended in an appropriate volume of culture medium and either transferred to a new flask (passaged) or seeded on desired plates for experiments.

For cryopreservation, cells were freeze at as low as a passage number as possible, with cell viability ≥ 90%. Cells were harvested, spin down and resuspended in freezing medium (10% DMSO in FBS) at a concentration of 1×10^6 to 5×10^6 viable cells/ml. Cells were then transferred to cryopreservation vials in 1-1.5 mL aliquots, labelled with cell line name, passage number, number of cells, user name and date. Vials were then put into a controlled-rate freezing chambers (Nalgene® Mr. Frosty, Sigma-Aldrich) at -80°C for at least 24 hours and kept in liquid nitrogen for long term storage.

2.2.2 Cytotoxicity and cell survival assays

2.2.2.1 MTT assay

The viability of cells was evaluated by MTT assay. In most viable cells, the mitochondrial activity is constant and thereby an increase or decrease in the number of viable cells is linearly related to mitochondrial activity, this is the principle behind the MTT assay. This colorimetric assay based on the conversion of MTT, a water-soluble tetrazolium salt to an insoluble purple formazan by cleavage of the tetrazolium ring by succinate dehydrogenase within the mitochondria. After solubilisation with an organic solvent such as DMSO, the formazan is measured spectrophotometrically. As the reduction of MTT can only happen in the metabolically active cells, this assay is an indicator of the viability of the cells under certain treatments.

For this assay, 5 mg/ml MTT is dissolved in sterile PBS, filtered with 0.22 µm single used filter unit and stored at 4°C avoiding light up to 3 months. Cells were seeded into 96-well plates and allowed to grow to approximately 70% confluency. The outer wells were susceptible to evaporation so filled with PBS only. Different treatments were then added to the cells, minimum 4 replications applied to each treatment with medium only as the blank and negative/vehicle/ positive control if applied. After treatment, media were removed, 100 µl of 0.5 mg/ml MTT solution in medium was added to each well and incubated in the dark at 37°C for 1 hour. Then 100 µl DMSO was added to each well and mixed thoroughly by pipetting. The absorbance was determined using the OMEG plate reader using 570 nm as the test wavelength and 670 nm as the background. Cell viability (%) was determined as [A570nm-A670nm (test)] / [A570nm-A670nm (control)] × 100%; the half-maximal inhibitory concentration (IC_{50}) were calculated with CalcuSyn software Version 2.0 (Biosoft, Cambridge, UK).

2.2.2.2 Alkaline comet assay

The comet assay or single cell gel electrophoresis assay is a rapid, sensitive and relatively simple method for detecting DNA strand breaks in eukaryotic cells. It is based on the ability of negatively charged loops/fragments of DNA to be drawn through an agarose gel in response to an electric field. The extent of DNA migration depends directly on the DNA damage present in the cells.

Cells were seeded on 24-well plates and allowed to grow to approximately 70% confluency, then placed in experimental conditions. Cells were then harvested and resuspended in PBS containing 10% DMSO and frozen at -80°C until the alkaline comet assay was performed. Samples were defrosted and 20-25,000 cells per sample were centrifuged at 108 g for 5 mins at 4°C. Pellets were resuspended in 0.6% low melting point agarose, dispensed in duplicate onto glass microscope slides (precoated in 1% normal melting point agarose), and allowed to set on ice under a glass coverslip. Once set, the coverslips were removed, and slides transferred into ice-cold lysis buffer (100 mM disodium EDTA 2.5 M NaCl, 10 mM Tris-HCl pH 10.0 with 1% Triton X-100 added immediately before use) for 1 hour. Slides were washed twice with ice-cold dH2O for 10 mins, transferred to a flatbed electrophoresis tank, and incubated in freshly prepared ice-cold electrophoresis buffer (300 mM NaOH 1 mM disodium EDTA, pH 13) for 30 mins, followed by electrophoresis in the same buffer at 21 V (1 V/cm) for 30 mins. Procedures were performed protected from direct light. Slides were drained of electrophoresis buffer and flooded with neutralization buffer (0.4 M Tris-HCl, pH 7.5) for 30 mins, washed twice in dH_2O for 10 mins, and dried at 37°C. Slides were stained with SYBR Green I nucleic acid stain diluted from a 10,000 X stock with 1X TE buffer (10 mM Tris-HCl, 1 mM EDTA) for 5 mins protected from light and dried at room temperature (RT) before visualization. For each sample, 100-200 comets were randomly analysed with images captured by fluorescence microscopy (Axioplan 2; Zeiss, Cambridge, UK) and scored using Comet Assay IV Lite analysis software (Perceptive Instruments, Bury St Edmunds, UK). DNA damage was expressed as tail intensity (% DNA in the comet tail) for statistical analysis because it has a linear relationship to DNA break frequency, is relatively unaffected by threshold settings and yields the widest possible range (i.e., 0%–100%)[239].

2.2.2.3 Annexin V/PI apoptosis assay

Annexin V/ propidium iodide (PI) double staining is a commonly used tool for studying apoptotic cells. During initiation of apoptosis, cells translocate the membrane phosphatidylserine (PS) from the inner side of the plasma membrane to the cell surface, which can be easily stained by a fluorescein isothiocyanate (FITC) conjugated Annexin V, a Ca^{2+}-dependent phospholipid-binding protein that has a high affinity for PS. PI does not stain live or early apoptotic cells due to the presence of an intact plasma membrane, while in late apoptotic and necrotic cells, PI passes through plasma and nucleus membrane and display red fluorescence. Therefore, cells that are considered viable are both Annexin V and PI

negative, while cells that are in early apoptosis are Annexin V positive and PI negative, and cells that are in late apoptosis or already dead are both Annexin V and PI positive.

HepG2 cells were seeded on 12-well plates at a density of 5×10^4 cells per well and incubated at 37°C for 48 hours. After treatment with 0, 1.25, 2.5, 5, 10, 20 µM SFN for 24 hours, cells were exposed to 700 µM hydrogen peroxide (H_2O_2) for another 24 hours. Medium and PBS used to wash the cell layer were then collected, cells were trypsinased and added to the collection. After centrifugation at 200 g for 5 min at 4°C, the formed pellets were washed with cold PBS before being re-suspended in 800 µl 1x binding buffer at a density of $1x10^5$/ml. 1x binding buffer was diluted from 10x binding buffer [0.1 M HEPES/NaOH (pH 7.4), 1.4 M NaCl, 25 mM $CaCl_2$] with MillQ-water (MQW). 5 µl Annexin V-FITC was used to label the apoptotic cells and 5 µl PI used to stain the necrotic cells. All reagent used were provided from AnnexinV-FITC Apoptosis Detection Kit (eBioscience). After incubation at RT for 20 mins in the dark, samples were run on a flow cytometer (Cube 6, Sysmex Partec, Germany). For each sample 10,000 events were collected, and the data were analysed using FlowJo software (Treestar Inc., USA). The gated cells were then filtered by FL1 on the X-axis and FL3 on the Y-axis on a new scatter plot, which then be divided into 4 squares showing the different stages between healthy (AnnexinV-/PI-), early apoptotic (AV+/PI-), late apoptotic (AV+/PI+), and necrotic (AV-/PI+) cells. Results were expressed as % of cells.

2.2.2.4 Colony formation assay

Clonogenic cell survival was first described in 1950s for the study of radiation effects. a cell that capable to divide and proliferate to produce a colony of cells is referred to as 'clonogenic'[240]. The loss of this ability is a basic function of radiation or chemotherapy agents. Therefore, this method has been used to examine the effects of various agents with potential applications in cancer treatment.

HepG2 cells were seeded in 6-well plates at a density of $2 X 10^5$ cell/ml and incubated for 24 hours. Then cells were treated with 0, 1.25, 5, 20 µM SFN for another 24 hours with DMSO (0.1%) as control. After that, cells were typsinized to make single-cell suspensions from the treated monolayer cultures, and seeded in new 6-well plates at 2000 cell/well in triplicate for each treatment group. Cells were maintained for at least 14 days to form colonies. The media were replaced every 3 days. Then colonies were fixed with ice-cold methanol and stained with 0.1% crystal violet for 30 mins. For quantitative analysis, 1 ml 33%

acetic acid were added to each well, then the plates were shaken for 1 hour. The absorbance at 560 nm of each well was measured in the microplate reader (BMG Labtech Ltd, UK). Colony formation % = (A560 test / A560 control) x100%. Results are given as means and standard deviations of three independent experiments with triplicate samples for every treatment condition.

2.2.3 Measurement of intracellular ROS

The production of intracellular ROS was measured using the chloromethyl derivative of the fluorescent probe 2',7'-dichlorodihydrofluorescein diacetate (CM-H2DCFDA) (Invitrogen). H2DCFDA diffuses through the cell membrane and is enzymatically hydrolysed by intracellular esterases to form the non-fluorescent compound 2',7'-dichlorofluorescein (DCFH), which is then rapidly oxidized to form the highly fluorescent 2',7'-dichlorofluorescin (DCF) in the presence of ROS. The DCF fluorescence intensity is believed to be parallel to the extent of ROS formed intracellularly. CM-H2DCFDA provides much better retention in live cells than H2DCFDA.

To evaluate SFN induced ROS changes, cells (2×10^4/well) were seeded on 96-well plates and left attached overnight. Different doses of SFN treatment were then added for 24 hours. Cells were then washed with PBS and incubated with 5 μM DCFH-DA for 30 mins at 37°C. Fluorescence was measured on the Omega microplate reader (BMG Labtech) with excitation/emission wavelengths as 485 nm/520 nm.

To evaluate AITC-SiQDs induced ROS changes, cells were seeded in 6-well plates and treated when they reached 70% confluence with 20 μM AITC or AITC-SiQDs for 1, 3, 6, 12 and 24 hours. The wells were then washed with PBS and incubated with 5 μM CM-H2DCFDA for 30 mins at 37°C. Subsequently, the cells were collected, centrifuged and re-suspended in 0.8 ml PBS. The fluorescent intensity of the oxidized product DCF was detected in the FL1-A channel with a flow cytometer (Cube 6, Sysmex Partec, Germany).

2.2.4 HPLC analysis of intracellular GSH

GSH is the most abundant non-enzymatic antioxidant molecule in the cell and is essential for redox regulation[241]. It maintains predominantly in its reduced form by the cytosolic enzyme, glutathione reductase, and can be rapid oxidized to glutathione disulfide (GSSG). In order to obtain a true measurement of the amount of reduced GSH in living cells, GSH was derivatized

using monobromobimane (mBBr)[242], weakly fluorescent reagent that can freely cross the cell membrane (Figure 2.1). The procedure was performed as described[178].

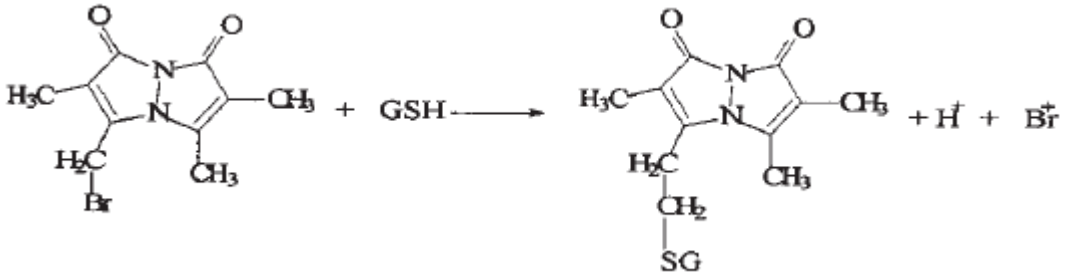

Figure 2.1 Reaction of mBBr with GSH[242].

Approximately 1×10^6 cells were collected from 6-well plates, washed twice in PBS and suspended in 75 µl PBS containing 5 mM diethylenetriaminepentaacetic acid. The suspensions were acidified by addition of 300 µl 50 mM methanesulfonic acid (MSA), and then subjected to three freeze-thaw cycles alternating between dry ices and a 37°C heat block for 6 mins each time and vortex 10 seconds at the highest setting. GSH-containing supernatants were obtained after centrifugation at 12,000 g for 10 mins and maintained in ice for protein quantifications by Bradford assay. GSH standards (0, 1.25, 5, 10, 20 µg/ml) were prepared from 1 mg/ml GSH stocking solution. All samples except the blank were prepared in triplicates.

For GSH derivatization, a 25 µl premix buffer (10 µl 0.5 M HEPES, pH 8.0, 1 µl 0.5 M EDTA, 1.5 µl 1M NaOH, 2 µl 0.1M mBBr and 10.5 µl 100% acetonitrile) was added to 75 µl cell extracts. The reaction was immediately vortexed and incubated for 15 mins in the dark at RT. After acidification with 1 µl 5 M MSA, the samples were vortexed and centrifuged at 12,000 g for 5 mins. The supernatants were diluted in 10 mM MSA if necessary and analysed by HPLC.

The GSH-mBBr adduct was then measured by high-performance liquid chromatography (HPLC) with a fluorescence detection. HPLC was run on a HiChrom ACE-AR C18 4.6 × 250 mm, 5 µm column (Phenomenex) with Solvent A (0.25%, v/v acetic acid and 10% methanol, pH 4). Samples were eluted with a gradient of Solvent B (90% methanol) at 1.0 ml/min flow rate as follow: 0-10 mins 0% Solvent B; 10-11 mins 50 % Solvent B; 11-15 mins 100% Solvent B; 16-20 mins 0% Solvent B. Detection was carried out with a Jasco fluorescence detector with excitation at 385 nm and emission at 460 nm. The gain of GSH-

mBBr adduct eluted at 8.9 mins and was quantified by the standard curve. The level of GSH was expressed as nmol/mg of cellular soluble protein.

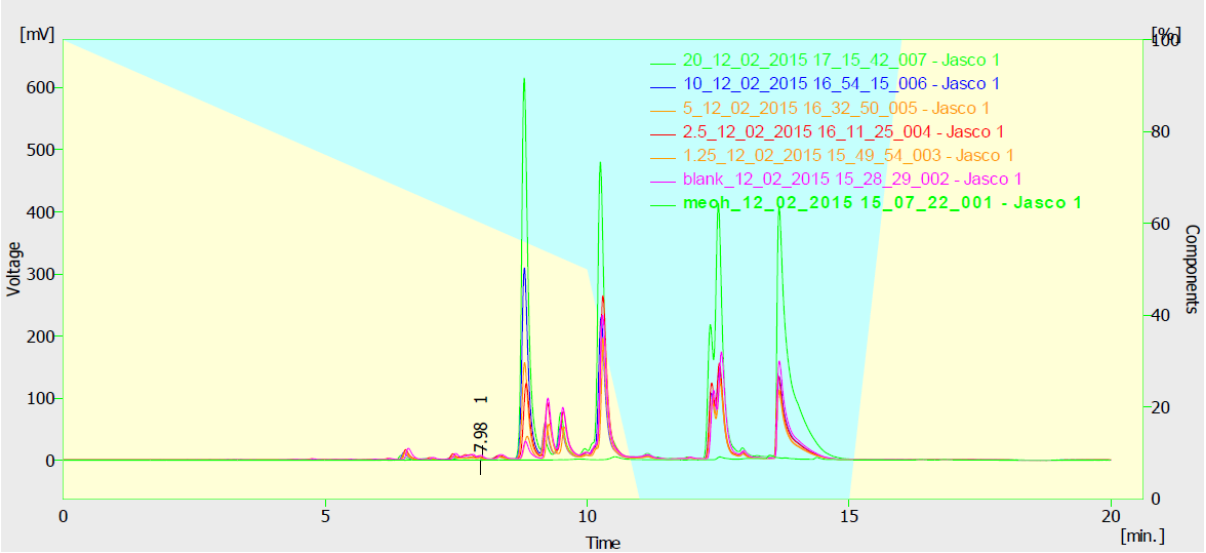

Figure 2.2 Chromatogram of the standards used for the determination of the standard curve.

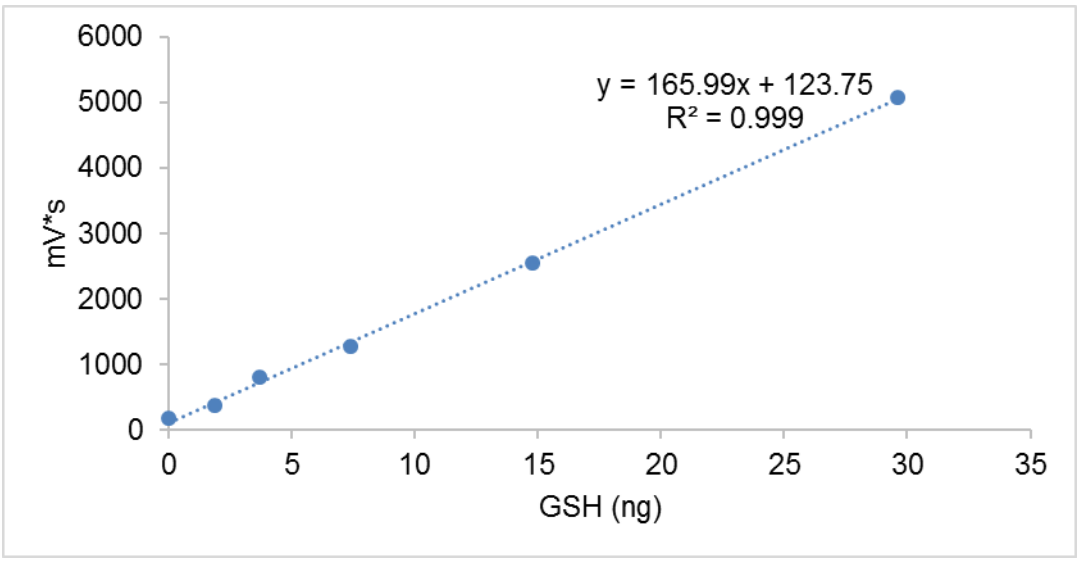

Figure 2.3 Standard curve of GSH.

2.2.5 Cell migration and adhesion assays

2.2.5.1 Wound assay

The wound assay, or gap closure migration assay, is an easy, low-cost and well-developed method to measure cell migration *in vitro*. The basic steps involve creating a wound/gap in a cell monolayer and capturing the images of the wound closure to provide migration characteristics of the cultured cells.

HepG2/Caco-2 cells were seeded in 24-well plates at 2×10^5 cells/ml. After cells reached 100% confluence, scratches were made with a 1 ml pipette tip across the center of the wells in a long-axial line to create a gap, without changing the medium. Detached cells were removed by gently washing twice with medium. The wells were then filled with fresh medium containing different treatments and vehicle control. Each treatment was performed at least in triplicate. Cells were grown for a further 48 hours, then washed twice with PBS, fixed with ice-cold methanol for 10 mins, and stained with 1% crystal violet for 30 mins. At least 3 pictures were taken within each well of the stained monolayer on an inverted microscope at 5x magnification. The wound area was quantitatively evaluated using ImageJ[243], at least 10 pictures were used in each treatment. Cell migration was calculated as follows: Migration % = 1- (Area W-Area C)/Area C %, where Area W is the wound area from treated wells and Area C is the wound area from the control wells.

For HUVECs, wound was created as above. The wells were then filled with fresh medium with different dose of SFN or conditioned medium (CM) from HepG2. Cells were grown for a further 12 hours as HUVECs under vehicle control (0.1% DMSO) reformed a confluent monolayer within 24 hours. Cells were then fixed and stained as above. CM was prepared by seeding HepG2 cells into 10 cm dishes with 10 ml complete culture medium and when at 80% confluence cells were washed with PBS and incubated with serum-free medium and SFN (0-20 μM) for another 24 hours. CM was collected from each dish and filter sterilized (0.2 μm, Minisart), then stored at −80°C for further experiments where serum-free medium was used as a negative control.

2.2.5.2 Cell adhesion assay

Cell adhesion, the ability of a cell to stick to another cell or ECM, plays an important role in cell communication and regulation including cell differentiation, migration and survival. It is mediated by adhesion molecules such as cadherins, integrins, selectins, immunoglobulins, glycoproteins and proteoglycans[244]. Tumor cells, especially the highly metastatic types,

usually obtain enhanced adhesion ability to facilitate the migration and adhesion to a new site to establish new tumors. Therefore, cell adhesion assay is used to evaluate the metastatic ability of cancer cells under certain treatment.

For cell-matrix adhesion assay, 96-well plate was coated with 50 µL of 10 ug/ml fibronectin (R&D Systems, MN, USA) or rat tail collagen I (Merck KGaA, Germany) or poly-l-lysine (PLL, Sigma) overnight at 4°C, and blocking with 1% bovine serum albumin (BSA; Thermo Scientific) for 1 hour at RT. HepG2 cells were seeded on the coated plate at a density of 5×10^4 cells/well in serum-free medium with treatment (12 replicates for each treatment) and incubated under normal growth condition for 1.5 hours. Unattached cells were removed by three times PBS washes. 50 µL of 4% paraformaldehyde (PFA) was added to each well for 10 mins at RT to fix the adherent cells. Plate was then washed with PBS again and stained with methylene blue immediately for 30 mins. The wells were then washed with dH2O to remove excess stain. To quantify the amount of adherent cells, 100 µL de-staining buffer (50% ethanol in 0.1 M HCl) were added to each well for 10 mins, and the absorbance was measured at 630 nm. Cell adhesion (%) was determined as [A630nm (test)] / [A630nm (control)] × 100%. Three independent assays were conducted per experimental design.

Adhesion between tumour cells and ECs was measured as described with modifications[245]. HepG2 were seeded in 96-well plates to 100% confluence then treated with 0-20 µM SFN for 24 hours. HUVECs was seeded on the HepG2-coated plate at a density of 5×10^4 cells/well in serum-free medium (12 replicates for each treatment). The plate was then incubated under normal growth condition for 1.5 hours, after which unattached cells were washed three times with PBS. 50 µl of 4% PFA was added to each well for 10 mins to fix the adherent cells. An in cell Western blotting for CD31 was then performed to measure the amount of adherent ECs. Briefly, cells were permeabilised by 0.5% Nonidet P40 lysis buffer (NP40) in PBS for 10 mins at RT, followed by PBS wash. Wells were blocked with Odyssey® blocking buffer for 10 mins at RT then 1:500 primary antibody CD31 in blocking buffer was added to each well (50 µl) for 1 hour at RT in humidified chamber, after PBST (0.1% Tween 20 in PBS) wash, 1:800 secondary antibody goat anti-mouse (IRDye® 800CW, LI-COR) in blocking buffer was added to each well (50 µl) for another 1 hour at RT in humidified chamber. Plates were protected from light from this point. After washing with PBST, plates were turn upside down to remove traces of wash buffer and scanned immediately using Odyssey® infrared imaging system (169 µm resolution, 3.0 mm focus offset). Background wells were incubated with secondary antibody but no primary antibody. Results were expressed as CD31

signal intensity (% of control). Three independent assays were conducted per experimental design.

2.2.6 Nrf2 siRNA knockdown

Nrf2 siRNA was obtained from Applied Biosystems (Sense strand: 5'-CCUUAUAUCUCGAAGUUUUtt-3'; antisense strand: 5'-AAAACUUCGAGAUAAGGtg-3'). AllStars negative control siRNA (Qiagen) has no homology to any known mammalian gene and was used to confirm the changes in phenotype or gene expression are non-specific. Transfection of siRNA was performed using HiPerFect transfection reagent (Qiagen) according to manufacturer's protocol.

For comet assay and wound assay, fast-forward transfection of adherent cells in 24-well plates was used. HepG2 cells were seeded at 0.5-1.5 x 10^5 cells/well of a 24-well plate in 0.5 ml of complete medium, and incubated under normal growth conditions shortly before transfection. 30 nM siRNA and 3 µl of HiPerFect transfection reagent were added to 100 µl culture medium without serum or antibiotics, mixed and incubated for 5-10 mins at RT to allow the formation of transfection complexes. The complexes were then added drop-wise to each well to give a final siRNA concentration of 5 nM. Plate were gently swirled to ensure uniform distribution of the transfection complexes. Cell were cultured under normal growth conditions for additional 24 hours. The comet assay/ wound assays were then performed as described.

For MTT assay, reverse transfection of adherent cells in 96-well plates was used as it is quicker, requires less pipetting and fewer materials. 12.5 ng siRNA was spotted in 25 µl of RNase-free water into each well (40 nM) of a 96-well plate. A mix of 0.75 µl of HiPerFect transfection reagent and 24.25 µl of culture medium without serum or antibiotics was then added to each well. The plate was incubated for 5-10 mins at RT to allow the formation of transfection complexes. HepG2 cells were then seeded at a density of 1 x 10^4 cells/well in 150 µl of culture medium on top of the transfection complexes. In each well, the final siRNA concentration was 5 nM. Cell were cultured under normal growth conditions for additional 24 hours. The MTT assay were then performed as described.

2.2.7 Western blotting

2.2.7.1 Protein extraction and quantification

For whole protein extraction, cell monolayers were washed twice with ice-cold PBS and lysed with a 6:1 mixture of NP40: proteinase inhibitor for 30 mins incubation at 4°C under gently agitation. NP40 lysis buffer, a non-denaturing detergent, was made as Tris-EDTA pH8 (2mM), NaCl (150mM), Glycerol (10% v/v) and NP40 (1% v/v); protease inhibitor solution was prepared by dissolving one complete protease inhibitor mini tablet [EDTA-free] in 1.5 ml of MQW. Cell lysates were further dislocated from the plates using sterile rubber cell scrapers followed by centrifugation at 13 600 g at 4°C for 15 min. Protein-containing supernatants were then transferred to pre-cold fresh tubes and stored at -80°C until used.

The Nuclear Extract Kit (Active Motif) was used to isolates nuclear and cytoplasmic extract from cell samples according to manufacturer's instructions. Briefly, cells were washed with ice-cold PBS with phosphatase inhibitors prior incubated with 1x hypotonic buffer at 4°C for 30 mins under gently agitation, to swell the cell membrane. Then cells were dislocated from the plates using cell scrapers and transferred to pre-cold Eppendorf tubes. Detergent was added to each tube to causes a leakage of the cytoplasmatic proteins into the supernatant. After vortexed for 10 seconds and centrifuged at 4°C, 14,000 g for 1.5 mins, the supernatant was collected as cytoplasmic fraction. The pellet was resuspended in complete lysis buffer, vortex and incubated at 4°C for another 30 mins. After vortexed for 10 seconds and centrifuged at 4°C, 14,000 g for 10 mins, the supernatant was collected as nuclear fraction. Samples were stored at -80°C until used.

The Bradford assay was used to determine concentrations of protein based on the colorimetric convert from the binding of Coomassie Brilliant Blue G-250 dye to protein. A range of protein standards (0, 0.25, 0.5, 1, 1.4 and 2 mg/ml) was obtained by dilution of BSA in MQW. A constant volume (5 µl) of protein standard or cell lysate samples was introduced into separate wells of a 96 well plate. If necessary, lysate samples could be diluted with MQW. All samples were tested in triplicates. Each well received 250 µl of Bradford reagents (50:1 v/v Bradford reagent: protein samples). The optical densities were measured at 595 nm using the Omega microplate reader (BMG Labtech). Using the standard curve and the linear regression formula, the protein concentrations from the samples could be calculated by the Omega Analysis Data Software. Proteins concentration in each sample was expressed in mg/ml of total solution and average protein concentration was used to calculate the loading volume for Western blot.

2.2.7.2 SDS-PAGE

Sodium dodecyl sulfate polyacrylamide gel electrophoresis (SDS-PAGE) was used to separate protein samples based on their electrophoretic mobility. SDS, an anionic detergent, binds to protein in a set ratio, approximately one molecule of SDS for every 2 amino acids. By doing so, SDS denatured protein, turning them into negatively charged linear poly peptide chains. Under the electric field, those negatively charged proteins migrated across the gel towards the positive electrode, and separated based on the difference of their mobility, which based on the difference of their molecular weight.

Loading samples were prepared with 4x loading buffer (NuPage LDS sample buffer; Invitrogen), 1M dithiothreitol (DTT, Sigma Aldrich) and known concentration of protein sample, to obtain final volume of 25% loading buffer, 5% DTT and 70% protein. After denatured at 98°C for 5 mins, the loading sample were loading in equivalent amounts of protein (20-40 µg) to the gel together with a molecular weight marker. 10-12% acrylamide gel were used as the resolving gel and 4% as the stocking gel. The gels were placed in a MINI Protean Tank (Bio Rad) according to manufacturer's instructions. The electrophoresis was run at 4°C, 200 V in 1x running buffer which diluted down from 10x running buffer (Bio Rad).

2.2.7.3 Protein transfer, immunoblotting and detection

The semi-dry transfer was applied using the Trans-Blot SD Semi-Dry Transfer Cell (Bio Rad) with the transfer buffer made up of 10% 10 x transfer buffer (Bio Rad), 20% methanol (Sigma Aldrich) and 70% MQW. 15-25 voltage was applied between 30 mins to 90 mins for different targets. Polyvinylidene fluoride membrane (PVDF, Millipore) was activated in methanol for 10 seconds before use. Two types of PVDF were used: Immobilon®-P membrane (0.45 µm) for chemiluminescent detection, and Immobilon®-FL membrane (0.45 µm) for fluorescence-based immunodetection by Odyssey® Infrared Imaging System (Li-COR, Cambridge UK).

For chemiluminescent detection, the membrane was blocked for 1 hour at RT with 5% w/v non-fat milk in 0.1% PBST, followed by incubation with diluted primary antibody (see Table 2) in blocking solution at 4°C overnight. Membrane was then washed 3 times with 0.1% PBST at 5-10 mins intervals with fast agitation and incubated with 1:10000 dilution of horseradish peroxidase (HRP)-conjugated secondary antibody with blocking solution for 1 hour at RT. After further washing, the membrane was developed with Amersham ECL Prime Detection kit (GE health) and visualised using a Fluor Chem Imager (Alpha Innotech). Band

intensity was determined with ImageJ. Results were normalised against loading control (β-actin for whole lysate protein and SAM68 for nuclear protein), and the protein expression from the different treatments was calculated relative to the control.

For fluorescent detection, the membrane was blocked for 1 hour at RT with the commercially supplied Odyssey® blocking buffer. The primary antibodies were prepared in recommended dilutions (Table 2) in the blocking buffer. IR-labelled secondary antibodies were used for detection: 800 nm channel with IRDye® 800CW and 700 nm channel with IRDye® 680LT, SDS was added to reach a final concentration of 0.02% to reduce the background of 700 nm channel. After washes, the imaging was proceed using LI-COR Odyssey Infrared Imaging System and analysed using the Odyssey® software, the intensity measured for each band should be within 10-200.

If stripping was required, blots were incubated with stripping buffer (Themo) for 15 mins at RT, then washed with 0.1% PBST and imaged to check any left signals. Then the membrane was re-blocked as before, prior to primary antibody probing.

Table 2. Primary antibodies used for Western blot.

Target/Antigen	Host	Dilution	Size	Supplier	Catalog No.
β-actin	Goat	1:5000	42 KDa	Santa Cruz	Sc-1615
HIF-1α	Rabbit	1:1000	120 KDa	Abcam	Ab2185
HO-1	Mouse	1:2000	30 KDa	Abcam	Ab13248
Ku70	Goat	1:5000	70 KDa	Santa Cruz	Sc-1486
Nrf2	Rabbit	1:2000	100 KDa	Santa Cruz	Sc-13032
SAM68	Rabbit	1:10000	68 KDa	Santa Cruz	Sc-333
STAT3	Mouse	1:2000	91/86 KDa	Santa Cruz	Sc-8019
p-STAT3	Mouse	1: 2000	91/86 KDa	Santa Cruz	Sc-8059
TrxR-1	Rabbit	1:2000	55 KDa	Abcam	Ab16840
VEGFA	Rabbit	1: 2000	15-40 KDa	Abcam	Ab46154

2.2.8 3D co-culture of HUVEC with pericytes/HepG2

Pericytes, defined by their close contacts with ECs, contribute to the stability of the endothelial tube, regulate hemodynamic processes and promote the survival of ECs. The three-dimensional co-culture of ECs and isolated murine pericyte-like cells offers a platform to study angiogenic processes not only the activation of ECs but also the recruitment of mural cells[236,246], which is essential for the formation and function of mature vascular network.

To expand beyond the limits of the pre-existing vascular supply, tumours recruit new blood vessels from surrounding vessels, an event known as the 'switch' to the angiogenic phenotype[247]. Numerous studies hypothesize that *in vivo* tumour-associated ECs receive biological signals from tumour cells, and subsequently induce tumour angiogenesis. Thus, co-culture HUVECs with HepG2 was used to study the effect of HepG2 cells on HUVECs behaviour.

2.2.8.1 3D culture in collagen I gels

Cells were trypsinized, washed with PBS, counted, and desired cell numbers were collected by centrifugation (2.5 x 10^5 HUVECs, 5 x 10^5 M2 or HepG2 cells per well). Collagen type I gels (2 mg/ml) were prepared in 1 × DMEM medium from concentrated rat tail type I collagen solution (>8 mg/ml in 0.02 N acetic acid; BD Bioscience) at 4°C, supplemented with final concentrations of 2% FBS, 22.5 mM $NaHCO_3$, 1 mM sodium pyruvate, 10 ng/ml VEGF and PDGF, 250 µg/ml ascorbic acid phosphate (ASAP) and neutralized by 0.1 M NaOH. Cells were suspended in the collagen I gel solution at 4°C and added into 24-well plates at 400 µl per well. After initial incubation in 37°C for 20 min, 400 µl EGM-2 culture medium was added to solidified collagen I gels with supplements of final concentrations of VEGF, PDGF, and ASAP as above, with treatment as experiment design. Medium was changed every 48 hours, and cultures were maintained for 4–6 days.

2.2.8.2 Whole-Mount Immunohistochemistry

3D collagen culture gels were washed in PBS, fixed with 20% DMSO in methanol overnight at 4°C, rehydrated in 50% methanol in PBS, 20% methanol in PBS and PBST for 1 hour each at RT. Gels were then incubated with blocking solution (10% FBS in PBS) overnight at 4°C. Primary antibody anti-human CD31 (Catalog No. 555444, BD Biosciences) were diluted in blocking buffer as 1:400 and incubated on top of the gels overnight at 4°C. After 5 times PBST

washes (1 hour each at RT), fluorescently labelled secondary antibody donkey anti-mouse conjugated with Cy3 (Jackson Immuno Research, 1: 500) were incubated in blocking buffer overnight at 4°C. After 3 times PBST washes (1 hour each at RT), gels were stained with DAPI (1:500) for 0.5 hour at RT, washed again and mounted in Gelvatol. Samples were examined by fluorescence microscopy (Axioplan2, Carl Zeiss). In five random fields from each sample, the total lengths of CD31-positive tube-like structures were measured by Volocity 4.0 (Improvision). Cumulative tube lengths per area are expressed as mm/mm^2.

2.2.9 Aortic ring assay

The quantitative three-dimensional *ex vivo* mouse aortic ring angiogenesis assays provides a more physiologically relevant *in vitro* model for angiogenesis study, in which developing microvessels undergo many key features of angiogenesis over a timescale similar to that observed *in vivo*.

This assay was performed per Baker and Robinson protocol[248]. Thoracic aortae are dissected from mixed background mice of 8–12 weeks of age, then cleaned and cut into rings with approximately 0.5 mm width. At least 20 rings from more than three separate aortae should be used per condition. Rings are starved in serum-free media (Opti-MEM®) at 37°C overnight to equilibrate their growth factor responses, effectively creating a uniform baseline state. Each ring was then embedded in separate wells of a 96 well plate containing 1.2 mg/ml of collagen I (50 µl/well, Millipore), which was polymerised by 5 N NaOH and leaving the plate at 37°C for 30 mins. Each ring was fed with 150 µl of fresh Opti-MEM supplemented with 2.5% FBS, 30 ng/ml VEGF and different concentration of SFN at 37°C every 3 days.

After 6 days, rings were fixed with 4% (v/v) formalin for 30 mins at RT, and the microvessel growth of each ring were counted by live phase-contrast microscopy. Immunofluorescence staining was then performed for a more informative view of microvessel sprouting, including the identification of supporting cells. Rings were permeabilised with 0.25% (v/v) Triton X-100 in PBS for 15 mins at RT twice, and blocked with 2% (v/v) BSA in PBLEC for 30 min at 37°C. 0.1 mg/ml FITC-conjugated BS-1 lectin (L2895, Sigma) were used to stain ECs and 1:1000 anti-actin α-smooth muscle Cy3 (Catalog No. 53142, Santa Cruz) were used to stain the supporting cells. 1 µg/ml DAPI were used to stain the nuclei. Images were taken by Axiovert 40 CFL inverted microscope (Carl Zeiss).

2.2.10 HepG2-bearing CAM assay

The chick embryo chorioallantoic membrane (CAM) has been used to study tumour angiogenesis and metastasis in human tumors[249]. Since the lymphoid system is not fully developed until late stages of incubation, the chick embryo serves as a naturally immunodeficient host capable of sustaining grafted tissues or cells. In addition, the highly-vascularized CAM promotes the efficiency of the grafting and provides a closed tumour growth system that mimics the physiological cancer cell microenvironment with low cost. Thus, it is a useful model to rapid assessment of tumour inhibition efficacy of potential candidates.

The growth and angiogenic characteristics of HepG2 cells were tested *in vivo* using a modified CAM assay as previously described[250]. Gallus gallus White leghorn fertilized eggs were obtained from a commercial breeder, Henry Stuart (Lincolnshire, UK). Eggs were stored at 16°C (up to one week) then incubated at 37°C for 9 days. A small window was made in the shell overlying the most vascularized area of each viable embryo and HepG2 cells ($1x10^6$) mixed with growth factor reduced matrigel (8.9 mg/mL, BD Biosciences) in a total volume of 25 µL with DMSO (0.05%) or SFN 20 µM was loaded on the top of the CAM ($n \geq 6$ CAMs per treatment). The window was resealed with adhesive tape and eggs were returned to the incubator for 3 days. Tumour samples were cut out from the membrane and their sizes were monitored with callipers, the tumour volume (V, mm^3) was calculated as L x W x D, where L = length (mm), W = width (mm) and D = depth (mm).

2.2.10.1 Hematoxylin and eosin (H&E) staining

Histological assessment was made to assess the development of the implanted tumour. Tumour samples from the modified CAM assay were fixed with 4% PFA overnight at 4°C then changed to cryopreservative medium (15% sucrose in PBS) overnight at 4°C. Tumours were then embedded in 8% gelatin (15% sucrose in PBS) and snap-frozen for -80°C storage. Serial sections (10 µm) were stained with hematoxylin and eosin. Sections were imaged under light microscope at magnification 5x.

2.2.10.2 Immunohistochemical staining

Briefly, section slides were blocked with 5% goat serum in PBS for 0.5 hour for nonspecific binding, and then incubated with a rabbit monoclonal antibody against human HIF-1α or a

mouse monoclonal antibody against human VEGF-A overnight at 4°C (each at 1:100 dilution in PBS). Slides were washed with PBS 3 times each for 5 mins, and incubated with the goat derived second antibody [AlexaFluo488 goat anti-rabbit for HIF-1α or AlexaFluo546 goat anti-mouse for VEGF-A (Invitrogen)] for 0.5 hours RT in a moist atmosphere, both were used at 1:500 dilution in PBS. Then sections were mounted with fluoromount G with DAPI (Thermo Fisher), and examined by fluorescence microscopy (Axioplan 2; Zeiss, Cambridge). The expression levels of HIF-1α and VEGF-A were assessed by measuring average pixel intensity per unit area of tumour in 5 random microscopic (400x) field in each slice using image J software.

2.2.11 Confocal laser scanning microscopy (CLSM)

HepG2 were plated onto sterile 10 mm glass coverslips in 24-well plates at a concentration of 2×10^5 cells/ml and incubated for 48 hours at 37°C, 5% CO_2. Cells were then treated with 50 μM AITC-SiQDs (excitation/emission: 350/440), or 0.1% DMSO as control for 1, 3, 6, 12, 24 hours. For lysosome staining, during the last 10 mins of AITC-SiQDs treatment, cells were exposed to 1 μM LysoTracker® Red DND-99 (excitation/emission: 577/590, ThermoFisher), then washed with fresh medium for 10 mins at 37°C, 5% CO_2. All cover slips were washed twice with PBS and fixed with 4% PFA for 10 mins. Cover slips with cells were inverted and mounted on a microscope slide. CLSM was performed on a Zeiss LSM510 META confocal microscope using a 10 × objective lens for imaging. Laser beams with 364, 488 and 543 nm excitation wavelengths were used to image AITC-SiQDs, bright field and lysosome respectively.

2.3 Statistics

Data are represented as the mean ± SD or mean ± SEM. Student's t-test was performed to determine any statistical difference between two groups; one-way analysis of variance (ANOVA) test was used to compare the means of serval different groups. A p value <0.05 was considered statistically significant. Unless otherwise indicated, these methods were done using GraphPad Prism software (GraphPad Software, La Jolla California USA, www.graphpad.com.) and used for all statistic comparisons presents.

Chapter 3. Antioxidant activities of SFN in HepG2 and HHL5 cells

3.1 Introduction

The cytoprotective effect of SFN largely comes from the activation of Nrf2 transcription factor, a master transcription factor involved in cell redox homeostasis and stress adaptation[86]. The interaction of SFN with Keap1 disrupts this function and allows nuclear accumulation of Nrf2. Although there are conflicting *in vitro* and *in vivo* data regarding which cysteine residues react with SFN, most biological data indicate that modification of C151 is essential for its action[251]. Nrf2 then binds to the ARE and enhances the transcription of more than 200 target genes, many of which provoke strong cytoprotective responses. Of significance is that Nrf2 controls the production, utilization and regeneration of GSH, the most abundant antioxidant cofactor within cells[252], by regulating γ-GCS, the rate-limiting enzyme for GSH synthesis[253], ROS-detoxifying enzymes such as GST[254], and NADPH-generating enzymes[255].

Apart from the cytoprotective effect, SFN has also been shown to exhibit cytotoxic effects including decreasing cell viability and proliferation[256–258]; disrupting mitochondria[259], tubulin and microtubule function[146,260,261]; inducing DNA damage[118], apoptosis and cell cycle arrest[262–265]; inhibiting telomerase activity[256,266]; and disrupting protein-protein interaction in Hsp90 complex[267]. The complex bioactivities of SFN could lead to different cell response upon SFN treatment which could depend on the cell type and dose/duration of the treatment. Therefore, increasing the understanding of the different effect of SFN in non-cancerous and cancerous cells has great importance in cancer management.

Selectivity towards cancer cells is the central requirement of any cancer therapy. However, compared results of SFN bioactivities on normal and cancerous cells have been inconsistent. Several normal epithelial cell lines are relatively resistant to apoptosis induction by SFN at concentrations which are lethal to cancer cells[268,269]. Zeng *et al* reported SFN activated survival signalling in non-tumorigenic NCM460 colon cells but apoptotic signalling in tumorigenic HCT116 colon cells and that may play a critical role in SFN's higher potential to inhibit cell proliferation in colon cancer cells than in normal colon cells[270]. While on the other hand, SFN has been reported as more cytotoxic for lymphoblastoid than for leukaemia cells[271]. The effects of SFN on non-transformed T-lymphocytes were similar to those recorded on Jurkat T-leukaemia cells[272]. According to Gamet-Payrastre *et al*, SFN affected the cell viability very effectively on undifferentiated intestinal HT29 cells but not differentiated CaCo-

2 cells[273]. SFN showed broad and complex effects on DNA methylation profiles in both normal and cancerous prostate epithelial cells[274] and regulated the Nrf2/ARE signalling pathway differently in human untransformed epithelial colon CRL-1790 cells and in HT-29 and Caco-2 colorectal cancer cells[275]. Negrette-Guzman *et al* demonstrated SFN modulates mitochondrial dynamics differentially in normal and cancer cells[276]. The transcriptional response to SFN on cell cycle related genes was dependent on the cell line and presumably the state of cancer progression[277,278]. However, to date, the understanding of why SFN has any specificity is far from conclusive.

The aim of this study was to compare the effect of the SFN in human hepatoma cell line HepG2 and immortalised human hepatocyte-derived cell line HHL5[235] in terms of its cytotoxic and cytoprotective effects, thereby shedding new light on the possible dual role of SFN in cancer management.

3.2 Results

3.2.1 Effect of SFN on cell viability and DNA damage

The cytotoxicity of SFN was measured by MTT assay (Figure 3.1) so that the appropriate experimental concentrations for further investigation can be established. Both HHL5 and HepG2 cells were cultured in 96-well plates to reach 70 to 80% confluency and then treated with SFN (1.25 to 160 μM) for 24 hours. Results indicated that SFN (≥20 μM) decreased the metabolic activities in both cell lines in a dose-dependent manner. With increasing SFN doses, a decrease of cell confluence and an increase of detached cells and cell debris were observed. The IC_{50} values of SFN were 30.2 and 54.9 μM in HHL5 and HepG2 cells respectively, which indicated that the normal cells were much more susceptible to cytotoxicity from SFN than the cancer cells. In addition, 1.25 μM SFN treatment increased cell viability in HepG2 cells significantly but not in HHL5 ($p < 0.05$).

The genotoxicity of SFN was also measured in both cell lines using comet assay (Figure 3.2A), doses tested were 1.25 to 20 μM to avoid strong cytotoxicity. Baseline DNA damage, represented as tail intensity percentage, in HHL5 and in HepG2 was 7.58 and 15.94% respectively. This difference may be caused the genomic instability of the cancer cells compared to the normal cells. After 24 hours, there was a significant increase of DNA damage from 20 μM SFN treatment in both cell lines, 21.15 and 24.57% in HHL5 and HepG2 respectively, i.e. 20 μM SFN induced a 2.8-fold increase in DNA damage in HHL5 compared to control but only 1.5-fold in HepG2. Furthermore, at 1.25 to 10 μM SFN decreased DNA damage in HepG2 cells but not in HHL5 cells.

To avoid activating the DNA repair process, which usually happens after 30 mins of genotoxic insults, the comet assay was performed with 20, 40, 80 μM SFN treatment for 30 min in both cell lines (Figure 3.2B). Results showed SFN caused DNA damage in a dose-dependent manner in both cell lines, with a 2.8-fold increase at 80 μM SFN treatment in HHL5 and 1.8-fold in HepG2 compared to their corresponding control. These data are consistent with the cytotoxicity observed between HHL5 and HepG2 cells, that SFN is more toxic to HHL5 than to HepG2 cells.

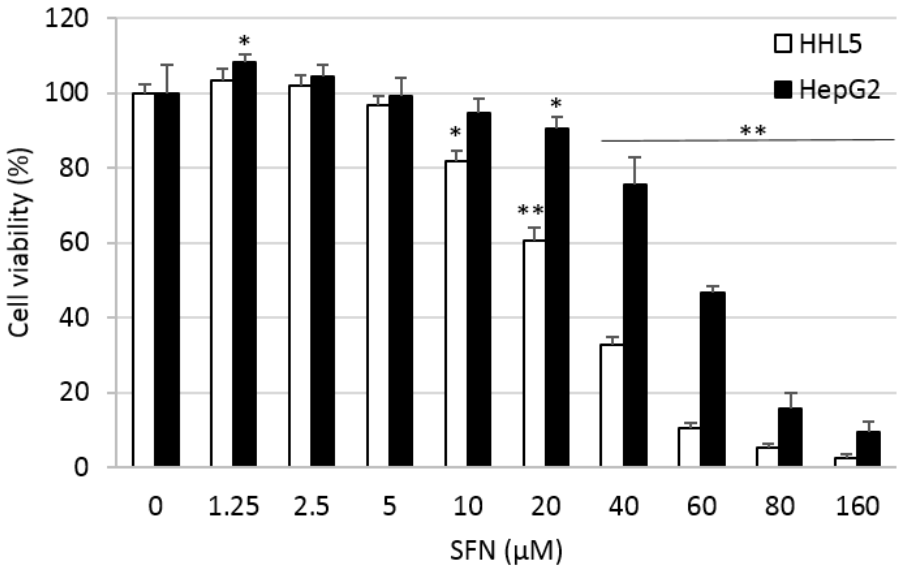

Figure 3.1 Effect of SFN on cell viability in HHL5 and HepG2 cells. Cells were treated with different doses of SFN with DMSO (0.1%) as control for 24 hours, then cell viability was determined by MTT assay. Result represents the mean ± SD ($n \geq 5$). Statistical significance from the control, *$p < 0.05$, **$p < 0.01$. Lines drawn on the graph indicates that all the bars included are significantly different from their corresponding control group.

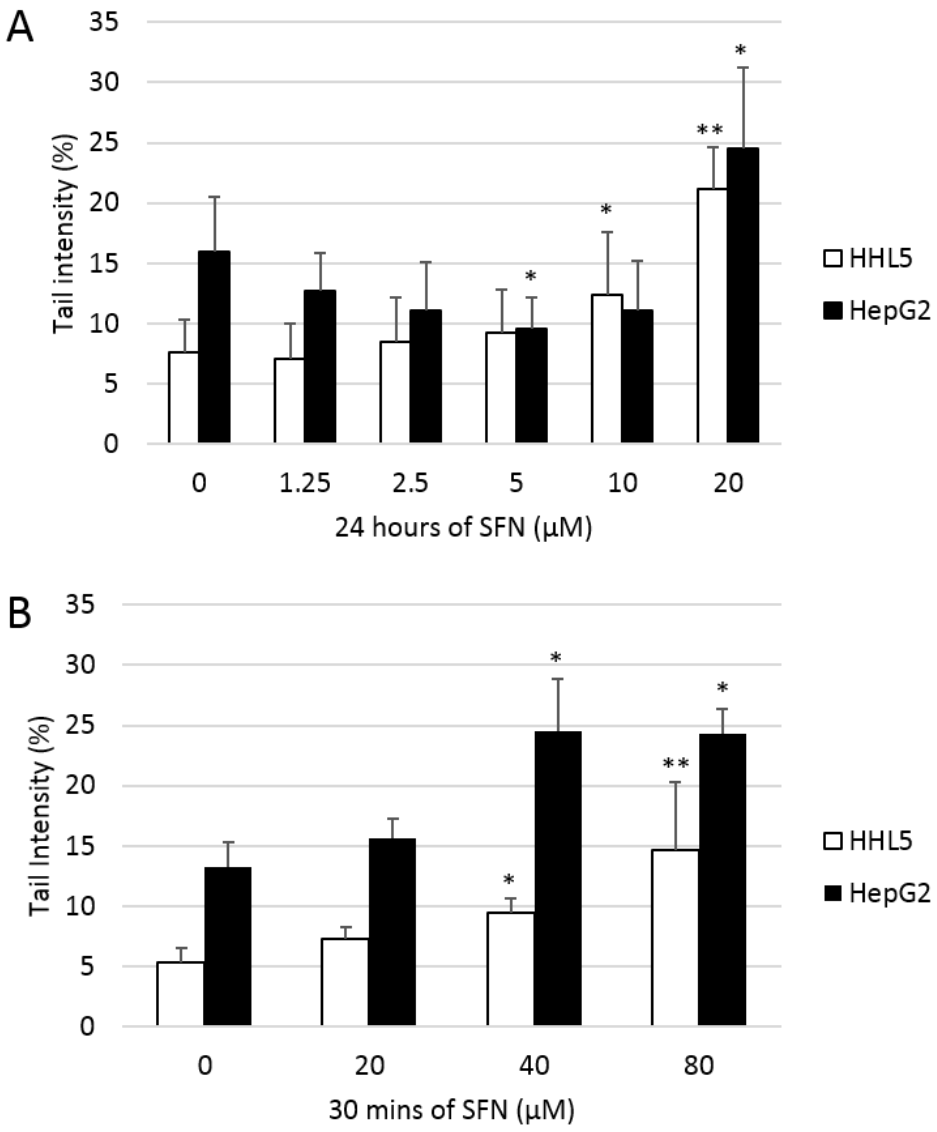

Figure 3.2 Effect of SFN on DNA damage in HHL5 and HepG2 cells. Cells were treated with different doses of SFN with DMSO (0.1%) as control for 24 hours (A) or 30 min (B), then DNA damage was determined by comet assay. Result represents the mean ± SD ($n \geq 3$). Statistical significance from the control, *$p < 0.05$, **$p < 0.01$.

3.2.2 Effect of H_2O_2 on cell viability and DNA damage

The cytotoxicity of 24 hours' treatment of H_2O_2 was measured by MTT assay in both HHL5 and HepG2 cells (Figure 3.3A). The IC_{50} values were 374.3 and 667.4 µM in HHL5 and HepG2 cells respectively. Interestingly, low doses of H_2O_2 (31.25 to 125 µM) significantly increased cell viability in HepG2 cells.

To establish the base line using H_2O_2 as an oxidative stress to induce DNA damage, cells were treated with different concentrations of H_2O_2 for 30 mins and the DNA damage was measured by comet assay. As shown in Figure 3.3B, H_2O_2 induced DNA damage in both cell lines in a dose-dependent manner at 30 mins. Also, the increased magnitude of DNA damage in HHL5 cells was higher in comparison to that of HepG2 cells at all the doses with greater significant differences at higher doses (90 and 120 µM). Taken together, these data indicated that HepG2 cells were much more resistant to H_2O_2 oxidative stress compared to HHL5 cells.

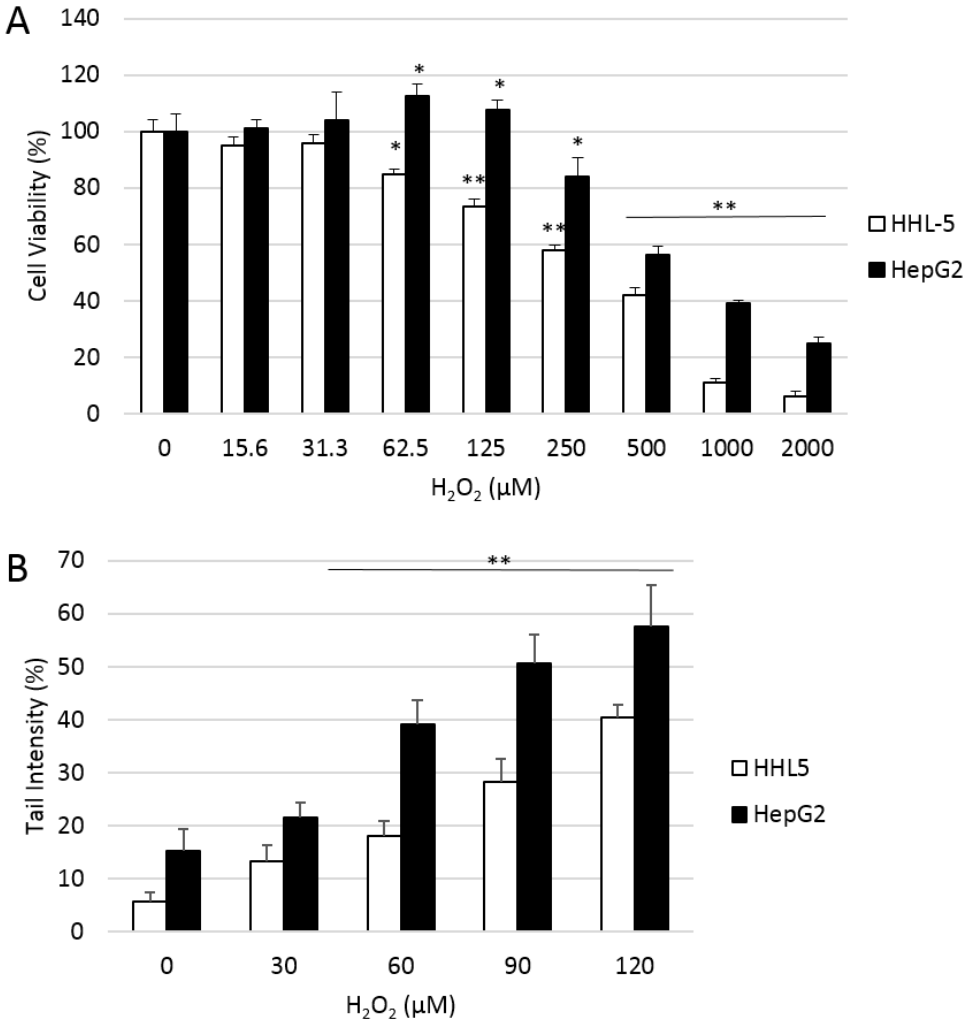

Figure 3.3 Effect of H_2O_2 on cell viability and DNA damage in HHL5 and HepG2 cells. (A) Cells viability was determined after 24 hours by MTT assay, result represents the mean ± SD ($n \geq 5$). (B) DNA damage was measured after 30 mins by comet assay. Tail intensity were measured for at least 100 comets per sample. Statistical significance from the control, *$p < 0.05$, **$p < 0.01$. Lines drawn on the graph indicates that all the bars included are significantly different from their corresponding control group.

3.2.3 Protective effect of SFN against H_2O_2-induced cell injury

The protective effect of SFN against H_2O_2-induced cell death in both cell lines was determined by MTT assay (Figure 3.4A). Cells were pre-treated with SFN (1.25 to 20 μM) for 24 hours then treated with H_2O_2 for another 24 hours. The dose of H_2O_2 treatment followed the IC_{50} value in each cell lines, i.e. 400 μM and 700 μM in HHL5 and HepG2 respectively. In HHL5, when the cells were pre-treated with 1.25 to 5 μM SFN, cell death induced by H_2O_2 was alleviated, however pre-treatment with 10 and 20 μM SFN lead to more cell death compared to H_2O_2 treatment (pre-treated with control). However, in HepG2, the protective effect was observed from 1.25 to 20 μM SFN pre-treatments in the MTT assay, which was further confirmed using an Annexin V/PI double staining. As shown in Figure 3.4B, H_2O_2 caused significant apoptotic cell death: 5.63% necrotic cells (PI positive) and 30.23% apoptotic cells (Annexin V positive). Pre-treatment with SFN (1.25 to 20 μM) significantly reduced the cytotoxicity induced by H_2O_2 with an observable increase in the viable cell percentage (double negative) relative to the non-pre-treated cells.

Next, whether SFN could protect against H_2O_2-induced DNA damage was tested by comet assay (Figure 3.5A). Cells were pre-treated with SFN (2.5, 5, 10 μM) for 24 hours then followed by 60 μM H_2O_2 treatment for 30 mins. Results showed that in HHL5, only SFN 5 μM pre-treatment provided significant protection against H_2O_2-induced DNA damage; while in HepG2, there was a dose-dependent protective effect from SFN pre-treatment. This result agreed with the changes of p-Chk2 (Thr68) at the protein level observed from Western blotting (Figure 3.5B). The phosphorylation of checkpoint kinase 2 (Chk2) indicates its activation, which is well documented as a cellular response to DNA damage[279]. H_2O_2 markedly increased the level of p-Chk2 whereas with SFN pre-treatment, p-Chk2 protein decreased in a dose-dependent manner in HepG2 but not in HHL5. These results indicated that SFN substantially reduced the DNA damage caused by H_2O_2 in HepG2 but not in HHL5 cells.

Together, these results suggested that HepG2 cells utilized the protective effect of SFN better than HHL5 against the cytotoxic effect of H_2O_2.

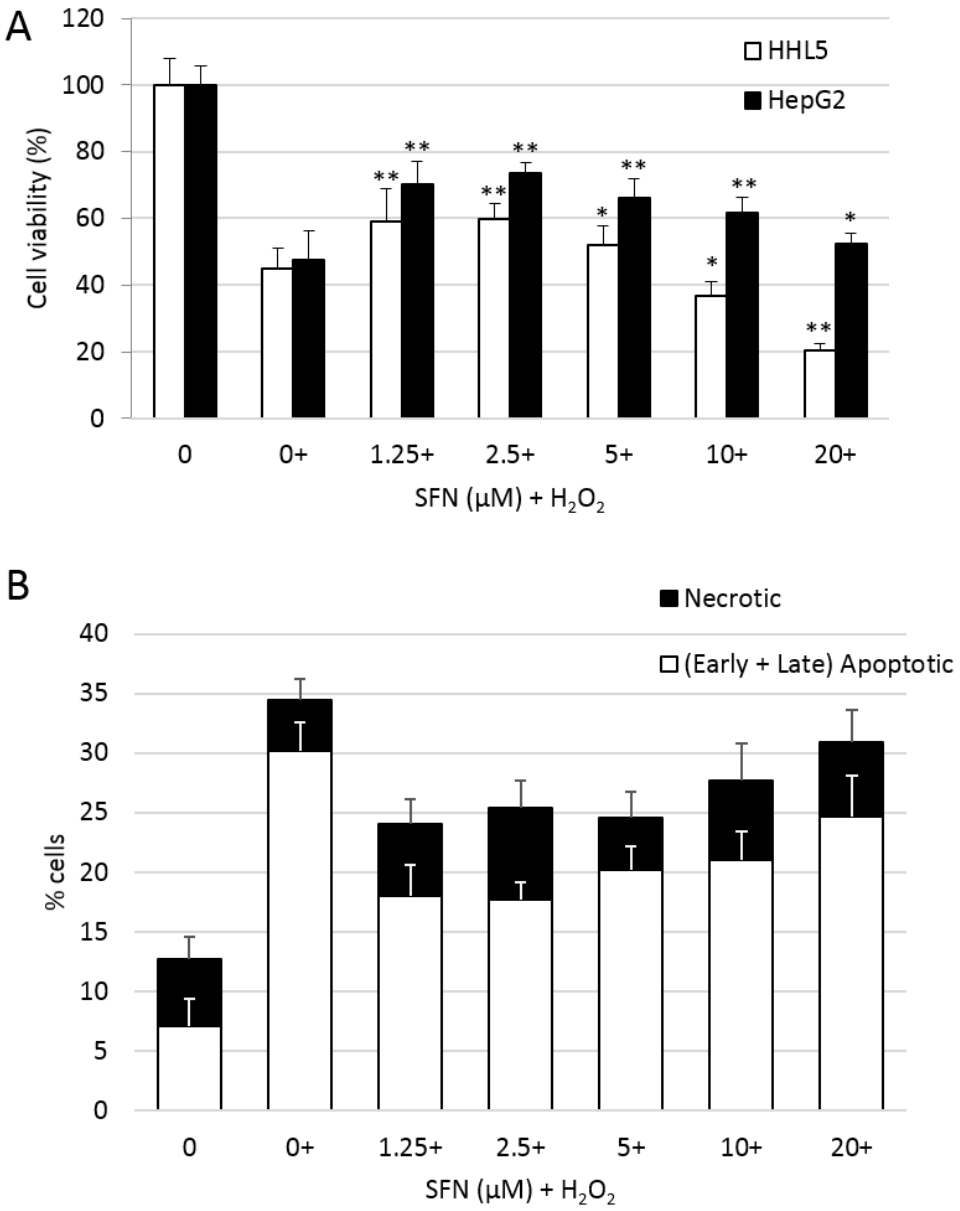

Figure 3.4 Protective effect of SFN against H_2O_2-induced cell injury. (A) Cells were pre-treated with different doses of SFN for 24 hours and then incubated with H_2O_2 (60 μM) for another 24 hours. Cell viability was measured by MTT assay, result represents the mean ± SD ($n \geq 5$). Statistical significance from H_2O_2 control, *$p < 0.05$, **$p < 0.01$. (B) HepG2 cells were pre-treated with SFN for 24 hours before exposure to H_2O_2 (700 μM) for 24 hours, followed by Annexin V/PI staining detected by a flow cytometer. Result represents apoptotic and necrotic cells percentage as mean ± SD ($n = 3$).

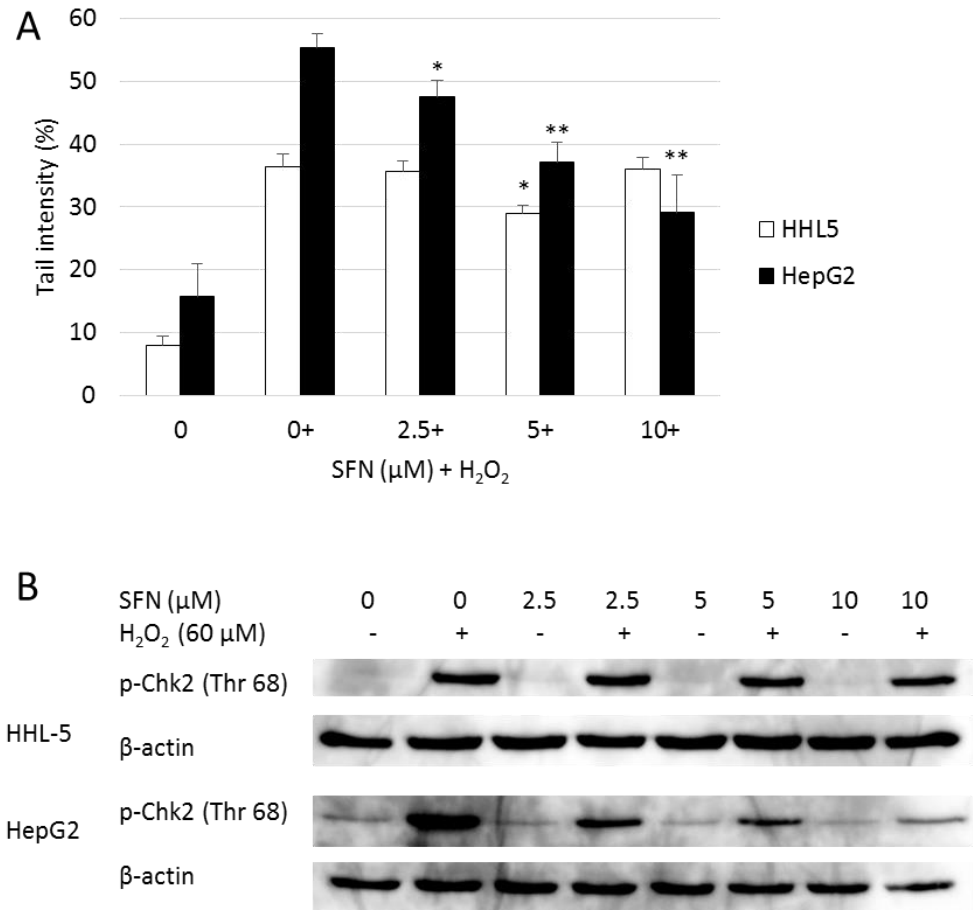

Figure 3.5 Protective effect of SFN against H_2O_2-induced DNA damage. Cells were pre-treated with different doses of SFN for 24 hours and then incubated with H_2O_2 for another 30 mins. DNA damage was measured by comet assay. (A) Tail intensity were measured for at least 100 comets per sample. Statistical significance from H_2O_2 control, *$p < 0.05$, **$p < 0.01$. (B) The protein level of p-Chk2 in whole cell lysates was detected by Western blot and normalized against β–actin.

3.2.4 Effect of SFN on intracellular ROS and GSH

The redox statues in HHL5 and HepG2 cells was investigated by examining the ROS and GSH levels under the basal and SFN treated conditions. HepG2 cells, which were observed to be less sensitive towards SFN and H_2O_2 treatment, had higher basal levels of ROS than HHL5 cells by approximately 1.5-fold (Figure 3.6A). The basal level of intracellular GSH was 43.9 ± 6.1 nmol/mg in HHL-5 and 60.7 ± 8.5 nmol/mg protein in HepG2. As shown in Figure 3.6B, 24 hours of SFN treatment dose-dependently increased the levels of ROS compared to control cells in HHL5 cells but decreased in HepG2 cells. On the other hand, in both cell lines SFN increased GSH levels compared to control after 24 hours in a dose-dependent manner. However, there was a drop of GSH level between 10 and 20 μM SFN treatment in HHL5 but not in HepG2 cells. In HHL5, GSH level was 2.2-fold increased with 10 μM SFN but only 1.8-fold increased with 20 μM SFN compared to control at 24 hours; while in HepG2, GSH level was 2.2-fold and 2.4-fold increased with 10 and 20 μM SFN treatment, respectively.

Further time courses of the GSH levels upon 10 μM SFN treatments in both cell lines were studied (Figure 3.6C). Result indicated SFN caused a biphasic depletion and restoration of GSH in both cell lines. The depletion happened in HHL5 cells at 3 and 6 hours after SFN exposure, the GSH level decreased to 60 and 72% of control levels respectively. In HepG2 cells, GSH level decreased to 51% at 3 hours of SFN treatment but back to control levels at 6 hours. At 24 hours, the GSH level increased around 2-fold of control in both cell lines. These results were in accordance with that demonstrated by Kim and coworkers[280] who showed the early down regulation between 0 and 4 hours and up regulation between 4 and 24 hours on HepG2-C8 cells.

Taken together, these data indicated that ROS and GSH levels in cancerous cells are higher than those in non-cancer cells, and different patterns of ROS and GSH changes caused by SFN treatment may link to the cytotoxic effect of itself and the protective effect of SFN against H_2O_2 insult.

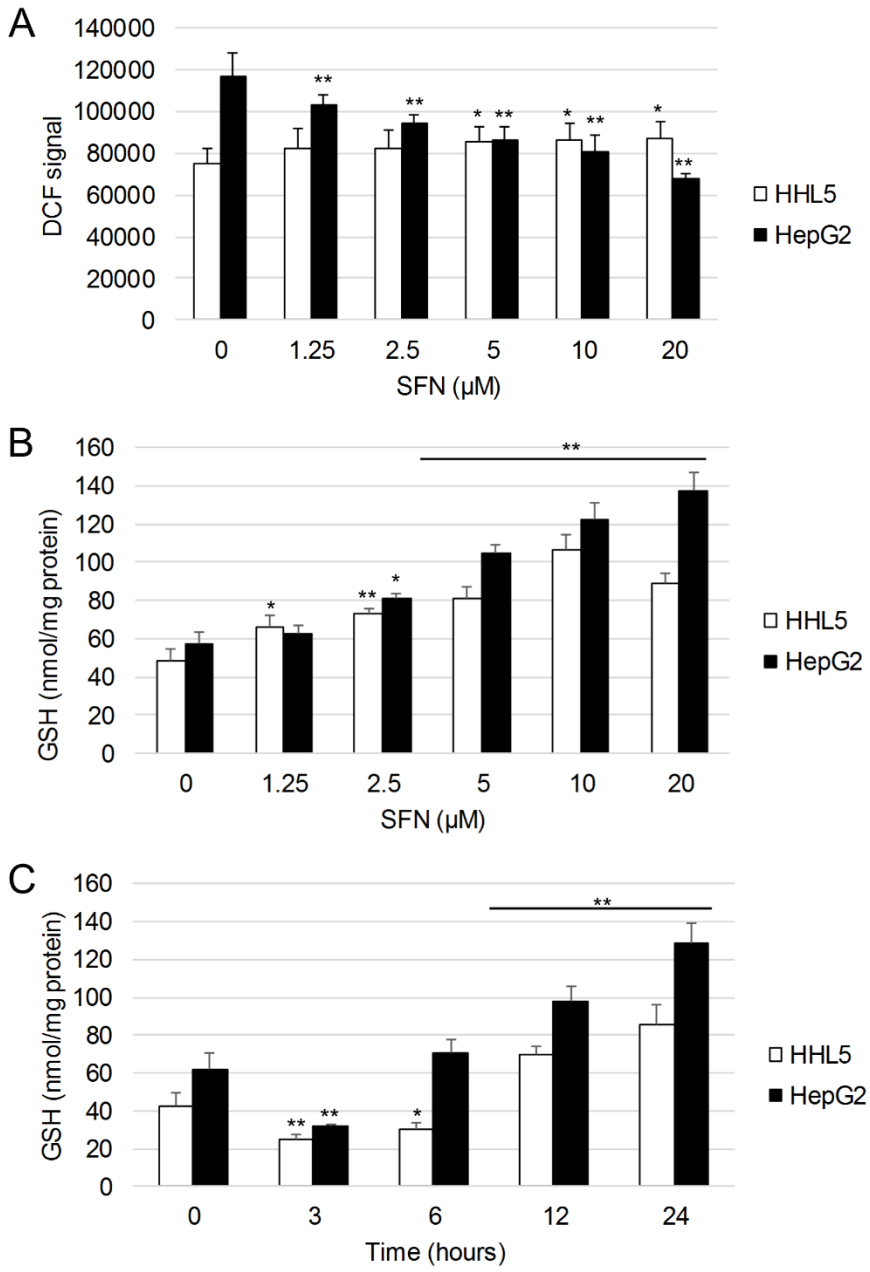

Figure 3.6 Effect of SFN on intracellular ROS and GSH levels in HHL5 and HepG2 cells. Cells were treated with different doses of SFN with DMSO (0.1%) as control for 24 hours. (A) The intracellular ROS was determined by measuring the fluorescent intensity of oxidized DCF, result represents the mean ± SD (n ≥ 5). Statistical significance from control, *p < 0.05, **p < 0.01. (B) The intracellular GSH level was measured by HPLC, result represents the mean ± SD (n = 3). Statistical significance from control, *p < 0.05, **p < 0.01. (C) Cells were treated with 10 μM SFN for 0, 3, 6, 12, 24 hours, the intracellular GSH level was measured by HPLC. Result represents the mean ± SD (n=3). Statistical significance from control, *p < 0.05, **p < 0.01.

3.2.5 Effect of SFN on nuclear Nrf2 accumulation

Since Nrf2 translocation to the nucleus is one of the key events required in the regulation of the Nrf2-Keap1-ARE signalling pathway, it is important to determine the time- and dose-response of SFN on this translocation in our cell lines. Here the time and dose courses of activation Nrf2 by SFN were tested in both cell lines. As shown in Figure 3.7, untreated HHL5 and HepG2 cells had low Nrf2 levels in the nucleus consistent with the continuous degradation of Nrf2 under homeostasis. Upon SFN treatment, a prompt increase of Nrf2 appeared after 1 hour in both cell lines, suggesting the liberation of Nrf2 from Keap1 suppression and subsequent Nrf2 nuclear translocation. The nuclear accumulation of Nrf2 plateaued after 2 hours and remained steady for 24 hours. The dose response from 4 hours SFN treatment in HHL5 cells agreed with previous studies[80]. In HepG2, SFN at 2.5 to 20 µM also induced significant and dose-dependent translocation of Nrf2 into the nucleus. Comparing the basal and induced level of nuclear Nrf2 in these two cell lines, HepG2 showed 3.3-fold higher basal level than HHL5. In addition, 5 µM SFN induced 2.9- and 6.2-fold increase of Nrf2 protein level in HHL5 and HepG2 cells respectively at 4 hours.

Taken together, there is time- and dose- dependent induction of nuclear Nrf2 level by SFN in both cell lines; HepG2 cells showed significantly higher basal level than HHL5 and SFN induced a higher level of Nrf2 translocation to the nucleus compared to control in HepG2 cells than that in HHL5 cells.

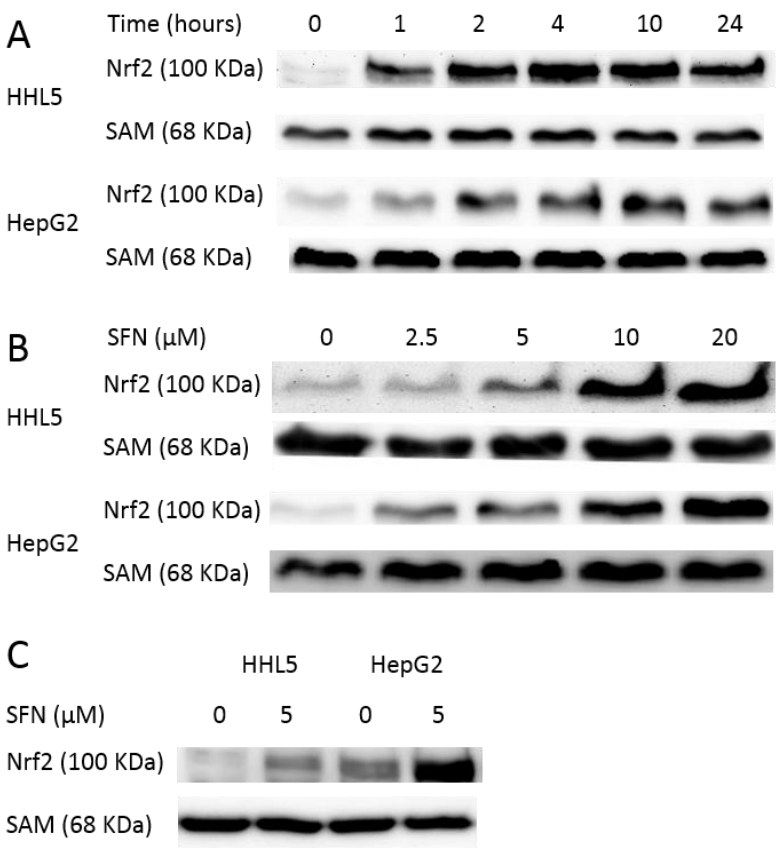

Figure 3.7 Effect of SFN on Nrf2 nuclear translocation. (A) Cells were treated with 10 μM SFN for 0, 1, 2, 4, 10, 24 hours. (B) Cells were treated with SFN 0, 2.5, 5, 10, 20 μM for 4 hours. (C) Cells were treated with SFN 5 μM or DMSO 0.1% for 4 hours. Nuclear protein was extracted and Nrf2 was detected by Western blotting. RNA-binding protein SAM was used as a loading control.

3.2.6 The role of Nrf2 and GSH in cytotoxic and cytoprotective effects of SFN

Since higher basal levels of Nrf2 and GSH were observed in HepG2 cells compared to that in HHL5 cells, their role in the cytotoxic effect of SFN was investigated further. BSO, a specific inhibitor of γ-GCS, was used to decrease the GSH level. The inhibition efficiency of BSO on the intracellular GSH level was characterized using HPLC (Appendix Figure 1). 50 μM BSO was chosen to be the co-treatment dose with SFN as it showed 60-80% reduction in the GSH level and abolished the SFN-induced GSH rise. Nrf2 knockdown was achieved by siRNA transfection. The siRNA knockdown efficiency of Nrf2 was measured using Western blot analysis (Appendix Figure 2).

As shown in Figure 3.8, at 24 hours, 50 μM BSO only reduced cell viability of HepG2 cells to 97.9%. 60 μM SFN decreased HepG2 cell viability to 47.6% which agreed with previous data; while co-treatment with BSO reduced the cell viability further to 25.7%. Furthermore, in Allstar transfected cells, SFN 60 μM decreased cell viability to 49.5% of DMSO control; while in siNrf2 transfected cells, SFN decreased cell viability to 15.3% of DMSO control. These data clearly indicated that by reducing Nrf2 and GSH level in HepG2 cells, SFN became more toxic.

Next, to investigate whether Nrf2 is the main gene responsible for the cytoprotective effect of SFN against H_2O_2-induced cell death in HepG2 cells, cells were transfected with siNrf2 (and Allstar as negative control), pre-treated with 5 μM SFN for 24 hours followed by H_2O_2 insult for another 24 hours. As shown in Figure 3.9, Nrf2 knockdown enhanced the cytotoxicity of H_2O_2, i.e. cell viability was 47.6, 40.0 and 24.6% in the non-transfected, Allstar transfected and siNrf2 transfected cells respectively. 5 μM SFN decreased the cytotoxicity of H_2O_2 in non-transfected and Allstar negative control cells, while the protective effect from SFN was abolished upon Nrf2 knockdown. The involvement of GSH in the SFN cytoprotective effect was also studied. Co-treatment with BSO and 5 μM SFN showed no protective effect against H_2O_2. Therefore, it can be concluded that the Nrf2/GSH signalling pathway plays an essential role in the protective effect of SFN against H_2O_2.

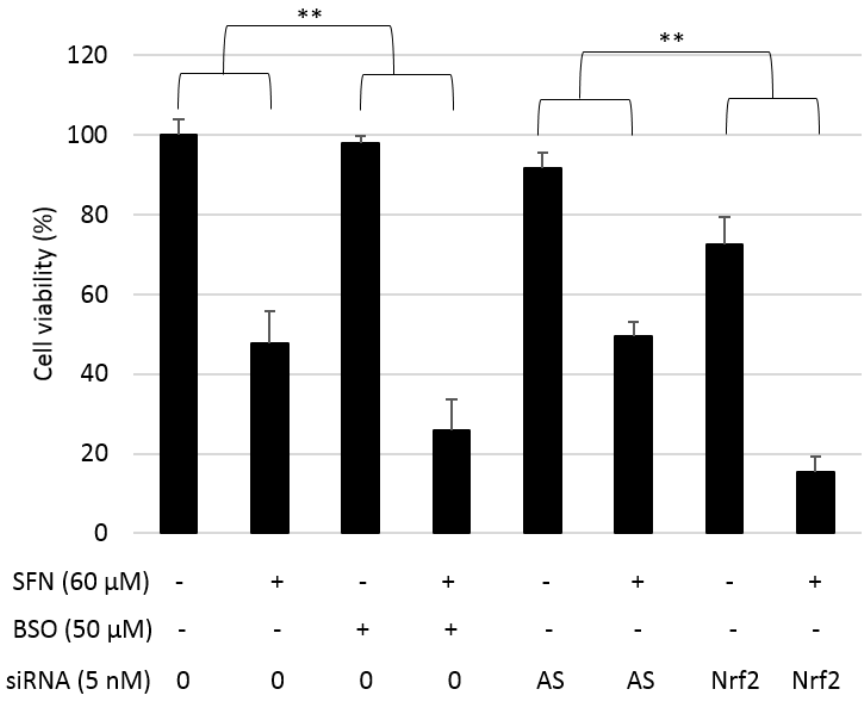

Figure 3.8 Effect of GSH inhibition and Nrf2 knockdown on cytotoxicity in HepG2 cells exposed to SFN. Nrf2 was knocked down using siRNA as described in Methods. Allstars (AS) was used as a negative control. Cells were incubated with 60 µM SFN or DMSO (0.1%) with or without 50 µM BSO for 24 hours. Cell viability was measured by MTT assay, result represents the mean ± SD ($n \geq 5$). Within indicated two columns, SFN treated groups were normalized against the mean of corresponding control groups. A student's t-test was then performed to determine any statistical difference between two groups. **$p < 0.01$ between the indicated groups.

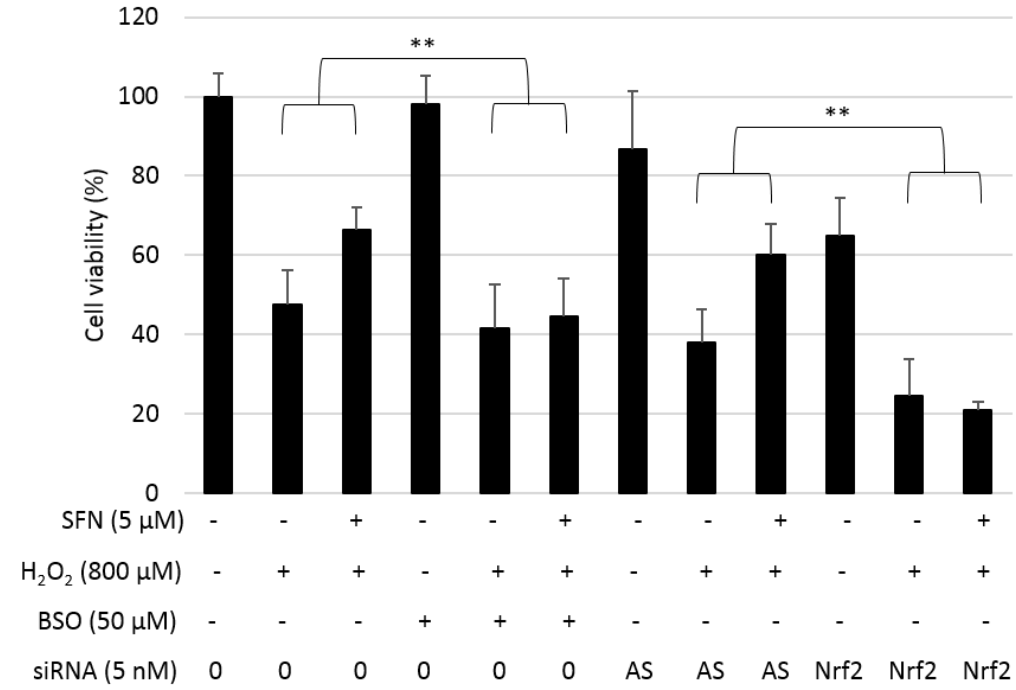

Figure 3.9 Effect of Nrf2 knockdown and GSH inhibition on the protective effect of SFN against H_2O_2 in HepG2 cells. Nrf2 was knocked down using siRNA as described in Methods. Allstars (AS) was used as a negative control. Cells were incubated with 5 µM SFN or DMSO (0.1%) with or without 50 µM BSO for 24 hours, then exposure to 800 µM H_2O_2 for another 24 hours. Cell viability was measured by MTT assay, result represents the mean ± SD ($n \geq 5$). Within indicated two columns, SFN treated groups were normalized against the mean of corresponding control groups. A student's t-test was then performed to determine any statistical difference between two groups. **$p < 0.01$ between the indicated groups.

3.3 Discussion

A successful chemopreventive agent should have a minimal effect on normal cells but a strong inhibitory effect on cell proliferation and carcinogenic pathways in cancer cells. While there are many studies on both protective and cytotoxic effects of SFN, there is little on comparing its effect on normal cells with cancer cells. The presented study is the first to compare the effects of SFN on the immortalised hepatocytes HHL5 versus the tumorigenic liver cell line HepG2.

SFN showed stronger cytotoxicity and genotoxicity in HHL5 than in HepG2. At 24 hours, 10 µM SFN started to inhibit cell viability and induce DNA damage in HHL5 while in HepG2 only 20 µM SFN started to have significant cytotoxic and genotoxic effect. HHL5 cells were also more susceptive to H_2O_2-induced cell death and DNA damage compare to HepG2 cells. H_2O_2 is continuously generated in living cells through metabolic pathways and serves as a source of ROS. The intracellular concentration of H_2O_2 is tightly controlled within 1 to 700 nM while above 1 µM is considered to cause oxidative stress inducing growth arrest and cell death[281]. The half-life of H_2O_2 is longer than that of other ROS and it has often been used in the oxidative stress injury model with hepatocytes as well as other cell types[282]. Therefore, H_2O_2 was chosen to induce oxidative stress in this study. Since the cytotoxic effects of SFN and H_2O_2 have been linked to the disruption of the redox status of the cells[283,284], the different sensitivities towards oxidative stress between these two cell lines observed is likely due to their differences in the basal redox status.

Indeed, results showed that HepG2 cells had higher basal levels of intracellular ROS, GSH and nuclear Nrf2 than HHL5. ROS such as hydroxyl radical ($^{\bullet}OH$), superoxide anion ($O_2^{\bullet-}$) and H_2O_2 are of importance in physiological functions such as second messengers[282]. A high ROS level is a common feature of cancer cells, which contributes to intracellular signalling cascades necessary for the tumour initiation, promotion and progression, as well as, tumour resistance to chemotherapy[285]. Elevated ROS in cancer cells could enhance cell proliferation and survival, increase genomic instability, thereby sustaining the oncogenic phenotype[282]. On the other hand, excessive ROS could also trigger redox imbalance which leads to apoptotic cell death[285]. In this study, the higher ROS level in HepG2 cells observed agreed with the higher basal level of DNA damage showed in comet assays compared with HHL5 cells; the higher basal level of GSH and Nrf2 in HepG2 cells could indicate an enhanced defence system against ROS compared to that in HHL5 cells.

More interestingly, SFN decreased the ROS level in HepG2 cells (1.25-20 μM) while increasing ROS in HHL5 cells (2-20 μM). SFN also increased nuclear Nrf2 levels and intracellular GSH levels in both cell lines but with slightly different patterns. Short term SFN exposure (3-6 hours) had a longer depletion effect on intracellular GSH and lower induction of Nrf2 nuclear accumulation in HHL5 cells compared to in HepG2 cells. These findings indicated SFN may exhibit strong pro-survival effects in HepG2 cells which is in line with the results demonstrated in 3.2.3. 24 hours pre-treatment of SFN provided protection against H_2O_2-induced cell injury in both cell lines. However, in HHL5 cells, SFN at high doses (10-20 μM) failed to show protective effect against H_2O_2-induced cell death and DNA damage.

Nrf2 is generally considered as the main defence mechanism of the cell and a major regulator of cell survival. Nrf2 deficient mice are more susceptive to carcinogenesis[286,287]. Many have reported the chemopreventive effect of Nrf2 in cancer[288]. The simultaneous induction of both Nrf2 and GSH from SFN is beneficial in healthy tissue. In mouse embryonic fibroblasts, the Nrf2-dependent up-regulation of GSH was found to be the principal mechanism by which SFN pre-treatment induced resistance to unsaturated carbonyl compounds, hydroperoxides and genotoxic electrophiles[177]. Li *et al* reported SFN protected human vascular endothelial cells against lysophosphatidylcholine-induced injury by the activation of Nrf2 and its downstream targets such as endogenous antioxidants GSH and phase II enzymes[289]. SFN also exerted neuroprotective effects with increased levels of Nrf2 expression and total GSH in the brain within an *in vivo* Parkinson's disease model[93]. In rat, SFN increased the level of Nrf2 and GSH and attenuated hepatic ischemia reperfusion injury[290]. During chemotherapy, such SFN activity might provide protection in normal cells against the effects of cytostatics. For example, the cytotoxicity of 5-fluorouracil and SFN mixture was lower than the sum of the effects of the single compounds in V-79 Chinese hamster lung fibroblasts[291].

However, the results of the presented study indicated that in HepG2, both Nrf2 and GSH substantially contributed to the preservation of cell integrity under conditions of SFN and H_2O_2 treatment, i.e., inhibition of Nrf2/GSH increased SFN cytotoxicity and decreased its cytoprotective effect against H_2O_2 in HepG2. The knockdown of Nrf2 increased the cell death even further in both cases compared to GSH inhibition, indicating that more Nrf2 targets might be involved. Essentially, Nrf2 protects not only normal cells but also transforming/cancer cells. With increasing evidence suggesting that Nrf2 was upregulated in cancer cells or resistance strains[292,293], and contributed to the aggressive cancer phenotype[294],

it became more important to rationalise the usage of Nrf2 activators such as SFN. In this study, HepG2 cells were more able to take advantage of the SFN-induced beneficial effects, and better resist SFN-induced disruptions than HHL5 cells, indicating a potential risk of using SFN for chemoprevention. More rigorous dose-response comparisons of efficacy versus toxicity need to be performed with consideration of the differences between normal and cancer cells.

In conclusion, HepG2 cells were more resistant to SFN exposure which may be due to their intrinsic high levels of Nrf2/GSH. SFN exhibited strong cytoprotective effects due to the activation of Nrf2 and the induction of GSH in both cell lines with a wider tested dose range observed in HepG2 compared to that in HHL5. Although *in vitro* studies do not necessarily predict *in vivo* outcomes, these findings raise a question that SFN may induce pro-survival effects in cancer cells.

Chapter 4. Anticancer activities of SFN compared with its metabolites

4.1 Introduction

The absorption, distribution, metabolism, and excretion characteristics of bioactive agents influence their ultimate effectiveness. SFN undergoes extensive first-pass metabolism in the gut epithelium or liver via the mercapturic acid pathway summarized in Figure 4.1. It has not been determined whether the bioactivity of SFN is due to its conjugates themselves or to parent SFN released by deconjugation reactions. According to Conaway *et al*, the half-life of decomposition for the Cys conjugates were several fold shorter than that for respective GSH conjugates, while the NAC conjugates had the longest at pH 7.4 and 37 °C[295]. Other studies agreed with Conaway *et al* that the stability of SFN metabolites increased as the pH decreased; and that SFN-NAC showed the longest decomposition half-life among all the metabolites in human plasma[296]. It was speculated that conjugates could be regarded as a transport form of SFN as they are unstable and readily dissociate to SFN or undergo exchange reactions with free thiols[297]. However, the greater solubility in aqueous media of these metabolites plus the different distribution of concentrations observed in the process of metabolism, suggests that they would be a preferred form for clinical chemoprevention trials in certain cases.

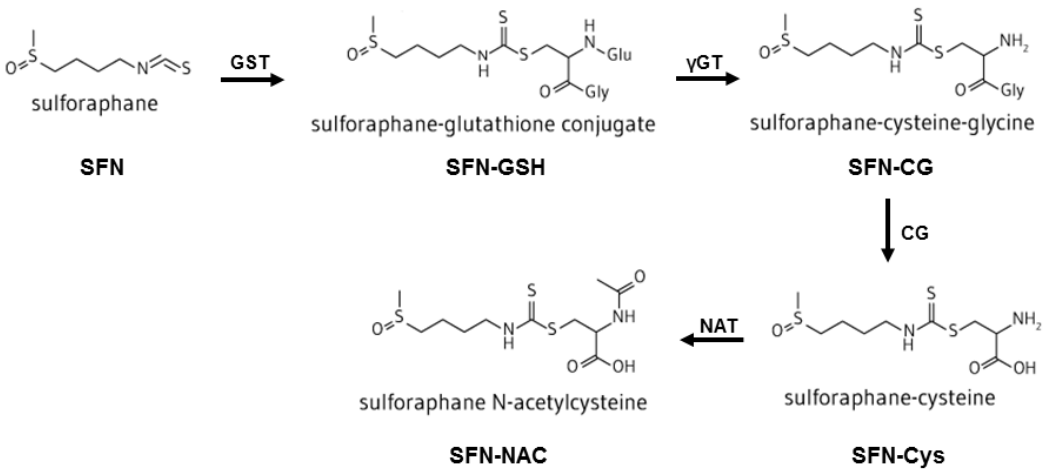

Figure 4.1 The mercapturic acid pathway of SFN.

Several studies have shown the potency of those metabolites as chemopreventive agents. SFN and SFN-GSH concentrations in the small intestine were 3 -13 nmol/g of tissue and 14-32 nmol/g of tissue respectively in a mouse feeding model[298], and both of them increased significantly the mRNA level of UGT1A1 and GSTA1 in HepG2 and HT29 cells[299]. SFN-Cys was reported to induce apoptosis in human non-small lung cancer cells[300] and to

suppress invasion in human prostate cancer cells[301]. SFN-NAC has been shown to exhibit equally if not more potent chemopreventive activities in comparison with SFN: in human prostate cancer LNCaP cell line model they have similar potentials to induce growth arrest and apoptosis[302]; they also inhibited lung adenoma induced by tobacco carcinogens and the development of adenomas to adenocarcinomas in mice[303]. In murine hepatoma cells both SFN and SFN-NAC caused dose-related cell growth inhibition and NQO1 induction[304]. Most importantly, as the major excretory product found in the urine with much higher concentrations compared to plasma[39], SFN-NAC has been studied to target bladder cancer[305]. Recent research has shown that SFN and its metabolites act as histone deacetylase (HDAC) inhibitors. Biochemical assays found that SFN metabolites did indeed inhibit HDAC activity *in vitro*, with the greatest inhibition involving SFN-NAC and SFN-Cys. Molecular modelling in the active site of an HDAC enzyme provided evidence that SFN-Cys fits within the HDAC pocket and had comparable geometry to known pharmacological HDAC inhibitors: trichostatin A and suberoylanilide hydroxamic acid in the active site, with the α-carboxyl group of the cysteine moiety forming a bidentate ligand with the buried zinc atom[306]. On the other hand, SFN is known to inhibit the activities of CYPs, namely CYP3A4 and CYP2D6, while these metabolites only showed inhibition on CYP2D6 in human liver microsomes[307]. Others reported that SFN-NAC were inactive as anti-initiators against azoxymethane induced colonic aberrant crypt foci compared with SFN in F344 rats feeding[308], and the induction of ARE by SFN was 8.6-fold higher than that by SFN-NAC in HepG2-C8 cells[280].

The cytotoxic and cytoprotective effect of SFN on HHL5 and HepG2 cells was demonstrated in the previous Chapter. Since there are very few studies that focused on the bioactivity of SFN metabolites, this study aims to compare the anticancer activity of SFN with its metabolites: SFN-GSH, SFN-Cys, and SFN-NAC.

4.2 Results

4.2.1 Cytotoxicity, genotoxicity and tumorigenicity of SFN vs its metabolites

The cytotoxic potential of SFN and its metabolites SFN-GSH, SFN-Cys and SFN-NAC were determined in HHL5 and HepG2 cells by MTT assay. As shown in Figure 4.2, all these compounds induced cytotoxicity in a dose-dependent manner in both cell lines. At the highest concentrations tested, SFN showed stronger cytotoxicity than three of its metabolites in both cell lines ($p < 0.01$). In HHL5, SFN-Cys exhibited less cytotoxicity than other metabolites; while in HepG2, there was no significant differences between the cytotoxicity from metabolites.

The genotoxicity of SFN was examined previously in Chapter 3, results showed that at 20 μM, SFN caused significant DNA damage in both cell lines after 24 hours. To test whether there was a significant difference between the genotoxicity of SFN and its metabolites, cells were treated with 20 μM SFN or its metabolites for 24 hours and the DNA damage was measured by comet assay. As shown in Figure 4.3, data from the SFN group agreed with previous data and there was no significant difference between SFN and these three metabolites.

To further evaluate the effects of SFN and its metabolites on cancer cell growth, a colony formation assay was conducted with HepG2 cells. Figure 4.4A showed colonies formed following SFN treatment compared to controls, quantitative results indicated that SFN suppressed the formation of colonies in a dose-dependent manner (Figure 4.4B). 10 μM was chosen when comparing SFN with its metabolites, as shown in Figure 4.4C, there was no significant difference between the inhibitory effect of SFN and its metabolites on HepG2 colony formation.

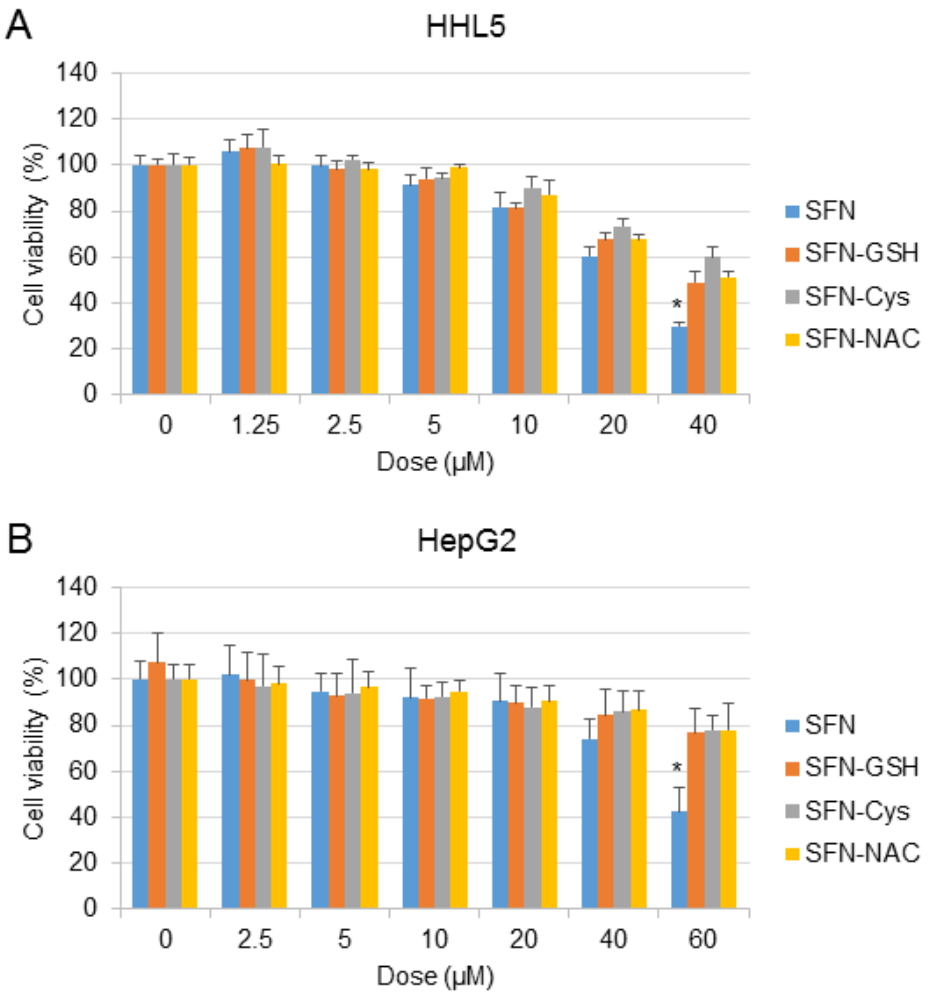

Figure 4.2 Effect of SFN and its metabolites on cell viability in HHL5 and HepG2 cells. (A) HHL5 and (B) HepG2 cells were treated with different doses of SFN or its metabolites for 24 hours, then cell viability was determined by MTT assay with DMSO (0.1%) as control. Result represents the mean ± SD ($n \geq 5$). Statistical significance within groups treated with the same dose, *$p < 0.05$, **$p < 0.01$.

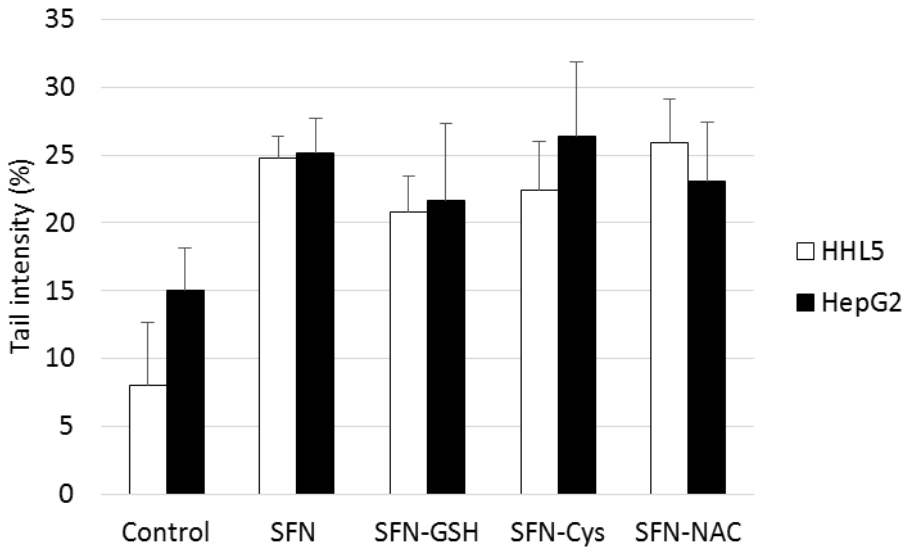

Figure 4.3 Effect of SFN and its metabolites on DNA damage in HHL5 and HepG2 cells. Cells were treated with 10 μM SFN or metabolites with DMSO (0.1%) as control for 24 hours, then DNA damage was determined by comet assay. Tail intensity was measured for at least 100 comets per sample.

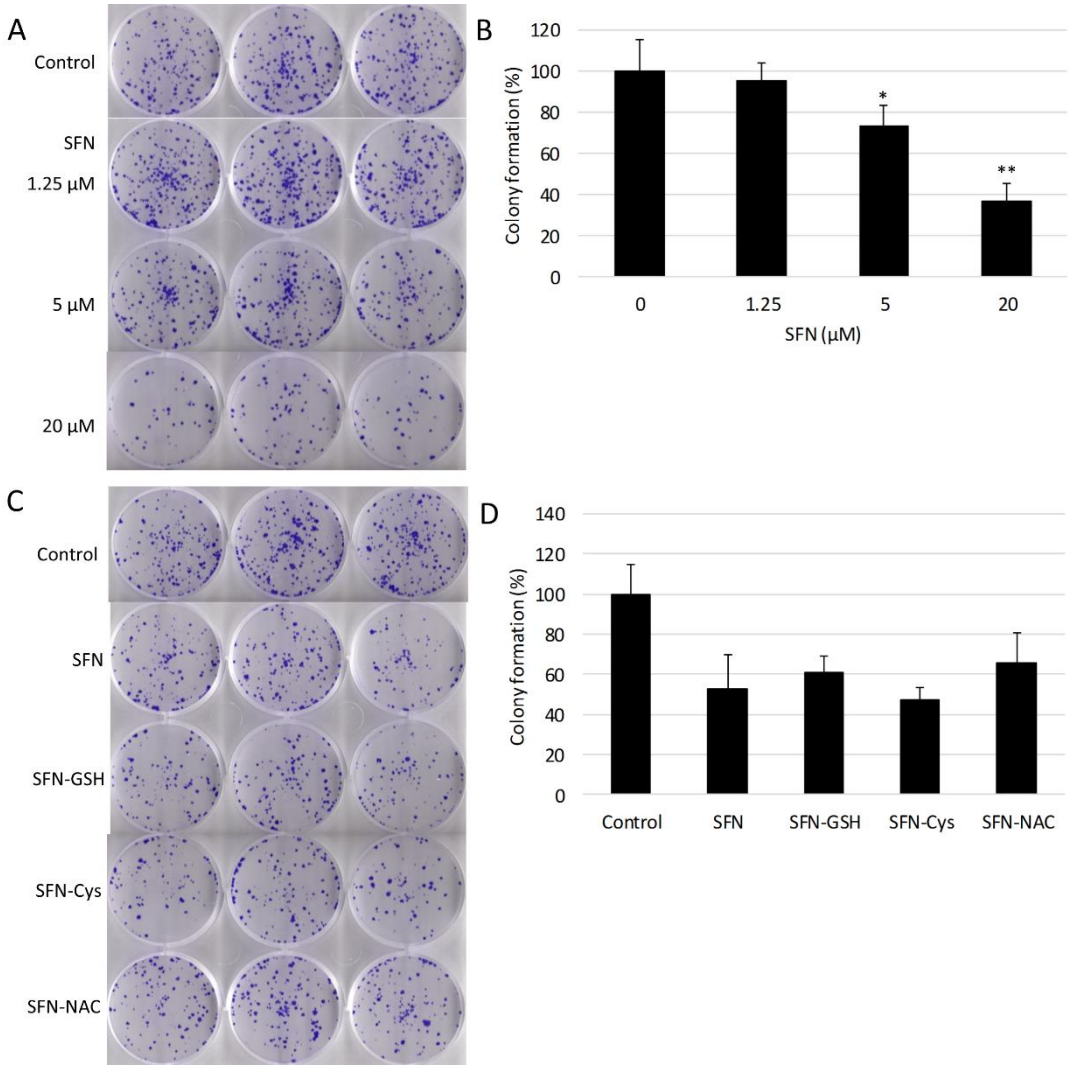

Figure 4.4 Effect of SFN and its metabolites on HepG2 colony formation. Cells were treated with 1.25, 5 and 20 µM SFN with DMSO (0.1%) as control for 24 hours, then seeded into 6-well plates at a density of 2 × 10^3 cells/well in triplicate per treatment. After 14 days of incubation, formed colonies were stained for photograph (A) and quantified (B). Statistical significance from the control, *$p < 0.05$, **$p < 0.01$. (C) HepG2 cells were treated with 10 µM SFN or metabolites with DMSO (0.1%) as control, followed by colony formation as above. Formed colonies were stained for photograph (C) and quantified (D). Result represents the mean ± SD (n = 3).

4.2.2 Effect of SFN vs its metabolites on cancer cell migration

Given that migration of cancer cells is an essential step for tumour metastasis and cell adhesion ability could help tumour cells colonize at new sites during metastasis[309], further investigation to whether SFN and its metabolites affect cell migration and adhesion was conducted.

Wound assays were performed to measure HepG2 cell migration after 48 hours under different doses of SFN treatment. As shown in Figure 4.5, SFN potently inhibited cell migration of HepG2 cells in a dose-dependent manner. At 20 μM, SFN reduced cell migration to 70.8% compared to control (0.1% DMSO). However, there was no significant difference between SFN and its metabolites in terms of their ability to inhibit cell migration.

The effect of SFN and its metabolites on cell-ECM interactions were measured by adhesion assay (Figure 4.6). 96-well plates were coated with two major kinds of ECM proteins: type I collagen and fibronectin, and PLL as a negative control for integrin-based cell adhesion. After a 1.5 hours incubation, HepG2 cell adhesion ability under different doses of SFN treatment was quantified. Results showed that SFN suppressed adhesion of HepG2 cells to all three coatings of ECM, with the strongest influence on collagen and weakest on PLL. 20 μM SFN significantly inhibited cell adhesion on both collagen and fibronectin but not PLL, further comparison studies with 20 μM SFN or its three metabolites in adhesion assays showed that the metabolites did not change the selectivity towards ECM and their inhibitory effects were not as strong as the effect of SFN.

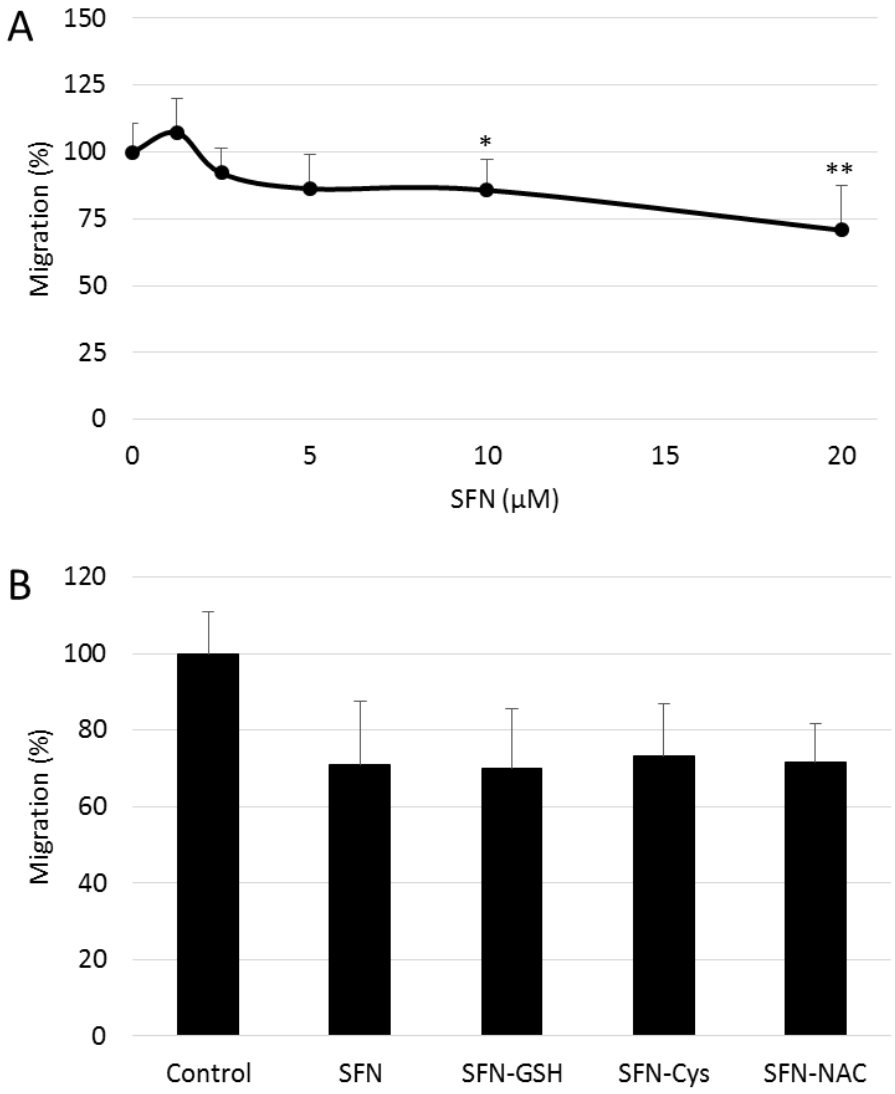

Figure 4.5 Effect of SFN and its metabolites on HepG2 cell migration. Cells were treated with 1.25 to 20 µM SFN (A) or 20 µM SFN or metabolites (B) for 48 hours with DMSO (0.1%) as control, cell migration was then measured by wound assay. Data are presented as mean ± SD ($n \geq 5$), *$p < 0.05$, ** $p < 0.01$ compared to control.

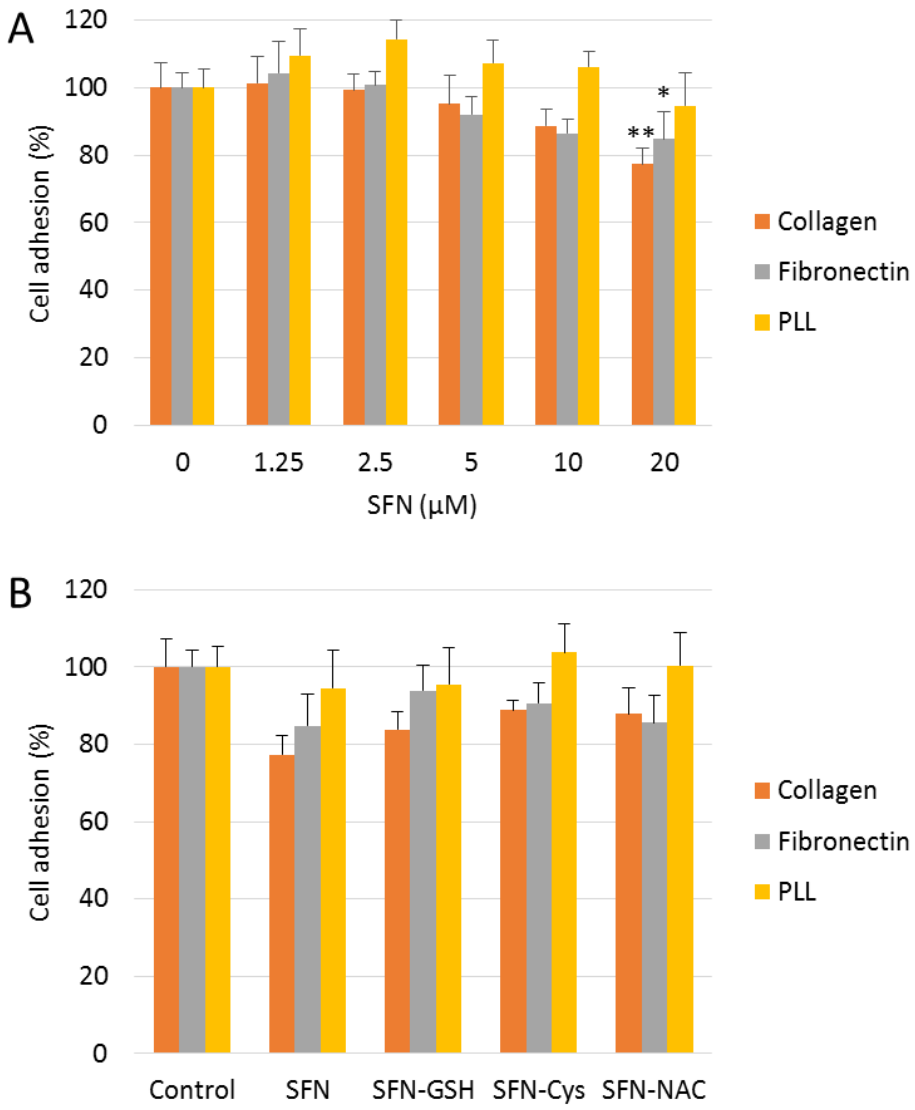

Figure 4.6 Effect of SFN and its metabolites on HepG2 cell adhesion. Cells were treated with 1.25 to 20 µM SFN (A) or 20 µM SFN or metabolites (B) for 1.5 hours with DMSO (0.1%) as control was measured by adhesion assay. Data are presented as mean ± SD ($n \geq 6$), *$p < 0.05$, ** $p < 0.01$ compared to control.

4.2.3 Effect of SFN vs its metabolites on angiogenesis

Angiogenesis, a process leading to the formation of new blood vessels, is required for both cancer progression and metastasis[247]. HUVEC populations are very responsive to compounds that modulate angiogenic responses, so HUVECs were used to examine the anti-angiogenic effects of SFN compared with its metabolites. Firstly, their effects on cell viability was tested by MTT assay after 24h treatment. As shown in Figure 4.7A, a dose-dependent inhibition in cell viability was observed from both SFN and its metabolites compared to DMSO control. SFN showed the highest cytotoxicity compared with SFN-Cys, SFN-NAC and SFN-GSH.

Secondly, the effect on HUVEC migration was measured using a wound assay (Figure 4.7B). At 12 hours, 20 µM SFN significantly reduced HUVEC migration to the wound area indicated by a nearly 2-fold increase of the wound area compared to control, while SFN-Cys and SFN-NAC exhibited inhibitory effects similar to that of SFN, but SFN-GSH significantly less effective in inhibiting HUVEC cell migration ($p < 0.01$).

Finally, the effect of SFN and its metabolites on tube formation was examined in the 3D co-culture HUVEC with pericytes model (Figure 4.8). 10 µM SFN significantly inhibited tube formation of HUVECs, the average total tube length was 3.37 and 0.99 mm/mm^2 in the control and SFN treated groups. At the same dose, there was no significant difference between this inhibitory effect using SFN, SFN-Cys or SFN-NAC; SFN-GSH however, showed a modestly weaker inhibition (1.46 mm/mm^2 total tube length).

In conclusion, SFN remain the strongest inhibitor to HUVEC cell viability, migration and tube formation, followed by SFN-Cys and SFN-NAC, SFN-GSH showed the weakest inhibitory effect among all the metabolites.

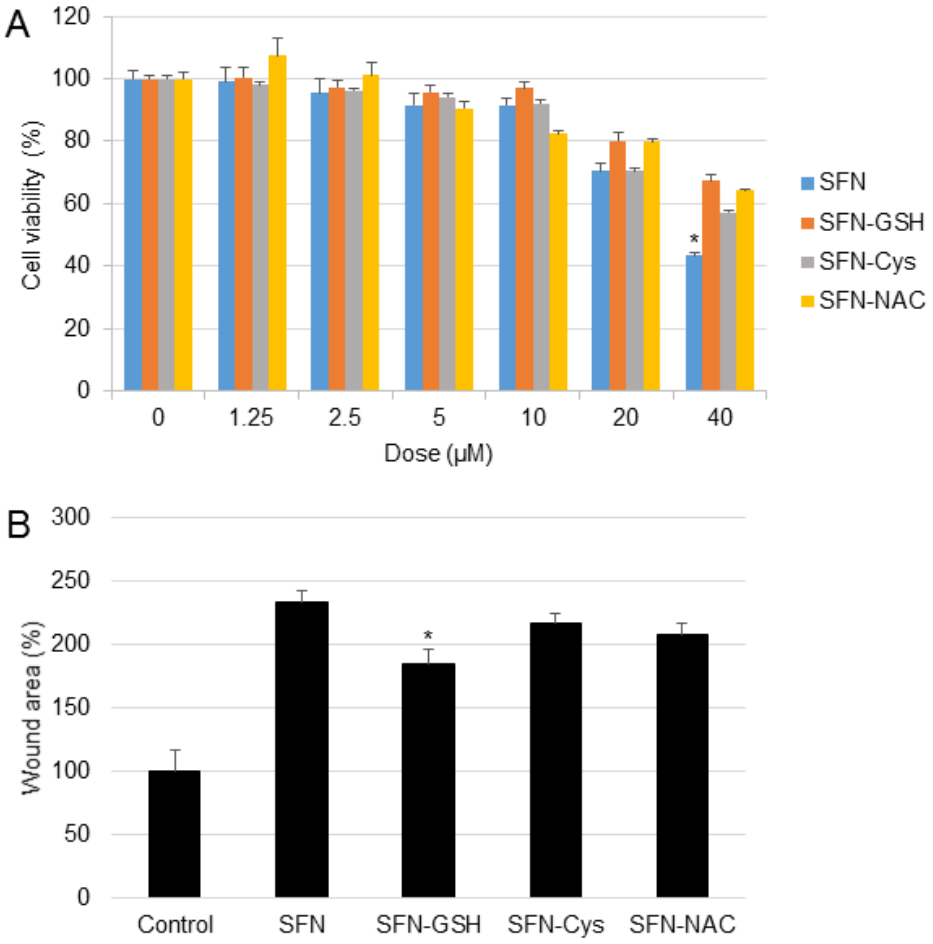

Figure 4.7 Effect of SFN and its metabolites on HUVEC cell viability and migration. (A) Cells were treated with 1.25 to 40 μM SFN or its metabolites for 24 hours with DMSO (0.1%) as control, cell viability was then determined by MTT assay. Result represents the mean ± SD (n ≥ 5). Statistical significance within groups treated with the same dose, *p < 0.05. (B) Cell migration at 12 hours 20 μM SFN or its metabolites with DMSO (0.1%) as control was measured by wound assay. Data are presented as mean ± SD (n ≥ 5), *p < 0.05 compared to SFN treated group.

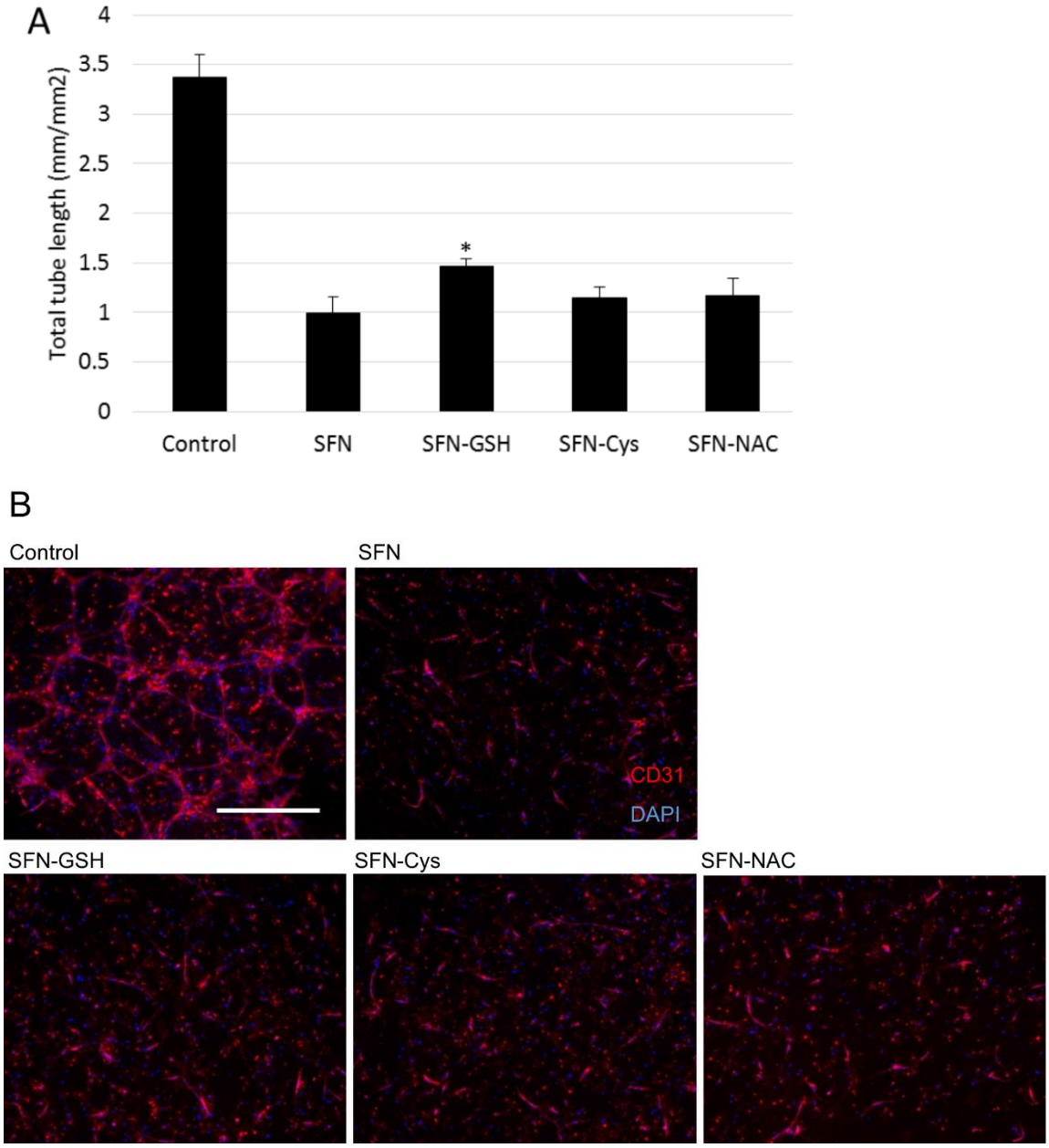

Figure 4.8 Effect of SFN and its metabolites on HUVEC tube formation in the 3D co-culture with pericytes. (A) The total lengths of CD31 positive tubes formed in treated groups (10 µM SFN or its metabolites) with DMSO (0.1%) as control were measured and expressed as mean ± SD (n≥3), *p < 0.05 compared to SFN treated group. (B) Representative pictures from 3D co-culture. HUVEC were identified by immunodetection of CD31 (red), nuclei were stained (blue) and merged pictures are shown. Scale bar = 500 µm.

4.2.4 Protective effect of SFN vs its metabolites against H_2O_2

Based on the results of the protective effect of SFN against H_2O_2-induced cell death in HHL5 and HepG2 (Figure 3.4A), 2.5 and 10 μM were chosen to be the tested concentrations for SFN and its metabolites. Cells were pre-treated with SFN or metabolites for 24 hours followed by H_2O_2 treatment for another 24 hours, cell viability was measured by MTT assay. Results indicated that in HHL5, pre-treatment of 2.5 μM but not 10 μM of SFN or its metabolites reduced H_2O_2-induced cell death; while in HepG2, both 2.5 and 10 μM pre-treatment showed a protective effect. In general, all three of the metabolites exhibited similar protective effects against H_2O_2 compared to SFN in both cell lines (Figure 4.9A);

According to previous data (Figure 3.5A), 24 hours pre-treatment with 5 μM SFN significantly inhibited H_2O_2-induced DNA damage in HHL5 and HepG2 cells. Here, the protective effect of 5 μM SFN and its metabolites in both cell lines was measured by comet assay as previously. As shown in Figure 4.9B, SFN pre-treatment agreed with previous data, and there was no significant difference between the protective effect of SFN and its metabolites in both cell lines.

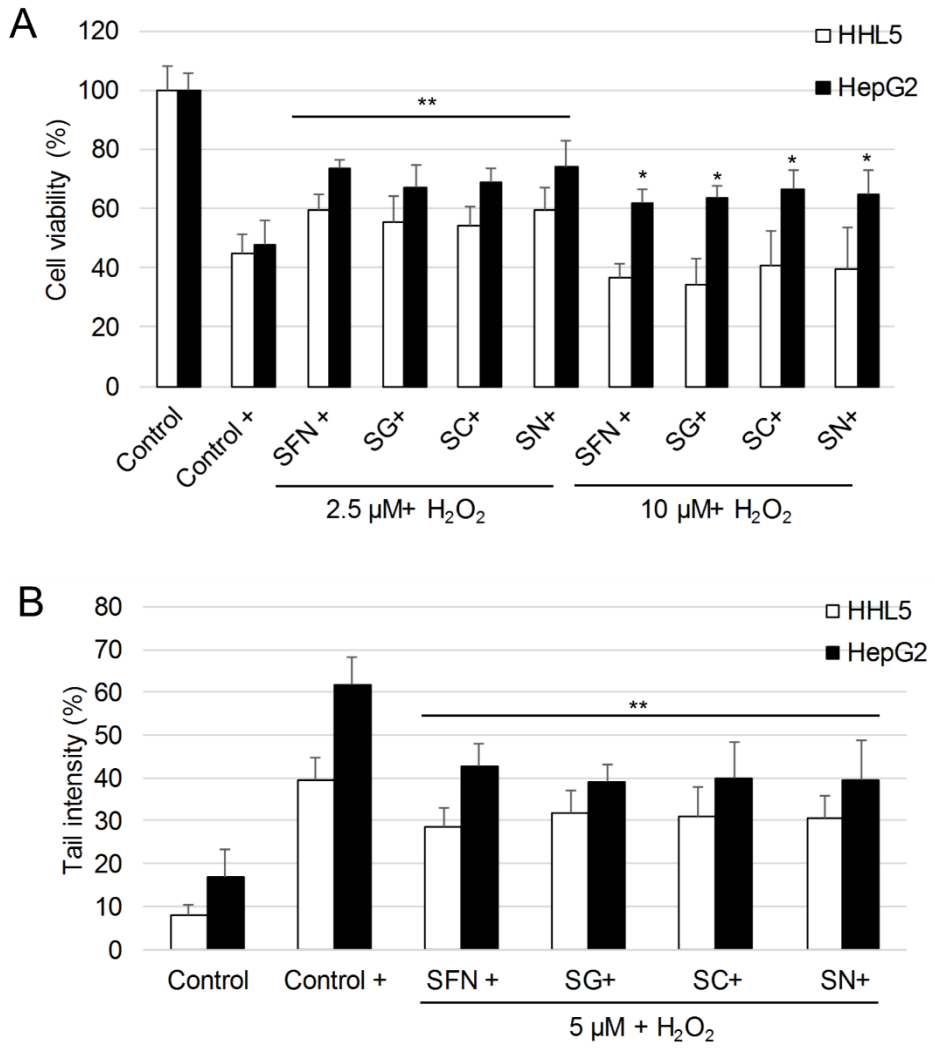

Figure 4.9. Protective effect of SFN and its metabolites against H_2O_2-induced cell injury. SG: SFN-GSH, SC: SFN-Cys, SN: SFN-NAC. (A) Cells were pre-treated with 2.5 or 10 µM SFN or metabolites for 24 hours and then incubated with H_2O_2 for another 24 hours. Cell viability was measured by MTT assay, result represents the mean ± SD ($n \geq 5$). (B) Cells were pre-treated with 5 µM SFN or metabolites for 24 hours and then incubated with H_2O_2 for another 30 mins. DNA damage was measured by comet assay. Tail intensity were measured for at least 100 comets per sample. Statistical significance from H_2O_2 control, *$p < 0.05$, **$p < 0.01$.

4.2.5 Effect of SFN vs its metabolites on Nrf2 and GSH

Since SFN can induce the translocation of Nrf2 to the nucleus in both cell lines in a time- and dose- dependent manner as shown in Figure 3.7, the same method was used to examine the function of its metabolites in terms of Nrf2 translocation and downstream phase II enzyme expression: TrxR1, NQO1 and HO-1.

As illustrated in Figure 4.10A, 10 μM SFN and its metabolites induced a clear increase of nuclear Nrf2 protein levels in both cell lines at 4 hours and 18 hours, and no significant difference was observed between SFN and its metabolites in activation of Nrf2 translocation into the nucleus. To determine whether the nuclear accumulation of Nrf2 by SFN and its metabolites resulted in the up-regulation of Nrf2 target genes, the expression of TrxR1, NQO1 and HO-1 was measured after 24 hours by Western blotting. Results showed remarkable increases of the target protein levels trigged by SFN and its metabolites, which suggested that the nuclear translocation of Nrf2 had a functional downstream effect. Again, the metabolites showed similar induction of TrxR1, NQO1 and HO-1 compared to SFN in both cell lines (Figure 4.10B).

The intracellular GSH changes at 24 hours in both cell lines were also measured using HPLC with DMSO (0.1%) as control. Both SFN and three of its metabolites induced at least a 2-fold increase of GSH level in HHL5 and HepG2 cells, and there was no significant difference between SFN and its metabolites (Figure 4.10C).

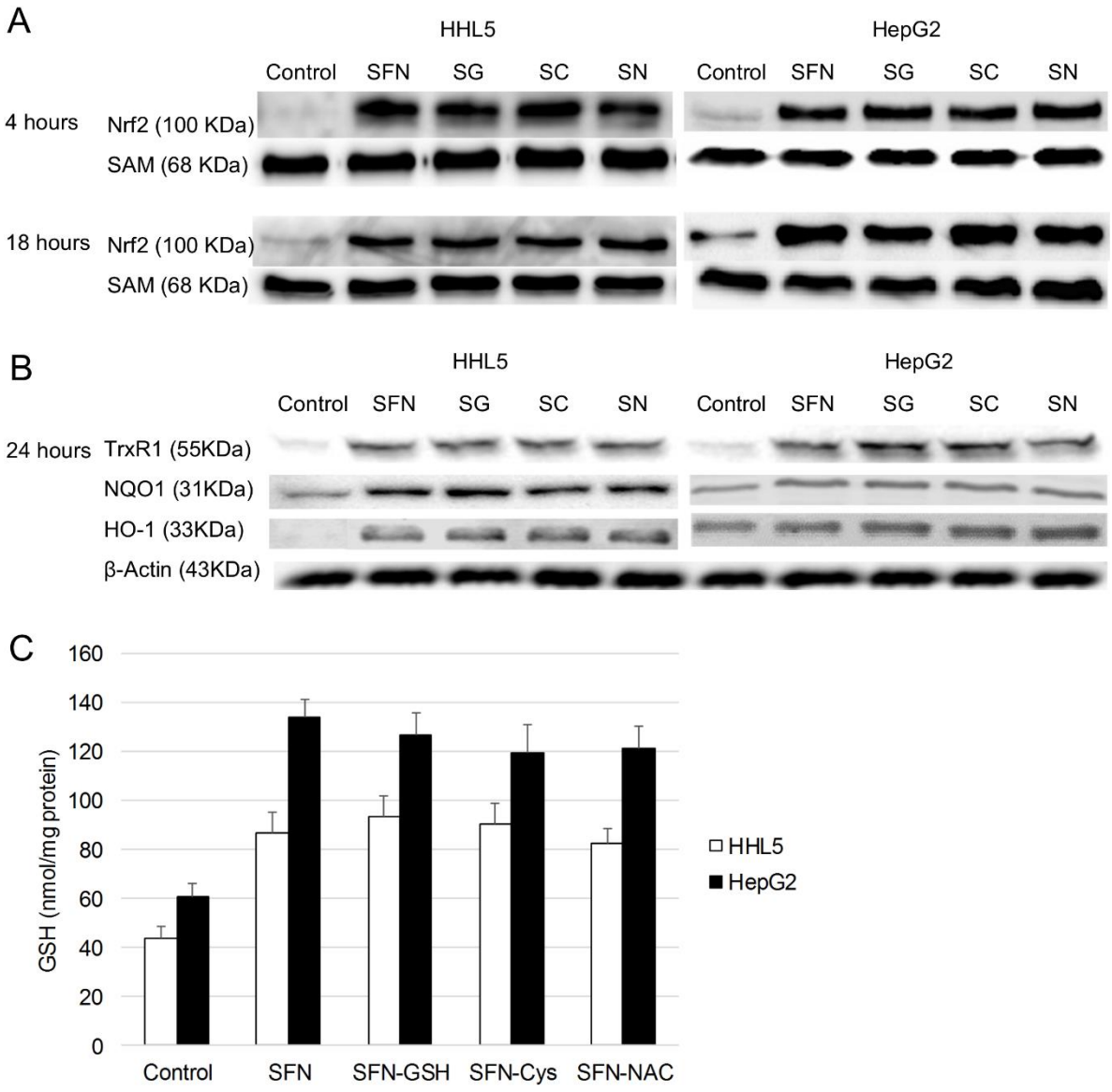

Figure 4.10 Effect of SFN and its metabolites on Nrf2 signalling activation and GSH induction. (A) Cells were treated with 10 μM SFN or its metabolites for 4 or 18 hours with DMSO (0.1%) as control. Nuclear protein was extracted and Nrf2 was detected by Western blotting. SAM was used as a loading control. (B) Cells were treated with 10 μM SFN or its metabolites for 24 hours with DMSO (0.1%) as control. Whole cell lysates were collected and TrxR1, NQO1, HO-1 were detected by Western blot. β-actin was used as a loading control. SG: SFN-GSH, SC: SFN-Cys, SN: SFN-NAC. (C) Cells were treated with 10 μM SFN or its metabolites for 24 hours with DMSO (0.1%) as control. The intracellular GSH level was measured by HPLC, results represented as the mean ± SD (n = 3).

4.3 Discussion

In mice, immediate increases in the levels of SFN and its metabolites in plasma have been shown after oral administration[310]. The metabolites were produced within minutes after cellular uptake of SFN, and some showed longer decomposition time than SFN in the plasma, and also a different tissue distribution profile[298,311,312]. These observations point to the potential relevance for cancer protection of greater knowledge about the biological activity of these metabolites.

SFN suppresses cancer development through various molecular targets that are involved in controlling cell proliferation, differentiation, apoptosis/autophagy, or cell cycle[67,313]. More recently, SFN has been found to induce DNA single[118] or double-strand[314] breaks and inhibit nucleotide-excision repair[123]; suppress cancer stemness[315]; metastatic and angiogenic potentials[67,316]. Here, three major metabolites of SFN: SFN-GSH, SFN-Cys and SFN-NAC were examined in terms of their cytotoxicity and genotoxicity in HHL5 and HepG2 cell lines, in comparison to SFN. The metabolites inhibited cell viability in a dose-dependent way without changing the selectivity of SFN, i.e. like SFN, all metabolites were more toxic towards HHL5 than HepG2. In addition, metabolites were less toxic compared to SFN especially in high doses (> 40 μM) in both cell lines. Both SFN and the metabolites induced significant DNA damage evidenced in comet assay, and no significant difference was found between the DNA damage caused by SFN or any of the metabolites in both cell lines.

To further compare the anticancer activities of the metabolites with SFN, their effects on colony formation, cell migration and adhesion were studied in HepG2 cells. SFN suppressed the formation of colonies and cell motility in HepG2 cells in a dose-dependent manner. Using the same dose, its metabolites showed similar or slight weaker inhibitory effects. Notably, SFN selectively inhibited HepG2 cell adhesion on collagen compared to that on fibronectin and poly-l-lysine; and its metabolites showed the same selectivity. This indicated SFN and its metabolites influenced collagen-mediated cell adhesion which could be associated with the integrins alpha 1,2,10,11 in a heterodimer with beta1[317,318]. The effects of SFN on cancer cell motility has been reported. It inhibited cell migration in human gastric cancer cells[132], bladder cancer cells[180], prostate cancer cells[319], oral carcinoma cells[130], and in human glioblastoma cells[320]. SFN also supressed cancer cell migration by supressing EMT[137,321]. It also inhibited hypoxia-induced migration of human colon cancer cells[134] and ovarian carcinoma cells[322]; and 12-O-tetradecanoyl phorbol-13-acetate induced cell invasion by suppressing NF-κB pathway in breast cancer cells[323]. Here SFN decreased HepG2 cell

migration which agreed with a previous study[136], and the inhibitory effect of SFN metabolites: SFN-GSH, SFN-Cys, and SFN-NAC was also confirmed consistent with SFN itself.

Angiogenesis is a prerequisite for tumour growth and metastasis[95]. The effects of SFN and its metabolites on HUVECs viability, migration and tube formation were compared for the first time. Results showed that SFN-Cys and SFN-NAC exhibited similar inhibition effects compared with SFN on HUVEC cell viability, migration and tube formation, while SFN-GSH showed significant weaker inhibition of HUVEC cell migration. ECs have been reported as a novel target of SFN action both *in vitro* and *in vivo*[145,146,324], further investigation was conducted in Chapter 5.

The nuclear accumulation of Nrf2 in both HHL5 and HepG2 cells was induced by SFN as well as three of its metabolites. Previous studies have demonstrated that SFN induced TrxR-1 expression in dose- and time-dependent manners in HHL-5 and HepG2[80,325]. Here the induction of TrxR1, NQO1 and HO-1 protein levels from 24 hours treatment of SFN or its metabolites in both cell lines were confirmed. No significant difference was observed between SFN and its metabolites in terms of their ability to activate Nrf2 translocation or to induce phase II enzymes. Further investigation of their effects on intracellular GSH also showed that SFN and its metabolites induced at least 2-fold increase of GSH after 24 hours in both cell lines. These data indicated the potential chemopreventive effect of SFN metabolites. Indeed, these metabolites showed similar protective effects against H_2O_2-induced cell death and DNA damage in HHL5 and HepG2 cells compared to SFN.

In summary, this study confirmed three of the major metabolites of SFN: SFN-GSH, SFN-Cys and SFN-NAC could decrease cell viability, induce DNA damage at high doses (>20 μM) whilst protecting against H_2O_2-induced cell damage at lower doses (2.5-10 μM). There was no significant difference between SFN and its metabolites in activation of Nrf2 and downstream gene expression, as well as to increase intracellular GSH. In HepG2 cells, they showed similar inhibitory effects on colony formation, cell migration and adhesion. Furthermore, both SFN and its metabolites inhibited angiogenic processes such as EC proliferation, migration and tube formation. These results provide compelling evidence that the principal metabolites of SFN retain the anticancer activity of the parent molecule, and that it is necessary to study SFN metabolites using *in vivo* models.

Chapter 5. Anti-angiogenic effects of SFN in HCC

5.1 Introduction

Hepatocellular carcinoma (HCC) is the sixth most common cancer worldwide, and one of the most common causes of cancer death[232]. High mortality rates were reported in Asia and Africa, especially in less-developed regions[326]. Surgical resection or transplantation of liver offers the best prognosis among other limited treatments, but only 15% of HCC patients are suitable for surgical intervention after initial diagnosis. Non-surgical treatment is still in demand; however, most forms of HCC are highly radio- and chemo-resistant and desirable therapeutic outcome is often elusive in clinical cases[327]. Therefore, the development of new therapeutic agents for HCC patients is a priority.

Angiogenesis is believed to play a central role in the development and progression of HCC which is one of the most vascularized solid tumours possessing high micro-vessel density[328]. Angiogenesis is a complex process consisting of the release of angiogenic factors, binding of angiogenic factors to receptors on ECs, EC activation, migration and proliferation, remodelling of the ECM and tube formation[141]. Recent evidence suggests that tumour angiogenesis, including HCC, involves cascades of signalling between tumour cells and the host stroma microenvironment and leads to the formation of structurally and functionally abnormal vessels which contribute to tumour growth and metastasis[329]. All these steps provide opportunities to halt tumour growth and even promote tumour regression, thus angiogenesis pathways represent an attractive therapeutic target for HCC. Sorafenib, a multi-kinase inhibitor targeting amongst others VEGFR1, VEGFR2, and VEGFR3, was approved in 2008 for patients with advanced HCC. Many more antiangiogenic agents have reached advanced phases of development for the treatment of HCC[330]. However, the therapeutic efficacy of these agents proved to be limited because of acquired drug resistance, serious toxic side effects and high cost[327,329,331]. Therefore, the identification of alternative agents targeting angiogenesis is considered an important strategy both for HCC prevention and treatment.

In the case of HCC, SFN has shown chemopreventive[332–334] and chemotherapeutic effects. It was found to decrease cell viability, telomerase activity[256], and to induce apoptosis in hepatocellular carcinoma cells[335,336] as well as in an orthotopic xenograft tumour model of HCC[266]. SFN also amplified TRAIL induced apoptotic signalling in TRAIL-resistant hepatoma cells[337] and sensitized the radiosensitivity of HCC cells by blocking the NF-kB pathway[338].

According to Wu *et al*, SFN also inhibits TGF-β-induced epithelial-mesenchymal transition of hepatocellular carcinoma cells via the ROS-dependent pathway[136]. A randomized, placebo-controlled trial showed that the disposition of aflatoxin and phenanthrene, both of which could lead to high risk of HCC, was altered by the administration of glucosinolate-rich broccoli sprout preparations[166].

More recently, the effects of SFN on endothelial cell functions have been reported *in vitro*[339,340] as well as *in vivo*[146]. SFN has been reported to inhibit NF-κB-regulated VEGF expression in human prostate cancer cells[341]; and hypoxia-induced HIF-1α and VEGF expression in human colon cancer cells[134]. It can also reduce the production of several pro-inflammatory cytokines and pro-angiogenic growth factors in human breast cancer cells[342]; and enhance the therapeutic efficacy of TRAIL in a prostate cancer orthotopic model through regulation of apoptosis, metastasis, and angiogenesis[147].

Significantly, the effect of SFN on HCC angiogenesis has not been reported. To test the hypothesis that SFN would not only affect EC function but also the interaction between HCC cells and ECs, which would result in the suppression of tumour growth, HUVEC and HepG2 cells were employed to investigate the anti-angiogenic potential of SFN *in vitro*. *Ex vivo* aortic ring and *in vivo* tumour-bearing CAM models were also used to confirm the anticancer properties of SFN. Our findings indicated that SFN inhibited HepG2-induced angiogenesis and that this was associated with the inhibition of STAT3/ HIF-1α /VEGF signalling. Thus, the use of SFN could present a strategy for prevention and treatment of HCC.

5.2 Results

5.2.1 Effect of SFN on HUVEC cell viability and migration

Proliferation and migration are essential characteristics of ECs for the generation of new blood vessels. The MTT assay was employed to evaluate the toxicity of SFN to HUVEC cells. Cells were incubated with different doses of SFN for 24 hours. Results showed SFN inhibited cell viability in a dose-dependent manner (Figure 5.1A). As determined with logarithmic regression analyses, the IC_{50} of 24 hour SFN treatment was approximately 39.1 μM against HUVEC. In further experiments, 0 - 20 μM SFN dose was used to avoid a strong toxicity effect.

To analyse the effect of SFN on HUVEC cell migration, a wound assay was performed on confluent monolayers of HUVEC cells. Vehicle control (0.1% DMSO) reformed a confluent monolayer within 24 hours so a 12-hour time point was chosen. SFN was tested across a concentration range of 1.25-20 μM. As showed in Figure 5.1B, SFN treatment inhibited HUVEC migration into the wound in a dose-dependent manner shown as the increased wound area compared to control.

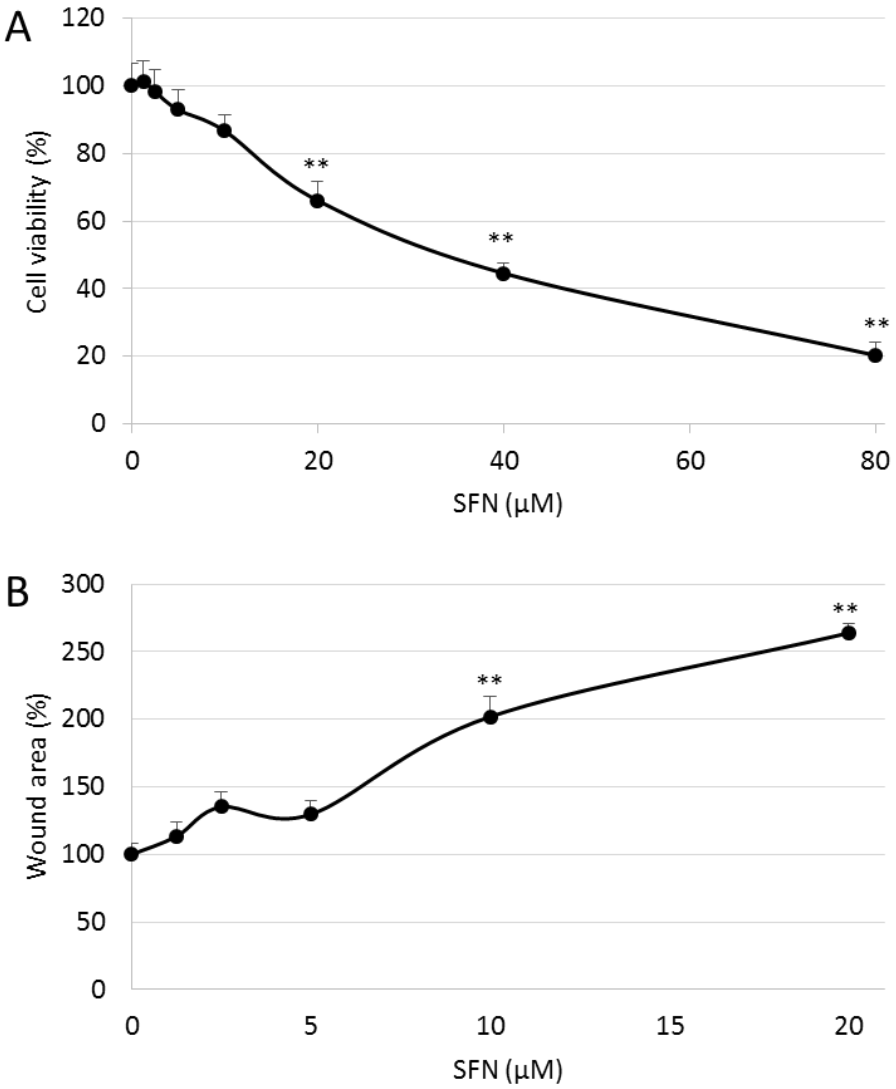

Figure 5.1 Effect of SFN on cell viability and migration of HUVECs. (A) Cell viability at 24 hours SFN treatment was determined by MTT assay. (B) Cell migration at 12 hours SFN treatment was measured by wound assay. Data are presented as mean ± SD ($n \geq 5$), **$p < 0.01$ compared to control.

5.2.2 Effect of SFN on tube formation and microvessel sprouting

It has become evident that the establishment of functional capillary networks by ECs, a crucial step for angiogenesis, depends heavily on the interactions and communications between ECs and the surrounding cells. A 3D co-culture model of HUVEC and pericytes M2 was used to study the effect of SFN on HUVEC tube formation (Figure 5.2A and B). When cultured in collagen with pericytes, HUVECs form three-dimensional, capillary-like tubular structures. SFN at 10 μM reduced tube formation by 46% compared to control. The destructive effect suggested that SFN could disrupt the formation of enclosed capillary networks of HUVECs.

The effect of SFN on angiogenesis was further explored in a 3D *ex vivo* mouse aortic ring assay (Figure 5.3A and B). This model approximates the complexities of angiogenesis *in vivo*, from endothelial cell activation to pericyte acquisition and remodelling. The microvessels sprouting from aortic rings embedded in collagen formed a network of vessels after around 5 days, while 5 μM SFN notably inhibited sprouting of microvessels. Together, these data demonstrated that SFN could inhibit angiogenesis.

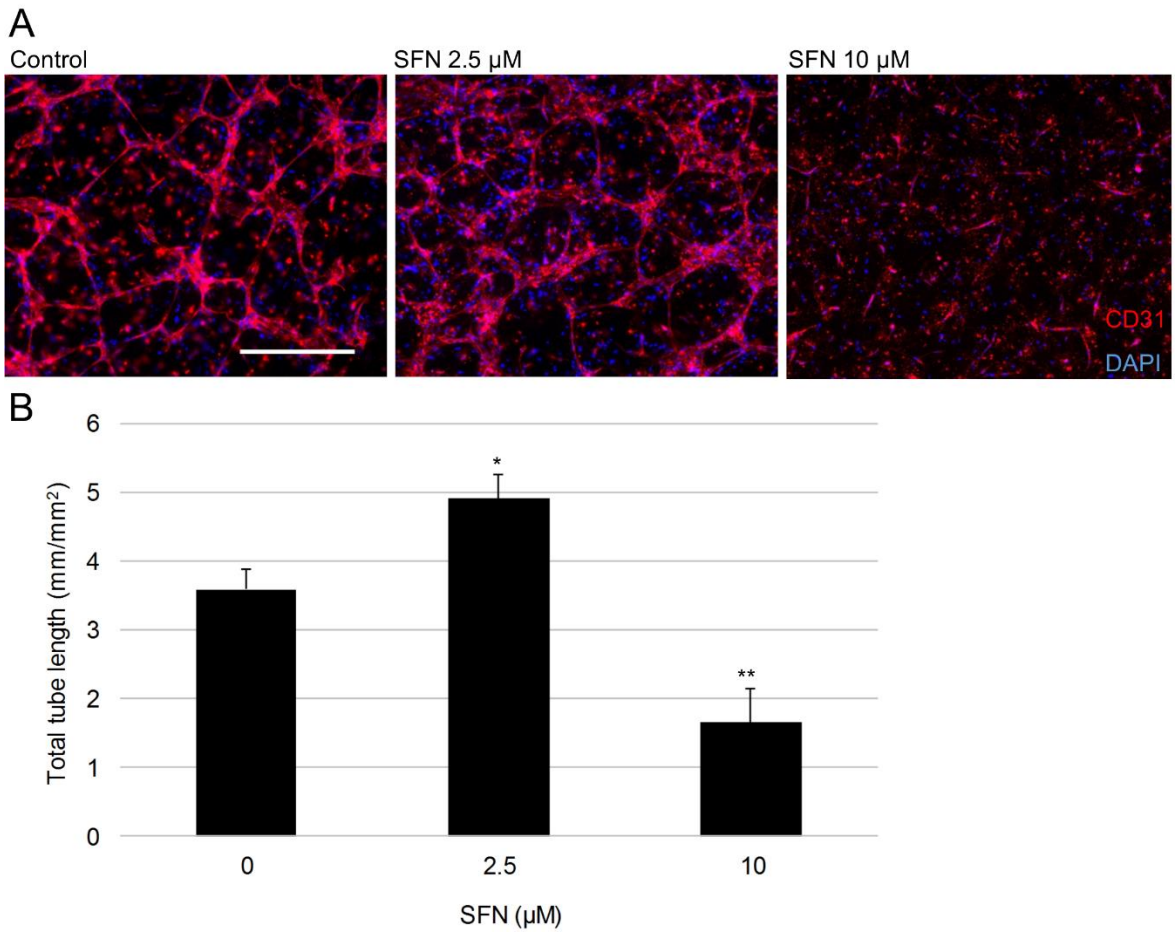

Figure 5.2 Effect of SFN on tube formation of HUVECs in the 3D co-culture with pericytes model. (A) Representative pictures from 3D co-culture of HUVECs and pericytes M2 at day 4 with SFN 0, 2.5, 10 µM. HUVEC were identified by immunodetection of CD31 (red), nuclei were stained (blue) and merged pictures are shown. Scale bar = 500 µm. (B) Total lengths of CD31 positive tubes were measured and expressed as mean ± SD (n≥5), *p < 0.05, ** p< 0.01 compared to control.

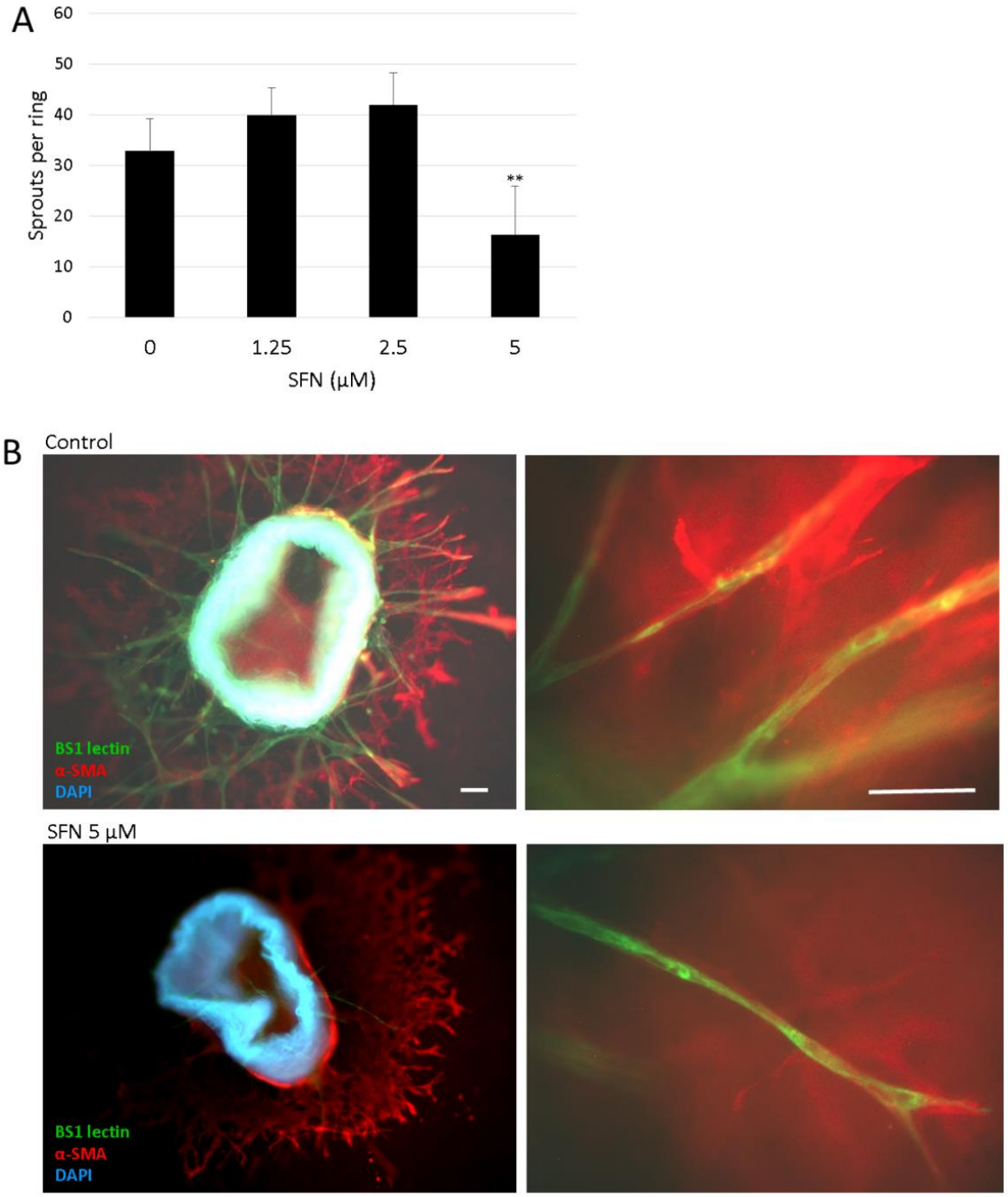

Figure 5.3 Effect of SFN on microvessel sprouting in mouse aortic rings. (A) Dose response of SFN on microvessel sprouting from aortic rings embedded in collagen with DMSO (0.1%) as control. Data are presented as mean ± SD ($n \geq 5$), $^{**}p < 0.01$ compared to control. (B) Representative pictures from the immunofluorescent staining of aortic rings. Endothelial sprouts were stained with BS1-lectin-FITC (green), supporting cells were stained for α-smooth muscle actin (red), nuclei were stained with DAPI (blue) and merged pictures are shown. Scale bar = 100 µm.

5.2.3 Effect of SFN on HepG2 stimulated migration, adhesion and tube formation of HUVECs

Interaction between cancer cells and ECs is implicated in tumour angiogenesis and metastasis[343]. Therefore, the effect of HepG2 cells on HUVEC cell migration, adhesion and tube formation, in addition to the role of SFN in the interaction between HepG2 and HUVEC cells was examined. The cytotoxicity of SFN on HepG2 was assessed (Figure 3.1) and doses without a significant cytotoxic effect (≤ 20 μM) were used in all experiments.

Firstly, the effect of SFN on the potential of HepG2 cells to promote migration of the HUVECs was investigated. HepG2 cells were treated with SFN at different doses for 24 hours, conditioned medium (CM) was then collected from DMSO treated groups (control CM) and from SFN (1.25-20 μM) treated groups. These CM were then used in the HUVEC wound assay to determine their effect on HUVEC migration (Figure 5.4A). Compared with serum-free controls, the gap area in control CM group was significantly smaller ($p<0.05$), indicating that CM from HepG2 cells stimulated HUVEC migration. In addition, this stimulation was suppressed by SFN treatment in a dose-dependent manner, which indicated that SFN treatment could inhibit the pro-migration effect of HepG2 cells on HUVECs.

The ability of HepG2 to recruit ECs was then tested using the cell adhesion assay. Adhesion of HUVECs was tested on the monolayer of HepG2 cells pre-treated with different doses of SFN for 24 hours; CD31 was used for in-well immunoblotting to measure the number of HUVECs. Results showed a dose-dependent decrease of HUVEC cell numbers adhered to SFN pre-treated HepG2 cells (Figure 5.4B), which indicated the potential of HepG2 cells to attract HUVEC was significantly compromised by SFN treatment.

Finally, the 3D co-culture tube formation model was modified, using HUVEC and HepG2 cells to investigate the effect of SFN on the formation of vascularization induced by HepG2. Co-culture of HUVECs with pericytes was used as positive control and HUVECs alone as negative control. As shown in Figure 5.5, HUVECs alone did not show any tubular structures after 3 days while HUVECs co-cultured with pericytes did. More interestingly, HUVEC co-cultured with HepG2 displayed scattered distribution of tubular structures indicating HepG2 could induce tube formation of HUVECs but the formed tubes were less mature compared to those induced by pericytes. This might because vessels induced by cancer cells either via angiogenesis or vasculogenesis are usually structurally and functionally abnormal[344]. Treatment with SFN inhibited the formation of the cellular network induced by HepG2, with almost no capillary tubes visible upon 20 μM treatment. Overall, these results

showed that SFN treatment inhibited the HepG2-induced chemotactic motility and tube formation of ECs.

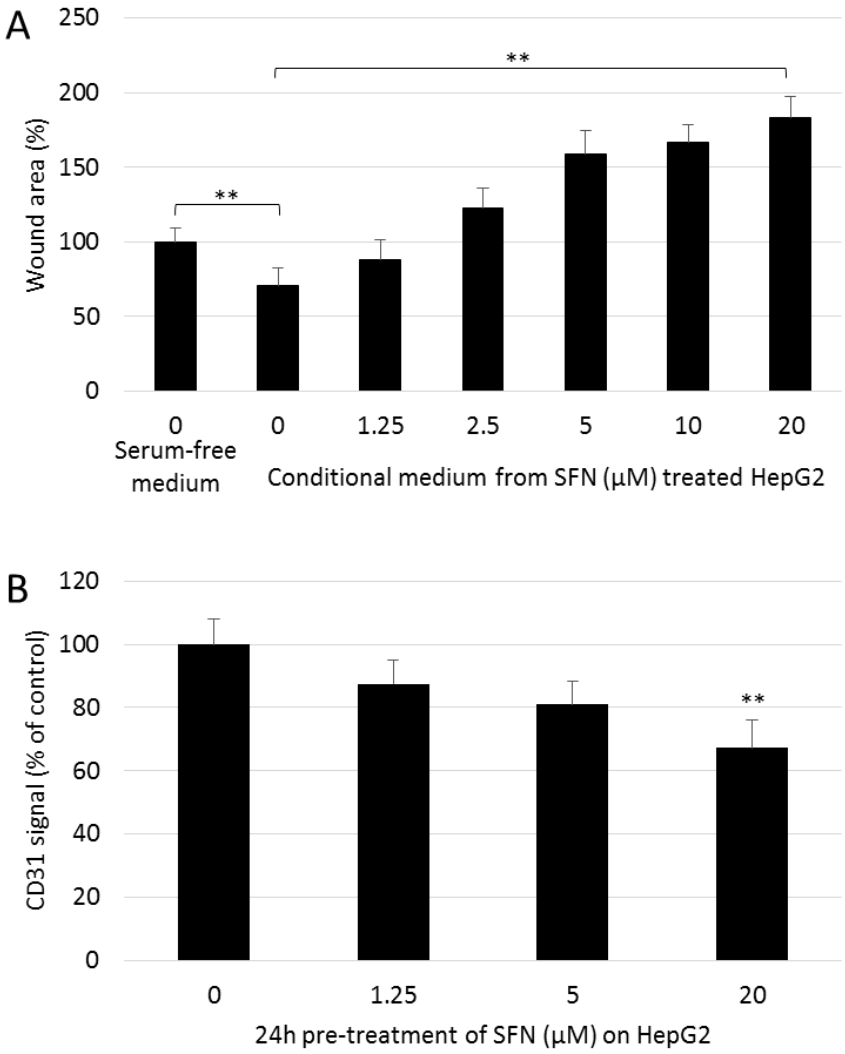

Figure 5.4 Effect of SFN on HepG2-stimulated migration and adhesion of HUVEC. (A) CM were collected from SFN treated HepG2 cells then added to HUVECs in the wound assay, with serum-free medium as control. Data are presented as mean ± SD ($n \geq 5$), **$p < 0.01$ between the indicated groups. (B) Adhesion assay of HUVECs on 24 hours SFN pre-treated HepG2 cells was performed. Adherent HUVECs were then stained for CD31. Data are presented as mean ± SEM ($n \geq 5$), **$p < 0.01$ compared to control.

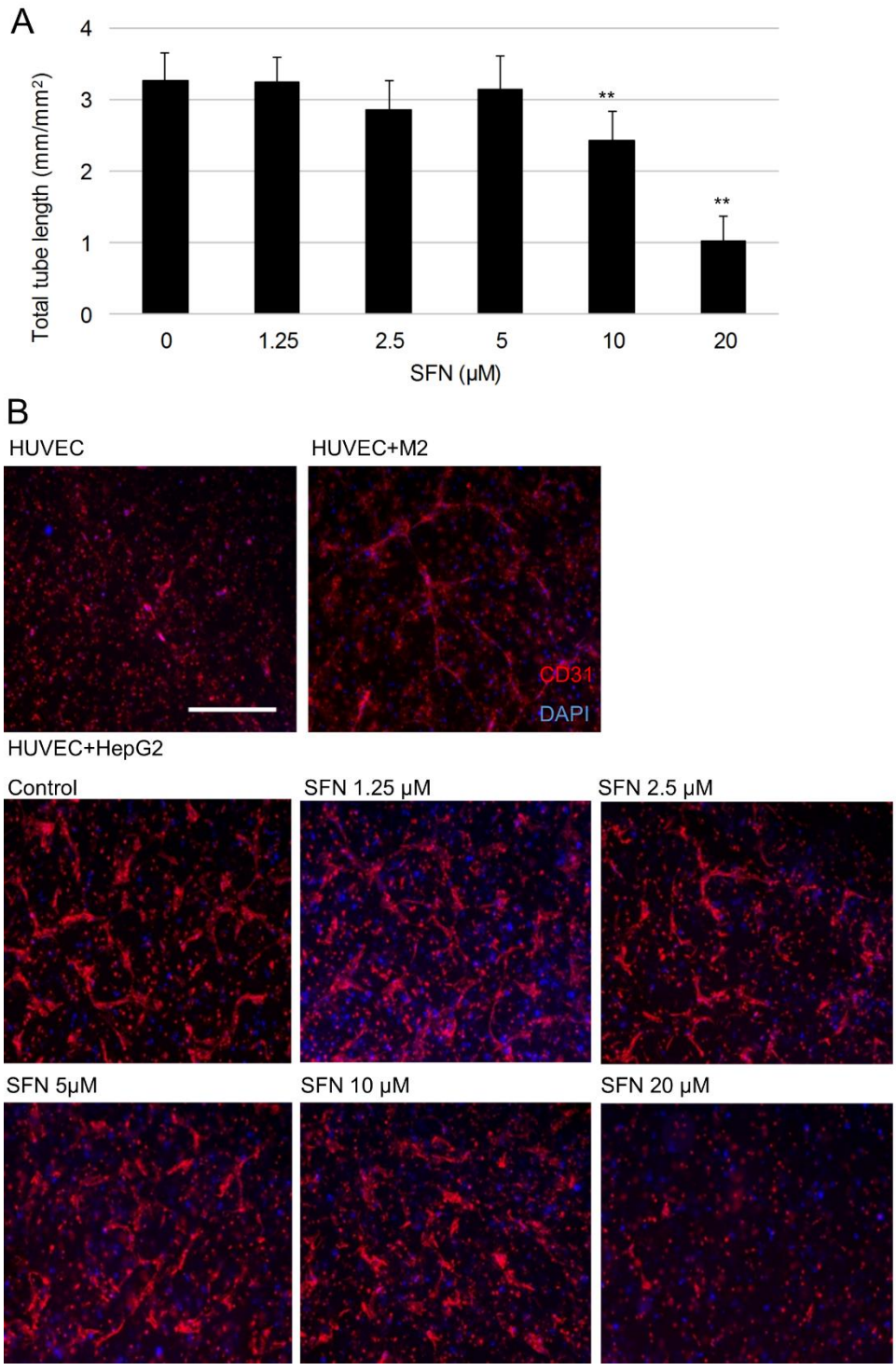

Figure 5.5 Effect of SFN on HepG2-stimulated tube formation of HUVEC. (A) 3D co-culture of HUVECs and HepG2 at day 3 treated with different doses of SFN. Total lengths of CD31 positive tubes were measured and expressed as mean ± SD (n=5), ** $p < 0.01$ compared to control. (B) Representative pictures from 3D co-culture of HUVECs and HepG2, cells were then fixed and stained with CD31 (red) and DAPI (blue). Scale bar = 500 μm.

5.2.4 Effect of SFN on STAT3, HIF-1a and VEGF in HepG2 cells

The induction of angiogenesis can be mediated by a variety of molecules released by tumour cells. VEGF is considered one of the most important angiogenic stimulators, and was identified as a key angiogenic signal in HCC. The expression of VEGF is largely controlled by two major transcription activators: signal transducer and activator of transcription 3 (STAT3) and HIF-1α. To further investigate the mechanism behind the inhibition effect of SFN on tumour angiogenesis, its effect on the STAT3/ HIF-1α /VEGF pathway was investigated in HepG2 cells. Immunoblotting revealed that STAT3 signalling is constitutively activated in HepG2 cells and SFN suppressed the expression of STAT3 in a dose-dependent manner. The effect of SFN on phospho-STAT3 (Tyr-705) was also investigated. However, reduced p-STAT3 (Tyr705) expression was associated with a reduction of the total STAT3 protein levels as the ratio of pSTAT3/STAT3 were close to 1 (Figure 5.6). SFN at 10 and 20 μM significantly down-regulated the expression of HIF-1α, and also dramatically inhibited cobalt chloride ($CoCl_2$)-induced accumulation of HIF-1α in a dose-dependent manner, indicating SFN inhibited the synthesis of HIF-1α. The protein expression level of VEGF-A was also reduced by SFN with or without $CoCl_2$ induction, in accordance with the results of HIF-1α (Figure 5.7). These results demonstrated that SFN could down-regulate the STAT3/ HIF-1α /VEGF-A pathway in HepG2 cells, and this could be the mechanism behind the inhibitory effect of SFN on HepG2-stimulated migration and tubulogenesis of ECs.

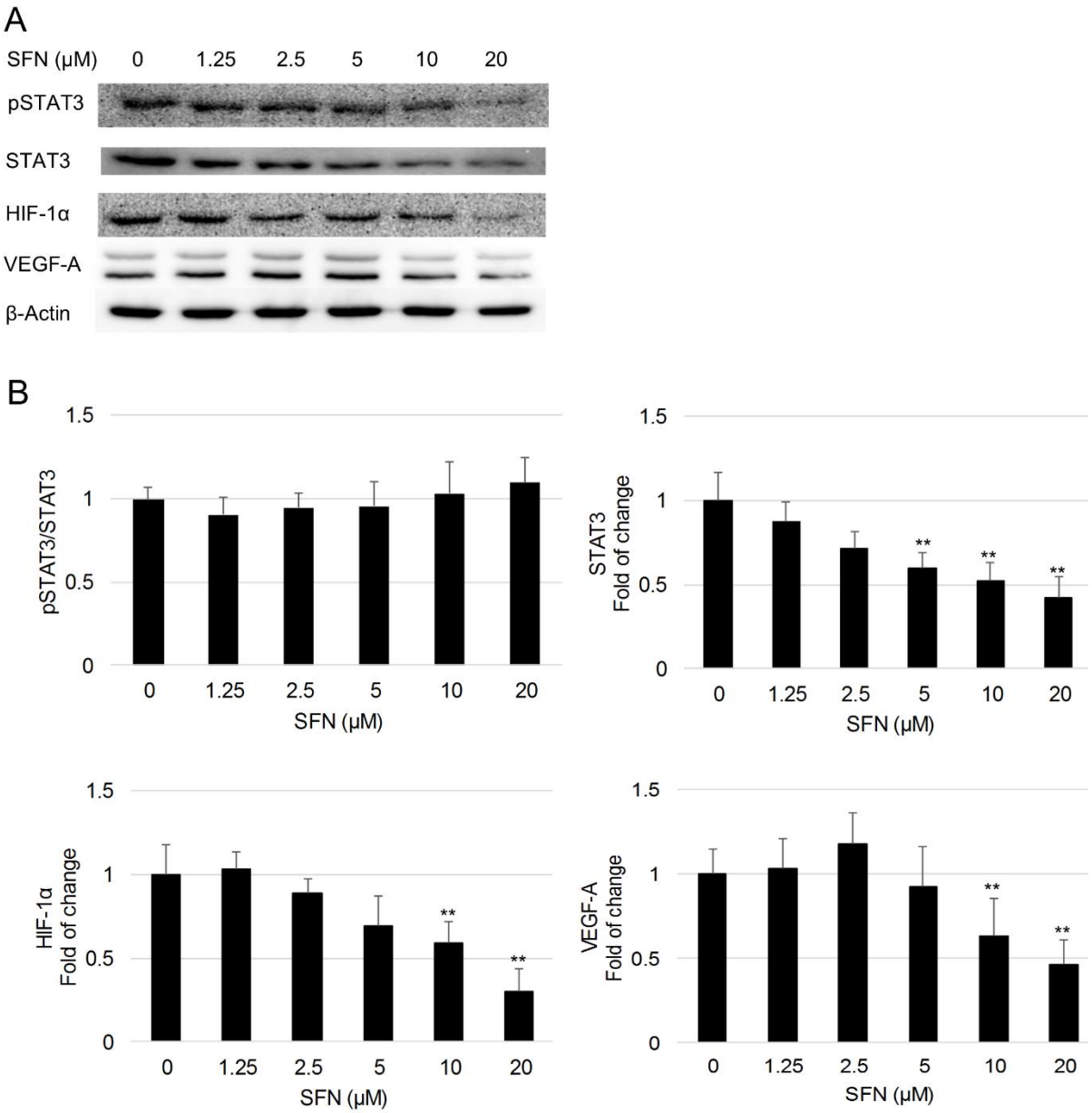

Figure 5.6 Dose response of SFN on protein expression in HepG2 cells. Cells were treated with 0-20 μM SFN for 24 hours, whole cell lysates were collected as described and subjected to Western blotting for STAT3, HIF-1α and VEGF-A. β-actin was used as a loading control (A). Band densities were normalized against β-actin, and results were expressed as fold induction relative to controls (B). Data are expressed as means ± SD (n = 3). *p < 0.05, ** p< 0.01 compared to control.

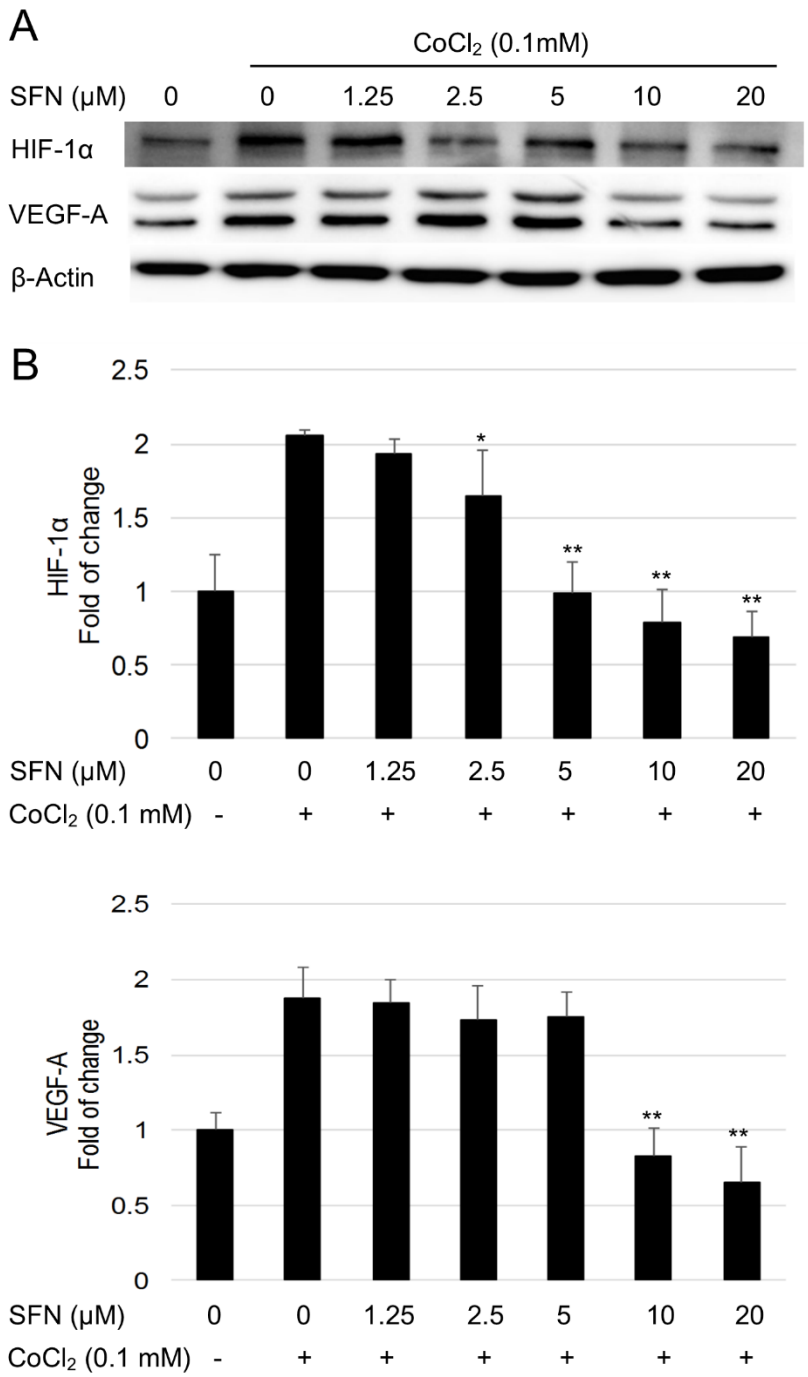

Figure 5.7 Dose response of SFN on protein expression in HepG2 cells under hypoxia. Cells were treated with 0-20 μM SFN without or with 0.1mM $CoCl_2$ for 24 hours, whole cell lysates were collected as described and subjected to Western blotting for HIF-1α and VEGF-A. β-actin was used as a loading control (A). Band densities were normalized against β-actin, and results were expressed as fold induction relative to controls (B). Data are expressed as means ± SD (n = 3). *$p < 0.05$, **$p < 0.01$ compared to control.

5.2.5 Effect of SFN on tumour growth and angiogenesis

A modified CAM assay was used to assess the influence of SFN on tumour growth and angiogenic potential of HepG2 cells *in vivo*. HepG2 cells (1×10^6) were mixed with growth factor reduced matrigel containing DMSO (0.1%) or SFN (20 μM), and incubated on top of the chicken embryo chorioallantoic membrane for 3 days. The tumours were then harvested and measured to calculate their volumes. The tumours treated with SFN had a significantly smaller volume compared with the control group (Figure 5.8A and B). H&E staining demonstrated massive areas of necrosis within SFN-treated tumours (Figure 5.8C). As HepG2 cells were resistant to SFN toxicity, the reduction in tumour size by SFN is less likely to result from its effect on tumour cell population but to its effects on vasculature formation within tumour stroma. The results of IHC analysis showed that SFN reduced the level of HIF-1α and VEGF in the tumour tissues (Figure 5.8D and E), which is consistent with the *in vitro* results. Thus, SFN reduced tumour growth and angiogenesis.

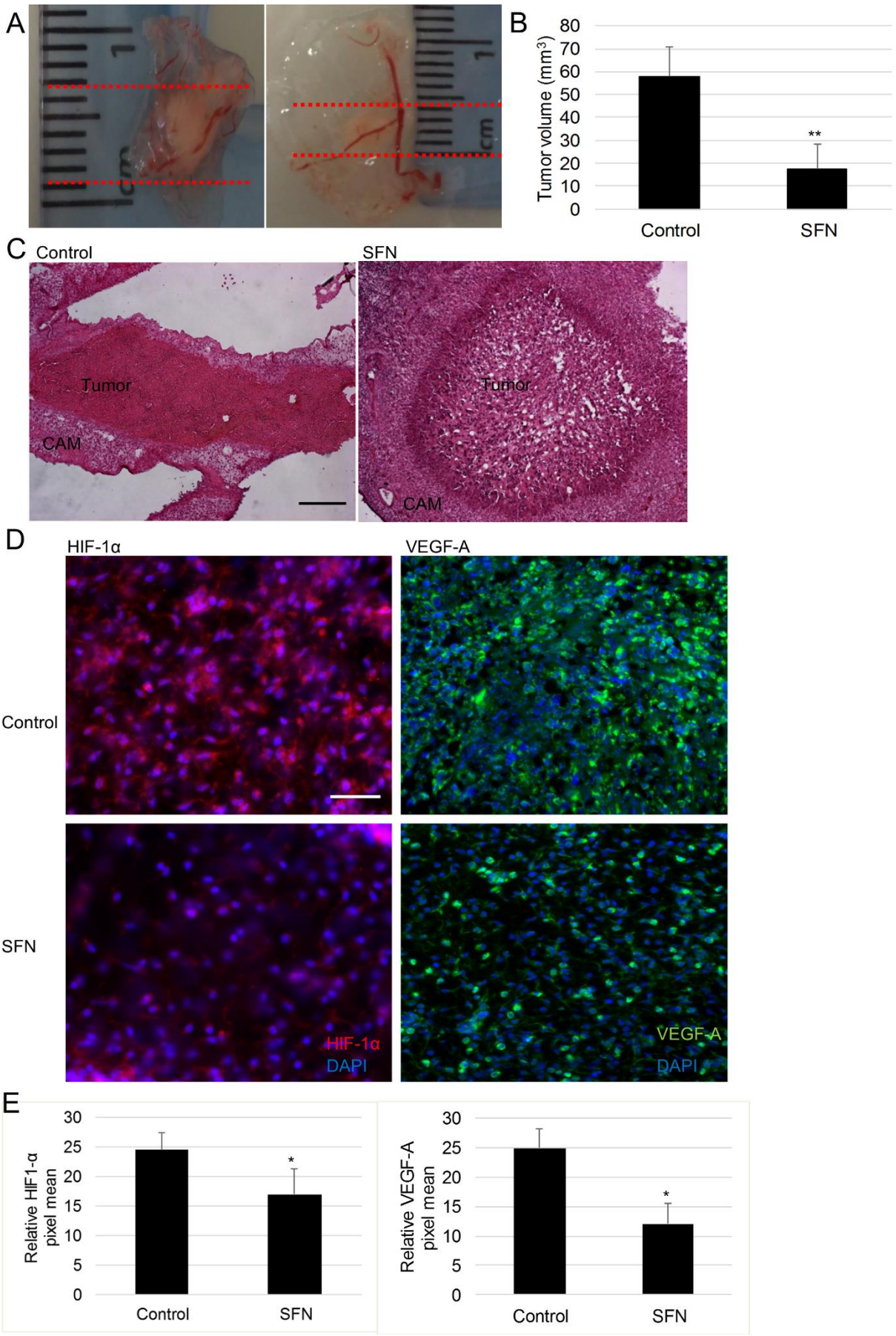
A
B
Tumor volume (mm3)
80
70
60
50
40
30
20
10
0
**
Control
SFN
C
Control
SFN
Tumor
CAM
Tumor
CAM
D
HIF-1α
VEGF-A
Control
SFN
HIF-1α
DAPI
VEGF-A
DAPI
E
Relative HIF1-α pixel mean
30
25
20
15
10
5
0
*
Control
SFN
Relative VEGF-A pixel mean
30
25
20
15
10
5
0
*
Control
SFN

Figure 5.8 Effect of SFN in the HepG2-bearing CAM model *in vivo*. (A) Representative photos of the tumour samples from control (0.1% DMSO) or SFN (20 μM) treatment. (B) The tumour volume was determined by direct measurement with callipers and results expressed as mean ± SD (n = 5; **p < 0.01). (C) Representative pictures from H&E staining of tumours, scale bar = 200 μm. (D) Representative pictures from IHC staining for HIF-1α and VEGF-A of tumours, scale bar = 200 μm. (E) HIF-1α and VEGF-A staining intensities (mean ± SD, n ≥ 5) were quantified. *p < 0.05 compared to control.

5.3 Discussion

HCC is one of the most common human cancers but is associated with poor prognosis. Growth and metastasis of HCC solid tumours depend on angiogenesis, thus preventing or inhibiting angiogenesis by non-toxic, affordable, and effective phytochemicals could be a useful strategy for better management of HCC. SFN, a predominant dietary phytochemical in CVs, has been studied intensively in terms of cancer prevention and treatment. In the present work, it is demonstrated that SFN not only interfered with endothelial cell proliferation, migration and tube formation, but, for the first time, inhibited the pro-angiogenic effect of HepG2 cells both *in vitro*, *ex vivo* and *in vivo*.

ECs are one of the critical components in the tumour microenvironment and play a crucial role in the growth and progression of cancer through angiogenesis[345]. Thus, the inhibition of their function is explored as a potential therapy. In this study, SFN significantly inhibited HUVEC viability and migration, in agreement with previous results[145,346]. High dose of SFN also disrupted the ability of HUVECs to form capillary-like tubular structure in 3D co-culture with pericytes, and blocked microvessel sprouting from mouse aortic rings *ex vivo*. These two angiogenesis models very closely mimic the physiology of vascular maturation because of the involvement of pericytes and smooth muscle cells[347]. Therefore, the anti-angiogenic effects of high dose SFN (> 5 μM) has been confirmed. Interestingly, 2.5 μM SFN simulated tube formation by 37% in the 3D co-culture model and sprouting by 28% in the aortic ring assay. The biphasic response of SFN has also been reported in other studies[173,180] as a potential risk factor in its application for cancer treatment. Further *in vivo* studies are needed to confirm this hormetic effect. As the physiological concentration of SFN by consumption of a meal rich in CVs or from supplements is around 1-7 μM in human plasma[35,37], it is crucial to achieve targeted delivery of high dose of SFN for cancer chemoprevention or treatment. Conversely, low dose SFN could be beneficial to patients with cardiovascular disease because of its stimulation effect on endothelial cell tube formation.

Intercellular communication and chemotaxis play key roles in the angiogenic process of HCC and can occur via direct contact or paracrine signalling between tumour cells and host microenvironment such as ECs[345]. However, the crosstalk between tumour cells and ECs is still in need of further investigation. In this study, the influence of HepG2 on HUVEC angiogenic behaviour, and the effect of SFN on the interaction between HepG2 and HUVEC have been studied. Results showed that HepG2 cells stimulated HUVEC migration and tube

formation, and that this stimulation could be inhibited by SFN pre-treatment on HepG2 cells. In addition, SFN could interrupt the ability of HepG2 cells to recruit HUVECs, indicating that SFN may influence not only paracrine factors but also cell-cell interactions between HepG2 and HUVEC.

VEGF-A has been implicated as a major paracrine mediator in the pathogenesis of HCC. In clinical trials, targeting VEGF pathways has been effective in treating HCC but is also prone to promoting resistance and more aggressive tumours, which could be due to the activation of transcriptional factors by anti-angiogenic agents[348]. Thus, targeting transcriptional factors may be more effective than targeting VEGF and its receptors. STAT3 and HIF-1α, two major transcription factors that regulate VEGF, have been found to be consistently upregulated in various cancers including HCC and associated with poor clinical outcomes in patients[349,350]. Suppression of STAT3 and HIF-1α activity was demonstrated to inhibit growth in HCC[351]. Here, the inhibition of STAT3 by SFN treatment was verified, which also coincided with reduced HIF-1α and VEGF expression in HepG2. These data were consistent with previous findings in other cell lines[352–354], indicating the STAT3/ HIF-1α /VEGF may be responsible for the anti-angiogenic effects of SFN.

Under normal conditions, HIF-1α is hydroxylated by prolyl hydroxylases (PHDs) at oxygen-dependent degradation domains at proline 402 and 564, and it then interacts with the von Hippel-Lindau (VHL)-ubiquitin E3 ligase complex before being degraded by the ubiquitin-proteasome system. Under hypoxia or stimulation with certain growth factors or cytokines, HIF-1α can escape degradation and bind with HIF-1β. The heterodimeric HIF1 formed rapidly translocates to the nucleus and activates hypoxia-responsive elements (HREs) which regulate many genes involved in cancer biology such as angiogenesis, metabolic adaption, cell survival and metastasis[349,355]. $CoCl_2$, widely used as a hypoxia mimicking agent, can stabilize HIF-1α by inhibiting PHD activity[356] as well as the binding between pVHL and hydroxylated HIF1[357]. HepG2 cells treated with $CoCl_2$ were shown here to increase expression of HIF-1α and VEGF, this increase was blocked by co-treatment of SFN in a dose-dependent manner. This indicates SFN could influence the synthesis of HIF-1α. The same result was found in MCF7, 4T1 and 293 cells by Zhou J and coworkers[358].

The antitumor efficacy was demonstrated *in vivo* by a modified CAM assay, which has been used previously to study tumour angiogenesis, invasion and metastasis in malignancies including HCC[359]. The highly-vascularized nature of the CAM enables the survival of embedded tumour cells and the presence of ECM proteins in CAM mimics the

physiological cancer cell environment. Here tumour volume was reduced by SFN treatment, which was consistent with the widespread tumour necrosis indicated by H&E staining. The expression of angiogenic factors tends to reflect aggressive tumour phenotype[329], whilst the inhibition of HIF-1α and VEGF expression was confirmed by IHC analysis in the SFN treated tumours. These results suggest that the antitumor activity of SFN may be mediated, at least in part, by inhibition of HIF-1α and subsequent VEGF expression.

In summary, the present study confirmed that SFN not only affects EC function but also the interaction between HCC cells and ECs by inhibiting STAT3/ HIF-1α /VEGF signalling in the cancer cells, which results in the suppression of angiogenesis induced by HCC cells leading to an anti-tumour effect. Based on these results, SFN has the potential to be considered as an anti-angiogenic agent against HCC and would warrant further *in vivo* investigation.

Chapter 6. Anticancer activities of AITC and its conjugated silicon quantum dots

6.1 Introduction

AITC is produced by the hydrolysis of its glucosinolate precursor, sinigrin, which can be found in many commonly consumed CVs and is particularly abundant in mustard, horseradish and wasabi where it is responsible for the pungent taste[17]. Because of the pungent flavour, AITC is also used as a food additive known as mustard oil. AITC has been shown to possess a broad spectrum of anticancer activities in both cultured cancer cell lines and animal tumour models[360]. The mode of action for the chemopreventive activity of AITC is attributed primarily to the detoxification of carcinogens through activation of Nrf2[361]. Previous studies also showed that AITC inhibited the growth of various human cancer cell lines such as colorectal carcinoma[140,362,363], lung cancer[127,364], leukemia[365], breast adenocarcinoma[366], bladder cancer[44,305,367], neuroblastoma[368], hepatoma[139] and prostate cancer cells[97,360,369]. The mechanisms are likely to involve DNA damage[127], cell cycle arrest[366], apoptosis[113] and the binding to thiol-reactive groups of several cellular targets such as DNA topoisomerase 2, p53 and tubulins[53,55,361]. In addition, AITC has been reported to suppress metastasis *via* inhibition of invasion and migration[139,362] in neoplastic cells. Antiangiogenic activity of AITC has also reported in *in vivo* studies[148,149]. However, findings from epidemiological studies on the association between CV intake and cancer risk are generally inconsistent[34,370]. The hormetic effects of ITCs may be the cause of the complex biological impact of a CV diet[371].

In toxicology, hormesis refers to a dose–response relationship with a stimulatory response at low doses and an inhibitory response at high doses[172]. Many drugs have been found to demonstrate such contradictory effects at high and low doses in the same individual. This reaction, also known as 'biphasic dose response', has shown significance in establishing the modality of a drug. On the other hand, mild stress stimuli can often trigger an adaptive stress response in order to maintain homeostasis, so that while a high dose of an insult brings harm, a low dose of the same could promote health[171]. Dietary phytochemicals have been reported to be prominent hormetic stressors that affect various signalling pathways associated with the progression of diverse diseases, especially cancer[173,174,371,372]. ITCs for example, have been reported to kill cancer cells at high doses but to promote cancer cell proliferation and survival at low doses[173,174,371]. Therefore, it is crucial to optimize the beneficial effects and minimize the potential risks of ITCs in cancer prevention and treatment.

The growth of nanotechnology has opened several new vistas in medical sciences, especially in the field of cancer treatment. SiQDs have been developed for both bio-imaging and therapeutic purposes because of their unique electronic and optical properties. As an interesting research area, further exploration of the surface functionalization of SiQDs has been shown to facilitate their application as drug carriers for chemotherapeutic agents, photosensitizers, siRNA and gene therapeutic agents and can also act as multifunctional entities for both imaging and therapy at the same time[217,373,374]. Here for the first time, the design of a new multifunctional nanoparticle system with SiQDs as carrier and AITC as surface ligand is reported. The objectives of the present study were to investigate the differences between the bioactivities of AITC and AITC-SiQDs; and the potential mechanisms/application of AITC-SiQDs to act as multifunctional vehicle for cancer therapy.

6.2 Results

6.2.1 A biphasic effect of AITC on cell viability, DNA integrity, migration and angiogenesis

The cytotoxicity of AITC was measured using the MTT assay. Results indicated that AITC decreased the metabolic activity of HepG2 cells in a dose-dependent manner after 24 hours. When cells were treated with AITC 40-320 μM, cellular viability was significantly inhibited (77.1-19.4% compared to control); however, a significant stimulation of cell viability was found with 5 μM AITC (Figure 6.1A).

The genotoxicity of AITC was then measured at non-cytotoxic concentrations (0-20 μM) using the comet assay. The baseline DNA damage, represented as tail intensity percentage, in control cells was 21.57% and there was a significant increase at 10 and 20 μM AITC treatment at 24 hours, 36.12 and 47.48% respectively; while at 2.5 μM AITC decreased DNA damage to 12.3% (Figure 6.1B-C). The induction of DNA damage with high dose AITC was accompanied by downregulation of DNA repair protein Ku70 (Figure 6.1D).

To assess whether AITC also affects cell migration, a wound assay was performed to measure the cell migration under different doses of AITC treatment after 48 hours. Around 30% inhibition of migration compared to the control was observed with 20 μM AITC exposure. This concentration is nontoxic, as is evident from the MTT assay; hence, the inhibitory effect could not be attributed to cytotoxic activity. Again, a significant increase in cell migration was observed with low dose (2.5 μM) AITC (130% compared to control) (Figure 6.2A-B).

The effect of AITC on the ability of HUVECs to form capillary-like tubular structures was tested in the 3D co-culture model with pericytes. Mature tube formation was clearly observed in control but was significantly disrupted with AITC treatment (>5 μM), showing as a sharp decrease in formed total tube length. However, at lower doses AITC (1.25 and 2.5 μM) significantly promoted the formation of capillary tubular structures (Figure 6.3A-B).

These data suggest that there was a biphasic dose response from AITC treatment in all tested endpoints. For cancer treatment, only high doses of AITC should be used, as low doses stimulated cancer cell viability and migration, and also restored genomic stability and promoted angiogenesis.

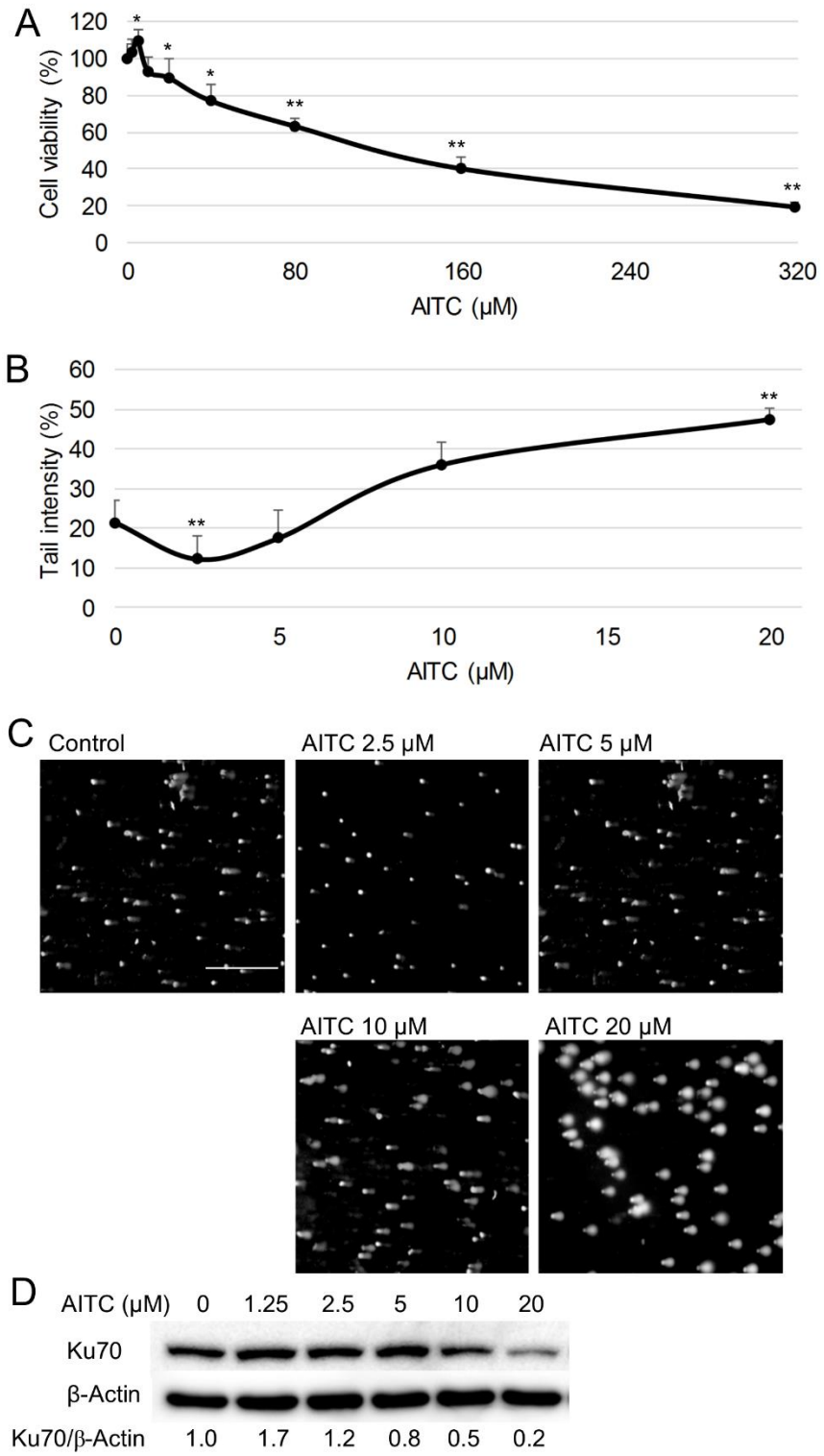

Figure 6.1 Effect of AITC on HepG2 cell viability and DNA integrity. (A) Cell viability at 24 hours AITC treatment was determined by MTT assay. Data are presented as mean ± SD (n ≥ 5), *p < 0.05, **p < 0.01 compared to control. (B) DNA damage at 24 hours AITC treatment was detected by comet assay. Data are presented as mean ± SD (n ≥ 5), **p < 0.01 compared to control. (C) Representative pictures from the comet assay. Scale bar = 500 μm.

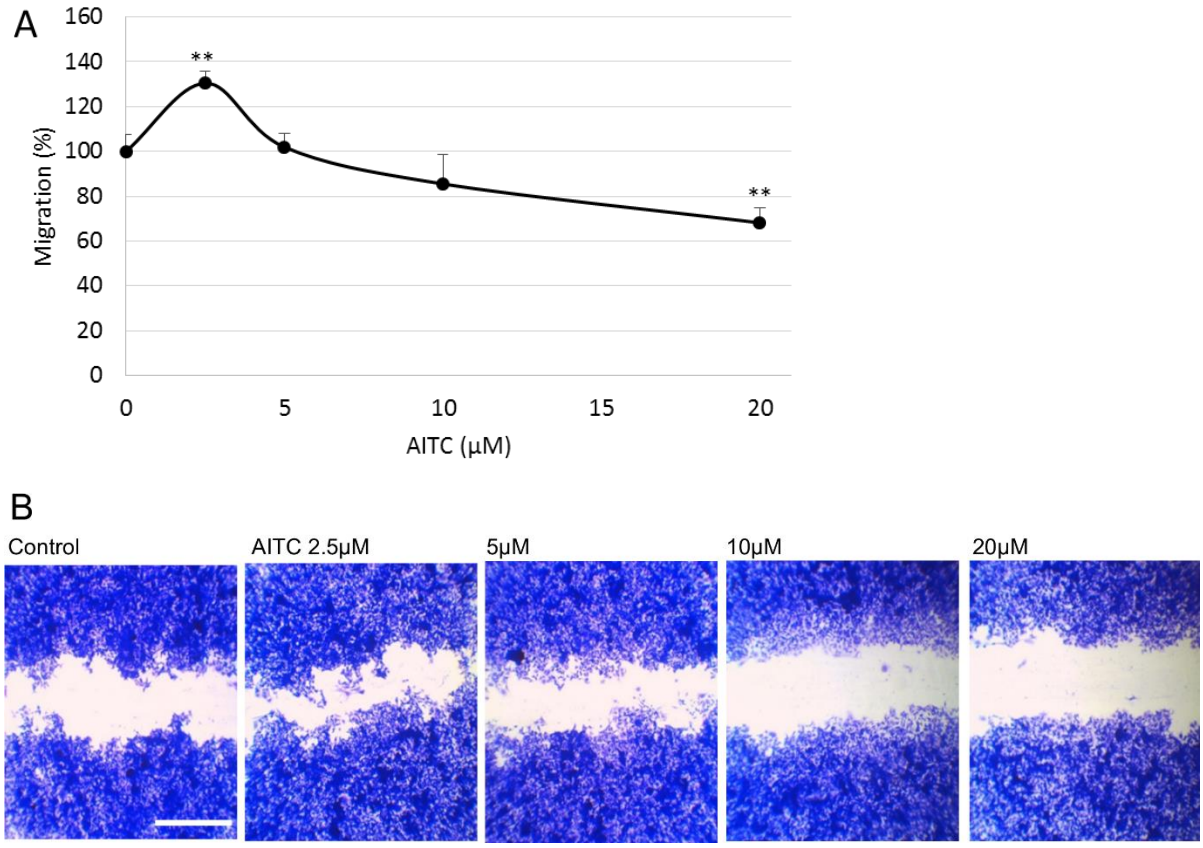

Figure 6.2 Effect of AITC on HepG2 cell migration. (A) HepG2 cell migration at 48 hours AITC treatment was measured by wound assay. Data are presented as mean ± SD ($n \geq 5$), $^{**}p < 0.01$ compared to control. (B) Representative phase contrast images from the wound assay. Scale bar = 1 mm.

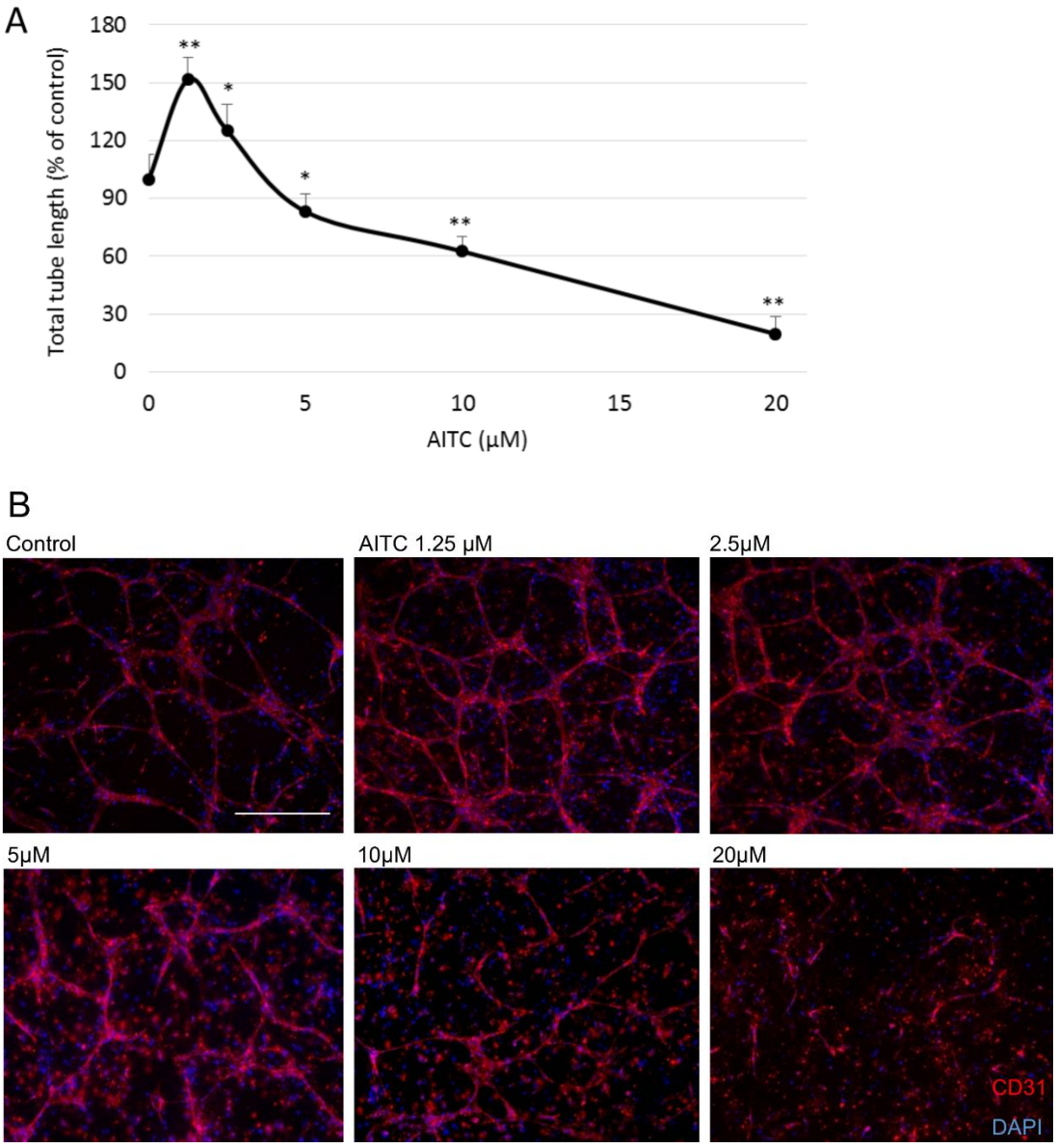

Figure 6.3 Effect of AITC on tube formation of HUVECs in a 3D co-culture with pericytes model. (A) The total lengths of CD31 positive tubes were measured and expressed as mean ± SD (n≥5), *p < 0.05, ** p< 0.01 compared to control. (B) Representative pictures from the immunostaining of CD31 (red) and DAPI (blue), scale bar = 500 μm.

6.2.2 Low dose AITC stimulation effect is mediated by Nrf2/GSH signaling

A low dose stimulation effect could be a risk factor for the use of AITC in cancer prevention and treatment. ITCs have been shown to activate Nrf2 signalling, which is important in stress adaptation and cytoprotection[375,376]. The role of Nrf2 in the low dose stimulation effect of AITC on DNA damage and cell migration was investigated using a siRNA knockdown approach. As shown in Figure 6.4, Nrf2 knockdown cells showed significantly increased DNA damage and reduced cell migration compared to non-transfected control cells. This suggested Nrf2 is involved in HepG2 cell genomic stability and migration. AITC at 2.5 μM reduced DNA damage and promoted cell migration in HepG2 cells. Cells transfected with Allstar negative control showed similar effects with AITC treatment as the non-transfected ones. In contrast, these stimulation effects from 2.5 μM AITC were abolished upon Nrf2 knockdown, i.e. DNA damage increased from 9.4% to 41.8%; cell migration decreased from 122.7 to 66.1% ($p<0.01$). These data strongly indicated that Nrf2 was involved in the low dose stimulation effect of AITC in DNA damage and cell migration. On the other hand, BSO treatment increased DNA damage by 1.5-fold and decreased cell migration by approximately 20% compared to control. Co-treated with BSO, 2.5 μM AITC treatment showed no stimulatory effect on DNA damage or cell migration. Therefore, it can be concluded that the Nrf2/GSH signalling pathway plays an essential role in low dose AITC inhibition of genomic instability and stimulation of cell migration.

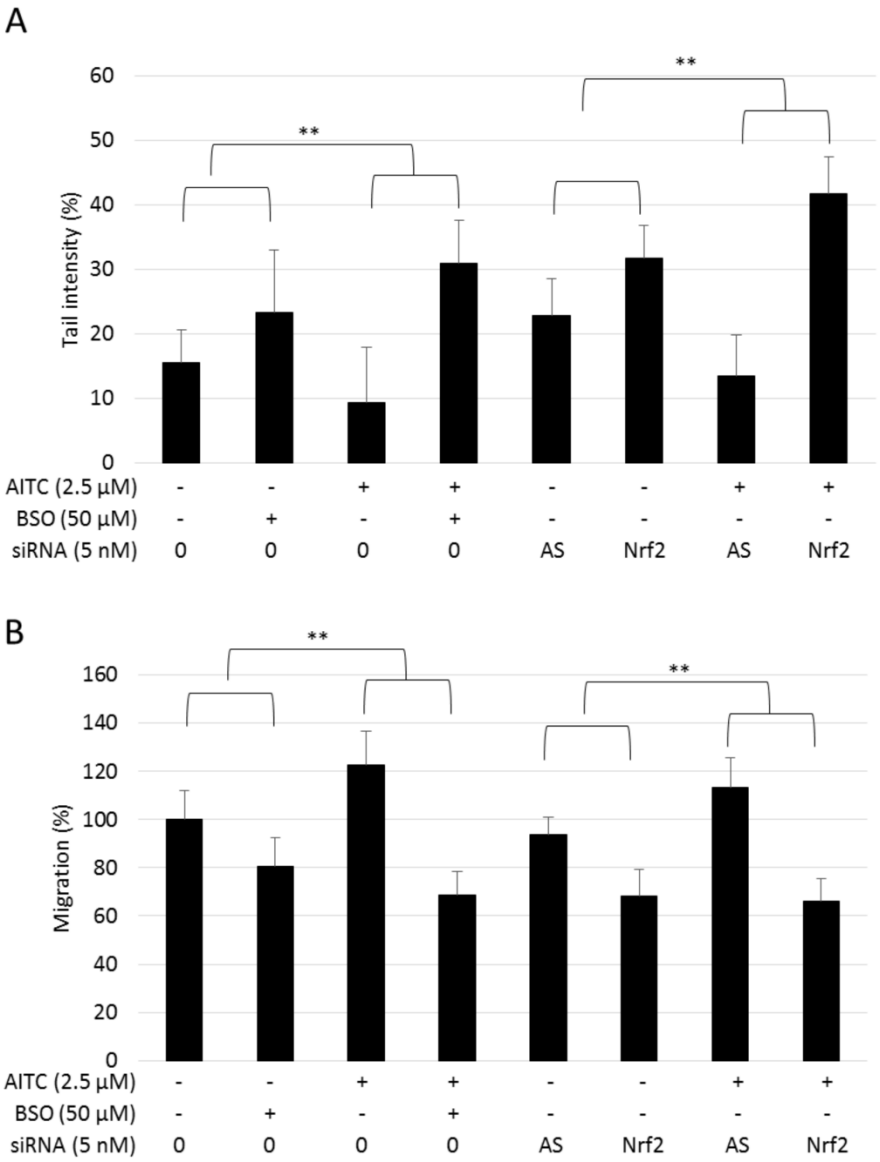

Figure 6.4 Effect of Nrf2 siRNA and GSH inhibition on HepG2 cell DNA damage and migration exposed to AITC. Allstars (AS) was used as a control for knockdown. Cells were incubated with 2.5 µM AITC or DMSO (0.1%) control with or without 50 µM BSO co-treatment. (A) After 24 hours DNA damage was measured by comet assay. (B) After 48 hours cell migration was measured by wound assay. Data are presented as mean ± SD ($n \geq 3$), $^{**}p < 0.01$ between the indicated groups (t-test).

6.2.3 AITC-SiQDs abolished the low dose stimulation effect of AITC

The effect of AITC-SiQDs on cell viability was initially determined using the MTT assay. Cells were incubated with different concentrations of AITC-SiQDs with AITC as the positive control for 24 hours. As shown in Figure 6.5A, there was no significant difference between the cytotoxicity of AITC-SiQDs and AITC at high dose (nearly 20% decrease from 40 µM treatment); but there was a significant difference between low dose AITC-SiQDs and AITC treatments on cell viability, i.e., cell viability was approximately 90% compared to control with 2.5 and 5 µM of AITC-SiQDs treatment while AITC treatment increased cell viability to 103-110% of the control. Amine-capped SiQDs (NH_2-SiQDs)[226] were used as negative control to confirm the cytotoxicity of AITC-SiQDs observed came from the surface ligand instead of the SiQDs core (Appendix Figure 3).

The effects of AITC-SiQDs on DNA damage, cell migration and angiogenesis were also examined (Figure 6.5B-D). At 20 µM AITC-SiQDs induced DNA damage (2.5-fold increase compared to control); inhibited cell migration (60% decrease compared to control); and inhibited tube formation in the 3D co-culture model (60% decrease compared to control). More importantly, AITC-SiQDs at 2.5 µM showed no stimulation in contrast to AITC.

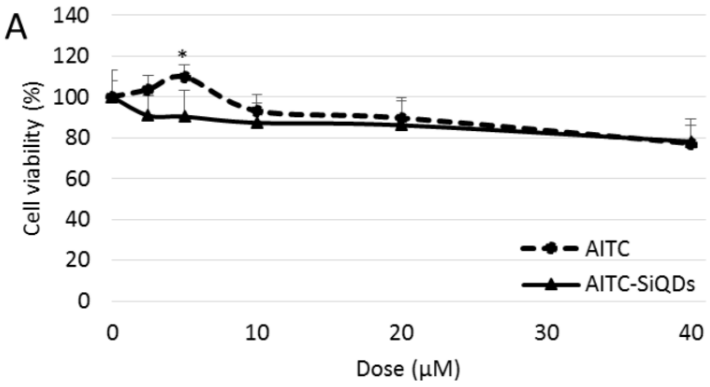
A
Cell viability (%)
140
120
100
80
60
40
20
0
*
AITC
AITC-SiQDs
0
10
20
30
40
Dose (μM)

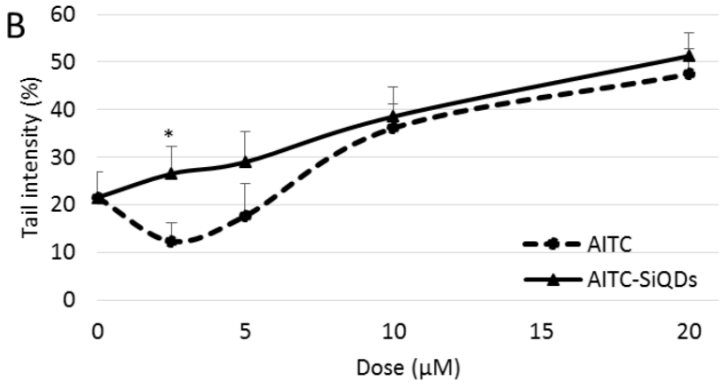
B
Tail intensity (%)
60
50
40
30
20
10
0
*
AITC
AITC-SiQDs
0
5
10
15
20
Dose (μM)

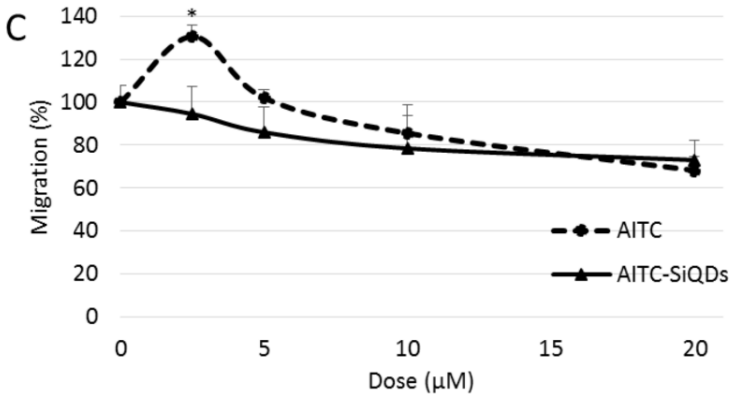
C
Migration (%)
140
120
100
80
60
40
20
0
*
AITC
AITC-SiQDs
0
5
10
15
20
Dose (μM)

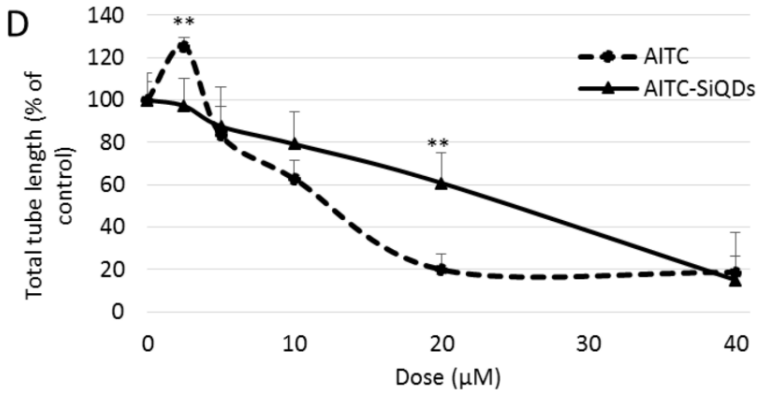
D
Total tube length (% of control)
140
120
100
80
60
40
20
0
**
**
AITC
AITC-SiQDs
0
10
20
30
40
Dose (μM)

Figure 6.5 Effect of AITC-SiQDs was compared with AITC on HepG2 cell viability (A), DNA integrity (B), migration (C) and tube formation in the 3D HUVEC co-culture with pericytes model (D). Data are presented as mean ± SD ($n \geq 3$), *$p < 0.05$, **$p < 0.01$ compared to corresponding AITC treatment.

6.2.4 Effect of AITC/AITC-SiQDs on the nuclear accumulation of Nrf2

The involvement of AITC-SiQDs in the activation of Nrf2 compared to AITC in HepG2 cells was examined. Nuclear protein was extracted and Nrf2 measured by Western blotting. As shown in Figure 6.6, untreated cancer cells had low Nrf2 levels in the nucleus consistent with the continuous degradation of Nrf2 under homeostasis. With 20 μM AITC treatment, a significant increase of Nrf2 protein in the nucleus was observed after 1 hour but this started to decrease after 4 hours, while at the same dose AITC-SiQD treatment caused the nuclear protein level of Nrf2 to increase compared to control for at least 24 hours. In addition, AITC treatment (1.25, 5, 20 μM) for 4 hours induced a significant and dose-dependent increase of Nrf2 in the nucleus, but AITC-SiQD treatment showed a much milder effect in this regard compared to the same dose of AITC treatment. These data indicated different dynamics of Nrf2 activation between AITC and AITC-SiQDs.

To check that the observed effect of AITC-SiQDs on abolishing the low dose stimulation effect was not specific to HepG2, the effect of AITC-SiQDs on colorectal adenocarcinoma cells, Caco-2, was investigated. Caco-2 cells were more sensitive towards AITC than HepG2 cells. As expected, results showed 80 μM AITC-SiQDs decreased cell viability to 31.77% compared to control in Caco-2 while only 78.19 % in Hepg2 (Figure 6.7A). As shown in Figure 6.7B-C, AITC-SiQDs abolished the stimulation effect seen with AITC (2.5 and 5 μM) on cell migration; and the prolonged induction of Nrf2 nuclear accumulation by AITC-SiQDs compared to the sharp induction by AITC was also observed in Caco-2. These results suggest that this effect of AITC-SiQDs is not cell line specific.

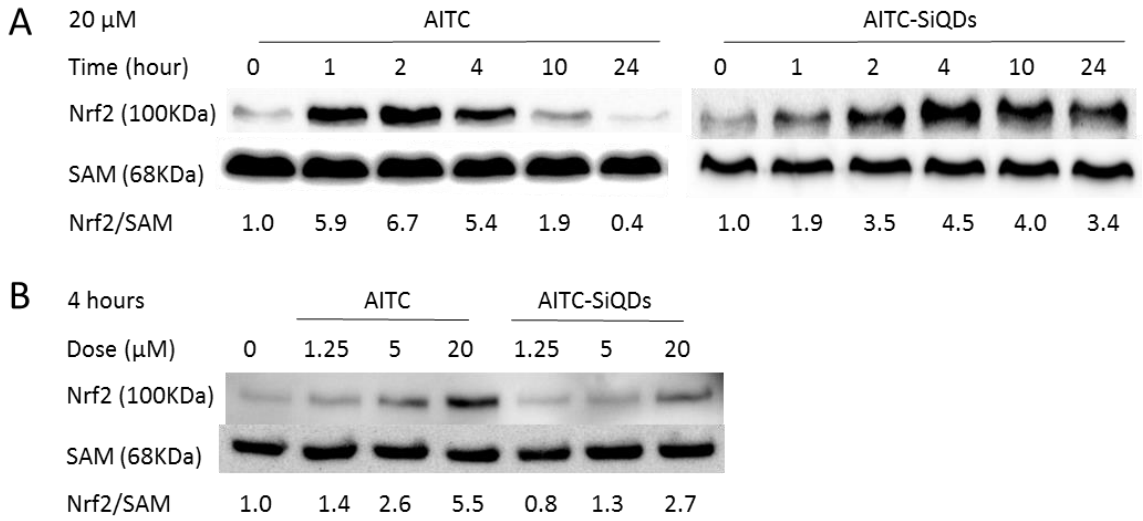

Figure 6.6 Effect of AITC or AITC-SiQDs on Nrf2 nuclear accumulation in HepG2 cells. Nuclear protein fractions were isolated as described in Methods. Nrf2 was detected by Western blot and quantified against SAM as a loading control, results were expressed as fold induction relative to controls. (A) Time course of the effect of 20 µM AITC or AITC-SiQDs on Nrf2 nuclear protein level. (B) Dose response of AITC or AITC-SiQDs at 4 hours on Nrf2 nuclear protein level.

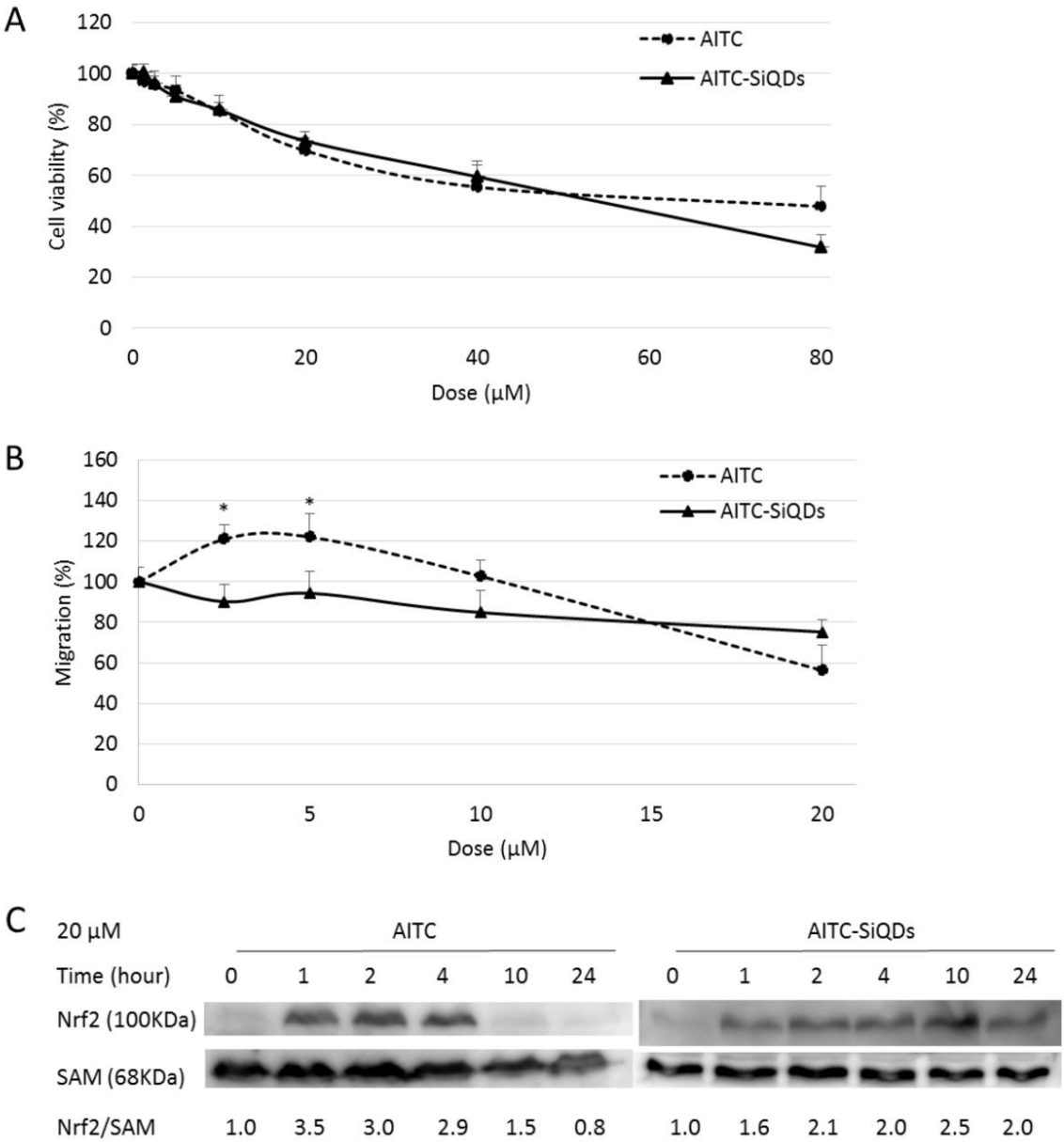

Figure 6.7. Effect of AITC or AITC-SiQDs on Caco2 cell viability, migration and nuclear Nrf2 accumulation. (A) Cell viability at 24 hours treatment was determined by MTT assay. (B) Cell migration at 48 hours treatment was measured by wound assay. Data are presented as mean ± SD ($n \geq 5$), *$p < 0.05$ compared to corresponding AITC treatment. (C) Time course of the effect of 20 μM AITC or AITC-SiQDs on Nrf2 nuclear protein level. Nuclear protein fractions were isolated as described in Methods. Nrf2 was detected by Western blot and quantified against SAM as a loading control.

6.2.5 Cellular uptake of AITC-SiQDs

The characterization of the interaction of NPs with cells is a key factor in their bioactivity. To investigate the cellular uptake of AITC-SiQDs, HepG2 cells were incubated with fluorescent AITC-SiQDs and analysed by CLSM; additional investigation was performed using Lysotracker red, a fluorescent cell-permeant acidic organelle-selective marker. The Lysotracker probes, which comprise a fluorophore linked with a weak base that is only partially protonated at neutral pH, freely penetrate cell membranes and are typically used to mark organelles including lysosomes and some late endosome at acidic pH[377]. The confocal microscopy images are shown in Figure 6.8. The control cells (treated with 0.1% DMSO) did not exhibit fluorescence. After 1 hour of incubation with AITC-SiQDs, a blue fluorescence signal was observed inside the cells, which peaked around 12 hours indicating the internalization of a large number of AITC-SiQDs. At 24 hours, there were still signals from internalized AITC-SiQDs which indicated the excretion of QDs took at least this length of time. Lysosomes were identifiable within HepG2 cells, and there was a clear co-localization of AITC-SiQDs within lysosomal structures at all time points investigated, which indicated that QDs were taken by the cells through endocytosis as is the case for most types of NPs[378].

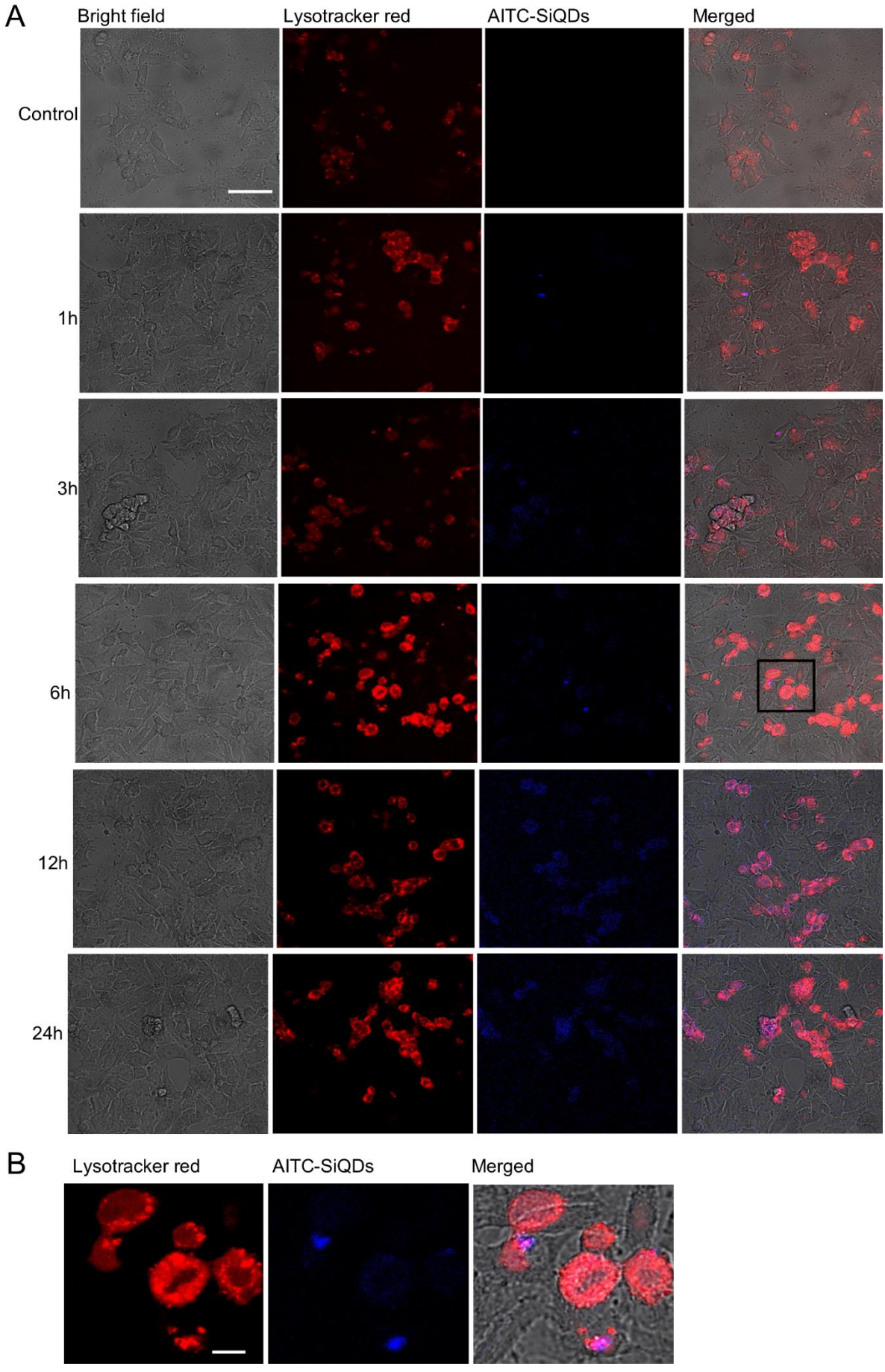
A
Bright field
Lysotracker red
AITC-SiQDs
Merged
Control
1h
3h
6h
12h
24h
B
Lysotracker red
AITC-SiQDs
Merged

Figure 6.8 Confocal imaging of AITC-SiQDs cellular uptake in HepG2. (A) Representative images of AITC-SiQDs signalling in HepG2 cells over 24 hours. Scale bar = 50 μm. (B) High resolution images from 6 hours of AITC-SiQDs localization into the lysosomes of HepG2 cells, area indicated by the black rectangle in the merged images. Scale bar = 10 μm.

6.2.6 Anticancer properties of AITC-SiQDs is mediated by ROS

ROS generation is one of the common mechanisms by which NPs exert toxicity; accordingly, the intracellular ROS was measured using a H2DCFDA probe, which is a stable nonpolar dye that diffuses readily into cells and yields DCFH. Intracellular ROS, in the presence of peroxidase, converts DCFH to fluorescent DCF. As shown in Figure 6.9A, 20 μM AITC or AITC-SiQD treatment both caused significant increase of ROS at 1 hour in Caco-2 cells, i.e., the DCF fluorescence intensity was measured as 124.6% and 149.6% of control from AITC and AITC-SiQDs respectively. ROS returned to control level after 3 hour in AITC-treated cells, but in AITC-SiQDs treated cells DCF intensity was 121.8% and 145.7% of control at 3 and 24 hours.

To examine further whether the AITC-SiQDs induced anti-proliferative response is related to ROS, a well-known antioxidant NAC was used to quench ROS production. Results from their co-treatment showed that NAC completely blocked the reduction in cell viability caused by AITC-SiQDs in Caco-2 (Figure 6.9B). This suggested that ROS generated by AITC-SiQDs participated in the anti-proliferation effect. Further results indicated that co-treatment with NAC reduced the DNA damage caused by AITC-SiQDs and impaired the inhibitory effect of AITC-SiQDs on cell migration (Figure 6.9C-D). Taken together, these data suggest a ROS mediated mechanism behind the bioactivities of AITC-SiQDs.

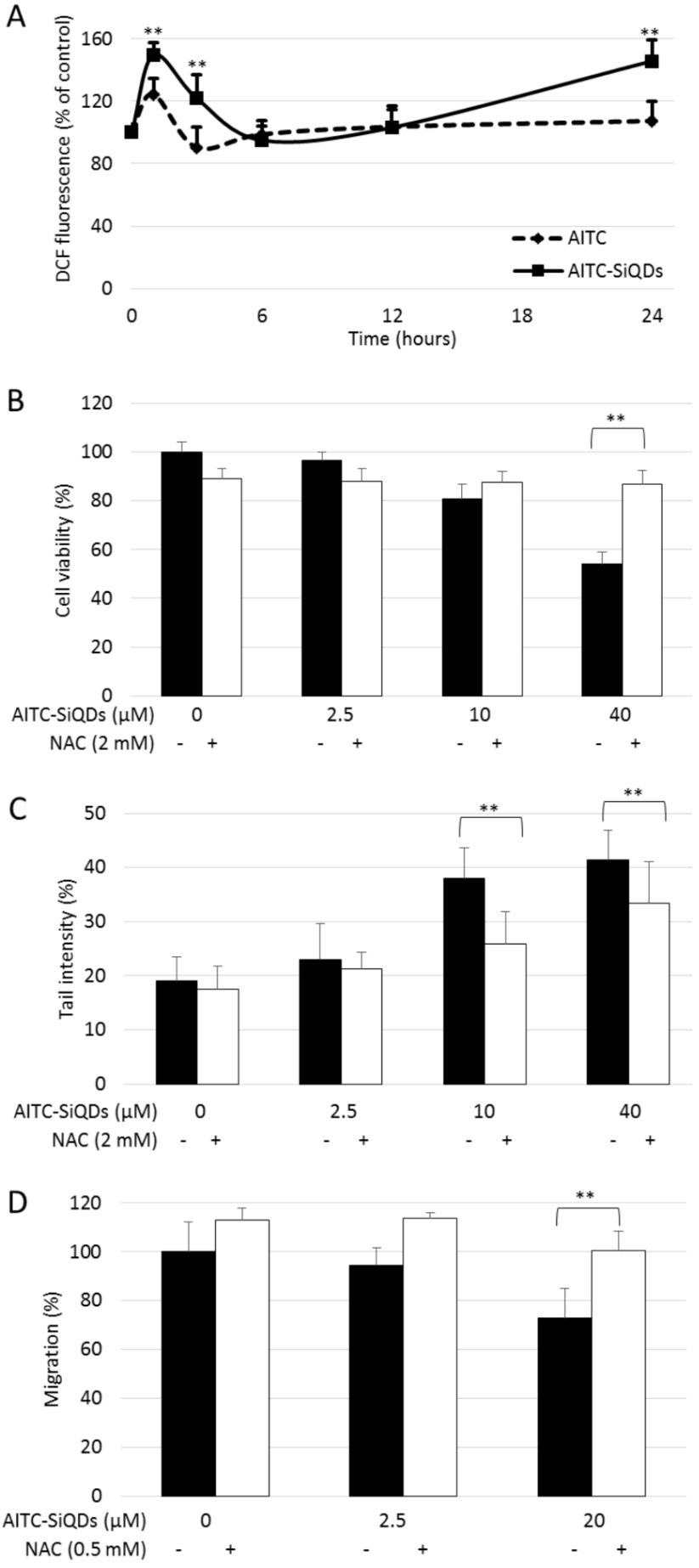
A
DCF fluorescence (% of control)
160
120
80
40
0
**
**
**
AITC
AITC-SiQDs
0
6
12
18
24
Time (hours)
B
Cell viability (%)
120
100
80
60
40
20
0
**
AITC-SiQDs (μM) 0 2.5 10 40
NAC (2 mM) - + - + - + - +
C
Tail intensity (%)
50
40
30
20
10
0
**
**
AITC-SiQDs (μM) 0 2.5 10 40
NAC (2 mM) - + - + - + - +
D
Migration (%)
120
100
80
60
40
20
0
**
AITC-SiQDs (μM) 0 2.5 20
NAC (0.5 mM) - + - + - +

Figure 6.9 Anticancer properties of AITC-SiQDs is mediated by ROS. (A) Caco-2 cells were incubated with 20 µM AITC or AITC-SiQDs over 24 hours with DMSO (0.1%) as control, ROS was measured at certain time points using flow cytometry. Data are presented as mean ± SD ($n \geq 3$), $^{**}p < 0.01$ compared to corresponding AITC treatment. (B) Caco-2 cells were incubated with different doses of AITC-SiQDs with or without 2 mM NAC for 24 hours. Cell viability was measured by MTT assay. (C) HepG2 cells were incubated with different doses of AITC-SiQDs with or without 2 mM NAC for 24 hours. DNA damage was measured by comet assay. (D) HepG2 cells were incubated with different doses of AITC-SiQDs with or without 0.5 mM NAC for 48 hours. Cell migration was measured by wound assay. Data are presented as mean ± SD ($n \geq 5$), $^{**}p < 0.01$ between the indicated groups (t-test).

6.3 Discussion

Recent findings suggest that several phytochemicals exhibit biphasic dose responses on cells with low doses activating signalling pathways that result in increased expression of genes encoding cytoprotective proteins such as antioxidant enzymes, protein chaperones, growth factors and mitochondrial proteins[173]. One example is the ITCs from CVs and their activation of Nrf2.

Nrf2 is receiving considerable attention regarding its dual role in cancer. A common mechanism behind the activity of chemopreventive agents is the activation of Nrf2, which leads to the induction of iron metabolism proteins, phase II detoxifying enzymes, phase III transporters and antioxidant proteins. Among these antioxidants, GSH synthesis and utilization are regulated by Nrf2[288,379]. However recent studies have demonstrated a dark side of Nrf2 in cancer. Several genes activated by Nrf2 are associated with cancer progression, such as those regulating proliferative signalling and reprograming energy metabolism[380,381]. Nrf2 has also been reported to be a major driver of hepatocarcinogenesis[382], and to be constitutively activated in many types of cancer cells or tumour samples from patients, which contributes to aggressive cancer phenotypes such as increased proliferation, metastasis and resistance to chemotherapy. The overexpression of Nrf2 is associated with poor prognosis in cancer patients[383,384]. In addition, recent application of Nrf2 inhibitors and shNrf2 treatment have been reported to effectively enhance chemotherapy[380,385]. Therefore, there is an urgent need to define the boundaries between the positive and negative effects of Nrf2 in cancer, and to establish a precise rationale for undertaking Nrf2 therapeutic targeting.

Results from Chapter 6.2.1 showed that AITC exhibited biphasic anticancer properties in HepG2 cells: high dose (≥ 20 μM) of AITC decreased cell viability, increased DNA damage and inhibited cell migration and angiogenesis; while low dose (1.25-2.5 μM) AITC exhibited an opposite effect. One of the main mechanisms behind the low dose stimulation effect is linked to the induction of Nrf2 signalling by AITC as siRNA knockdown treatment abolished the stimulations. BSO co-treatment also significantly reduced the effects of low dose AITC indicating the involvement of GSH in the stimulation effect. It should be noted that the physiological concentration of AITC following consumption of a meal rich in CVs or from supplements is around 1-5 μM in human plasma[101], which means for most people the exposure of AITC would be within the subtoxic stimulatory dose range, which could be a risk factor for those who have transformed cells in the body.

It has been demonstrated here for the first time that by using nanotechnology, the biphasic effect of AITC can be avoided. The biological and optical properties of AITC-SiQDs, particularly the anticancer activity of AITC as the surface ligand and the PL of the SiQDs core, were both exploited in this nanoscale system. Results showed that at high doses AITC-SiQDs exhibited similar effects to that of AITC while at low dose free from the adverse effect. The accumulation of nuclear Nrf2 induced by AITC-SiQDs was found to be much less and over a longer time than that induced by AITC. The cellular uptake studies confirmed that the internalization and excretion of AITC-SiQDs took at least 24 hours which was distinctively different from the free diffusion of AITC. The role of ROS in the anticancer activities of AITC-SiQDs was also demonstrated. Although the underlying mechanism is not fully understood, the different patterns of Nrf2 activation may be the key of AITC-SiQDs escaping the biphasic response shown by AITC.

One limitation of the current study was the usage of NH_2-SiQDs as negative controls applied only to the measurement of cytotoxicity, but not to other endpoints of efficacy discussed here such as DNA integrity, migration and angiogenesis. Based on the significant differences observed from the cytotoxicity experiments and previous studies of the bioactivities of NH_2-SiQDs, it is safe to assume that NH_2-SiQDs do not possess strong toxic effect *in vitro*. Yet it would be interesting to further compare the possible different effects between these two SiQDs, as it has been proved that the surface decoration plays a vital role in *in vivo* stability, internalization and functionality of stealth NPs.

In summary, this nano delivery system presents an encouraging platform to avoid the biphasic effect of AITC. Further *in vivo* studies must be performed to extrapolate the dose-effects found in the *in vitro* experiments. Together with other advantages that could be provided by this nanoscale delivery system, such as passive tumour targeting and real time monitoring[386], AITC-SiQDs have the potential to be used in anticancer drug delivery.

Chapter 7. Conclusion and future perspectives

7.1 Findings and final discussion

The US National Cancer Institute has identified more than 1,000 different phytochemicals that possess cancer-preventive activity, and more than half of the anticancer drugs in clinical use are natural products or their derivatives and many are plant-derived phytochemicals[387]. Dietary ITCs from CVs have attracted extensive research interest for cancer management, as they are easy accessible and have shown strong evidence of anticancer bioactivities in *in vitro* and animal studies. However, the epidemiological evidence regarding the consumption of dietary ITCs as chemopreventive agents has been inconsistent. Further detailed mechanistic studies of the bioactivities of ITCs are needed to better harness their potential beneficial effects in clinical application.

SFN has been found to exert a variety of bio-active effects including anti-oxidation, anti-inflammation, cytotoxicity and cytoprotection. Furthermore, *in vitro* and *in vivo* studies have revealed that SFN affects many stages of cancer development: it modulates the initiation phase of cancer by inhibiting phase I enzymes and inducing phase II enzymes; the promotion phase by inducing apoptosis, autophagy and cell-cycle inhibition; and the progression phase by inhibiting EMT, angiogenesis and metastasis[66,67]. Here, the effect of SFN on normal and cancerous liver cells, HHL5 and HepG2 respectively, were compared in terms of its cytotoxic and cytoprotective effects in Chapter 3; three of its metabolites (SFN-GSH, SFN-Cys, and SFN-NAC) were studied in Chapter 4; and the anti-angiogenic effect of SFN in HCC was examined in Chapter 5.

Results from these chapters confirmed the chemopreventive effects of SFN. In HepG2 cells, SFN inhibited cell viability, induced DNA damage, inhibited colony formation, disrupted cell migration and adhesion at high doses (≥ 20 μM). It also impaired EC function and suppressed tumour growth and angiogenesis in the HepG2-bearing CAM model. From the cytoprotective point of view, SFN potently induced the activation of Nrf2 and its downstream target: TrxR1, NQO1 and HO-1. It also increased the intracellular GSH level at 24 hours (with a depletion effect around 3 - 6 hours). Low dose SFN (≤ 5 μM) provided protection against H_2O_2-induced apoptosis, DNA damage and cell death. A conclusion which can be drawn is that beyond a certain concentration threshold SFN exerts pro-death activities and below the threshold it may promote pro-survival signalling. However, SFN (and its metabolites) was more toxic towards HHL5 compared to HepG2, which is likely due to the

differences in Nrf2/GSH basal level between these two cell lines. BSO inhibition and Nrf2 knockdown both increased HepG2 cell sensitivity towards SFN toxicity. In addition, HepG2 cells were able to benefit from the cytoprotective effect of SFN against oxidative stress within a wider dose range (1.25 - 20 μM) compared to HHL5, in which the essential role of Nrf2 and GSH has also been confirmed. All these results raise important questions about the selectivity of SFN towards cancer cells.

One of the characteristics of cancer cells is to maintain a much higher ROS level than normal cells. This enables cancer cells to constitutively activate growth factor pathways, such as PI3K/Akt, MARK and STATs, to sustain cellular growth and proliferation[95,389]. Consequently, the hyper-metabolism of cancer cells causes abundant generation of ROS from mitochondria, endoplasmic reticulum and NADPH oxidases, which lead to genomic instability to promote tumorigenesis, reinforcement of proliferative signals, and activation of NF-kB and EMT to support survival and progression of the tumour cells[282]. The elevated ROS level also activates HIFs to adapt to the metabolic stress and to stimulate angiogenesis[355]. More interesting, the high ROS production is counterbalanced by the high antioxidant activity in cancer cells. The major mechanism by which cancer cells increased their ROS scavenging potential is through activating Nrf2 signalling. Elevated ROS can oxidize redox sensitive cysteine residues on Keap1 and even stimulate PI3K, MAPK, etc. signalling to activate Nrf2 translocation to the nucleus. In addition, certain tumour cells were found to have Keap1 mutations resulting in constitutive activation of Nrf2[85]. Other tumour suppressor genes such as FOXOs and p53 also repress tumorigenesis by inducing antioxidants[282].

In summary, tumorigenic cells require high level of ROS to promote proliferation, survival and metabolic adaption. At the same time, if cancer cells lose control of their ROS levels, they are susceptible to oxidative stress induced cell death. The dual function of ROS in cancer biology presents a conundrum for therapeutic use of ITCs. Many chemopreventive phytochemicals, including ITCs, are considered as antioxidants. However, no evidence was found to support antioxidant supplements for primary or secondary prevention, β-carotene and vitamin E even seemed to increase mortality[390]. The indirect antioxidant capacity of ITCs largely involves the activation of Nrf2 and phase II detoxification system, leading to an increase the cellular defences against oxidative damage. However, this may be hijacked by malignant cells to sustain high ROS levels without oxidative damage, thus promote more aggressive phenotypes.

Nrf2 has been traditionally deemed to be a tumour suppressor[86,288]. However, increasing evidence has been revealing the dark side of Nrf2 in cancer prevention and treatment[293,381]. It is a fact that Nrf2 exhibits a beneficial effect not only in normal cells but also in cancer cells, thus the effect of Nrf2 activation will dependent on cancer types and stages. A simple hypothesis is that because oxidative stress is needed to initiate cancer, activation of Nrf2 at that time may play a chemopreventive role. While at the later stage, Nrf2 hyperactivation favours the survival of the cancer cells by protecting them from excessive oxidative stress, triggering malignant progression and even increasing resistances against chemotherapeutic agents and radiotherapy[383]. Satoh *et al* reported that Nrf2 prevented initiation but accelerated progression during lung carcinogenesis[391]. Some studies suggest that dietary ITCs exert tumour inhibitory effects especially during earlier stages of carcinogenesis[392,393]. As potent inducers of Nrf2/ARE signalling, the use of ITCs needs to be carefully reconsidered when defining the boundaries between the positive and negative effects of Nrf2 in individual cases.

Importantly, there is no significant difference between SFN and three of its metabolites in the induction of Nrf2 nuclear translocation and downstream protein expression, which further proves the necessity to study the mechanism behind not only SFN but also its metabolites. In addition, theses metabolites possess greater solubility in aqueous media and different distribution profiles during metabolism (see section 4.1), all of which indicate that they would be a preferred form for clinical chemoprevention trials in certain cases.

Apart from the hormetic effect and lack of selectivity of SFN discussed above, there are other factors that hinder the clinical use of SFN (and many other ITCs). Many ITCs are unstable under normal conditions. Their bioavailability can be influenced by many factors (see section 1.2). It is also difficult to reach therapeutically doses of ITCs in the systemic circulation due to the rapid clearance and metabolism in the human body. Notably, the cytotoxic and anticancer activity of ITCs occur at higher concentrations (> 5 μM), which is difficult to achieve and maintain through dietary intake. These limitations could be improved by application of nanotechnology to provide protection against degradation and to achieve controlled and targeted release.

In Chapter 6, the biphasic effect of AITC was confirmed on cell viability, DNA damage and migration in HepG2 cells; and on tube formation in the 3D co-culture of HUVEC with pericytes model. siRNA knockdown of Nrf2 and GSH inhibition abolished the stimulation

effect of AITC on cell migration and DNA damage, indicating the role of Nrf2 and GSH in the hormetic effect of ITCs. Furthermore, the biological activity of a novel NP delivery system with AITC conjugated on the surface of SiQDs (AITC-SiQDs) was investigated. AITC-SiQDs showed similar anticancer properties at high doses while avoiding the stimulation effect of low doses compared to free AITC. In addition, AITC-SiQDs showed a lower and long-lasting activation of Nrf2 translocation into nucleus which correlated with their levels of cellular uptake as detected by the intrinsic fluorescence of SiQDs. ROS production could be one of the mechanisms behind the anticancer effect of AITC-SiQDs. These data provide novel insights into the biphasic effect of AITC and highlight the application of nanotechnology to optimize the therapeutic potential of dietary ITCs in cancer treatment.

7.2 Limitations and future research

Assessing hormesis can be challenging. One crucial component of the hormetic dose response is time[171], however it requires the response to be evaluated using many doses with multiple time points. In the database compiling toxicological studies assessing the occurrence of hormetic dose responses built by Calabrease *et al*, only 20% of the 9000 dose responses include a time component[394]. In addition, the magnitude of the low-dose stimulation is mostly (60%) modest with maximum responses typically only 30-60% greater than control group[394], which makes it difficult to distinguish the stimulatory response from the variation between groups. Study designs need to be more rigorous, with at least 3-4 properly spaced doses below a well-characterized threshold and higher statistical power (more animals, more repeats, etc.). The observation and reproducibility of hormesis would also be further challenged by the high variability within the control group. To this end, besides experiments *in vitro*, long-term animal model experiments are needed to confirm the hormetic window of ITCs in different pathological conditions (either in the process of carcinogenesis or aggressive cancer progression).

On the other hand, *in vivo* models should be used to explore other advantages that could be provided by this nanoscale delivery system, such as passive tumour targeting via the enhanced permeability and retention (EPR) effect[395] and real time monitoring, as there is limited similarity between NP delivery *in vitro* and *in vivo*. Further design of NPs could also enable active targeting via ligand/receptor mediated, and/or microenvironment-responsive cellular uptake. In addition, various physical stimuli, such as electric pulse, ultrasound,

magnetic field, radiation, light and so on, have been used to trigger the release of drug and improve the efficacy of NPs[396]**.** Thus, the application of nano-vectors could enable targeted delivery of ITCs with a controlled dose based on the engineering of the NPs to achieve the maximum beneficial effects.

Emerging as a new strategy for cancer chemotherapy, combination therapy (either the co-administration of more than two therapeutic agents or the combination of different types of therapy) allows targeting of multiple pathways involved in drug resistance or cancer cell survival, and are usually more effective than monotherapy due to the heterogeneous nature of cancer[397]. ITCs have multiple targets in the process of cancer development, therefore they have been considered as promising candidates for combination therapy. In tumour-bearing mice experiments, SFN was found to be able to enhance the therapeutic potential of TRAIL through regulation of apoptosis, metastasis and angiogenesis[147]; sensitized non-small cell lung cancer cells to cisplatin by inhibiting c-Myc accumulation[398]; and enhanced the anticancer activity of taxanes against triple negative breast cancer by targeting cancer stem cells[399]. There is also *in vivo* evidence that supports AITC as a potential candidate to overcome platinum resistance[400]; and to synergistically inhibit bladder cancer growth, angiogenesis and invasion with celecoxib[401].

Current combination approaches through cocktail administration face several challenges, one of which is to ensure the correct ratio of the combined agents reaches the target under dissimilar pharmacokinetics. The application of nanotechnology could be of help in this aspect, offering controlled drug delivery and opportunities in novel combination strategies[397]. NPs have been proved to be able to deliver various materials from hydrophobic small molecules (e.g. most inhibitors and chemotherapies) to hydrophilic macromolecules (e.g. antibodies and nucleic acids). Liposomes, generally considered as amphiphilic lipid bilayered spherical vesicles, are one of the most stable platforms for multi-drug delivery. Another class of FDA-approved materials for NPs is a variety of biodegradable polymers such as polyethylene glycol (PEG), polyvinyl alcohol (PVA), hydrophobic polylactic acid (PLA), polyglycolic acid (PGA), etc. Along with other nanoparticulate systems, promising studies of their application in combination therapy have been summarized in several reviews[402,403].

There are several successful NP delivery systems for combination therapy using phytochemicals as chemosensitizers with various drugs. However, there are very few reports on the application of ITCs. One combination regimen of aspirin and curcumin (encapsulated with solid lipid NPs) with free SFN has shown 10-fold lower effective dosages against the progression of pancreatic intraepithelial neoplasms in comparison with the free form

mixtures[404]; and later been confirmed as safe for acute, subacute, and subchronic oral administration in mice[405]. The same lab has also published another regimen of ibuprofen (encapsulated in solid lipid NPs) and SFN, which again provided evidence of a promising approach for pancreatic cancer prevention and therapy[406]. Why do they not encapsulate SFN into the NPs is not explained. Hossein *et al* reported a delivery system of SFN and curcumin with PEGylated gold coated Fe_3O_4 magnetic NPs with a size of 20 nm and enhanced therapeutic effects by apoptosis and necrosis induction as well as inhibition of migration in human breast adenocarcinoma cells[407]. With many available formulations of ITCs in combination therapies, surely there is space to explore utilizing nano delivery systems to achieve maximum therapeutic effect.

The application of nanotechnology in combination therapy could also play an important role in the evolving field of personalized medicine. With the growing knowledge of molecular distinct subtypes of various cancers and the fast-developed technology of genetic profiling of the patients, it is possible to optimize treatment for each patient. Nanomedicine, in addition, could integrate diagnostic and therapeutic function in one system, and offer fine-tuning of the pharmacological properties of the treatment with specific targeting and controlled release, thus maximising the clinical potency for the benefit of patients. Current nanotechnology-based therapeutic systems are not yet sufficient, however it is a fast-growing field for future biomedicine, especially in cancer[408].

In conclusion, ITCs show great promise as chemopreventive agents, but there is a significant need to understand the dynamic molecular networks that respond to ITCs leading to the hormetic effects and any possible selectivity in cancer prevention and treatment. The utilization of nanotechnology could increase the therapeutic benefit of ITCs by tailoring time/dose according to the specificities of the disease, while minimizing any possible detrimental effects at nonspecific targets, thus providing us with an opportunity to use ITCs as therapeutic agents for cancer treatment. Further detailed studies are required to establish the safety and efficacy profiles of ITCs and their nano-form to pursue their clinical application.

Appendices

Appendix 1. BSO inhibiton of GSH, dose-dependent efficiency

The dose response from 24 hours treatment of BSO on intracellular GSH level was examined in Appendix Figure 1A. 50 µM BSO was chosen to be the co-treatment dose with SFN as it showed 60-80% reduction in the GSH level without significant cytotoxicity. Co-treatment with BSO (50 µM) abolished SFN (5 µM) induced GSH rise, from 98.7 to 13.8 nmol/mg protein (Appendix Figure 1B).

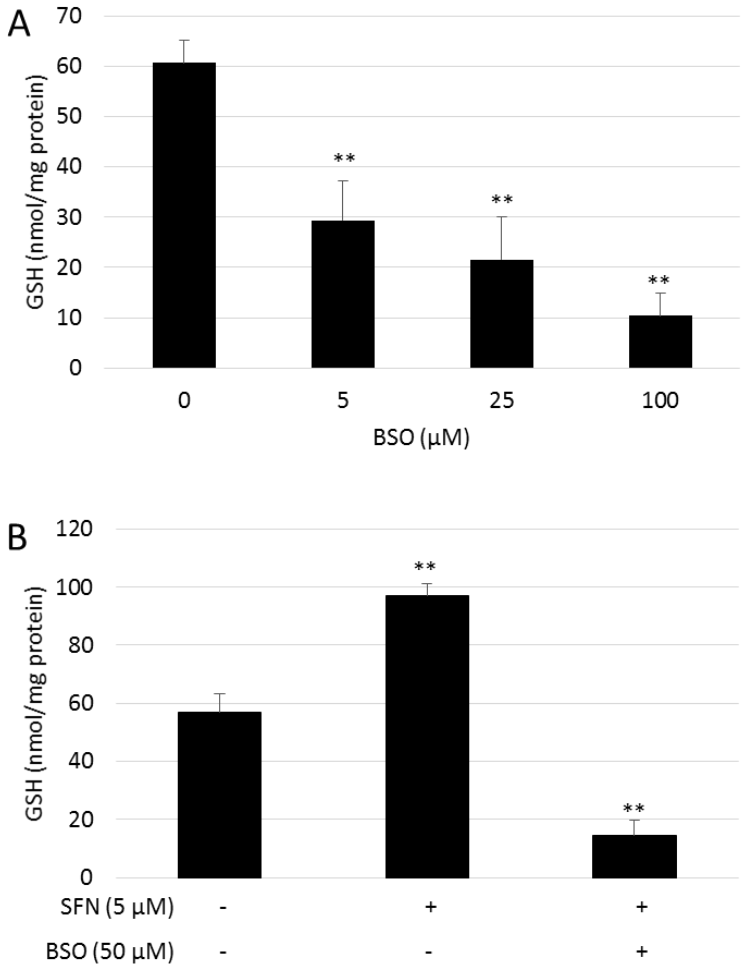

Appendix Figure 1. Effect of BSO on intracellular GSH levels in HepG2 cells. Cells were treated with different doses of BSO with water as vehicle control for 24 hours (A) or 5 µM SFN +/- 50 µM BSO for 24 hours (B). The intracellular GSH level was measured by HPLC, result represents the mean ± SD (n = 3). Statistical significance from control, **p < 0.01.

Appendix 2. siNrf2 efficiency

The siRNA knockdown efficiency of Nrf2 was characterized using Western blot analysis. Transfection was done following the protocol of large-scale transfection of adherent cells from the HiPerFect transfection reagent handbook. HepG2 cells were seeded in 60 mm dishes at 1 x 10^6 cells/dish in 3.5 ml of complete medium, and incubated under normal growth conditions for 24 hours. 40 nM siRNA and 20 µl of HiPerFect transfection reagent were added to 0.5 ml culture medium without serum or antibiotics, mixed and incubated for 5-10 mins at RT to allow the formation of transfection complexes. The complexes were then added drop-wise to each well to give a final siRNA concentration of 5 nM. Plate were gently swirled to ensure uniform distribution of the transfection complexes. Cell were cultured under normal growth conditions for additional 48 hours before adding AITC 2.5 µM or DMSO (0.1%) for 4 hours. Nuclear protein extraction and Western blotting were then performed as described. As shown in Appendix Figure 2, AITC induced nuclear accumulation of Nrf2 in control and cells transfected with Allstar, while an 80% inhibition Nrf2 level was observed in siNrf2 transfected cells compared to that in Allstar transfected cells under AITC treatment. This confirmed the transfection could abolish the induction effect of AITC on nuclear Nrf2 accumulation.

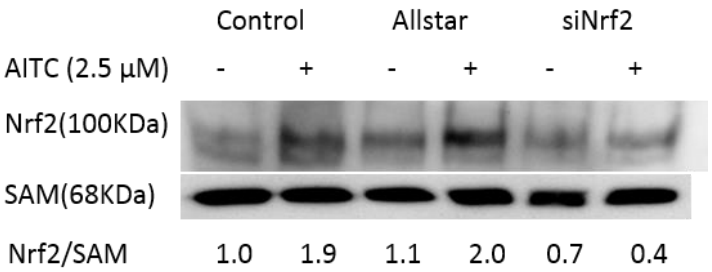

Appendix Figure 2. Effect of Nrf2 siRNA in HepG2 cells. Cells were seeded in 6 cm dishes, after 24 hours cells were treated with siNrf2 as per the manufacturer's instructions. Allstars was used as a negative control. After another 48 hours, medium was changed with 2.5 µM AITC or DMSO (0.1%) treatment for 4 hours. Nrf2 in nuclear extract was detected using Western blot analysis.

Appendix 3. SiQDs control for cytotoxicity experiments

The effect of AITC-SiQDs on the cell viability was initially screened using MTT assay with amine-capped SiQDs (NH_2-SiQDs)[226] as negative control. As the ligand coverage of NH_2-SiQDs is unknown, the unit μg/mL was used here to compare these two kinds of NPs. Results in Appendix Figure 3 confirmed that the cytotoxicity of AITC-SiQDs came from the surface ligand instead of the SiQDs core.

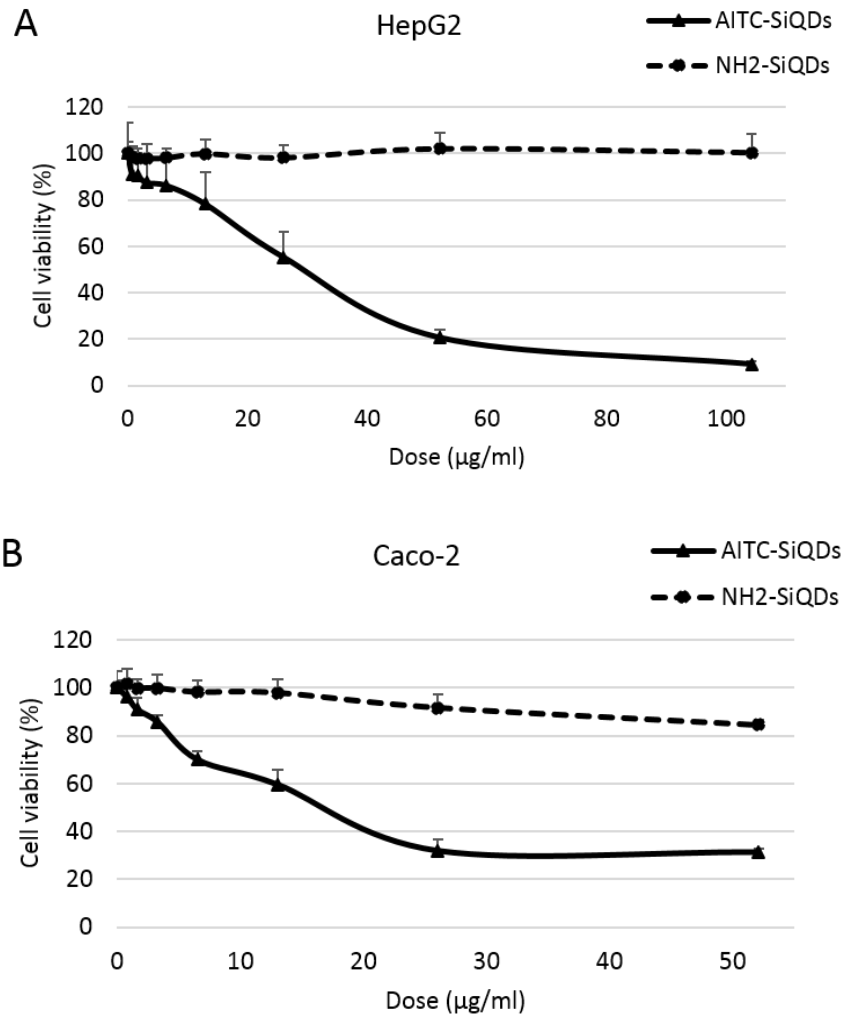

Appendix Figure 3. Effects of NH_2-SiQDs on cell viability. Cells were treated with different dose of AITC-SiQDs or NH_2-SiQDs at 70–80% confluence for 24 hours. The control cells were treated with DMSO (0.1%), and cell viability was determined by the MTT assay. Results from (A) HepG2, (B) Caco-2. Each data point represents the mean ± SD of at least 5 biological replicates.

References

1. Siegel, R. L., Miller, K. D. & Jemal, A. Cancer Statistics, 2017. *CA Cancer J Clin* **67,** 7–30 (2017).

2. Steward, W. P. & Brown, K. Cancer chemoprevention: a rapidly evolving field. *Br. J. Cancer* **109,** 1–7 (2013).

3. Landis-Piwowar, K. R. & Iyer, N. R. Cancer Chemoprevention: Current State of the Art. *Cancer Growth Metastasis* **7,** 19–25 (2014).

4. Tuorkey, M. J. Cancer Therapy with Phytochemicals : Present and Future Perspectives. *Biomed. Environ. Sci.* **28,** 808–819 (2015).

5. Zubair, H. *et al.* Cancer chemoprevention by phytochemicals: Nature's healing touch. *Molecules* **22,** 395 (2017).

6. Baena Ruiz, R. & Salinas Hernández, P. Cancer chemoprevention by dietary phytochemicals: Epidemiological evidence. *Maturitas* **94,** 13–19 (2016).

7. Surh, Y.-J. Cancer chemoprevention with dietary phytochemicals. *Nat. Rev. Cancer* **3,** 768–780 (2003).

8. World Cancer Research Fund & American Institute for Cancer Research. *Food, Nutrition, Physical Activity, and the Prevention of Cancer: a Global Perspective.* Washington DC: AICR (2007)

9. Wattenberg, L. W. Chemoprevention of Cancer. *Cancer Res.* **45,** 1–8 (1985).

10. Watson, G. W., Beaver, L. M., Williams, D. E., Dashwood, R. H. & Ho, E. Phytochemicals from cruciferous vegetables, epigenetics, and prostate cancer prevention. *AAPS J.* **15,** 951–61 (2013).

11. Issa, A. Y., Volate, S. R. & Wargovich, M. J. The role of phytochemicals in inhibition of cancer and inflammation: New directions and perspectives. *Journal of Food Composition and Analysis* **19,** 405–419 (2006).

12. Angelino D., Jeffery E. Glucosinolate hydrolysis and bioavailability of resulting isothiocyanates: Focus on glucoraphanin. *J. Funct. Foods* **7,** 67–76 (2014).

13. Rask, L. *et al.* Myrosinase: Gene family evolution and herbivore defense in Brassicaceae. *Plant Mol. Biol.* **42,** 93–113 (2000).

14. Nakagawa, K. *et al.* Evaporative light-scattering analysis of sulforaphane in broccoli samples: Quality of broccoli products regarding sulforaphane contents. *J. Agric. Food*

Chem. **54,** 2479–2483 (2006).

15. Gu, Z., Guo, Q. & Gu, Y. Factors Influencing Glucoraphanin and Sulforaphane Formation in Brassica Plants: A Review. *J. Integr. Agric.* **11,** 1804–1816 (2012).

16. Matusheski, N. V. *et al.* Epithiospecifier protein from broccoli (Brassica oleracea L. ssp. italica) inhibits formation of the anticancer agent sulforaphane. *J. Agric. Food Chem.* **54,** 2069–2076 (2006).

17. Uematsu, Y. *et al.* Determination of isothiocyanates and related compounds in mustard extract and horseradish extract used as natural food additives. *Shokuhin Eiseigaku Zasshi.* **43,** 10–17 (2002).

18. Sultana, T. *et al.* Effects of fertilisation on the allyl isothiocyanate profile of above-ground tissues of New Zealand-grown wasabi. *J. Sci. Food Agric.* **82,** 1477–1482 (2002).

19. Cavanaugh, E. J., Simkin, D. & Kim, D. Activation of transient receptor potential A1 channels by mustard oil, tetrahydrocannabinol and Ca2+ reveals different functional channel states. *Neuroscience* **154,** 1467–1476 (2008).

20. Agudo, A. *et al.* Consumption of cruciferous vegetables and glucosinolates in a Spanish adult population. *Eur. J. Clin. Nutr.* **62,** 324–331 (2008).

21. Fowke, J. H. *et al.* Urinary Isothiocyanate Excretion, Brassica Consumption, and Gene Polymorphisms among Women Living in Shanghai, China. *Cancer Epidemiol. Biomarkers Prev.* **12,** 1536–1539 (2003).

22. McNaughton, S. A. & Marks, G. C. Development of a food composition database for the estimation of dietary intakes of glucosinolates, the biologically active constituents of cruciferous vegetables. *Br. J. Nutr.* **90,** 687–697 (2003).

23. Matusheski, N. V., Juvik, J. A. & Jeffery, E. H. Heating decreases epithiospecifier protein activity and increases sulforaphane formation in broccoli. *Phytochemistry* **65,** 1273–1281 (2004).

24. Saha, S. *et al.* Isothiocyanate concentrations and interconversion of sulforaphane to erucin in human subjects after consumption of commercial frozen broccoli compared to fresh broccoli. *Mol. Nutr. Food Res.* **56,** 1906–1916 (2012).

25. Vermeulen, M., Klöpping-Ketelaars, I. W., Van Den Berg, R. & Vaes, W. H. Bioavailability and kinetics of sulforaphane in humans after consumption of cooked versus raw broccoli. *J. Agric. Food Chem.* **56,** 10505–10509 (2008).

26. Fahey, J. W. *et al.* Sulforaphane bioavailability from glucoraphanin-rich broccoli:

Control by active endogenous myrosinase. *PLoS One* **10,** (2015).

27. McClements, D. J. Enhancing nutraceutical bioavailability through food matrix design. *Current Opinion in Food Science* **4,** 1–6 (2015).

28. Krul, C. *et al.* Metabolism of sinigrin (2-propenyl glucosinolate) by the human colonic microflora in a dynamic in vitro large-intestinal model. *Carcinogenesis* **23,** 1009–1016 (2002).

29. Seow, A. *et al.* Urinary total isothiocyanate (ITC) in a population-based sample of middle-aged and older Chinese in Singapore: Relationship with dietary total ITC and glutathione S-transferase M1/T1/P1 genotypes. *Cancer Epidemiol. Biomarkers Prev.* **7,** 775–781 (1998).

30. Zhang, Y., Kolm, R. H., Mannervik, B. & Talalay, P. Reversible conjugation of isothiocyanates with glutathione catalyzed by human glutathione transferases. *Biochem. Biophys. Res. Commun.* **206,** 748–755 (1995).

31. Zhang, Y. & Talalay, P. Mechanism of differential potencies of isothiocyanates as inducers of anticarcinogenic Phase 2 enzymes. *Cancer Res.* **58,** 4632–4639 (1998).

32. Zhang, Y. Role of glutathione in the accumulation of anticarcinogenic isothiocyanates and their glutathione conjugates by murine hepatoma cells. *Carcinogenesis* **21,** 1175–1182 (2000).

33. Zhang, Y. The molecular basis that unifies the metabolism, cellular uptake and chemopreventive activities of dietary isothiocyanates. *Carcinogenesis* **33,** 2–9 (2012).

34. Higdon, J. V., Delage, B., Williams, D. E. & Dashwood, R. H. Cruciferous vegetables and human cancer risk: epidemiologic evidence and mechanistic basis. *Pharmacological Research* **55,** 224–236 (2007).

35. Ye, L., Dinkova-Kostova, A. & Wade, K. Quantitative determination of dithiocarbamates in human plasma, serum, erythrocytes and urine: pharmacokinetics of broccoli sprout isothiocyanates in humans. *Clin. Chim. Acta* **316,** 43–53 (2002).

36. Petri, N. *et al.* Absorption/metabolism of sulforaphane and quercetin, and regulation of phase II enzymes, in human jejunum in vivo. *Drug Metab. Dispos.* **31,** 805–813 (2003).

37. Gasper, A. V. *et al.* Glutathione S-transferase M1 polymorphism and metabolism of sulforaphane from standard and high-glucosinolate broccoli. *Am. J. Clin. Nutr.* **82,** 1283–1291 (2005).

38. Davidson, R. *et al.* Isothiocyanates are detected in human synovial fluid following broccoli consumption and can affect the tissues of the knee joint. *Sci. Rep.* **7,** (2017).

39. Cornblatt, B. S. *et al.* Preclinical and clinical evaluation of sulforaphane for chemoprevention in the breast. *Carcinogenesis* **28,** 1485–1490 (2007).

40. Bricker, G. V. *et al.* Isothiocyanate metabolism, distribution, and interconversion in mice following consumption of thermally processed broccoli sprouts or purified sulforaphane. *Mol. Nutr. Food Res.* **58,** 1991–2000 (2014).

41. Veeranki, O., Bhattacharya, A., Marshall, J. R. & Zhang, Y. Organ-specific exposure and response to sulforaphane, a key chemopreventive ingredient in broccoli: implications for cancer prevention. *Br. J. Nutr.* **109,** 25–32 (2013).

42. Ioannou, Y. M., Burka, L. T. & Matthews, H. B. Allyl isothiocyanate: Comparative disposition in rats and mice. *Toxicol. Appl. Pharmacol.* **75,** 173–181 (1984).

43. Bollard, M., Stribbling, S., Mitchell, S. & Caldwell, J. The disposition of allyl isothiocyanate in the rat and mouse. *Food Chem. Toxicol.* **35,** 933–943 (1997).

44. Bhattacharya, A. *et al.* Inhibition of bladder cancer development by allyl isothiocyanate. *Carcinogenesis* **31,** 281–286 (2010).

45. Shapiro, T. A., Fahey, J. W., Wade, K. L., Stephenson, K. K. & Talalay, P. Chemoprotective glucosinolates and isothiocyanates of broccoli sprouts: Metabolism and excretion in humans. *Cancer Epidemiol. Biomarkers Prev.* **10,** 501–508 (2001).

46. Kristensen, M., Krogholm, K. S., Frederiksen, H., Bügel, S. H. & Rasmussen, S. E. Urinary excretion of total isothiocyanates from cruciferous vegetables shows high dose-response relationship and may be a useful biomarker for isothiocyanate exposure. *Eur. J. Nutr.* **46,** 377–382 (2007).

47. Munday, R. *et al.* Evaluation of isothiocyanates as potent inducers of carcinogen-detoxifying enzymes in the urinary bladder: critical nature of in vivo bioassay. *Nutr. Cancer* **54,** 223–231 (2006).

48. Shapiro, T. a *et al.* Safety, tolerance, and metabolism of broccoli sprout glucosinolates and isothiocyanates: a clinical phase I study. *Nutr. Cancer* **55,** 53–62 (2006).

49. Alumkal, J. J. *et al.* A phase II study of sulforaphane-rich broccoli sprout extracts in men with recurrent prostate cancer. *Invest. New Drugs* **33,** 480–489 (2015).

50. Poulton, E. J. *et al.* Sulforaphane is not an effective antagonist of the human pregnane X-receptor in vivo. *Toxicol. Appl. Pharmacol.* **266,** 122–131 (2013).

51. Miyoshi, N. Chemical alterations and regulations of biomolecules in lifestyle-related diseases. *Biosci. Biotechnol. Biochem.* **80,** 1046–1053 (2016).

52. Lewis, S. M. *et al.* Inactivation of protein tyrosine phosphatases by dietary isothiocyanates. *Bioorganic Med. Chem. Lett.* **25,** 4549–4552 (2015).

53. Mi, L. *et al.* Covalent binding to tubulin by isothiocyanates. A mechanism of cell growth arrest and apoptosis. *J. Biol. Chem.* **283,** 22136–22146 (2008).

54. Cross, J. V, Foss, F. W., Rady, J. M., Macdonald, T. L. & Templeton, D. J. The isothiocyanate class of bioactive nutrients covalently inhibit the MEKK1 protein kinase. *BMC Cancer* **7,** 183 (2007).

55. Lin, R. K. *et al.* Dietary isothiocyanate-induced apoptosis via thiol modification of DNA topoisomerase IIα. *J. Biol. Chem.* **286,** 33591–33600 (2011).

56. Youn, H. S. *et al.* Sulforaphane Suppresses Oligomerization of TLR4 in a Thiol-Dependent Manner. *J. Immunol.* **184,** 411–419 (2010).

57. Shibata, T., Kimura, Y., Mukai, A. & Mori, H. Transthiocarbamoylation of proteins by thiolated isothiocyanates. *J. Biol. Chem.* **286,** 42150–42161 (2011).

58. Cross, J. V *et al.* Nutrient isothiocyanates covalently modify and inhibit the inflammatory cytokine macrophage migration inhibitory factor (MIF). *Biochem. J* **423,** 315–321 (2009).

59. Healy, Z. R., Liu, H., Holtzclaw, W. D. & Talalay, P. Inactivation of tautomerase activity of macrophage migration inhibitory factor by sulforaphane: A potential biomarker for anti-inflammatory intervention. *Cancer Epidemiol. Biomarkers Prev.* **20,** 1516–1523 (2011).

60. Traka, M. *et al.* Broccoli consumption interacts with GSTM1 to perturb oncogenic signalling pathways in the prostate. *PLoS One* **3,** (2008).

61. Brown, K. K. & Hampton, M. B. Biological targets of isothiocyanates. *Biochim. Biophys. Acta* **1810,** 888–894 (2011).

62. Cheung, K. L. & Kong, A. N. Molecular targets of dietary phenethyl isothiocyanate and sulforaphane for cancer chemoprevention. *Am. Assoc. Pharm. Sci.* **12,** 87–97 (2010).

63. Lim, Y. P. *et al.* Allyl isothiocyanate (AITC) inhibits pregnane X receptor (PXR) and constitutive androstane receptor (CAR) activation and protects against acetaminophen- and amiodarone-induced cytotoxicity. *Arch. Toxicol.* **89,** 57–72 (2015).

64. La Marca, M. *et al.* Structural influence of isothiocyanates on expression of cytochrome P450, phase II enzymes, and activation of Nrf2 in primary rat hepatocytes. *Food Chem. Toxicol.* **50,** 2822–2830 (2012).

65. Yeh, C. T. & Yen, G. C. Chemopreventive functions of sulforaphane: A potent inducer of antioxidant enzymes and apoptosis. *J. Funct. Foods* **1,** 23–32 (2009).

66. Clarke, J. D., Dashwood, R. H. & Ho, E. Multi-targeted prevention of cancer by sulforaphane. *Cancer Letters* **269,** 291–304 (2008).

67. Lenzi, M., Fimognari, C. & Hrelia, P. Sulforaphane as a promising molecule for fighting cancer. *Cancer Treat. Res.* **159,** 207–223 (2014).

68. Yu, R. *et al.* Role of a mitogen-activated protein kinase pathway in the induction of phase II detoxifying enzymes by chemicals. *J. Biol. Chem.* **274,** 27545–27552 (1999).

69. Chen, Z. *et al.* MAP kinases. *Chem. Rev.* **101,** 2449–2476 (2001).

70. Keum, Y. S., Owuor, E. D., Kim, B. R., Hu, R. & Kong, A. N. T. Involvement of Nrf2 and JNK1 in the activation of antioxidant responsive element (ARE) by chemopreventive agent phenethyl isothiocyanate (PEITC). *Pharm. Res.* **20,** 1351–1356 (2003).

71. Shan, Y., Wang, X., Wang, W., He, C. & Bao, Y. p38 MAPK plays a distinct role in sulforaphane-induced up-regulation of ARE-dependent enzymes and down-regulation of COX-2 in human bladder cancer cells. *Oncol. Rep.* **23,** 1133–1138 (2010).

72. Keum, Y. S. *et al.* Mechanism of action of sulforaphane: Inhibition of p38 mitogen-activated protein kinase isoforms contributing to the induction of antioxidant response element-mediated heme oxygenase-1 in human hepatoma HepG2 cells. *Cancer Res.* **66,** 8804–8813 (2006).

73. Salazar, M., Rojo, A. I., Velasco, D., De Sagarra, R. M. & Cuadrado, A. Glycogen synthase kinase-3β inhibits the xenobiotic and antioxidant cell response by direct phosphorylation and nuclear exclusion of the transcription factor Nrf2. *J. Biol. Chem.* **281,** 14841–14851 (2006).

74. Rada, P. *et al.* SCF/β-TrCP promotes glycogen synthase kinase 3-dependent degradation of the Nrf2 transcription factor in a Keap1-independent manner. *Mol. Cell. Biol.* **31,** 1121–33 (2011).

75. Jain, A. K. & Jaiswal, A. K. GSK-3β Acts Upstream of Fyn Kinase in Regulation of Nuclear Export and Degradation of NF-E2 Related Factor 2.pdf. *J. Biol. Chem.* **282,** 16502–16510 (2007).

76. Shang, G. *et al.* Sulforaphane attenuation of experimental diabetic nephropathy involves GSK-3 beta/Fyn/Nrf2 signaling pathway. *J. Nutr. Biochem.* **26,** 596–606 (2015).

77. Lee, Y. J. *et al.* Reactive oxygen species and PI3K/Akt signaling play key roles in the induction of Nrf2-driven heme oxygenase-1 expression in sulforaphane-treated human mesothelioma MSTO-211H cells. *Food Chem. Toxicol.* **50,** 116–123 (2012).

78. Yu, J. S. *et al.* Sulforaphane suppresses hepatitis C virus replication by up-regulating heme oxygenase-1 expression through PI3K/Nrf2 pathway. *PLoS One* **11,** (2016).

79. Keum, Y. S. *et al.* Pharmacokinetics and pharmacodynamics of broccoli sprouts on the suppression of prostate cancer in transgenic adenocarcinoma of mouse prostate (TRAMP) Mice: Implication of induction of Nrf2, HO-1 and apoptosis and the suppression of Akt-dependent kinase p. *Pharm. Res.* **26,** 2324–2331 (2009).

80. Li, D. *et al.* Synergy between sulforaphane and selenium in the up-regulation of thioredoxin reductase and protection against hydrogen peroxide-induced cell death in human hepatocytes. *Food Chem.* **133,** 300–307 (2012).

81. Zhang, D. D. *et al.* Ubiquitination of Keap1, a BTB-Kelch substrate adaptor protein for Cul3, targets Keap1 for degradation by a proteasome-independent pathway. *J. Biol. Chem.* **280,** 30091–30099 (2005).

82. Katoh, Y. *et al.* Evolutionary conserved N-terminal domain of Nrf2 is essential for the Keap1-mediated degradation of the protein by proteasome. *Arch. Biochem. Biophys.* **433,** 342–350 (2005).

83. Tong, K. I. *et al.* Different electrostatic potentials define ETGE and DLG motifs as hinge and latch in oxidative stress response. *Mol. Cell. Biol.* **27,** 7511–7521 (2007).

84. Eggler, A. L., Small, E., Hannink, M. & Mesecar, A. D. Cul3-mediated Nrf2 ubiquitination and antioxidant response element (ARE) activation are dependent on the partial molar volume at position 151 of Keap1. *Biochem. J.* **422,** 171–180 (2009).

85. Jaramillo, M. C. & Zhang, D. D. The emerging role of the Nrf2-Keap1 signaling pathway in cancer. *Genes Dev.* **27,** 2179–91 (2013).

86. Baird, L. & Dinkova-Kostova, A. T. The cytoprotective role of the Keap1-Nrf2 pathway. *Archives of Toxicology* **85,** 241–272 (2011).

87. Mitsuishi, Y., Motohashi, H. & Yamamoto, M. The Keap1-Nrf2 system in cancers: stress response and anabolic metabolism. *Front. Oncol.* **2,** 200 (2012).

88. Hong, F., Freeman, M. L. & Liebler, D. C. Identification of sensor cysteines in human Keap1 modified by the cancer chemopreventive agent sulforaphane. *Chem. Res. Toxicol.* **18,** 1917–1926 (2005).

89. Jeong, W.S. *et al.* Differential expression and stability of endogenous nuclear factor E2-related factor 2 (Nrf2) by natural chemopreventive compounds in HepG2 human hepatoma cells. *J. Biochem. Mol. Biol.* **38,** 167–176 (2005).

90. Toyama, T. *et al.* Isothiocyanates reduce mercury accumulation via an Nrf2-dependent mechanism during exposure of mice to methylmercury. *Environ. Health Perspect.* **119,** 1117–1122 (2011).

91. Xu, C. *et al.* Inhibition of 7,12-dimethylbenz(a)anthracene-induced skin tumorigenesis in C57BL/6 mice by sulforaphane is mediated by nuclear factor E2-related factor 2. *Cancer Res.* **66,** 8293–8296 (2006).

92. Bai, Y. *et al.* Prevention by sulforaphane of diabetic cardiomyopathy is associated with up-regulation of Nrf2 expression and transcription activation. *J. Mol. Cell. Cardiol.* **57,** 82–95 (2013).

93. Zhou, Q. *et al.* Sulforaphane protects against rotenone-induced neurotoxicity in vivo: Involvement of the mTOR, Nrf2, and autophagy pathways. *Sci. Rep.* **6,** 32206 (2016).

94. Wagner, A. E., Boesch-Saadatmandi, C., Dose, J., Schultheiss, G. & Rimbach, G. Anti-inflammatory potential of allyl-isothiocyanate--role of Nrf2, NF-(κ) B and microRNA-155. *J. Cell. Mol. Med.* **16,** 836–43 (2012).

95. Hanahan, D. & Weinberg, R. A. Hallmarks of cancer: The next generation. *Cell* **144,** 646–674 (2011).

96. Wang, F. & Shan, Y. Sulforaphane retards the growth of UM-UC-3 xenographs, induces apoptosis, and reduces survivin in athymic mice. *Nutr. Res.* **32,** 374–380 (2012).

97. Xu, C. *et al.* ERK and JNK signaling pathways are involved in the regulation of activator protein 1 and cell death elicited by three isothiocyanates in human prostate cancer PC-3 cells. *Carcinogenesis* **27,** 437–445 (2006).

98. Wagner, A. E., Terschluesen, A. M. & Rimbach, G. Health promoting effects of brassica-derived phytochemicals: From chemopreventive and anti-inflammatory activities to epigenetic regulation. *Oxid. Med. Cell. Longev.* **2013,** (2013).

99. Kaufman-Szymczyk, A., Majewski, G., Lubecka-Pietruszewska, K. & Fabianowska-

Majewska, K. The role of sulforaphane in epigenetic mechanisms, including interdependence between histone modification and DNA methylation. *International Journal of Molecular Sciences* **16,** 29732–29743 (2015).

100. Heiss, E., Herhaus, C., Klimo, K., Bartsch, H. & Gerhäuser, C. Nuclear Factor κB Is a Molecular Target for Sulforaphane-mediated Anti-inflammatory Mechanisms. *J. Biol. Chem.* **276,** 32008–32015 (2001).

101. Zhang, Y. Allyl isothiocyanate as a cancer chemopreventive phytochemical. *Molecular Nutrition and Food Research* **54,** 127–135 (2010).

102. Li, Y. & Zhang, T. Targeting cancer stem cells with sulforaphane, a dietary component from broccoli and broccoli sprouts. *Future Oncol.* **9,** 1097–103 (2013).

103. Kim, S.H., Sehrawat, A. & Singh, S. V. Dietary chemopreventative benzyl isothiocyanate inhibits breast cancer stem cells in vitro and in vivo. *Cancer Prev. Res. (Phila).* **6,** 782–90 (2013).

104. Pereira, L. P. *et al.* Targeting colorectal cancer proliferation, stemness and metastatic potential using Brassicaceae extracts enriched in isothiocyanates: A 3D cell model-based study. *Nutrients* **9,** 368 (2017).

105. Alberts, B. *et al. Molecular Biology of the Cell, Fourth Edition*. *Garland Science* (2002).

106. Wong, R. S. Y. Apoptosis in cancer: from pathogenesis to treatment. *J. Exp. Clin. Cancer Res.* **30,** 87 (2011).

107. Cotter, T. G. Apoptosis and cancer: the genesis of a research field. *Nat. Rev. Cancer* **9,** 501–507 (2009).

108. Kumar, G. *et al.* Isothiocyanates: a class of bioactive metabolites with chemopreventive potential. *Tumor Biology* **36,** 4005–4016 (2015).

109. Zou, X., Qu, Z., Fang, Y., Shi, X. & Ji, Y. Endoplasmic reticulum stress mediates sulforaphane-induced apoptosis of HepG2 human hepatocellular carcinoma cells. *Mol. Med. Rep.* **15,** 331–338 (2017).

110. Rudolf, K., Cervinka, M. & Rudolf, E. Sulforaphane-induced apoptosis involves p53 and p38 in melanoma cells. *Apoptosis* **19,** 734–747 (2014).

111. Choi, S. *et al.* D,L-Sulforaphane-induced cell death in human prostate cancer cells is regulated by inhibitor of apoptosis family proteins and Apaf-1. *Carcinogenesis* **28,** 151–162 (2007).

112. Račkauskas, R. *et al.* Sulforaphane sensitizes human cholangiocarcinoma to cisplatin via the downregulation of anti-apoptotic proteins. *Oncol. Rep.* **37,** 3660–3666 (2017).

113. Geng, F. *et al.* Allyl isothiocyanate arrests cancer cells in mitosis, and mitotic arrest in turn leads to apoptosis via Bcl-2 protein phosphorylation. *J. Biol. Chem.* **286,** 32259–32267 (2011).

114. Li, G. *et al.* Mitochondrial translocation of cofilin is required for allyl isothiocyanate-mediated cell death via ROCK1/PTEN/PI3K signaling pathway. *Cell Commun. Signal.* **11,** 50 (2013).

115. Curtin, N. J. DNA repair dysregulation from cancer driver to therapeutic target. *Nat. Rev. Cancer* **12,** 801–817 (2012).

116. Lord, C. J. & Ashworth, A. The DNA damage response and cancer therapy. *Nature* **481,** 287–294 (2012).

117. Dueva, R. & Iliakis, G. Alternative pathways of non-homologous end joining (NHEJ) in genomic instability and cancer. *Transl. Cancer Res.* **2,** 163–177 (2013).

118. Sestili, P. *et al.* Sulforaphane induces DNA single strand breaks in cultured human cells. *Mutat. Res.* **689,** 65–73 (2010).

119. Kassie, F. & Knasmüller, S. Genotoxic effects of allyl isothiocyanate (AITC) and phenethyl isothiocyanate (PEITC). *Chem. Biol. Interact.* **127,** 163–180 (2000).

120. Ferreira de Oliveira, J. M. P. *et al.* Sulforaphane Induces DNA Damage and Mitotic Abnormalities in Human Osteosarcoma MG-63 Cells: Correlation with Cell Cycle Arrest and Apoptosis. *Nutr. Cancer* **66,** 325–334 (2014).

121. Savio, A. L. V., da Silva, G. N., Camargo, E. A. de & Salvadori, D. M. F. Cell cycle kinetics, apoptosis rates, DNA damage and TP53 gene expression in bladder cancer cells treated with allyl isothiocyanate (mustard essential oil). *Mutat. Res. - Fundam. Mol. Mech. Mutagen.* **762,** 40–46 (2014).

122. Rajendran, P. *et al.* HDAC turnover, CtIP acetylation and dysregulated DNA damage signaling in colon cancer cells treated with sulforaphane and related dietary isothiocyanates. *Epigenetics* **8,** 612–623 (2013).

123. Piberger, A. L., Köberle, B. & Hartwig, A. The broccoli-born isothiocyanate sulforaphane impairs nucleotide excision repair: XPA as one potential target. *Arch. Toxicol.* **88,** 647–658 (2014).

124. Naumann, P. *et al.* Sulforaphane enhances irradiation effects in terms of perturbed

cell cycle progression and increased DNA damage in pancreatic cancer cells. *PLoS One* **12(7): e01,** 1–13 (2017).

125. Charron, C. S. *et al.* Assessment of DNA damage and repair in adults consuming allyl isothiocyanate or Brassica vegetables. *J. Nutr. Biochem.* **24,** 894–902 (2013).

126. Murata, M., Yamashita, N., Inoue, S. & Kawanishi, S. Mechanism of oxidative DNA damage induced by carcinogenic allyl isothiocyanate. *Free Radic. Biol. Med.* **28,** 797–805 (2000).

127. Tripathi, K. *et al.* Allyl isothiocyanate induces replication-associated DNA damage response in NSCLC cells and sensitizes to ionizing radiation. *Oncotarget* **6,** 5237–5252 (2015).

128. Steeg, P. S. Targeting metastasis. *Nat. Rev. Cancer* **16,** 201–18 (2016).

129. Wells, A., Grahovac, J., Wheeler, S., Ma, B. & Lauffenburger, D. Targeting tumor cell motility as a strategy against invasion and metastasis. *Trends in Pharmacological Sciences* **34,** 283–289 (2013).

130. Jee, H.G., Lee, K. E., Kim, J. Bin, Shin, H.-K. & Youn, Y.-K. Sulforaphane inhibits oral carcinoma cell migration and invasion in vitro. *Phytother. Res.* **25,** 1623–8 (2011).

131. Lee, C. S. *et al.* Isothiocyanates inhibit the invasion and migration of C6 glioma cells by blocking FAK/JNK-mediated MMP-9 expression. *Oncol. Rep.* **34,** 2901–2908 (2015).

132. Mondal, A., Biswas, R., Rhee, Y. H., Kim, J. & Ahn, J. C. Sulforaphene promotes Bax/Bcl2, MAPK-dependent human gastric cancer AGS cells apoptosis and inhibits migration via EGFR, p-ERK1/2 down-regulation. *Gen. Physiol. Biophys.* **35,** 25–34 (2016).

133. Bao, C. *et al.* Sulforaphene Interferes with Human Breast Cancer Cell Migration and Invasion through Inhibition of Hedgehog Signaling. *J. Agric. Food Chem.* **64,** 5515–5524 (2016).

134. Kim, D. H. *et al.* Sulforaphane inhibits hypoxia-induced HIF-1α and VEGF expression and migration of human colon cancer cells. *Int. J. Oncol.* **47,** 2226–2232 (2015).

135. Wang, D. *et al.* Sulforaphane suppresses EMT and metastasis in human lung cancer through miR-616-5p-mediated GSK3β/β-catenin signaling pathways. *Acta Pharmacol. Sin.* **38,** 241–251 (2017).

136. Wu, J. *et al.* Sulforaphane inhibits TGF-β-induced epithelial-mesenchymal transition of hepatocellular carcinoma cells via the reactive oxygen species-dependent pathway.

Oncol. Rep. **35,** 2977–2983 (2016).

137. Shan, Y. *et al.* Epithelial-mesenchymal transition, a novel target of sulforaphane via COX-2/MMP2, 9/Snail, ZEB1 and miR-200c/ZEB1 pathways in human bladder cancer cells. *J. Nutr. Biochem.* **24,** 1062–1069 (2013).

138. Kaczyńska, A. & Herman-Antosiewicz, A. Combination of lapatinib with isothiocyanates overcomes drug resistance and inhibits migration of HER2 positive breast cancer cells. *Breast Cancer* **24,** 271–280 (2017).

139. Hwang, E. S. & Kim, G. H. Allyl isothiocyanate influences cell adhesion, migration and metalloproteinase gene expression in SK-Hep1 cells. *Exp. Biol. Med. (Maywood).* **234,** 105–11 (2009).

140. Lai, K. C. *et al.* Allyl isothiocyanate inhibits cell metastasis through suppression of the MAPK pathways in epidermal growth factor-stimulated HT29 human colorectal adenocarcinoma cells. *Oncol. Rep.* **31,** 189–196 (2014).

141. Carmeliet, P. & Jain, R. K. Angiogenesis in cancer and other diseases. *Nature* **407,** 249–257 (2000).

142. Weis, S. M. & Cheresh, D. A. Tumor angiogenesis: molecular pathways and therapeutic targets. *Nat. Med.* **17,** 1359–1370 (2011).

143. Bertl, E., Bartsch, H. & Gerhäuser, C. Inhibition of angiogenesis and endothelial cell functions are novel sulforaphane-mediated mechanisms in chemoprevention. *Mol. Cancer Ther.* **5,** 575–585 (2006).

144. Wang, Y., Zhou, Z., Wang, W., Liu, M. & Bao, Y. Differential effects of sulforaphane in regulation of angiogenesis in a co-culture model of endothelial cells and pericytes. *Oncol. Rep.* **37,** 2905–2912 (2017).

145. Davis, R., Singh, K. P., Kurzrock, R. & Shankar, S. Sulforaphane inhibits angiogenesis through activation of FOXO transcription factors. *Oncol. Rep.* **22,** 1473–1478 (2009).

146. Jackson, S. J. T., Singletary, K. W. & Venema, R. C. Sulforaphane suppresses angiogenesis and disrupts endothelial mitotic progression and microtubule polymerization. *Vascul. Pharmacol.* **46,** 77–84 (2007).

147. Shankar, S., Ganapathy, S. & Srivastava, R. K. Sulforaphane enhances the therapeutic potential of TRAIL in prostate cancer orthotopic model through regulation of apoptosis, metastasis, and angiogenesis. *Clin. Cancer Res.* **14,** 6855–6866 (2008).

148. Thejass, P. & Kuttan, G. Inhibition of endothelial cell differentiation and

proinflammatory cytokine production during angiogenesis by allyl isothiocyanate and phenyl isothiocyanate. *Integr Cancer Ther* **6,** 389–399 (2007).

149. Thejass, P. & Kuttan, G. Allyl isothiocyanate (AITC) and phenyl isothiocyanate (PITC) inhibit tumour-specific angiogenesis by downregulating nitric oxide (NO) and tumour necrosis factor-alpha (TNF-alpha) production. *Nitric Oxide - Biol. Chem.* **16,** 247–257 (2007).

150. Kumar, A., D'Souza, S. S., Tickoo, S., Salimath, B. P. & Singh, H. B. Antiangiogenic and proapoptotic activities of allyl isothiocyanate inhibit ascites tumor growth in vivo. *Integr. Cancer Ther.* **8,** 75–87 (2009).

151. Wu, Q. J. *et al.* Pre-diagnostic cruciferous vegetables intake and lung cancer survival among Chinese women. *Sci. Rep.* **5,** 10306 (2015).

152. Mori, N. *et al.* Cruciferous vegetable intake is inversely associated with lung cancer risk among current nonsmoking men in the Japan public health center (JPHC) study. *J. Nutr.* **147,** (2017).

153. Wang, L. I. *et al.* Dietary intake of Cruciferous vegetables, Glutathione S-transferase (GST) polymorphisms and lung cancer risk in a Caucasian population. *Cancer Causes Control* **15,** 977–985 (2004).

154. Tse, G. & Eslick, G. D. Cruciferous vegetables and risk of colorectal neoplasms: a systematic review and meta-analysis. *Nutr. Cancer* **66,** 128–39 (2014).

155. Yang, G. *et al.* Isothiocyanate exposure, glutathione S-transferase polymorphisms, and colorectal cancer risk. *Am. J. Clin. Nutr.* **91,** 704–711 (2010).

156. Vogtmann, E. *et al.* Cruciferous vegetables, glutathione S-transferase polymorphisms, and the risk of colorectal cancer among Chinese men. *Ann. Epidemiol.* **24,** 44–49 (2014).

157. Suzuki, R. *et al.* Fruit and vegetable intake and breast cancer risk defined by estrogen and progesterone receptor status: the Japan Public Health Center-based Prospective Study. *Cancer Causes Control* **24,** 2117–28 (2013).

158. Boggs, D. A. *et al.* Fruit and vegetable intake in relation to risk of breast cancer in the black women's health study. *Am. J. Epidemiol.* **172,** 1268–1279 (2010).

159. Nechuta, S. *et al.* Postdiagnosis cruciferous vegetable consumption and breast cancer outcomes: A report from the after breast cancer pooling project. *Cancer Epidemiol. Biomarkers Prev.* **22,** 1451–1456 (2013).

160. Liu, B., Mao, Q., Cao, M. & Xie, L. Cruciferous vegetables intake and risk of prostate cancer: a meta-analysis. *Int. J. Urol.* **19,** 134–41 (2012).

161. Richman, E. L., Carroll, P. R. & Chan, J. M. Vegetable and fruit intake after diagnosis and risk of prostate cancer progression. *Int. J. Cancer* **131,** 201–10 (2012).

162. Van Die, M. D. *et al.* Phytotherapeutic interventions in the management of biochemically recurrent prostate cancer: A systematic review of randomised trials. *BJU International* **117,** 17–34 (2016).

163. Li, L. Y. *et al.* Cruciferous vegetable consumption and the risk of pancreatic cancer: a meta-analysis. *World J. Surg. Oncol.* **13,** 454 (2015).

164. Larsson, S. C., Håkansson, N., Näslund, I., Bergkvist, L. & Wolk, A. Fruit and vegetable consumption in relation to pancreatic cancer risk: a prospective study. *Cancer Epidemiol. Biomarkers Prev.* **15,** 301–305 (2006).

165. Nothlings, U. *et al.* Vegetable intake and pancreatic cancer risk: the multiethnic cohort study. *Am J Epidemiol* **165,** 138–147 (2007).

166. Kensler, T. W. *et al.* Effects of glucosinolate-rich broccoli sprouts on urinary levels of aflatoxin-DNA adducts and phenanthrene tetraols in a randomized clinical trial in He Zuo Township, Qidong, People's Republic of China. *Cancer Epidemiol. Biomarkers Prev.* **14,** 2605–2613 (2005).

167. Wu, Q. J. *et al.* Urinary isothiocyanates level and liver cancer risk: a nested case-control study in Shanghai, China. *Nutr. Cancer* **66,** 1023–1029 (2014).

168. Bosetti, C. *et al.* Cruciferous vegetables and cancer risk in a network of case-control studies. *Ann. Oncol.* **23,** 2198–2203 (2012).

169. Voorrips, L. E. *et al.* Vegetable and fruit consumption and risks of colon and rectal cancer in a prospective cohort study: The Netherlands Cohort Study on Diet and Cancer. *Am. J. Epidemiol.* **152,** 1081–1092 (2000).

170. Conzatti, A., Telles da Silva Froes, F. C., Schweigert Perry, I. D. & Guerini de Souza, C. Clinical and Molecular Evidence of the Consumption of Broccoli, Glucoraphanin and Sulforaphane in Humans. *Nutr. Hosp.* **31,** 559–569 (2014).

171. Calabrese, E. J., Iavicoli, I. & Calabrese, V. Hormesis: its impact on medicine and health. *Hum. Exp. Toxicol.* **32,** 120–52 (2013).

172. Calabrese, E. J. & Baldwin, L. A. Applications of hormesis in toxicology, risk assessment and chemotherapeutics. *Trends in Pharmacological Sciences* **23,** 331–337 (2002).

173. Son, T. G., Camandola, S. & Mattson, M. P. Hormetic dietary phytochemicals. *NeuroMolecular Medicine* **10,** 236–246 (2008).

174. Speciale, a., Chirafisi, J., Saija, a. & Cimino, F. Nutritional Antioxidants and Adaptive Cell Responses: An Update. *Curr. Mol. Med.* **11,** 770–789 (2011).

175. Zanichelli, F. *et al.* Low concentrations of isothiocyanates protect mesenchymal stem cells from oxidative injuries, while high concentrations exacerbate DNA damage. *Apoptosis* **17,** 964–974 (2012).

176. Zanichelli, F. *et al.* Dose-dependent effects of R-sulforaphane isothiocyanate on the biology of human mesenchymal stem cells, at dietary amounts, it promotes cell proliferation and reduces senescence and apoptosis, while at anti-cancer drug doses, it has a cytotoxic effect. *Age (Omaha).* **34,** 281–293 (2012).

177. Higgins, L. G. *et al.* Transcription factor Nrf2 mediates an adaptive response to sulforaphane that protects fibroblasts in vitro against the cytotoxic effects of electrophiles, peroxides and redox-cycling agents. *Toxicol. Appl. Pharmacol.* **237,** 267–280 (2009).

178. Wang, W. *et al.* Sulforaphane protects the liver against CdSe quantum dot-induced cytotoxicity. *PLoS One* **10,** (2015).

179. Calabrese, E. J. Cancer Biology and Hormesis: Human Tumor Cell Lines Commonly Display Hormetic (Biphasic) Dose Responses. *Crit. Rev. Toxicol.* **35,** 463–582 (2005).

180. Bao, Y., Wang, W., Zhou, Z. & Sun, C. Benefits and Risks of the Hormetic Effects of Dietary Isothiocyanates on Cancer Prevention. *PLoS One* **e114764,** 1–19 (2014).

181. Barrera, L. N. *et al.* TrxR1 and GPx2 are potently induced by isothiocyanates and selenium, and mutually cooperate to protect Caco-2 cells against free radical-mediated cell death. *Biochim. Biophys. Acta - Mol. Cell Res.* **1823,** 1914–1924 (2012).

182. Farrell, D. *et al.* Recent advances from the national cancer institute alliance for nanotechnology in cancer. in *ACS Nano* **4,** 589–594 (2010).

183. Ferrari, M. Cancer nanotechnology: opportunities and challenges. *Nat. Rev. Cancer* **5,** 161–171 (2005).

184. Hassanzadeh, P., Fullwood, I., Sothi, S. & Aldulaimi, D. Cancer nanotechnology. *Gastroenterol. Hepatol. from Bed to Bench* **4,** 63–69 (2011).

185. Xie, J. *et al.* Nanotechnology for the delivery of phytochemicals in cancer therapy. *Biotechnology Advances* **34,** 343–353 (2016).

186. Yallapu, M. M. *et al.* Anti-cancer activity of curcumin loaded nanoparticles in prostate cancer. *Biomaterials* **35,** 8635–8648 (2014).

187. Ranjan, A. P., Mukerjee, A., Helson, L., Gupta, R. & Vishwanatha, J. K. Efficacy of liposomal curcumin in a human pancreatic tumor xenograft model: Inhibition of tumor growth and angiogenesis. *Anticancer Res.* **33,** 3603–3610 (2013).

188. Zaman, M. S. *et al.* Curcumin Nanoformulation for Cervical Cancer Treatment. *Sci. Rep.* **6,** 20051 (2016).

189. Orunoğlu, M. *et al.* Effects of curcumin-loaded PLGA nanoparticles on the RG2 rat glioma model. *Mater. Sci. Eng. C* **78,** 32–38 (2017).

190. Tan, B. J., Liu, Y., Chang, K. L., Lim, B. K. W. & Chiu, G. N. C. Perorally active nanomicellar formulation of quercetin in the treatment of lung cancer. *Int. J. Nanomedicine* **7,** 651–661 (2012).

191. Jung, K. H. *et al.* Resveratrol-loaded polymeric nanoparticles suppress glucose metabolism and tumor growth in vitro and in vivo. *Int. J. Pharm.* **478,** 251–257 (2015).

192. Siddiqui, I. A. *et al.* Introducing nanochemoprevention as a novel approach for cancer control: Proof of principle with green tea polyphenol epigallocatechin-3-gallate. *Cancer Res.* **69,** 1712–1716 (2009).

193. Khan, N. *et al.* Oral administration of naturally occurring chitosan-based nanoformulated green tea polyphenol EGCG effectively inhibits prostate cancer cell growth in a xenograft model. *Carcinogenesis* **35,** 415–423 (2014).

194. Hsieh, D. S. *et al.* The treatment of bladder cancer in a mouse model by epigallocatechin-3-gallate-gold nanoparticles. *Biomaterials* **32,** 7633–40 (2011).

195. Chen, C. C. *et al.* Improving anticancer efficacy of (-)-epigallocatechin-3-gallate gold nanoparticles in murine B16F10 melanoma cells. *Drug Des. Devel. Ther.* **8,** 459–473 (2014).

196. Sanna, V. *et al.* Targeted biocompatible nanoparticles for the delivery of (-)-epigallocatechin 3-gallate to prostate cancer cells. *J. Med. Chem.* **54,** 1321–1332 (2011).

197. El-Gogary, R. I. *et al.* Polyethylene glycol conjugated polymeric nanocapsules for targeted delivery of quercetin to folate-expressing cancer cells in vitro and in vivo. *ACS Nano* **8,** 1384–1401 (2014).

198. Bu, L. *et al.* Trans-resveratrol loaded chitosan nanoparticles modified with biotin and

avidin to target hepatic carcinoma. *Int. J. Pharm.* **452,** 355–362 (2013).

199. Ji, G., Yang, J. & Chen, J. Preparation of novel curcumin-loaded multifunctional nanodroplets for combining ultrasonic development and targeted chemotherapy. *Int. J. Pharm.* **466,** 314–320 (2014).

200. Li, T. *et al.* pH-Sensitive mesoporous silica nanoparticles anticancer prodrugs for sustained release of ursolic acid and the enhanced anti-cancer efficacy for hepatocellular carcinoma cancer. *Eur. J. Pharm. Sci.* **96,** 456–463 (2017).

201. Almeida, E. A. M. S. *et al.* Curcumin-loaded dual pH- and thermo-responsive magnetic microcarriers based on pectin maleate for drug delivery. *Carbohydr. Polym.* **171,** 259–266 (2017).

202. Yan, J. *et al.* Targeted nanomedicine for prostate cancer therapy: docetaxel and curcumin co-encapsulated lipid–polymer hybrid nanoparticles for the enhanced anti-tumor activity in vitro and in vivo. *Drug Deliv.* **23,** 1757–1762 (2015).

203. Fang, J. H. *et al.* Magnetic core-shell nanocapsules with dual-targeting capabilities and co-delivery of multiple drugs to treat brain gliomas. *Adv. Healthc. Mater.* **3,** 1250–1260 (2014).

204. Anitha, A., Sreeranganathan, M., Chennazhi, K. P. rasad, Lakshmanan, V. K. & Jayakumar, R. In vitro combinatorial anticancer effects of 5-fluorouracil and curcumin loaded N,O-carboxymethyl chitosan nanoparticles toward colon cancer and in vivo pharmacokinetic studies. *Eur. J. Pharm. Biopharm.* **88,** 238–251 (2014).

205. Hu, K. *et al.* Quercetin Remodels the Tumor Microenvironment To Improve the Permeation, Retention, and Antitumor Effects of Nanoparticles. *ACS Nano* **11,** 4916–4925 (2017).

206. Mohan, A., Narayanan, S., Sethuraman, S. & Krishnan, U. M. Novel resveratrol and 5-fluorouracil coencapsulated in PEGylated nanoliposomes improve chemotherapeutic efficacy of combination against head and neck squamous cell carcinoma. *Biomed Res. Int.* **2014,** (2014).

207. Singh, M. *et al.* Enhancement of cancer chemosensitization potential of cisplatin by tea polyphenols poly(lactide-co-glycolide) nanoparticles. *J. Biomed. Nanotechnol.* **7,** 202 (2011).

208. Narayanan, N. K., Nargi, D., Randolph, C. & Narayanan, B. A. Liposome encapsulation of curcumin and resveratrol in combination reduces prostate cancer incidence in

PTEN knockout mice. *Int. J. Cancer* **125,** 1–8 (2009).

209. Danafar, H., Sharafi, A., Kheiri Manjili, H. & Andalib, S. Sulforaphane delivery using mPEG-PCL co-polymer nanoparticles to breast cancer cells. *Pharm. Dev. Technol.* 1–10 (2016).

210. Kheiri Manjili, H., Sharafi, A., Attari, E. & Danafar, H. Pharmacokinetics and in vitro and in vivo delivery of sulforaphane by PCL-PEG-PCL copolymeric-based micelles. *Artif Cells Nanomed Biotechnol* 1–12 (2017).

211. Kheiri Manjili, H. *et al.* D, l-sulforaphane loaded Fe3O4@ gold core shell nanoparticles: A potential sulforaphane delivery system. *PLoS One* **11,** (2016).

212. Encinas-Basurto, D. *et al.* Poly (lactic-co-glycolic acid) nanoparticles for sustained release of allyl isothiocyanate: Characterization, in vitro release and biological activity. *J. Microencapsul.* 1–30 (2017).

213. Li, Y. *et al.* Enhancement of aqueous stability of allyl isothiocyanate using nanoemulsions prepared by an emulsion inversion point method. *J. Colloid Interface Sci.* **438,** 130–137 (2015).

214. Pulliero, A. *et al.* Nanoparticles increase the efficacy of cancer chemopreventive agents in cells exposed to cigarette smoke condensate. *Carcinogenesis* **36,** 368–377 (2014).

215. Yang, Y. T., Shi, Y., Jay, M. & Di Pasqua, A. J. Enhanced toxicity of cisplatin with chemosensitizer phenethyl isothiocyanate toward non-small cell lung cancer cells when delivered in liposomal nanoparticles. *Chem. Res. Toxicol.* **27,** 946–948 (2014).

216. Bera, D., Qian, L., Tseng, T. K. & Holloway, P. H. Quantum dots and their multimodal applications: A review. *Materials* **3,** 2260–2345 (2010).

217. O'Farrell, N., Houlton, A. & Horrocks, B. R. Silicon nanoparticles: Applications in cell biology and medicine. *International Journal of Nanomedicine* **1,** 451–472 (2006).

218. Samia, A. C. S., Chen, X. & Burda, C. Semiconductor Quantum Dots for Photodynamic Therapy. *J. Am. Chem. Soc.* **125,** 15736–15737 (2003).

219. Medintz, I. L., Uyeda, H. T., Goldman, E. R. & Mattoussi, H. Quantum dot bioconjugates for imaging, labelling and sensing. *Nat. Mater.* **4,** 435–446 (2005).

220. Bakalova, R. *et al.* Quantum dot anti-CD conjugates: Are they potential photosensitizers or potentiators of classical photosensitizing agents in photodynamic therapy of cancer? *Nano Lett.* **4,** 1567–1573 (2004).

221. Probst, C. E., Zrazhevskiy, P., Bagalkot, V. & Gao, X. Quantum dots as a platform for nanoparticle drug delivery vehicle design. *Advanced Drug Delivery Reviews* **65,** 703–718 (2013).

222. Wang, Y. & Chen, L. Quantum dots, lighting up the research and development of nanomedicine. *Nanomedicine: Nanotechnology, Biology, and Medicine* **7,** 385–402 (2011).

223. Volkov, Y. Quantum dots in nanomedicine: Recent trends, advances and unresolved issues. *Biochem. Biophys. Res. Commun.* **468,** 419–427 (2015).

224. O'Farrell, N., Houlton, A. & Horrocks, B. R. Silicon nanoparticles: applications in cell biology and medicine. *Int. J. Nanomedicine* **1,** 451–72 (2006).

225. Lie, L. H., Duerdin, M., Tuite, E. M., Houlton, A. & Horrocks, B. R. Preparation and characterisation of luminescent alkylated-silicon quantum dots. *J. Electroanal. Chem.* **538 -539,** 183–190 (2002).

226. Ahire, J. H. *et al.* Highly luminescent and nontoxic amine-capped nanoparticles from porous silicon: Synthesis and their use in biomedical imaging. *ACS Appl. Mater. Interfaces* **4,** 3285–3292 (2012).

227. Cheng, X., Lowe, S. B., Reece, P. J. & Gooding, J. J. Colloidal silicon quantum dots: from preparation to the modification of self-assembled monolayers (SAMs) for bio-applications. *Chem. Soc. Rev.* **43,** 2680–700 (2014).

228. Alsharif, N. H. *et al.* Alkyl-capped silicon nanocrystals lack cytotoxicity and have enhanced intracellular accumulation in malignant cells via cholesterol-dependent endocytosis. *Small* **5,** 221–8 (2009).

229. Ahire, J. H. *et al.* Synthesis of Carbohydrate Capped Silicon Nanoparticles and their Reduced Cytotoxicity, In Vivo Toxicity, and Cellular Uptake. *Adv. Healthc. Mater.* **4,** 1877–1886 (2015).

230. Behray, M. *et al.* Synthesis of Diagnostic Silicon Nanoparticles for Targeted Delivery of Thiourea to Epidermal Growth Factor Receptor-Expressing Cancer Cells. *ACS Appl. Mater. Interfaces* **8,** 8908–8917 (2016).

231. Wang, Q., Bao, Y., Ahire, J. & Chao, Y. Co-encapsulation of biodegradable nanoparticles with silicon quantum dots and quercetin for monitored delivery. *Adv. Healthc. Mater.* **2,** 459–66 (2013).

232. Forner, A., Llovet, J. M. & Bruix, J. Hepatocellular carcinoma. *Lancet* **379,** 1245–55

(2012).

233. Nishimori, H. *et al.* Silica nanoparticles as hepatotoxicants. *Eur. J. Pharm. Biopharm.* **72,** 496–501 (2009).

234. Xie, G., Sun, J., ZhonG., G., Shi, L. & ZhanG., D. Biodistribution and toxicity of intravenously administered silica nanoparticles in mice. *Arch. Toxicol.* **84,** 183–190 (2010).

235. Clayton, R. F. *et al.* Liver cell lines for the study of hepatocyte functions and immunological response. *Liver Int.* **25,** 389–402 (2005).

236. Cooley, L. S. *et al.* Reversible transdifferentiation of blood vascular endothelial cells to a lymphatic-like phenotype in vitro. *J. Cell Sci.* **123,** 3808–3816 (2010).

237. Fogh, J., Fogh, J. M. & Orfeo, T. One hundred and twenty-seven cultured human tumor cell lines producing tumors in nude mice. *J. Natl. Cancer Inst.* **59,** 221–226 (1977).

238. Jumarie, C. & Malo, C. Caco-2 cells cultured in serum-free medium as a model for the study of enterocytic differentiation in vitro. *J Cell Physiol* **149,** 24–33 (1991).

239. Collins, A. R. The comet assay for DNA damage and repair: principles, applications, and limitations. *Mol. Biotechnol.* **26,** 249–261 (2004).

240. Franken, N. A. P., Rodermond, H. M., Stap, J., Haveman, J. & van Bree, C. Clonogenic assay of cells in vitro. *Nat. Protoc.* **1,** 2315–2319 (2006).

241. Meister, A. Glutathione deficiency produced by inhibition of its synthesis, and its reversal; Applications in research and therapy. *Pharmacology and Therapeutics* **51,** 155–194 (1991).

242. Cotgreave, I. A. & Moldéus, P. Methodologies for the application of monobromobimane to the simultaneous analysis of soluble and protein thiol components of biological systems. *J. Biochem. Biophys. Methods* **13,** 231–249 (1986).

243. Schneider, C. a, Rasband, W. S. & Eliceiri, K. W. NIH Image to ImageJ: 25 years of image analysis. *Nat. Methods* **9,** 671–675 (2012).

244. Aplin, A. E., Howe, A. K. & Juliano, R. L. Cell adhesion molecules, signal transduction and cell growth. *Curr. Opin. Cell Biol.* **11,** 737–44 (1999).

245. Sun, D. *et al.* Bisacurone inhibits adhesion of inflammatory monocytes or cancer cells to endothelial cells through down-regulation of VCAM-1 expression. *Int.*

Immunopharmacol. **8,** 1272–1281 (2008).

246. Davis, G. E., Stratman, A. N., Sacharidou, A. & Koh, W. Molecular Basis for Endothelial Lumen Formation and Tubulogenesis During Vasculogenesis and Angiogenic Sprouting. *Int. Rev. Cell Mol. Biol.* **288,** 101–165 (2011).

247. Weis, S. M. & Cheresh, D. A. Tumor angiogenesis: molecular pathways and therapeutic targets. *Nat. Med.* **17,** 1359–1370 (2011).

248. Baker, M. *et al.* Use of the mouse aortic ring assay to study angiogenesis. *Nat. Protoc.* **7,** 89–104 (2012).

249. Ribatti, D. The chick embryo chorioallantoic membrane (CAM) assay. *Reprod. Toxicol.* **70,** 97–101 (2017).

250. Han, S. Y. *et al.* MicroRNA-33a-3p suppresses cell migration and invasion by directly targeting PBX3 in human hepatocellular carcinoma. *Oncotarget* **7,** 42461–42473 (2016).

251. Hu, C., Eggler, A. L., Mesecar, A. D. & Van Breemen, R. B. Modification of Keap1 cysteine residues by sulforaphane. *Chem. Res. Toxicol.* **24,** 515–521 (2011).

252. Townsend, D. M., Tew, K. D. & Tapiero, H. The importance of glutathione in human disease. *Biomedicine and Pharmacotherapy* **57,** 145–155 (2003).

253. Lu, S. C. Regulation of glutathione synthesis. *Molecular Aspects of Medicine* **30,** 42–59 (2009).

254. Thimmulappa, R. K. *et al.* Identification of Nrf2-regulated genes induced by the chemopreventive agent sulforaphane by oligonucleotide microarray. *Cancer Res.* **62,** 5196–5203 (2002).

255. Mitsuishi, Y. *et al.* Nrf2 Redirects Glucose and Glutamine into Anabolic Pathways in Metabolic Reprogramming. *Cancer Cell* **22,** 66–79 (2012).

256. Moon, D. O. *et al.* Sulforaphane decreases viability and telomerase activity in hepatocellular carcinoma Hep3B cells through the reactive oxygen species-dependent pathway. *Cancer Lett.* **295,** 260–266 (2010).

257. Chaudhuri, D., Orsulic, S. & Ashok, B. T. Antiproliferative activity of sulforaphane in Akt-overexpressing ovarian cancer cells. *Mol. Cancer Ther.* **6,** 334–45 (2007).

258. Chung, Y. K. *et al.* Sulforaphane down-regulates SKP2 to stabilize $p27^{KIP1}$ for inducing antiproliferation in human colon adenocarcinoma cells. *J. Biosci. Bioeng.* **119,** 35–42

(2015).

259. Tang, L. & Zhang, Y. Mitochondria are the primary target in isothiocyanate-induced apoptosis in human bladder cancer cells. *Mol. Cancer Ther.* **4,** 1250–1259 (2005).

260. Jackson, S. J. T. & Singletary, K. W. Sulforaphane: A naturally occuring mammary carcinoma mitotic inhibitor, which disrupts tubulin polymerization. *Carcinogenesis* **25,** 219–227 (2004).

261. Byun, S. *et al.* Sulforaphene suppresses growth of colon cancer-derived tumors via induction of glutathione depletion and microtubule depolymerization. *Mol. Nutr. Food Res.* **60,** 1068–1078 (2016).

262. Pham, N. A. *et al.* The dietary isothiocyanate sulforaphane targets pathways of apoptosis, cell cycle arrest, and oxidative stress in human pancreatic cancer cells and inhibits tumor growth in severe combined immunodeficient mice. *Mol Cancer Ther* **3,** 1239–1248 (2004).

263. Gamet-Payrastre, L. *et al.* Sulforaphane, a naturally occurring isothiocyanate, induces cell cycle arrest and apoptosis in HT29 human colon cancer cells. *Cancer Res.* **60,** 1426–1433 (2000).

264. Suppipat, K., Park, C. S., Shen, Y., Zhu, X. & Lacorazza, H. D. Sulforaphane Induces Cell Cycle Arrest and Apoptosis in Acute Lymphoblastic Leukemia Cells. *PLoS One* **7,** (2012).

265. Park, H. S. *et al.* Sulforaphane induces reactive oxygen species-mediated mitotic arrest and subsequent apoptosis in human bladder cancer 5637 cells. *Food Chem. Toxicol.* **64,** 157–165 (2014).

266. Herz, C. *et al.* The isothiocyanate erucin abrogates telomerase in hepatocellular carcinoma cells in vitro and in an orthotopic xenograft tumour model of HCC. *J. Cell. Mol. Med.* **18,** 2393–2403 (2014).

267. Li, Y. *et al.* Sulforaphane inhibits pancreatic cancer through disrupting Hsp90-p50Cdc37 complex and direct interactions with amino acids residues of Hsp90. *J. Nutr. Biochem.* **23,** 1617–1626 (2012).

268. Pledgie-Tracy, A., Sobolewski, M. D. & Davidson, N. E. Sulforaphane induces cell type-specific apoptosis in human breast cancer cell lines. *Mol. Cancer Ther.* **6,** 1013–1021 (2007).

269. Clarke, J. D., Hsu, A., Yu, Z., Dashwood, R. H. & Ho, E. Differential effects of sulforaphane on histone deacetylases, cell cycle arrest and apoptosis in normal

prostate cells versus hyperplastic and cancerous prostate cells. *Mol. Nutr. Food Res.* **55,** 999–1009 (2011).

270. Zeng, H., Trujillo, O.N., Moyer, M.P., Botnen, J. H. Prolonged sulforaphane treatment activates survival signaling in nontumorigenic NCM460 colon cells but apoptotic signaling in tumorigenic HCT116 colon cells. *Nutr. Cancer* **15,** 2379–2381 (2013).

271. Misiewicz, I., Skupinska, K. & Kasprzycka-Guttman, T. Differential response of human healthy lymphoblastoid and CCRF-SB leukemia cells to sulforaphane and its two analogues: 2-oxohexyl isothiocyanate and alyssin. *Pharmacol. Reports* **59,** 80–87 (2007).

272. Fimognari, C. *et al.* Isothiocyanates as novel cytotoxic and cytostatic agents: Molecular pathway on human transformed and non-transformed cells. in *Biochemical Pharmacology* **68,** 1133–1138 (2004).

273. Gamet-Payrastre, L. *et al.* Selective cytostatic and cytotoxic effects of glucosinolates hydrolysis products on human colon cancer cells in vitro. *Anticancer. Drugs* **9,** 141–8 (1998).

274. Wong, C. P. *et al.* Effects of sulforaphane and 3,3'-diindolylmethane on genome-wide promoter methylation in normal prostate epithelial cells and prostate cancer cells. *PLoS One* **9,** (2014).

275. Lubelska, K. *et al.* Sulforaphane Regulates NFE2L2/Nrf2-Dependent Xenobiotic Metabolism Phase II and Phase III Enzymes Differently in Human Colorectal Cancer and Untransformed Epithelial Colon Cells. *Nutr. Cancer* **68,** 1338–1348 (2016).

276. Negrette-Guzman, M. *et al.* Sulforaphane induces differential modulation of mitochondrial biogenesis and dynamics in normal cells and tumor cells. *Food Chem. Toxicol.* **100,** 90–102 (2017).

277. Constantinescu, S. *et al.* Transcriptomic responses of cancerous and noncancerous human colon cells to sulforaphane and selenium. *Chem. Res. Toxicol.* **27,** 377–386 (2014).

278. Agyeman, A. S. *et al.* Transcriptomic and proteomic profiling of KEAP1 disrupted and sulforaphane-treated human breast epithelial cells reveals common expression profiles. *Breast Cancer Res. Treat.* **132,** 175–187 (2012).

279. Atsushi, H. *et al.* DNA Damage-Induced Activation of p53 by the Checkpoint Kinase Chk2. *Science (80-.).* **287,** 1824–1827 (2000).

280. Kim, B. R. *et al.* Effects of Glutathione on Antioxidant Response Element-Mediated Gene Expression and Apoptosis Elicited by Sulforaphane. *Cancer Res.* **63,** 7520–7525 (2003).

281. Stone, J. & Yang, S. Hydrogen peroxide: a signaling messenger. *Antioxid. Redox Signal.* **8,** 243–270 (2006).

282. Schieber, M. & Chandel, N. S. ROS Function in Redox Signaling and Oxidative Stress. *Curr. Biol.* **24,** R453–R462 (2014).

283. Sestili, P. & Fimognari, C. Cytotoxic and Antitumor Activity of Sulforaphane: The Role of Reactive Oxygen Species. *Biomed Res. Int.* **2015,** 1–9 (2015).

284. Sies, H. Role of metabolic H2O2 generation: Redox signaling and oxidative stress. *Journal of Biological Chemistry* **289,** 8735–8741 (2014).

285. Trachootham, D., Alexandre, J. & Huang, P. Targeting cancer cells by ROS-mediated mechanisms: a radical therapeutic approach? *Nat. Rev. Drug Discov.* **8,** 579–591 (2009).

286. Yokoo, Y. *et al.* Effects of Nrf2 silencing on oxidative stress-associated intestinal carcinogenesis in mice. *Cancer Med.* **5,** 1228–1238 (2016).

287. Cheung, K. L. *et al.* Nrf2 knockout enhances intestinal tumorigenesis in Apcmin/+ mice due to attenuation of anti-oxidative stress pathway while potentiates inflammation. *Mol. Carcinog.* **53,** 77–84 (2014).

288. Kensler, T. W. *et al.* Keap1-Nrf2 signaling: A target for cancer prevention by sulforaphane. *Top. Curr. Chem.* **329,** 163–178 (2013).

289. Li, B. *et al.* Sulforaphane protected the injury of human vascular endothelial cell induced by LPC through up-regulating endogenous antioxidants and phase II enzymes. *Food Funct.* **6,** 1984–91 (2015).

290. Chi, X. *et al.* Sulforaphane reduces apoptosis and oncosis along with protecting liver injury-induced ischemic reperfusion by activating the Nrf2/ARE pathway. *Hepatol. Int.* **9,** 321–329 (2015).

291. Milczarek, M., Misiewicz-Krzemińska, I., Lubelska, K. & Wiktorska, K. Combination treatment with 5-fluorouracil and isothiocyanates shows an antagonistic effect in Chinese hamster fibroblast cells line-V79. *Acta Pol. Pharm. - Drug Res.* **68,** 331–342 (2011).

292. Taguchi, K., Motohashi, H. & Yamamoto, M. Molecular mechanisms of the Keap1-Nrf2

pathway in stress response and cancer evolution. *Genes to Cells* **16,** 123–140 (2011).

293. Menegon, S., Columbano, A. & Giordano, S. The Dual Roles of NRF2 in Cancer. *Trends in Molecular Medicine* **22,** 578–593 (2016).

294. Kansanen, E., Kuosmanen, S. M., Leinonen, H. & Levonenn, A. L. The Keap1-Nrf2 pathway: Mechanisms of activation and dysregulation in cancer. *Redox Biol.* **1,** 45–49 (2013).

295. Conaway, C. & Krzeminski, J. Decomposition rates of isothiocyanate conjugates determine their activity as inhibitors of cytochrome p450 enzymes. *Chem. Res. Toxicol.* **14,** 1170–1176 (2001).

296. Al Janobi, A. A. *et al.* Quantitative measurement of sulforaphane, iberin and their mercapturic acid pathway metabolites in human plasma and urine using liquid chromatography-tandem electrospray ionisation mass spectrometry. *J. Chromatogr. B Anal. Technol. Biomed. Life Sci.* **844,** 223–234 (2006).

297. Baille, T. A. & Slatter, J. . Glutathione - a vehicle for the transport of chemically reactive metabolites in vivo. *Acc. Chem. Res.* **24,** 264–270 (1991).

298. Hu, R. *et al.* Cancer chemoprevention of intestinal polyposis in ApcMin/+ mice by sulforaphane, a natural product derived from cruciferous vegetable. *Carcinogenesis* **27,** 2038–2046 (2006).

299. Basten, G. P., Bao, Y. & Williamson, G. Sulforaphane and its glutathione conjugate but not sulforaphane nitrile induce UDP-glucuronosyl transferase (UGT1A1) and glutathione transferase (GSTA1) in cultured cells. *Carcinogenesis* **23,** 1399–1404 (2002).

300. Lin, K. *et al.* Sulforaphane-cysteine-induced apoptosis via phosphorylated ERK1/2-mediated maspin pathway in human non-small cell lung cancer cells. *Cell Death Discov.* **3,** 17025 (2017).

301. Tian, H. *et al.* Sulforaphane-cysteine suppresses invasion via downregulation of galectin-1 in human prostate cancer DU145 and PC3 cells. *Oncol. Rep.* **36,** 1361–1368 (2016).

302. Chiao, J. W. *et al.* Sulforaphane and its metabolite mediate growth arrest and apoptosis in human prostate cancer cells. *Int. J. Oncol.* **20,** 631–636 (2002).

303. Conaway, C. C. *et al.* Phenethyl isothiocyanate and sulforaphane and their N-acetylcysteine conjugates inhibit malignant progression of lung adenomas induced by

tobacco carcinogens in A/J mice. *Cancer Res.* **65,** 8548–8557 (2005).

304. Hwang, E. S. & Jeffery, E. H. Induction of quinone reductase by sulforaphane and sulforaphane N-acetylcysteine conjugate in murine hepatoma cells. *J. Med. Food* **8,** 198–203 (2005).

305. Tang, L., Li, G., Song, L. & Zhang, Y. The principal urinary metabolites of dietary isothiocyanates, N-acetylcysteine conjugates, elicit the same anti-proliferative response as their parent compounds in human bladder cancer cells. *Anticancer. Drugs* **17,** 297–305 (2006).

306. Myzak, M. C., Karplus, P. A., Chung, F. L. & Dashwood, R. H. A novel mechanism of chemoprotection by sulforaphane: Inhibition of histone deacetylase. *Cancer Res.* **64,** 5767–5774 (2004).

307. Vanduchova, A., Tomankova, V., Anzenbacher, P. & Anzenbacherova, E. Influence of Sulforaphane Metabolites on Activities of Human Drug-Metabolizing Cytochrome P450 and Determination of Sulforaphane in Human Liver Cells. *J. Med. Food* **19,** 1141–1146 (2016).

308. Chung, F. L., Conaway, C. C., Rao, C. V & Reddy, B. S. Chemoprevention of colonic aberrant crypt foci in Fischer rats by sulforaphane and phenethyl isothiocyanate. *Carcinogenesis* **21,** 2287–2291 (2000).

309. Friedl, P. & Wolf, K. Tumour-cell invasion and migration: diversity and escape mechanisms. *Nat. Rev. Cancer* **3,** 362–74 (2003).

310. Li, Y. *et al.* Kinetics of sulforaphane in mice after consumption of sulforaphane-enriched broccoli sprout preparation. *Mol. Nutr. Food Res.* **57,** 2128–2136 (2013).

311. Abbaoui, B. *et al.* Inhibition of bladder cancer by broccoli isothiocyanates sulforaphane and erucin: Characterization, metabolism, and interconversion. *Mol. Nutr. Food Res.* **56,** 1675–1687 (2012).

312. Clarke, J. D. *et al.* Metabolism and tissue distribution of sulforaphane in Nrf2 knockout and wild-type mice. *Pharm. Res.* **28,** 3171–3179 (2011).

313. Fofaria, N. M., Ranjan, A., Kim, S. H. & Srivastava, S. K. in *Enzymes* **37,** 111–137 (2015).

314. Sekine-Suzuki, E., Yu, D., Kubota, N., Okayasu, R. & Anzai, K. Sulforaphane induces DNA double strand breaks predominantly repaired by homologous recombination pathway in human cancer cells. *Biochem. Biophys. Res. Commun.* **377,** 341–345 (2008).

315. Scarpa, E. S. & Ninfali, P. Phytochemicals as innovative therapeutic tools against cancer stem cells. *International Journal of Molecular Sciences* **16,** 15727–15742 (2015).

316. Feitelson, M. A. *et al.* Sustained proliferation in cancer: Mechanisms and novel therapeutic targets. *Seminars in Cancer Biology* **35,** S25–S54 (2015).

317. Hynes, R. O. Cell-matrix adhesion in vascular development. *Journal of Thrombosis and Haemostasis* **5,** 32–40 (2007).

318. Popova, S. N., Lundgren-Åkerlund, E., Wiig, H. & Gullberg, D. Physiology and pathology of collagen receptors. *Acta Physiologica* **190,** 179–187 (2007).

319. Vyas, A. R. & Singh, S. V. Functional relevance of d,l-sulforaphane-mediated induction of vimentin and plasminogen activator inhibitor-1 in human prostate cancer cells. *Eur. J. Nutr.* **53,** 843–852 (2014).

320. Li, C. *et al.* Sulforaphane inhibits invasion via activating ERK1/2 signaling in human glioblastoma U87MG and U373MG cells. *PLoS One* **9,** (2014).

321. Wang, L. *et al.* Sulforaphane inhibits thyroid cancer cell growth and invasiveness through the reactive oxygen species-dependent pathway. *Oncotarget* **6,** 25917–31 (2015).

322. Pastorek, M. *et al.* Sulforaphane reduces molecular response to hypoxia in ovarian tumor cells independently of their resistance to chemotherapy. *Int. J. Oncol.* **47,** 51–60 (2015).

323. Lee, Y. R. *et al.* Sulforaphane controls TPA-induced MMP-9 expression through the NF-kB signaling pathway, but not AP-1, in MCF-7 breast cancer cells. *BMB Rep.* **46,** 201–206 (2013).

324. Bertl, E., Bartsch, H. & Gerhäuser, C. Inhibition of angiogenesis and endothelial cell functions are novel sulforaphane-mediated mechanisms in chemoprevention. *Mol. Cancer Ther.* **5,** 575–85 (2006).

325. Bacon, J. R. *et al.* Dual action of sulforaphane in the regulation of thioredoxin reductase and thioredoxin in human HepG2 and caco-2 cells. *J. Agric. Food Chem.* **55,** 1170–1176 (2007).

326. Sartorius, K., Sartorius, B., Aldous, C., Govender, P. S. & Madiba, T. E. Global and country underestimation of hepatocellular carcinoma (HCC) in 2012 and its implications. *Cancer Epidemiol.* **39,** 284–290 (2015).

327. De Lope, C. R., Tremosini, S., Forner, A., Reig, M. & Bruix, J. Management of HCC. *J. Hepatol.* **56,** S75–S87 (2012).

328. Li, S. *et al.* Expression characteristics of hypoxia-inducible factor-1α and its clinical values in diagnosis and prognosis of hepatocellular carcinoma. *Hepat. Mon.* **11,** 36–43 (2011).

329. Zhu, A. X., Duda, D. G., Sahani, D. V & Jain, R. K. HCC and angiogenesis: possible targets and future directions. *Nat. Rev. Clin. Oncol.* **8,** 292–301 (2011).

330. Pang, R. & Poon, R. T. P. Angiogenesis and antiangiogenic therapy in hepatocellular carcinoma. *Cancer Letters* **242,** 151–167 (2006).

331. Pazo-Cid, R. A. *et al.* Novel antiangiogenic therapies against advanced hepatocellular carcinoma (HCC). *Clin. Transl. Oncol.* **14,** 564–574 (2012).

332. Moreno, F. S., Heidor, R. & Pogribny, I. P. Nutritional epigenetics and the prevention of hepatocellular carcinoma with bioactive food constituents. *Nutr. Cancer* **68,** 719–733 (2016).

333. Okano, J. I., Fujise, Y., Abe, R., Imamoto, R. & Murawaki, Y. Chemoprevention against hepatocellular carcinoma. *Clinical Journal of Gastroenterology* **4,** 185–197 (2011).

334. Yang, G., Lee, H. E. & Lee, J. Y. A pharmacological inhibitor of NLRP3 inflammasome prevents non-alcoholic fatty liver disease in a mouse model induced by high fat diet. *Sci. Rep.* **6,** 24399 (2016).

335. Jeon, Y. K., Yoo, D. R., Jang, Y. H., Jang, S. Y. & Nam, M. J. Sulforaphane induces apoptosis in human hepatic cancer cells through inhibition of 6-phosphofructo-2-kinase/fructose-2,6-biphosphatase4, mediated by hypoxia inducible factor-1-dependent pathway. *Biochim. Biophys. Acta - Proteins Proteomics* **1814,** 1340–1348 (2011).

336. Park, S. Y., Kim, G. Y., Bae, S. J., Yoo, Y. H. & Choi, Y. H. Induction of apoptosis by isothiocyanate sulforaphane in human cervical carcinoma HeLa and hepatocarcinoma HepG2 cells through activation of caspase-3. *Oncol. Rep.* **18,** 181–187 (2007).

337. Kim, H. *et al.* Sulforaphane sensitizes tumor necrosis factor-related apoptosis-inducing ligand (TRAIL)-resistant hepatoma cells to TRAIL-induced apoptosis through reactive oxygen species-mediated up-regulation of DR5. *Cancer Res.* **66,** 1740–1750 (2006).

338. Ren, K., Li, Z., Li, Y., Zhang, W. & Han, X. Sulforaphene enhances radiosensitivity of

hepatocellular carcinoma through suppression of the NF-κB pathway. *J. Biochem. Mol. Toxicol.* **e21917,** (2017).

339. Juge, N., Mithen, R. & Traka, M. Molecular basis for chemoprevention by sulforaphane: a comprehensive review. *Cell. Mol. Life Sci.* **64,** 1105–1127 (2007).

340. Gupta, S. C., Kim, J. H., Prasad, S. & Aggarwal, B. B. Regulation of survival, proliferation, invasion, angiogenesis, and metastasis of tumor cells through modulation of inflammatory pathways by nutraceuticals. *Cancer Metastasis Rev.* **29,** 405–34 (2010).

341. Xu, C., Shen, G., Chen, C., Gélinas, C. & Kong, A. N. T. Suppression of NF-kappaB and NF-kappaB-regulated gene expression by sulforaphane and PEITC through IkappaBalpha, IKK pathway in human prostate cancer PC-3 cells. *Oncogene* **24,** 4486–95 (2005).

342. Hunakova, L. *et al.* Modulation of markers associated with aggressive phenotype in MDA-MB-231 breast carcinoma cells by sulforaphane. *Neoplasma* **56,** 548–556 (2009).

343. Labelle, M. & Hynes, R. O. The initial hours of metastasis: The importance of cooperative host-tumor cell interactions during hematogenous dissemination. *Cancer Discovery* **2,** 1091–1099 (2012).

344. Chung, A. S., Lee, J. & Ferrara, N. Targeting the tumour vasculature: insights from physiological angiogenesis. *Nat. Rev. Cancer* **10,** 505–514 (2010).

345. Whiteside, T. L. The tumor microenvironment and its role in promoting tumor growth. *Oncogene* **27,** 5904–12 (2008).

346. Asakage, M. *et al.* Sulforaphane induces inhibition of human umbilical vein endothelial cells proliferation by apoptosis. *Angiogenesis* **9,** 83–91 (2006).

347. Eberhard, A. *et al.* Heterogeneity of angiogenesis and blood vessel maturation in human tumors: Implications for antiangiogenic tumor therapies. *Cancer Res.* **60,** 1388–1393 (2000).

348. Carmeliet, P. & Jain, R. Molecular mechanisms and clinical applications of angiogenesis. *Nature* **473,** 298–307 (2011).

349. Luo, D., Wang, Z., Wu, J., Jiang, C. & Wu, J. The role of hypoxia inducible factor-1 in hepatocellular carcinoma. *BioMed Research International* **2014,** (2014).

350. He, G. & Karin, M. NF-kappaB and STAT3 - key players in liver inflammation and cancer. *Cell Res.* **21,** 159–168 (2011).

351. Moser, C. *et al.* ENMD-1198, a novel tubulin-binding agent reduces HIF-1alpha and STAT3 activity in human hepatocellular carcinoma(HCC) cells, and inhibits growth and vascularization in vivo. *BMC Cancer* **8,** 206 (2008).

352. Hahm, E. R. & Singh, S. V. Sulforaphane inhibits constitutive and interleukin-6-induced activation of signal transducer and activator of transcription 3 in prostate cancer cells. *Cancer Prev. Res. (Phila).* **3,** 484–94 (2010).

353. Miao, Z., Yu, F., Ren, Y. & Yang, J. D,L-sulforaphane induces ROS-dependent apoptosis in human gliomablastoma cells by inactivating STAT3 signaling pathway. *Int. J. Mol. Sci.* **18,** 1–14 (2017).

354. Wang, X. *et al.* Sulforaphane improves chemotherapy efficacy by targeting cancer stem cell-like properties via the miR-124/IL-6R/STAT3 axis. *Sci. Rep.* **6,** 36796 (2016).

355. Semenza, G. L. Defining the role of hypoxia-inducible factor 1 in cancer biology and therapeutics. *Oncogene* **29,** 625–634 (2009).

356. Al Okail, M. S. Cobalt chloride, a chemical inducer of hypoxia-inducible factor-1α in U251 human glioblastoma cell line. *J. Saudi Chem. Soc.* **14,** 197–201 (2010).

357. Yuan, Y., Hilliard, G., Ferguson, T. & Millhorn, D. E. Cobalt inhibits the interaction between hypoxia-inducible factor-alpha and von Hippel-Lindau protein by direct binding to hypoxia-inducible factor-alpha. *J. Biol. Chem.* **278,** 15911–15916 (2003).

358. Zhou, J., Joplin, D. G., Cross, J. V. & Templeton, D. J. Sulforaphane Inhibits Prostaglandin E2 Synthesis by Suppressing Microsomal Prostaglandin E Synthase 1. *PLoS One* **7,** e49744 (2012).

359. Li, M. *et al.* The In Ovo Chick Chorioallantoic Membrane (CAM) Assay as an Efficient Xenograft Model of Hepatocellular Carcinoma. *J. Vis. Exp.* **104,** e52411 (2015).

360. Srivastava, S. K. *et al.* Allyl isothiocyanate, a constituent of cruciferous vegetables, inhibits growth of PC-3 human prostate cancer xenograft in vivo. *Carcinogenesis* **24,** 1665–1670 (2003).

361. Gupta, P., Kim, B., Kim, S. H. & Srivastava, S. K. Molecular targets of isothiocyanates in cancer: Recent advances. *Mol. Nutr. Food Res.* **0,** 1–23 (2014).

362. Bhattacharya, A. *et al.* Allyl isothiocyanate-rich mustard seed powder inhibits bladder cancer growth and muscle invasion. *Carcinogenesis* **31,** 2105–2110 (2010).

363. Lau, W. S., Chen, T. & Wong, Y. S. Allyl isothiocyanate induces G2/M arrest in human colorectal adenocarcinoma SW620 cells through down-regulation of Cdc25B and

Cdc25C. *Mol. Med. Rep.* **3,** 1023–1030 (2010).

364. Schaefer, E. A. M. *et al.* Stimulation of the chemosensory TRPA1 cation channel by volatile toxic substances promotes cell survival of small cell lung cancer cells. *Biochem. Pharmacol.* **85,** 426–438 (2013).

365. Xu, K. & Thornalley, P. J. Studies on the mechanism of the inhibition of human leukaemia cell growth by dietary isothiocyanates and their cysteine adducts in vitro. *Biochem. Pharmacol.* **60,** 221–231 (2000).

366. Tsai, S. C. *et al.* ERK-modulated intrinsic signaling and G2/M phase arrest contribute to the induction of apoptotic death by allyl isothiocyanate in MDA-MB-468 human breast adenocarcinoma cells. *Int. J. Oncol.* **41,** 2065–2072 (2012).

367. Sávio, A. L. V., da Silva, G. N. & Salvadori, D. M. F. vero. Inhibition of bladder cancer cell proliferation by allyl isothiocyanate (mustard essential oil). *Mutat. Res. - Fundam. Mol. Mech. Mutagen.* **771,** 29–35 (2015).

368. Louhivuori, L. M. *et al.* Differentiation dependent expression of TRPA1 and TRPM8 channels in IMR-32 human neuroblastoma cells. *J. Cell. Physiol.* **221,** 67–74 (2009).

369. Xiao, D. *et al.* Allyl isothiocyanate, a constituent of cruciferous vegetables, inhibits proliferation of human prostate cancer cells by causing G2/M arrest and inducing apoptosis. *Carcinogenesis* **24,** 891–897 (2003).

370. Wu, Q. J. *et al.* Cruciferous vegetables intake and the risk of colorectal cancer: a meta-analysis of observational studies. *Ann. Oncol.* **24,** 1079–87 (2013).

371. Bao, Y., Wang, W., Zhou, Z. & Sun, C. Benefits and risks of the hormetic effects of dietary isothiocyanates on cancer prevention. *PLoS One* **9,** (2014).

372. Pietsch, K. *et al.* Hormetins, antioxidants and prooxidants: Defining quercetin-, caffeic acid- and rosmarinic acid-mediated life extension in C. elegans. *Biogerontology* **12,** 329–347 (2011).

373. Zrazhevskiy, P., Sena, M. & Gao, X. Designing multifunctional quantum dots for bioimaging, detection, and drug delivery. *Chem. Soc. Rev.* **39,** 4326–54 (2010).

374. Qi, L. & Gao, X. Emerging application of quantum dots for drug delivery and therapy. *Expert Opin. Drug Deliv.* **5,** 263–267 (2008).

375. Niture, S. K., Kaspar, J. W., Shen, J. & Jaiswal, A. K. Nrf2 signaling and cell survival. *Toxicology and Applied Pharmacology* **244,** 37–42 (2010).

376. Kaspar, J. W., Niture, S. K. & Jaiswal, A. K. Nrf2:INrf2 (Keap1) signaling in oxidative stress. *Free Radical Biology and Medicine* **47,** 1304–1309 (2009).

377. Urano, Y. *et al.* Selective molecular imaging of viable cancer cells with pH-activatable fluorescence probes. *Nat. Med.* **15,** 104–9 (2009).

378. Iversen, T. G., Skotland, T. & Sandvig, K. Endocytosis and intracellular transport of nanoparticles: Present knowledge and need for future studies. *Nano Today* **6,** 176–185 (2011).

379. Kou, X., Kirberger, M., Yang, Y. & Chen, N. Natural products for cancer prevention associated with Nrf2–ARE pathway. *Food Sci. Hum. Wellness* **2,** 22–28 (2013).

380. Lau, A., Villeneuve, N. F., Sun, Z., Wong, P. K. & Zhang, D. D. Dual roles of Nrf2 in cancer. *Pharmacological Research* **58,** 262–270 (2008).

381. Sporn, M. B. & Liby, K. T. NRF2 and cancer: the good, the bad and the importance of context. *Nat. Rev. Cancer* **12,** 564–71 (2012).

382. Karin, M. & Dhar, D. Liver carcinogenesis: From naughty chemicals to soothing fat and the surprising role of NRF2. *Carcinogenesis* **37,** 541–546 (2016).

383. Moon, E. J. & Giaccia, A. Dual roles of NRF2 in tumor prevention and progression: Possible implications in cancer treatment. *Free Radical Biology and Medicine* **79,** 292–299 (2015).

384. Zhang, D. D. The Nrf2-Keap1-ARE signaling pathway: The regulation and dual function of Nrf2 in cancer. *Antioxid. Redox Signal.* **13,** 1623–1626 (2010).

385. Zhu, J. *et al.* An overview of chemical inhibitors of the Nrf2-ARE signaling pathway and their potential applications in cancer therapy. *Free Radical Biology and Medicine* **99,** 544–556 (2016).

386. Wang, A. Z., Langer, R. & Farokhzad, O. C. Nanoparticle Delivery of Cancer Drugs. *Annu. Rev. Med.* **63,** 185–198 (2012).

387. González-Vallinas, M., González-Castejón, M., Rodríguez-Casado, A. & Ramírez de Molina, A. Dietary phytochemicals in cancer prevention and therapy: A complementary approach with promising perspectives. *Nutr. Rev.* **71,** 585–599 (2013).

388. Zhang, Y., Talalay, P., Cho, C. G. & Posner, G. H. A major inducer of anticarcinogenic protective enzymes from broccoli: isolation and elucidation of structure. *Proc. Natl. Acad. Sci. U. S. A.* **89,** 2399–2403 (1992).

389. Bourgeais, J., Gouilleux-Gruart, V. & Gouilleux, F. Oxidative metabolism in cancer: A STAT affair? *Jak-Stat* **2,** e25764 (2013).

390. Bjelakovic, G., Nikolova, D., Gluud, L. L., Simonetti, R. G. & Gluud, C. Antioxidant supplements for prevention of mortality in healthy participants and patients with various diseases. *Sao Paulo Med. J.* **133,** 164 (2015).

391. Satoh, H., Moriguchi, T., Takai, J., Ebina, M. & Yamamoto, M. Nrf2 prevents initiation but accelerates progression through the kras signaling pathway during lung carcinogenesis. *Cancer Res.* **73,** 4158–4168 (2013).

392. Moy, K. A. *et al.* Urinary total isothiocyanates and colorectal cancer: a prospective study of men in Shanghai, China. *Cancer Epidemiol. Biomarkers Prev.* **17,** 1354–9 (2008).

393. Giovannucci, E., Rimm, E. B., Liu, Y., Stampfer, M. J. & Willett, W. C. A Prospective Study of Cruciferous Vegetables and Prostate Cancer. *Cancer Epidemiol. Biomarkers Prev.* **12,** 1403–1409 (2003).

394. Calabrese, E. J. & Blain, R. B. The hormesis database: The occurrence of hormetic dose responses in the toxicological literature. *Regul. Toxicol. Pharmacol.* **61,** 73–81 (2011).

395. Bertrand, N., Wu, J., Xu, X., Kamaly, N. & Farokhzad, O. C. Cancer nanotechnology: The impact of passive and active targeting in the era of modern cancer biology. *Advanced Drug Delivery Reviews* **66,** 2–25 (2014).

396. Jhaveri, A., Deshpande, P. & Torchilin, V. Stimuli-sensitive nanopreparations for combination cancer therapy. *Journal of Controlled Release* **190,** 352–370 (2014).

397. Ma, L., Kohli, M. & Smith, a. Nanoparticles for combination drug therapy. *ACS Nano* **7,** 9518–9525 (2013).

398. Li, Q. Q. *et al.* Sulforaphane inhibits cancer stem-like cell properties and cisplatin resistance through miR-214-mediated downregulation of c-MYC in non-small cell lung cancer. *Oncotarget* **8,** 12067–12080 (2017).

399. Burnett, J. P. *et al.* Sulforaphane enhances the anticancer activity of taxanes against triple negative breast cancer by killing cancer stem cells. *Cancer Lett.* **394,** 52–64 (2017).

400. Ling, X. *et al.* Synergistic effect of allyl isothiocyanate (AITC) on cisplatin efficacy in vitro and in vivo. *Am. J. Cancer Res.* **5,** 2516–2530 (2015).

401. Bhattacharya, A., Li, Y., Shi, Y. & Zhang, Y. Enhanced inhibition of urinary bladder

cancer growth and muscle invasion by allyl isothiocyanate and celecoxib in combination. *Carcinogenesis* **34,** 2593–2599 (2013).

402. Eldar-Boock, A., Polyak, D., Scomparin, A. & Satchi-Fainaro, R. Nano-sized polymers and liposomes designed to deliver combination therapy for cancer. *Current Opinion in Biotechnology* **24,** 682–689 (2013).

403. Glasgow, M. D. K. & Chougule, M. B. Recent developments in active tumor targeted multifunctional nanoparticles for combination chemotherapy in cancer treatment and imaging. *Journal of Biomedical Nanotechnology* **11,** 1859–1898 (2015).

404. Grandhi, B. K., Thakkar, A., Wang, J. & Prabhu, S. A novel combinatorial nanotechnology-based oral chemopreventive regimen demonstrates significant suppression of pancreatic cancer neoplastic lesions. *Cancer Prev. Res.* **6,** 1015–1025 (2013).

405. Thakkar, A. *et al.* Preclinical systemic toxicity evaluation of chitosan-solid lipid nanoparticle-encapsulated aspirin and curcumin in combination with free sulforaphane in BALalB/c mice. *Int. J. Nanomedicine* **11,** 3265–3276 (2016).

406. Thakkar, A., Chenreddy, S., Wang, J. & Prabhu, S. Evaluation of ibuprofen loaded solid lipid nanoparticles and its combination regimens for pancreatic cancer chemoprevention. *Int. J. Oncol.* **46,** 1827–1834 (2015).

407. Danafar, H., Sharafi, A., Askarlou, S. & Kheiri Manjili, H. Preparation and characterization of PEGylated iron oxide-gold nanoparticles. *Drug Res (Stuttg).* 10.1055/s-0043-115905. (2017).

408. Mura, S. & Couvreur, P. Nanotheranostics for personalized medicine. *Advanced Drug Delivery Reviews* **64,** 1394–1416 (2012).